Geodetic and seismological study of slow earthquakes and inter-plate coupling in the Ryukyu subduction zone

by

Yoko TaoLin Tu

Department of Natural History Science
Graduate School of Science, Hokkaido University

September 2018

Contents

Chapter 3. Slow Slip Events (SSEs)

Chapter 4. Very Low Frequency Earthquakes (VLFEs)

Chapter 5. Repeating Very Low Frequency Earthquakes (RVLFEs)

Chapter 6. Conclusions

Acknowledgement

I greatly appreciate my advisor Prof. K. Heki. Without his guidance, I cannot finish this thesis. Moreover, I am deeply grateful to Prof. M. Ando of Shizuoka University, Prof. H. Kumagai, and Prof. Y. Yamanaka of Nagoya University for their suggestions and assistance for this study. I also want to thank my family, friends, and people who I met in Japan. Thank you for giving me the warmest friendship and great support. Finally, I would like to thank the Japan-Taiwan Exchange Association and the Hokkaido University for the grant. The economic supports let me can concentrate on my research and enjoy the life in Japan.

Moreover, the broadband seismograms used in this study are provided by the NIED F-net in Japan (http://www.fnet.bosai.go.jp/top.php?LANG=ja) and BATS in Taiwan (http://tecws.earth.sinica.edu.tw/BATS/index_login3.php). The GNSS data are supplied by GSI GONET in Japan (http://terras.gsi.go.jp/geo_info/geonet_top.html). This work used GMT, SAC, and Seis-PC software. Here, I express my appreciation to above research and development groups.

Abstract

Slow earthquakes are important phenomena in discussing how plates converge in subduction zones. Here I detected slow slip events (SSEs) and very low-frequency earthquakes (VLFEs) in the Ryukyu Trench using GEONET (GNSS Earth Observation Network) GNSS (Global Navigation Satellite System) data and board-band seismic data of F-net and BATS (Broadband Array in Taiwan for Seismology) in order to investigate interplate coupling in this subduction zone.

From 1997 to 2016, I identified 38 SSEs beneath the Iriomote Island, southwestern Ryukyu Arc. These events occurred biannually on the same fault patch at a depth of ~30 km on the subducting Philippine Sea Plate slab with average moment magnitudes (M_w) of ~6.6. Their slip accumulation rate varies in time and increases in 2002 and 2013, coinciding with the activation of the back-arc spreading as indicated by the earthquakes swarms in the Okinawa Trough. It suggests that episodic activations of the back-arc spreading at the Okinawa Trough caused extra southward movement of the block south of the trough and accelerated convergence at the Ryukyu Trench.

From 2005 to 2012, a total of 29,841 VLFEs were detected in the Ryukyu area also. These events are distributed near the Ryukyu Trench axis and have shallow thrust-faulting mechanisms, which indicates that they probably occur in the accretional prism or on the shallow plate interface of the Ryukyu subduction zone. Moreover, these VLFEs are characteristic of high *b*-values (2.3-5.0), and nearby SSEs often influence their activities. For example, in the Sakishima, Okinawa, and Amami areas, VLFEs are activated in 5-30 days,

0-15 days, and 0-5 days, respectively, after the start of SSEs.

Among these VLFEs, 97 events south of the Miyako Island showed notable similarities in waveforms, amplitudes, magnitudes, and source mechanisms. These events recurred in the same area with an average interval of ~50 days. This new type of VLFEs, named as repeating very low frequency earthquakes (RVLFEs), are similar to small repeating earthquakes in the creeping zone of the plate boundaries. Seismic slip released by the RVLFEs is about 3-42 % of the average plate convergence in this segment of the subduction zone, significantly smaller than that of 72 % released by the repeating SSEs.

From the locations of SSEs and VLFEs detected in this study, and two suspect megathrust earthquakes (M_w>8) in the Ryukyu area, slow and ordinary earthquakes in the Ryukyu Trench are found to occur in following depths, Sakishima: megathrusts (locked zone, ~10 km), VLFEs (~20 km), and SSEs (~30 km), and Okinawa: VLFEs (~20 km) and SSEs (~30 km). However, the situation in the Amami area is not well understood due to the complex tectonic setting and inaccurate hypocenters of large earthquakes and VLFEs.

Chapter 1.

Ryukyu Subduction Zone

1.1 Subduction zones

1.1.1 What are subduction zones?

The lithosphere (containing the crust and shallow upper mantle) forms the outermost layer of the solid earth, which consists of several hundred tectonic plates. These plates (including oceanic and continental plates) float upon the asthenosphere and move relative to one another by the thermal convection of the mantle (Figure 1.1). Based on the relative movement of plates, their boundaries can be classified into three types, i.e., convergent, divergent, and transform fault (Figure 1.1). At convergent boundaries, plates collide with each other and often form majestic mountain ranges (e.g., Himalaya, the highest mountain system on Earth, caused by the convergence of two continental plates) or oceanic trenches (e.g., Mariana, the deepest trench on Earth, due to the convergence of two oceanic plates). In contrast, at divergent boundaries, plates are pushed apart by magma rising from the mantle to the surface. This process renews the oceanic plates and let the marine basins spread. Two typical cases for the type of boundaries are the mid-ocean ridge in the Atlantic Ocean and the Great Rift Valley in the continent of Africa. Moreover, at transform fault boundaries, plates slide sideways in front of each other. These boundaries are different from the convergent and divergent types; they cannot produce spectacular landforms such as high mountains or deep oceans but still can generate large earthquakes (e.g., the M_w 7.9 San Francisco earthquakes of Apr. 18, 1906 along the San Andreas Fault in California).

Subduction is a geological process that occurs at the convergent plate boundaries. When two tectonic plates (usually consists of two oceanic plates or one oceanic and one continental plates) converge, the heavier plate will sink into the mantle under the lighter plate due to the gravitational force. This is called subduction. In this process, a large number of earthquakes occur along the slabs subducting to the depth. Additionally, the volcanism caused by the arc magmatism related to the melting of the upper mantle at the upper surface of the subduction slab is also activated. The region influenced by the subduction process can extend landward one to several hundreds of kilometers from the trench axis depending on the dip angle of the subduction slabs. Such an area is known as the *subduction zone*.

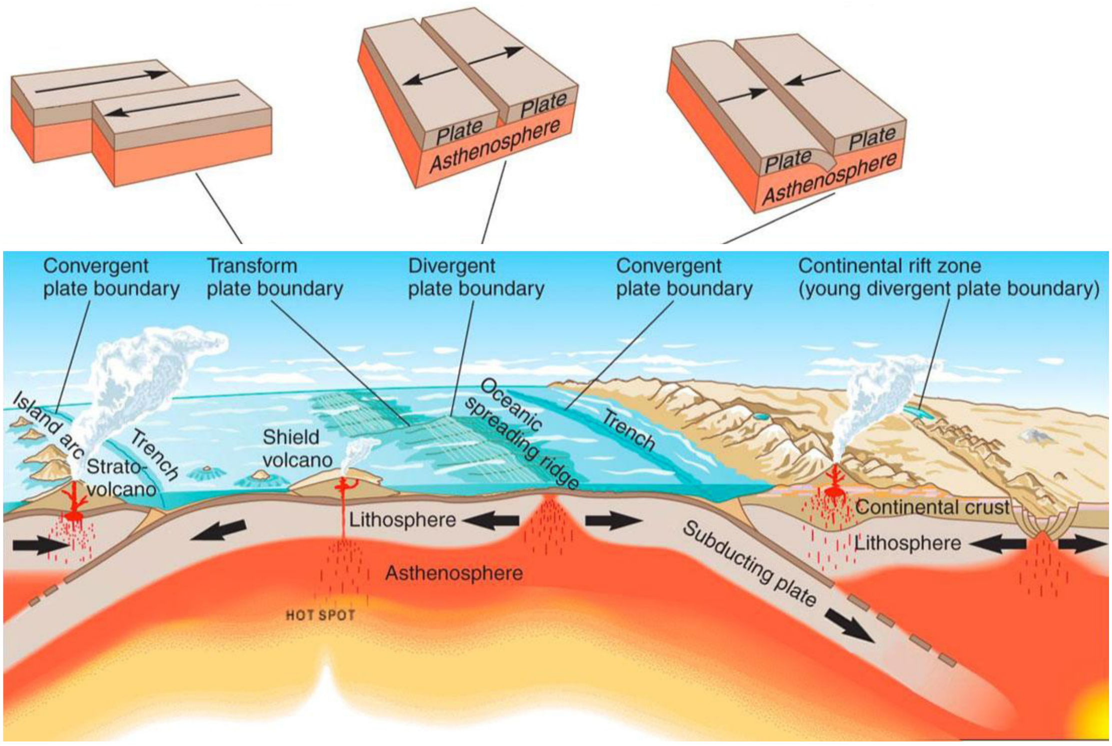

Figure 1.1. Schematic image of plate tectonics and three types of plate boundaries. (Diagram by the courtesy of the U.S. Geological Survey, https://pubs.usgs.gov/gip/dynamic/Vigil.html)

1.1.2 Where are subduction zones?

Subduction zones exist along convergent plate boundaries, where at least one of tectonic plates is an oceanic plate. As shown in Figure 1.2, most subduction zones are located around the Pacific Ocean. These subduction zones can be divided into two major groups based on the type of plates (Figure 1.3). One of the groups is related to the convergence of two oceanic plates, characterized by an island arc parallel to the trench axis (Figure 1.3a). One typical example for this type of subduction zones is the Mariana Trench at the west margin of the Pacific Plate (Figure 1.2). The other group of subduction zones is caused by the oceanic-continental plate convergence (Figure 1.3b). This type of subduction zones forms a remarkable chain of volcanoes at the border of continental plates, and its oceanic trench is closer to the coastline in comparison to the type of the oceanic-oceanic plate convergence (Figure 1.3b). The Cascadia subduction zone in North America (Cascadia faces Canada and USA.) and the Peru-Chile Trench in South America are two typical examples (Figure 1.2).

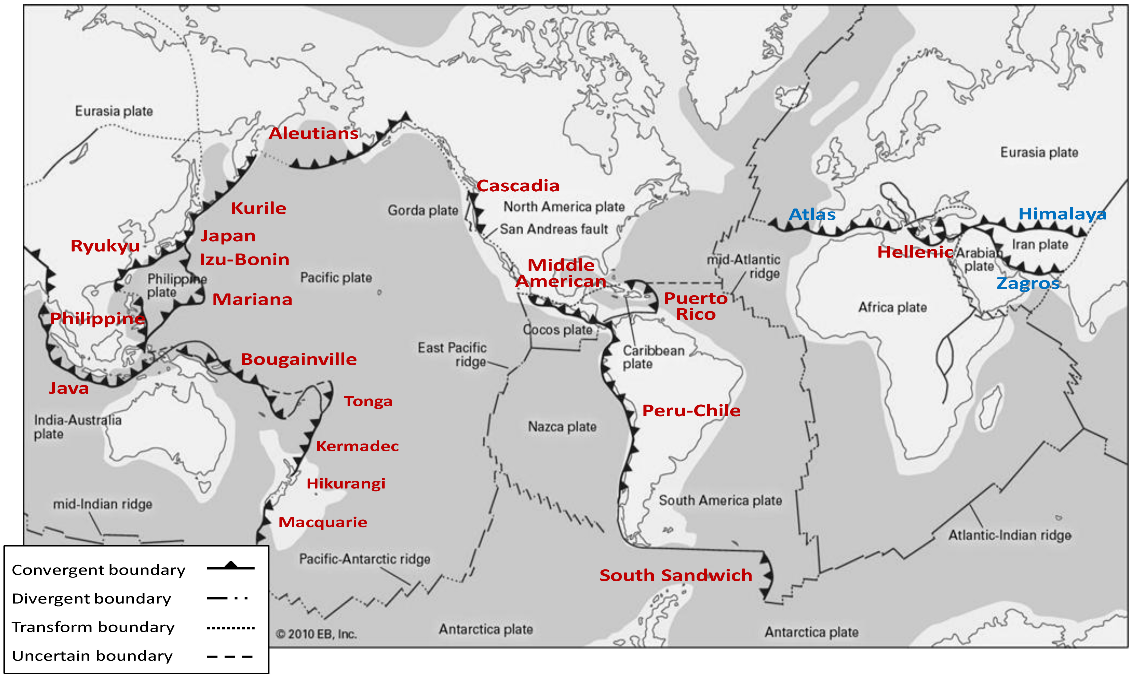

Figure 1.2. Distribution of convergent plate boundaries (barbed lines) including subduction zones, whose names are shown in red, and continental collision zones, whose names are shown in blue. (Modified from Figure 1 of Stern, 2002) (Base-map by the courtesy of the Encyclopaedia Britannica, https://www.britannica.com/science/subduction-zone)

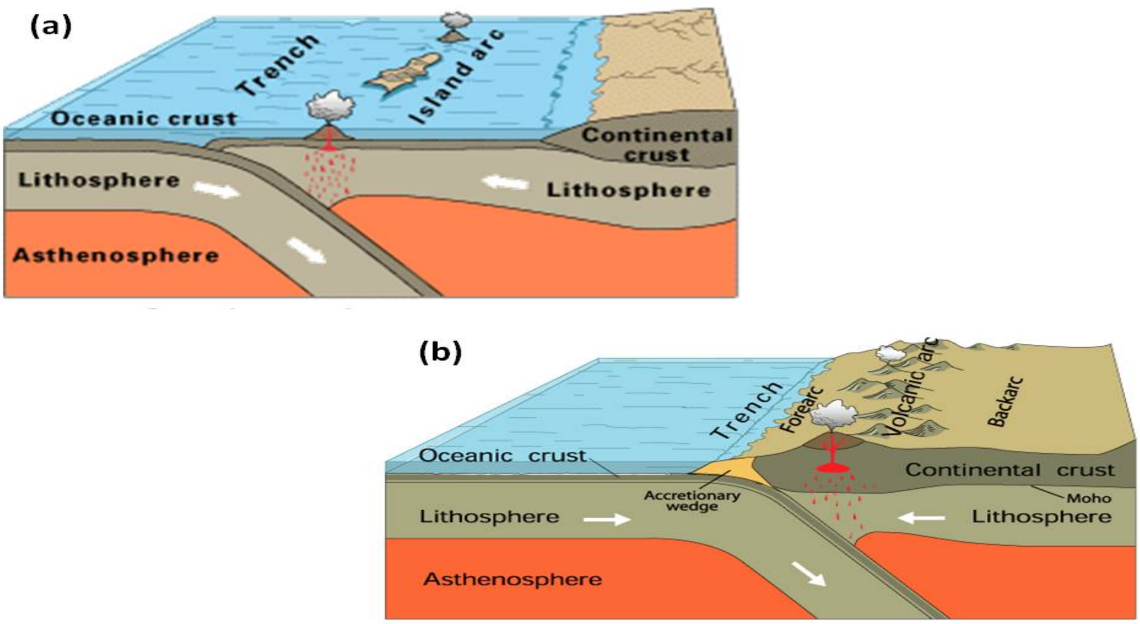

Figure 1.3. Schematic image of two types of subduction zones as (a) oceanic-oceanic plate convergence, and (b) oceanic-continental plate convergence. (Diagram courtesy of the U.S.

Geological Survey, https://www.usgs.gov/media/images/subduction-fault-zone-diagram; https://walrus.wr.usgs.gov/tsunami/sumatraEQ/tectonics.html)

1.1.3 Large earthquakes and subduction zones

Although approximately 90 % of earthquakes occur in subduction zone areas, large interplate earthquakes (M_w >8) only occur in few subduction zones and do not show a random distribution (Figure 1.4). Uyeda and Kanamori (1979) first discussed this phenomenon and attempted to understand its causes by analyzing characteristics of subduction zones where large interplate earthquakes occur. They found that these subduction zones seemed to have similar properties. Moreover, all subduction zones on Earth probably followed an evolution mode and could be classified into several different stages based on the age of subducting sea floor, the arc-normal stress, and the existence of active back-arc basins. The two extreme cases of this evolution mode are the Chilean and the Mariana types, respectively (Figure 1.5).

In the Chilean type subduction zones, a young (< 50 Ma), hot, and thin oceanic plate subducts beneath a continental plate (Figure 1.5). Such a relatively light subducting plate resists the subduction process due to high buoyant. This causes high seismicity and high coupling between the upper and lower slabs and induces the occurrence of large interplate earthquakes. Moreover, this type of subduction zones also has other significant characteristics, such as shallow dip angles, shallow seismic zones, and shallow oceanic trenches (Figure 1.5). The most famous example is the Peru-Chile Trench in South America (Figure 1.2). There, several large interplate earthquakes have occurred in the past 100 years, including the M_w 9.5 Chile earthquake in 1960, the largest earthquake recorded in the human history (Figure 1.4).

In contrast, the subducting plate in the Mariana type subduction zones is an old (> 50 Ma), cold, and thick oceanic plate. Such a relatively dense subducting plate can dive smoothly into the mantle, and causes low seismicity and low interplate coupling. Large interplate earthquakes rarely occur in such subduction zones. Moreover, they are also characterized by steep dip angles, deep oceanic trenches, and the existence of active back-arc opening systems (Figure 1.5). A typical case for this type of subduction zones is the Mariana Trench in the western Pacific Ocean (Figure 1.2).

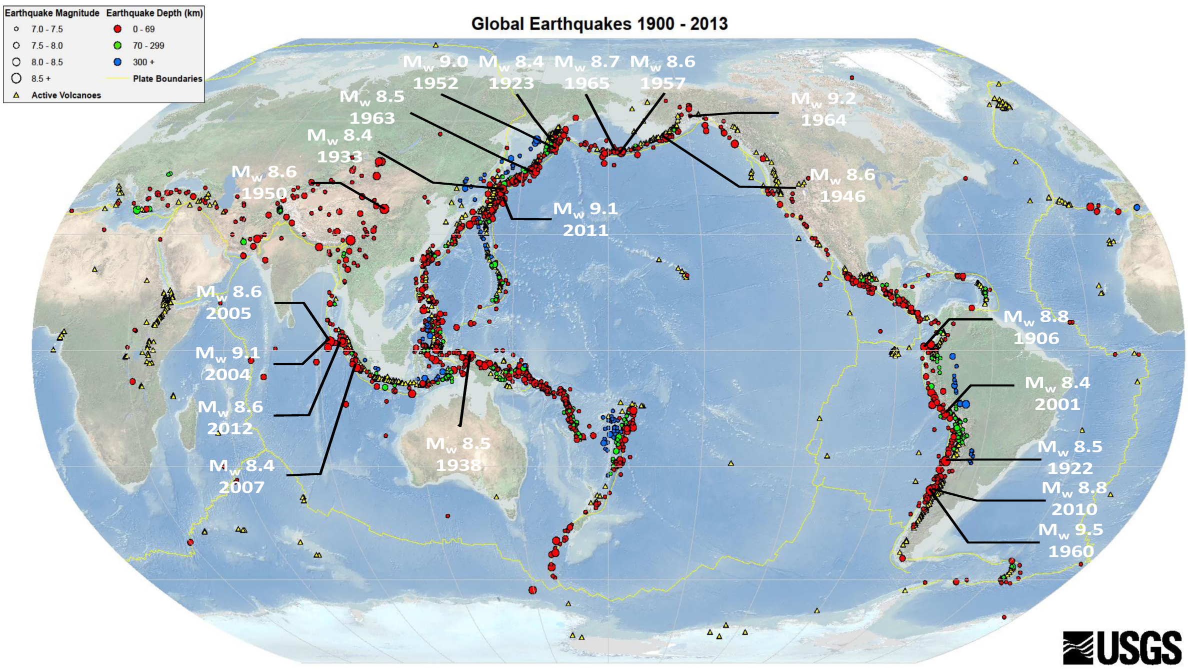

Figure 1.4. Global earthquake distribution and 20 largest earthquakes in the world. (Diagram courtesy of the U.S. Geological Survey, https://earthquake.usgs.gov/earthquakes/byregion)

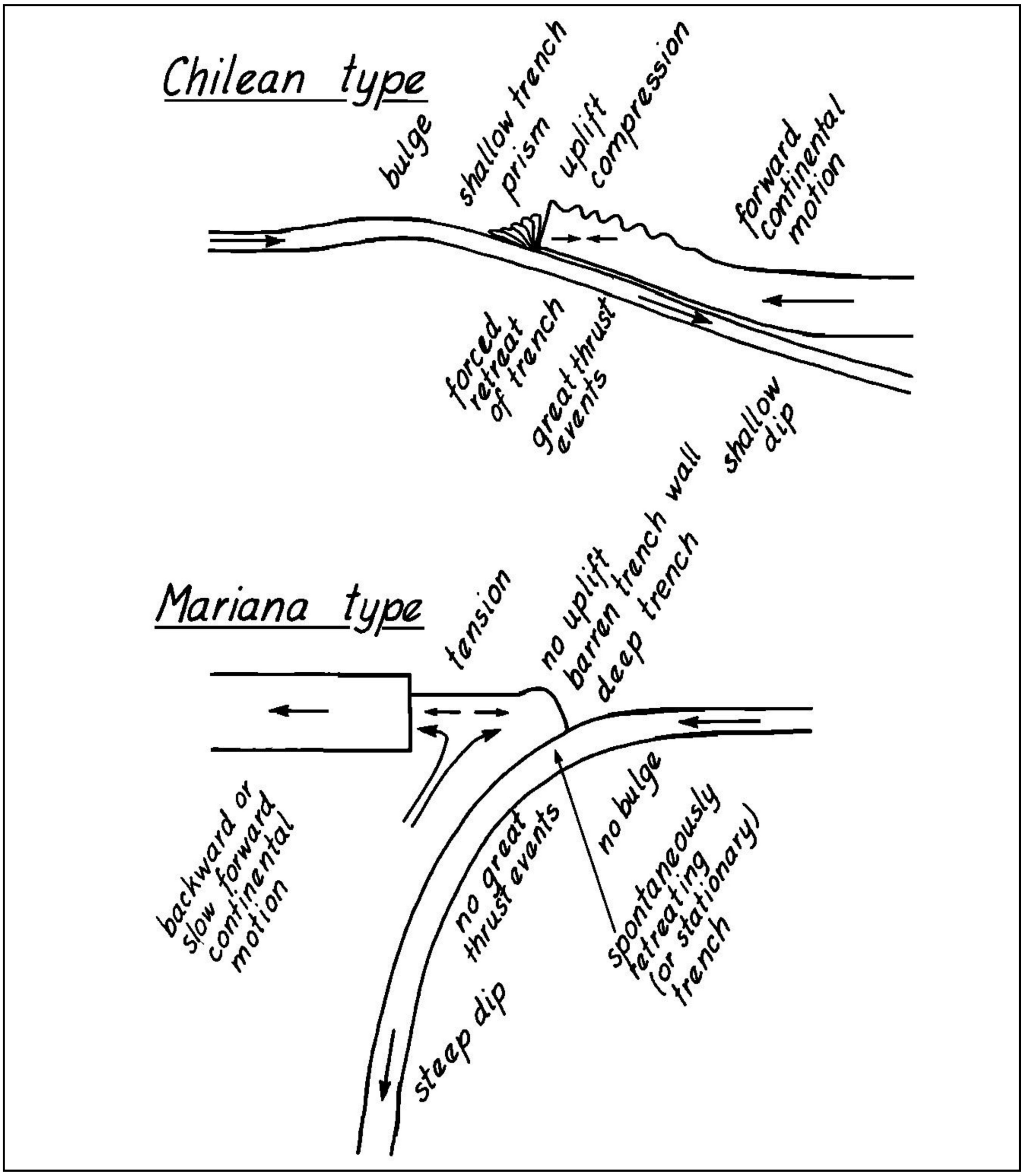

Figure 1.5. Two extreme types of subduction zones. (From Figure 7 of Uyeda and Kanamori, 1979)

1.2 Geological setting of the Ryukyu Trench

1.2.1 Plate tectonics

Japan is surrounding by several subduction zones, such as the Japan Trench, Nankai Trough, and Ryukyu Trench, generated by the interaction of the Eurasian, Philippine Sea, North America, and the Pacific plates (Figure 1.6). The southernmost Ryukyu Trench is a convergence plate boundary between the Eurasian Plate and the Philippine Sea Plate, extending ~2000 km from southern Kyushu to eastern Taiwan (Figure 1.6). Along this trench, the Philippine Sea Plate subducts beneath the Eurasian plate at a rate of ~8 cm/year (Hsu et al., 2012; Nakamura, 2009).

Northeast of the Ryukyu Trench runs the Ryukyu Arc and the Okinawa Trough (Figure 1.6). Unlike general island-arcs dominated by igneous rocks made by subduction magma activities, the Ryukyu Islands are composed of Holocene sediments and Pleistocene conglomerate and limestone (Ando et al., 2018). In addition, both geological (e.g., Yamano et al., 2001; 2003) and geodetic (Iwasa and Heki, 2018) data reveal that the uplift of these islands is non-uniform both in time and space. The Okinawa Trough lying behind the Ryukyu Arc is an active back-arc spreading system (Sibuet al., 1987). It causes the Ryukyu islands move trench-ward as demonstrated by the rapid southward movements of the Globe Navigation Satellite System (GNSS) stations there (Figure 1.7). Given the opening rate of the Okinawa Trough at the southwest segment is ~5 cm/year (Nishimura et al., 2004), the convergent rate between the southwestern part of the Ryukyu Arc and the Philippine Sea plate is probably up to 12.5 cm/year (Heki and Kataoka, 2008; Hsu et al., 2012).

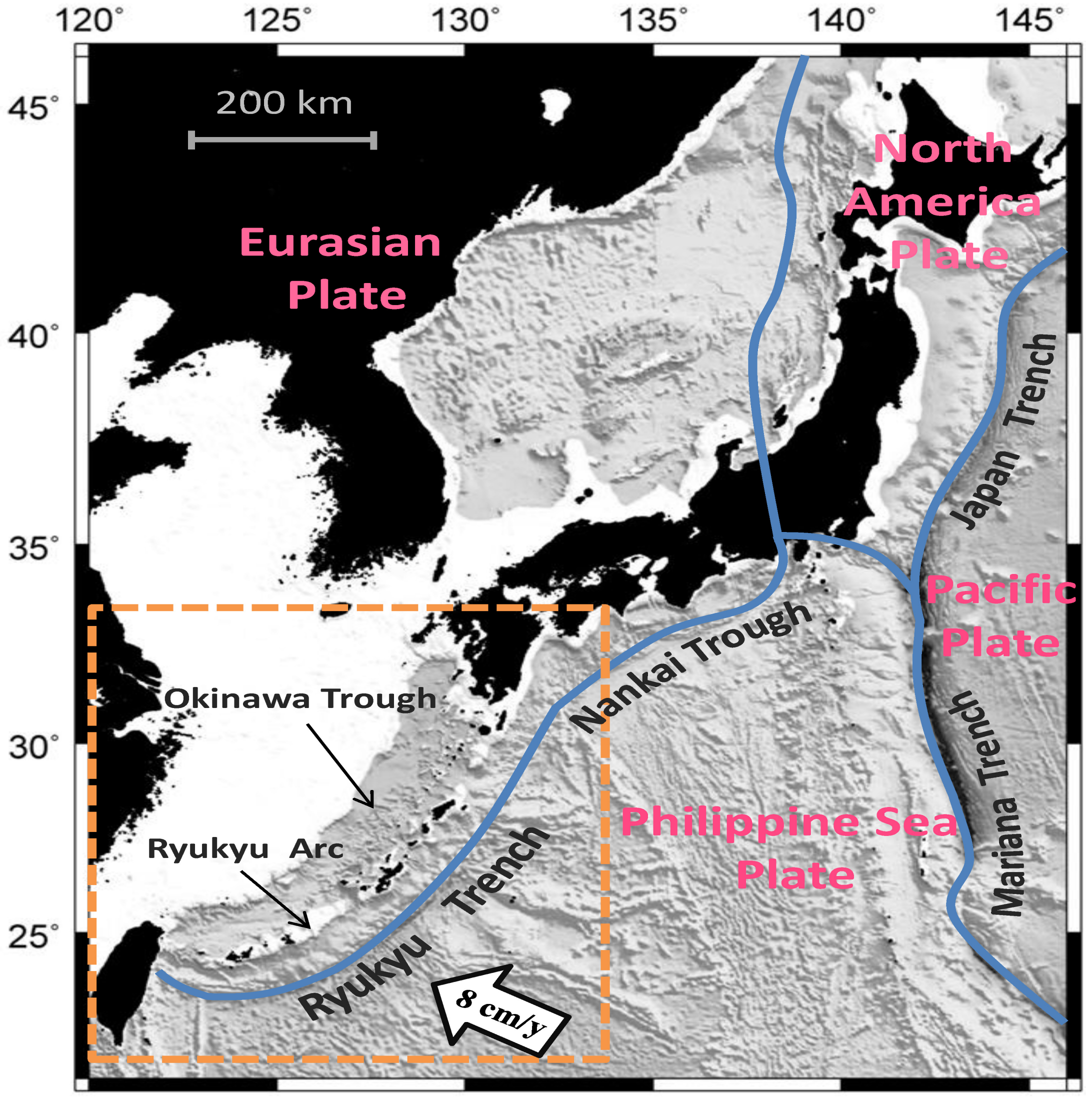

Figure 1.6. The plate tectonic map around the Japan Islands. The blue curves show the plate boundaries with the Eurasian, Philippine Sea, North America, and the Pacific plates. The orange dashed rectangle represents the geometry range of the Ryukyu area, studied here. The Ryukyu Trench, Ryukyu Arc, and Okinawa Trough, three major geological structures in the Ryukyu area, run in parallel. Along the Ryukyu Trench, the Philippine Sea Plate subducts beneath the Eurasian Plate at a rate of ~8 cm/year (Nakamura, 2009; Hsu et al., 2012).

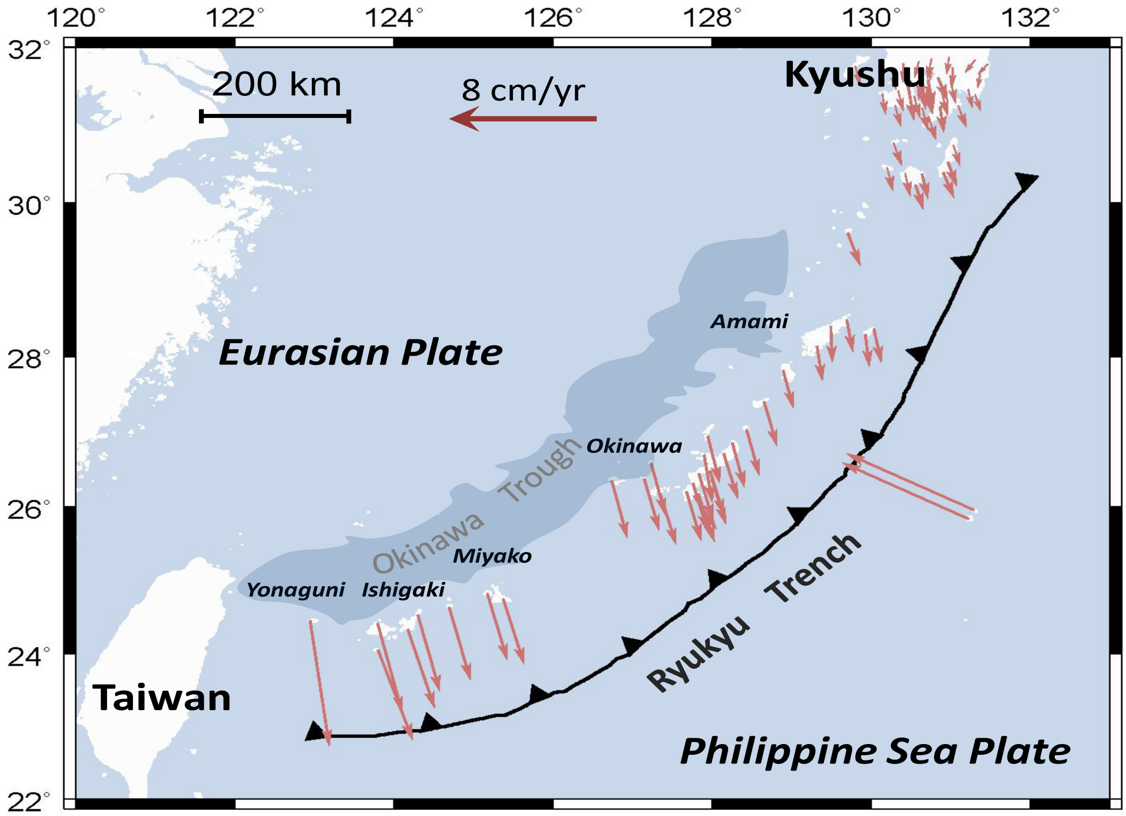

Figure 1.7. Velocities of GNSS stations (red arrows) relative to the Eurasian Plate during the period of 2000-2010. The data is from GEONET (GNSS Earth Observation Network), run by Geographical Information Authority (GSI) of Japan.

1.2.2 Bathymetry

The northern Philippine Sea Plate consists of two inactive marginal basins, i.e., the Shikoku Basin and the West Philippine Basin (Figure 1.8), whose evolutionary histories have been described in detail in several studies (e.g., Okino et al 1999; Deschamps and Lallemand, 2002). The West Philippine Basin subducts northward along the Ryukyu Trench and is bounded by the Kyushu-Palau ridge in the east and by the Gagua ridge in the west (Figure 1.8). Based on the bathymetry, the West Philippine Basin can be divided into two distinct subareas, i.e., the southwest block close to the Ishigaki, Miyako, and Okinawa Islands with a smooth seabed, and the northeast block near the Amami Island with several bathymetric highs (Figure 1.8). These marine ridges at the northeast block of the West Philippine Basin are Oki-Daito ridge, Daito ridge, and Amami Plateau from SW to NE. They are considered to be the remnants of paleo-island arcs subducting beneath the Ryukyu Trench together with the Philippine Sea Plate (Nishizawa et al., 2014).

The Kyushu-Palau Ridge near the Kyushu Island separates the Shikoku Basin from the West Philippine Basin (Figure 1.8). The two basins are subducting at the Ryukyu Trench and the Nankai Trough, respectively, and the Kyushu-Palau Ridge bounds these two subduction zones (Figure 1.8). The bathymetry of the Shikoku Basin is similar to the west block of the West Philippine Basin, i.e., smooth seafloor without significant bathymetric highs.

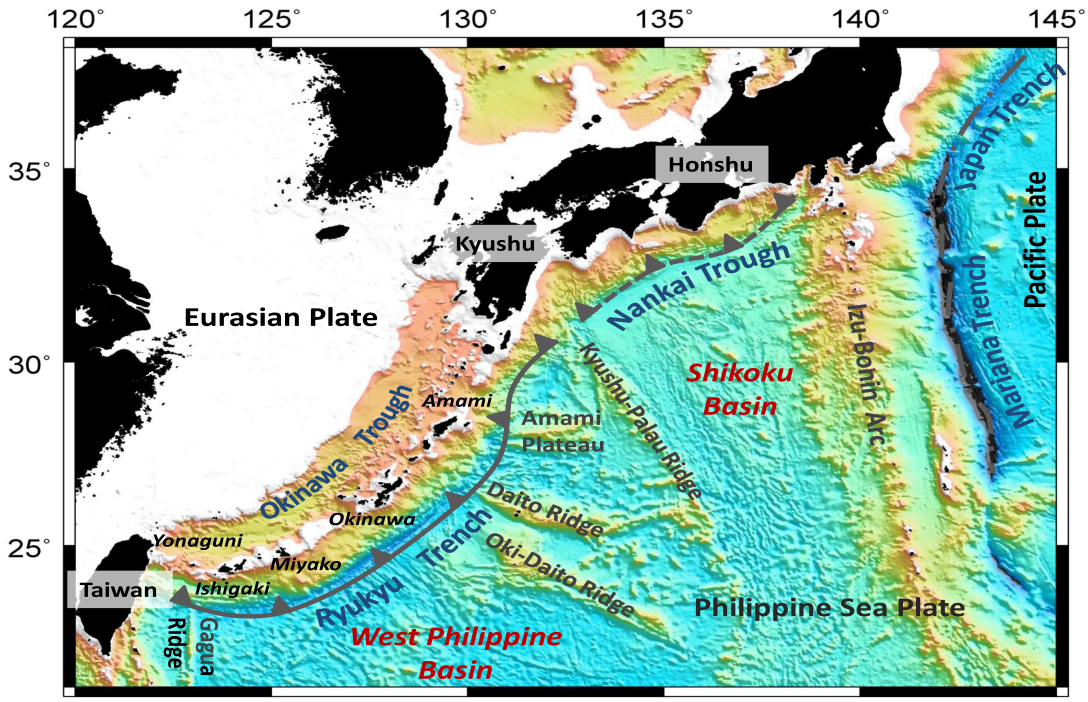

Figure 1.8. Bathymetry map of the northern Philippine Sea Plate. It is composed of the West

Philippine Basin and the Shikoku Basin. The two basins are bounded by the Kyushu-Palau Ridge and subduct beneath the Eurasian Plate along the Ryukyu Trench and Nankai Trough, respectively. Several linear structures lie on the eastern block of the West Philippine Basin. They are the remnants of paleo-island arcs subducting at the Ryukyu Trench (Nishizawa et al., 2013). The bathymetry of the Shikoku Basin is similar to the western block of the West Philippine Basin, having smooth seafloors with few bathymetric highs.

1.2.3 Seafloor ages

The seafloor ages of the northern Philippine Sea Plate vary from region to region. As illustrated in Figure 1.9, the seafloor ages along the Ryukyu Trench (i.e., the west block of the West Philippine Basin) falls within 50-70 Ma, while those along the Nankai Trough (i.e., the Shikoku Basin) are only 20-35 Ma. As for the region around the Amami Island (i.e., the east block of the West Philippine Basin), the seafloor is considered to have a younger age due to the existence of paleo-island arcs (Muller et al., 2008). Such a difference significantly influences the subduction process of the Philippine Sea Plate and causes diverse seismic activities and complex crustal deformations in this region. Furthermore, based on this factor, several studies classified the Nankai Trough and the Ryukyu Trench into the Chilean type and the Mariana type subduction zone, respectively (e.g., Peterson and Seno, 1984; Scholz and Campos 2012), even though these two subduction zones belong to the same tectonic plate.

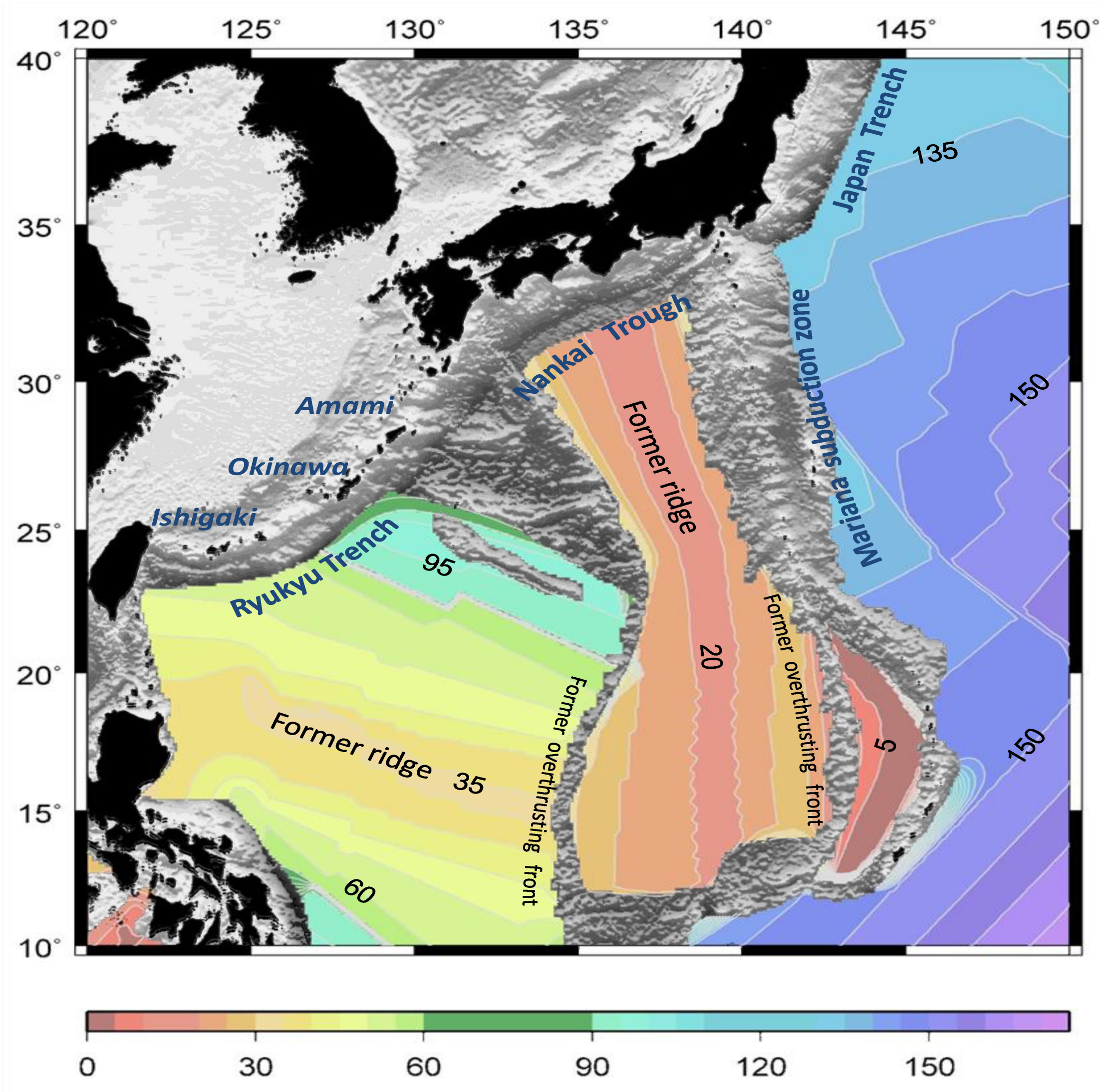

Figure 1.9. The seafloor age of the Philippine Sea Plate and the Pacific Plate around Japan. The data are provided by Muller et al. (2008). The seafloor age along the Ryukyu Trench falls into 50-70 Ma, which is significantly older than that of 20-35 Ma along the Nankai Trough. However, due to the existence of oceanic paleo-island arcs, the age of the seafloor subducting around the Amami Island are much younger than other regions.

1.3 Historical large earthquakes in the Ryukyu Trench

The Ryukyu Trench is different from the Nankai Trough or the Japan Trench; large interplate earthquakes ($M_w \geq 8$) have not been reported in this region (Peterson and Seno, 1984; Ando et al., 2009; Nakamura, 2009; Scholz and Campos 2012). Figure 1.10 exhibits the disaster earthquakes ($M_w \geq 7.0$) that have occurred along the Ryukyu Trench from 1700 to 2015. It is interesting to note that most of the earthquakes are located in eastern Taiwan and the offshore of Kyushu. Only very few events have occurred near the Ryukyu Trench axis. Among these earthquakes, I marked two significant events on this map, i.e., the 1771 Yaeyama earthquake and the 1911 Kikai earthquake, because they have larger magnitudes ($M_w \geq 8$) and seem to have occurred on the plate boundary of the Ryukyu subduction zone.

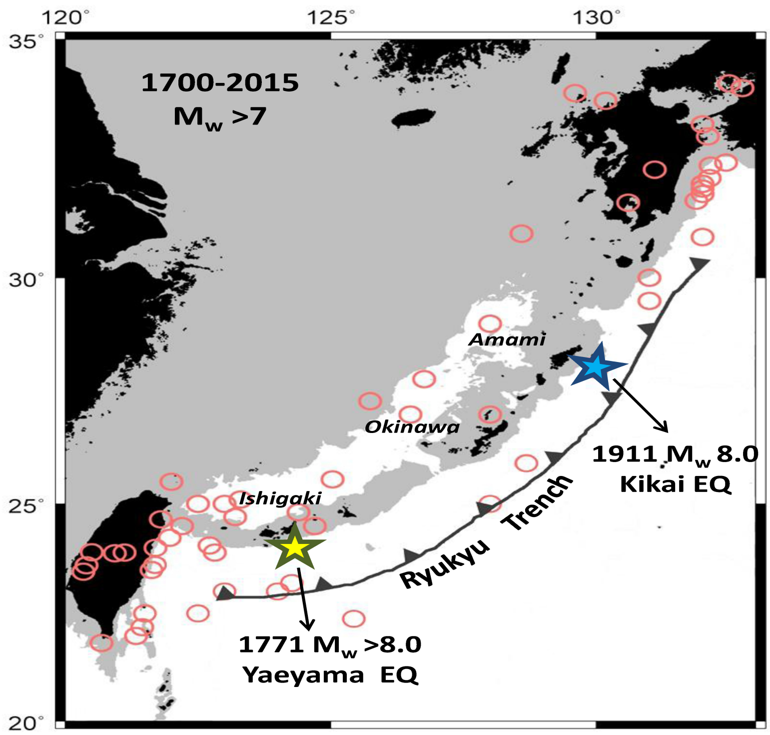

Figure 1.10. Distribution of disaster earthquakes ($M_w \geq 7$) in the Ryukyu area. The yellow and blue stars show the epicenters of the 1771 Yaeyama earthquake and the 1911 Kikai earthquake, respectively. The data are from the earthquake catalog of Japan Meteorological Agency (JMA).

1.3.1 1771 Yaeyama earthquake

The 1771 Yaeyama earthquake occurred near the Ishigaki Island, southwestern Ryukyu Arc (Figure 1.10). This event was accompanied by a disastrous tsunami that struck Ishigaki and surrounding islands with the maximum run-up height of ~30 m and caused fatalities of one-third of the populations on the Ishigaki Island (Goto et al., 2012). For the mechanism of this event, Imamura et al. (2001, 2008) suggested that it was an extensive submarine landslide triggered by an M7-class intraplate earthquake, whereas Nakamura (2009b) considered that it should be an M_w 8.0 tsunami (slow) earthquake near the Ryukyu Trench axis. Recently, Ando et al., (2018) investigated paleotsunami deposits on the Ishigaki Island and proposed that this earthquake might be an ordinary subduction thrust earthquake of $M_w > 8.0$ based on earthquake-induced ground cracks observed in the soil bed underlying the Yaeyama tsunami sediments. It means that the 1771 earthquake is probably a large interplate earthquake ($M_w \geq 8.0$) that occurred on the subduction plate interface of the southwestern Ryukyu Trench.

1.3.2 1911 Kikai earthquake

The 1911 Kikai earthquake occurred near Amami Island (Figure 1.10), and its signal was recorded as far as Tokyo (> 1000 km) (Usami, 1988). This earthquake generated strong ground shaking that destroyed approximately 400 houses on Kikai Island and caused a tsunami (< 3m) with slight damage to surrounding islands (Hatori, 1988; Goto, 2013). Several studies considered this earthquake as an intraplate earthquake with a depth of ≥

100 km (M_w ≥8) (e.g., Utsu, 1982; Abe and Kanamori, 1979). However, Goto (2013) relocated its hypocenter using old smoked seismograms and proposed that this event was a large shallow interplate earthquake (M_w 8.0) near the Ryukyu Trench axis. That is, the 1911 Kikai earthquake may be another case of large interplate earthquakes that occurred in the Ryukyu subduction zone.

1.4 Issue of the Ryukyu Trench: coupled or decoupled?

As mentioned by Uyeda and Kanamori (1979), all subduction zones on Earth could be roughly divided into the Chilean and Mariana types based on the sea floor age, the arc-normal stress, and the existence of active back-arc basins (Figure 1.5). The Chilean type subduction zones have a young (< 50 Ma) subducting plate, which causes a low dipping seismic zone due to weaker negative buoyancy. The plate motion of this type of subduction zones is seismic, i.e., their coupled is high, and large interplate earthquakes may occur. In contrast, the Mariana type subduction zones possess an old (> 50 Ma) subducting plate, which results in a large dip-angle seismic zone and low coupling ratio between the upper and lower slabs. There, the plate motion is aseismic, and large interplate earthquakes seldom occur.

Under this hypothesis, the Ryukyu Trench should be classified into the Mariana type subduction zone because it has an older subducting plate (> 50 Ma, Figure 1.9) and an active back-arc opening system (Okinawa Trough; Sibuet al., 1987). Additionally, the absence of large interplate earthquakes in the past 300 years (Ando et al., 2009; Scholz and Campos

2012) and the trenchward monition of the Ryukyu Arc from GNSS observations (Figure 1.7) all indicate that the plate motion of the Ryukyu Trench is aseismic, i.e., the plate boundary here may be decoupled or weakly coupled (Peterson and Seno, 1984; Scholz and Campos 2012).

However, several investigations, such as the excavation of palotsunami sediments (e.g., Ando et al., 2018), slow earthquake detections (Heki and Kataoka, 2008; Ando et al., 2012; Nishimara, 2014; Nakamura and Sunakawa, 2015, Arai et al., 2016, Nakamura 2017), seafloor geodetic observations (Nakamura et al., 2010; Chen at al., 2018), the analysis of geological structures (e.g., Lin et al., 2014), and the estimation of locked zones from GNSS observations (e.g., Hsu et al., 2012) also suggest that the Ryukyu Trench may have slight, but significant interplate coupling and has potential to generate large interplate earthquakes. Such diverse views indicate that we have only insufficient understandings of the subduction process in the Ryukyu Trench. Hence, more detailed and multiple-approach studies are crucial.

1.5 Primary purposes of this study

The primary purpose of this study is to clarify the interplate coupling of the Ryukyu subduction zone. To achieve this goal, I focus on the subject of slow earthquakes. Slow earthquakes are a newly discovered type of earthquakes within the past of 50 years (Beroza and Ide, 2011). Theses earthquakes often observed in strongly coupled subduction plate boundaries, such as the Nankai Trough and the Cascadia subduction zone, and were considered to be related to large interplate earthquakes (Obara and Kato, 2016). However, they are also detected in the Ryukyu Trench (e.g., Heki and Kataoka, 2008; Ando et al., 2012). Hence, I selected this subject for this study and expected that the properties of slow earthquakes and its relation with other seismic events could help us understand the general feature of the plate convergence in the Ryukyu subduction zone.

Chapter 2.

Slow Earthquakes

2.1 What are slow earthquakes?

Earthquakes are the ground shaking of the Earth, which release strain by fault ruptures/slips in the Earth's interior. Ordinarily, earthquake faults are locked due to the friction of fault planes, but the rupture/slip starts when the accumulated strain exceeds the friction. Because the way of fault slips and strain release is diverse, the velocity of fault slips can range from 10^{-9} (creeping along plate boundaries) to 10^{0} m/s (fast slippage along faults). A rapid slip of faults generates high-frequency elastic waves that propagate in the Earth and cause detectable ground shaking, i.e., ordinary (or regular) earthquakes (Utsu, 2001). In contrast, a slow fault slip predominantly generates low-frequency elastic waves (Beroza and Ide, 2011). Such earthquakes known as slow earthquakes are undetectable with short-period seismometers and do not cause significant ground shaking.

Although both slow earthquakes and ordinary earthquakes are phenomena of fault slips, the frequency contents of seismic energy radiated from them are fairly different. For example, slow earthquakes release energy over a period of seconds to years (Figure 2.1), significantly longer than that of seconds to minutes of ordinary earthquakes (Obara and Kato, 2016). Moreover, this type of earthquakes generates seismic waves inefficiently relative to ordinary earthquakes, especially at the high-frequency components (Figure 2.2) (Beroza and Ide, 2011). That is, they are characterized by low-frequency signals, and only high-sensitivity broadband seismometers and long-term geodetic/strain measurements can record these events (Beroza and Ide, 2011).

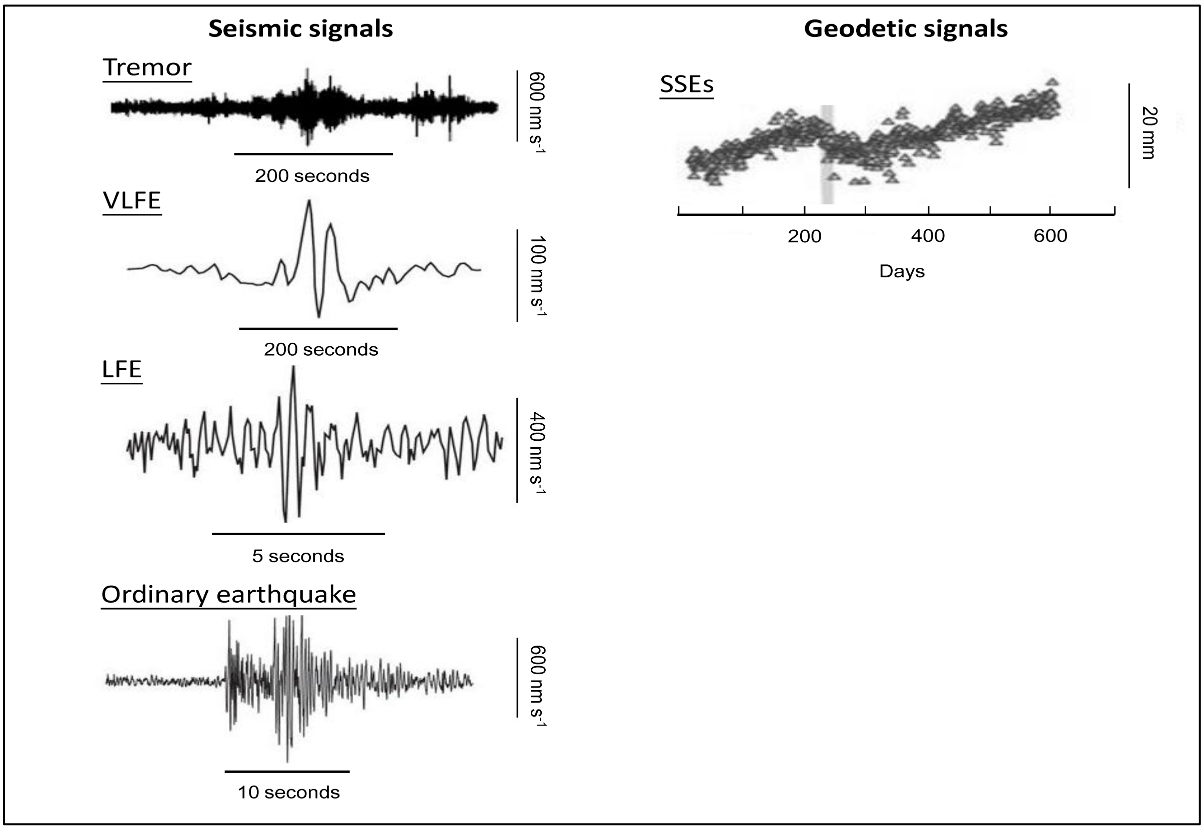

Figure 2.1. Waveforms of an ordinary earthquake and four types of slow earthquakes, i.e., low-frequency tremor, very low-frequency earthquake (VLFE), low-frequency earthquake (LFE), and slow slip event (SSE). Most of the slow earthquakes have a longer duration than the ordinary earthquake. (Modified from Figure 1 of Peng and Gonberg, 2010)

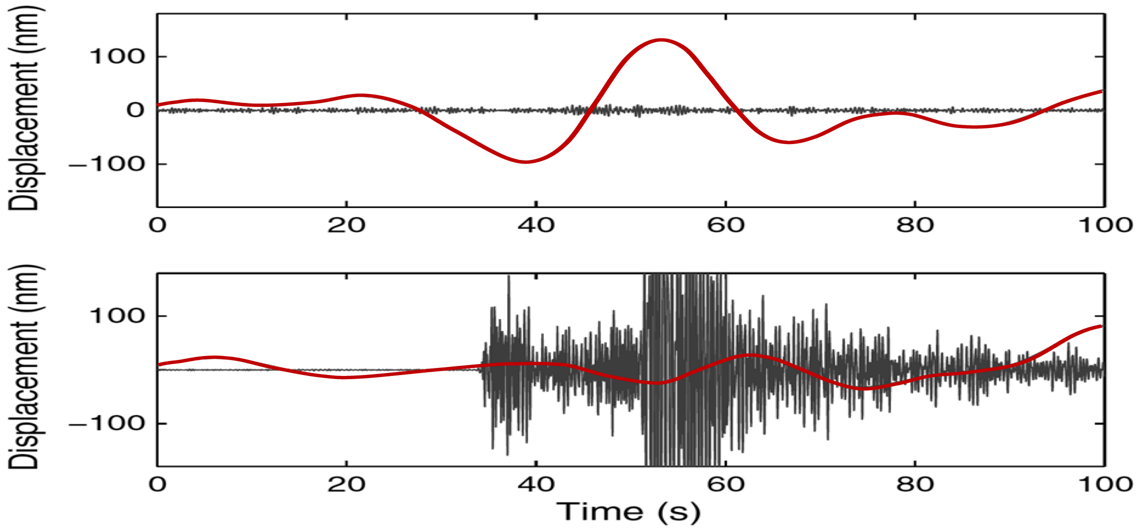

Figure 2.2. EW-component waveforms of a slow earthquake (upper) and an ordinary

earthquake (bottom) in the Cascadia subduction zone. The seismograms are filtered in 0.02-0.05 Hz (red) and 2-8 Hz (black), respectively. Waves from the slow earthquake are dominated by low-frequency signals and depleted in high-frequency components (From Figure 2 of Ghosh et al., 2015)

2.2 Development of slow earthquake research

Over the past 50 years, scientists have noted some seismic events that occurred much more slowly than regular earthquakes (Beroza and Ide, 2011). These anomalous events such as creeping tremors (e.g., Kanamori and Setwart, 1979), tsunami earthquakes (e.g., Kanamori, 1972; Kanamori and Kikuchi, 1993), and silent earthquakes (e.g., Beroza & Jordan 1990; Kawasaki et al., 1995) all have remarkably long durations and seismic waves of unusually long periods. At the early stage, silent earthquakes were considered to be the extreme case situated at the end of the seismic spectrum, in which they were the boundary of seismic events that could generate detectable seismic radiation (Beroza & Jordan 1990). This is the earliest stage of the slow earthquake research, but no detailed investigations could be done due to the limit of seismometer networks.

In the 1990s, with the development of the global positioning system (GPS), slow surface deformations after large earthquakes were determined as slow post-seismic slips (afterslips) (e.g., Heki et al., 1997; Heki and Tamura; 1997). Subsequently, more and more silent earthquakes/slips and slow crust movements were detected over the world by space geodesy (e.g., Hirose et al., 1999; Dragert et al., 2001; Ozawa et al., 2002, 2003; Kawasaki, 2004). These studies all demonstrate that slow aseismic slips are common phenomena on the Earth, not exceptional cases, and their results built essential foundations for further studies.

In the 21st Century, the slow earthquake research evolved into a new stage due to the improvement of observation instruments. Applying high-sensitive borehole and broadband seismometers, scientists discovered a series of slow earthquakes that had never been observed, such as low-frequency tremors (e.g., Obara, 2002), very low-frequency earthquakes (VLFEs) (e.g., Obara and Ito, 2005; Ito and Obara, 2006a), and low-frequency earthquakes (LFEs) (e.g., Katsumata and Kamaya, 2003). Moreover, the dense and continuous observations by Global Navigation Satellite System (GNSS) also provided abundant high-quality coordinate data of ground stations, which made significant advances in detection of slow crust movements. Hirose et al. (1999) first used the name "slow slip events (SSEs)" to signify anomalous crustal deformations that occurred on subduction plate boundaries but were not directly related to large earthquakes. Afterward, plenty of SSEs was detected in subduction zones worldwide (e.g., Dragert et al., 2001; Lowry et al., 2001; Douglas et al., 2005; Hirose and Obara, 2005; Heki and Kataoka, 2008) although sometimes they had different names, e.g., aseismic slips (Ozawa et al., 2002, 2004), silent slips (e.g., Shibazaki and Iio, 2003), and characteristic silent earthquakes (Ozawa et al., 2003). Furthermore, episodic tremor and slip (ETS) is another significant finding during this period. Rogers and Dragert (2003) first discovered that slow slips and low-frequency tremors at the same source depth in the Cascadia subduction zone coincided both temporally and spatially (Figure 2.3). The same phenomena were also found in the Nankai Trough, SW Japan (e.g., Obara et al., 2004a; Hirose and Obara, 2006), while their correlation extended from the slow slips and tremors to LFEs and VLFEs (e.g., Shelly et al., 2006; Ito et al., 2007).

At the later period of this stage, the direction of slow earthquake research started to shift from observations to the comparative analysis due to the accumulation of large amounts of seismic data. For example, Ide et al. (2007) compared characteristics of SSEs, VLFEs, LFEs, ETSs, and silent earthquakes detected over the world and found that their durations and seismic moments are proportional. This is entirely different from regular earthquakes (Figure 2.4). Shelly et al. (2006, 2007) also analyzed low-frequency tremors and LFEs in Shikoku area, SW Japan. They proposed that various slow seismic events are different manifestations of a single process, possibly related to the fluid on the plate boundary of subduction zones. Since then, slow earthquakes are believed to have similar seismogenic processes and belong to the same family independent from regular earthquakes.

During the last decade, slow earthquake research has been getting diverse. In addition to observational studies (e.g., Ando et al., 2012; Nishimura, 2014; Matsuzawa et al., 2015, Arai et al, 2016, Arisa and Heki, 2017), scientists pay much attention to particular subjects, such as the correlation between different types of slow earthquakes (e.g., Hirose et al., 2010; Nakamura and Sunagawa, 2015; Nakamura, 2017; Nakano et al., 2018), migration of the slow earthquakes (e.g., Asano at al., 2015; Yamashita at al., 2015; Ghosh et al., 2015; Nakamura, 2017), and tidal trigging (e.g., Thomas et al., 2012). Moreover, several comprehensive reviews have been published during this period (e.g., Peng and Gonberg, 2010; Beroza and Ide, 2011; Obara and Kato, 2016). Following the establishment of the community of slow earthquake science in Japan in 2016, large integrated studies, i.e., those involving two or more disciplines (e.g., geophysics, geology, and physics), will become the mainstream of slow earthquake research in the future.

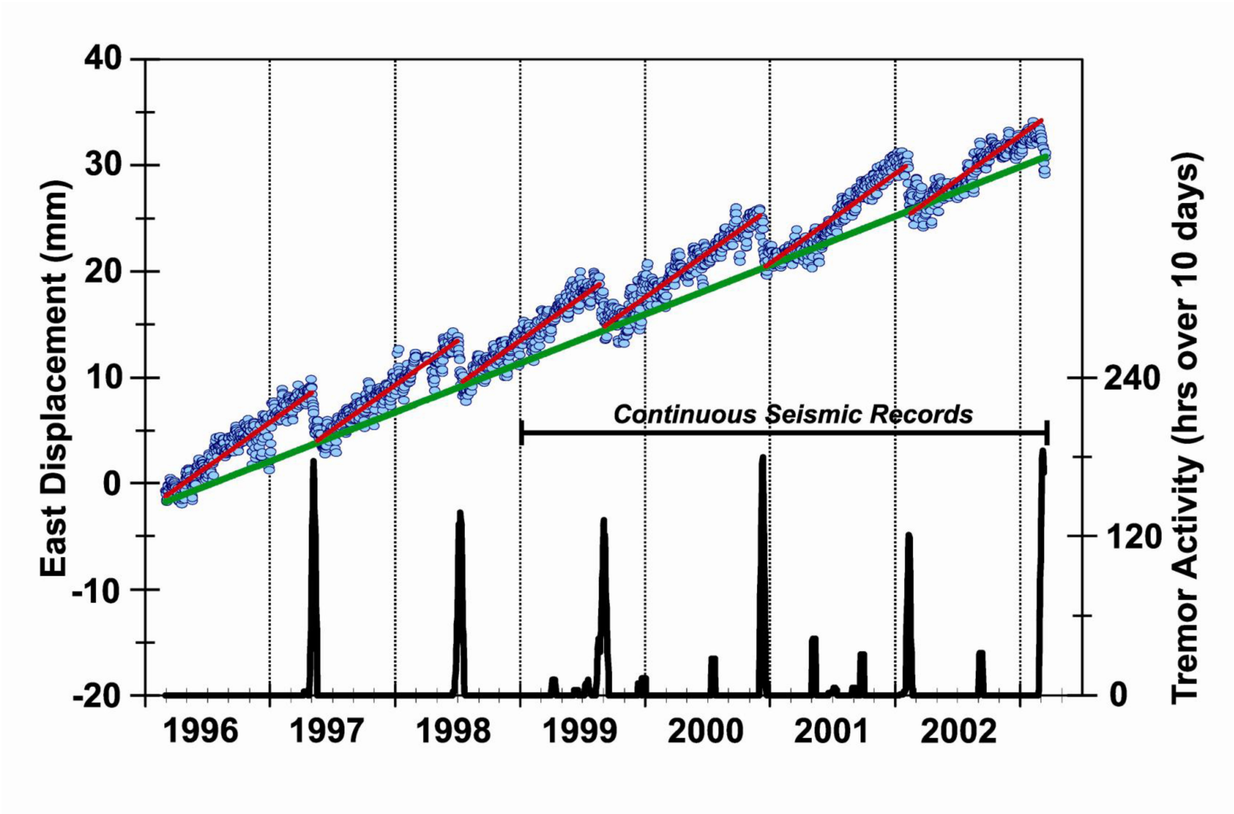

Figure 2.3. Synchronous activities of low-frequency tremors and slow slips in the Cascadia subduction zone. (From Figure 2 of Rogers and Dragert, 2003)

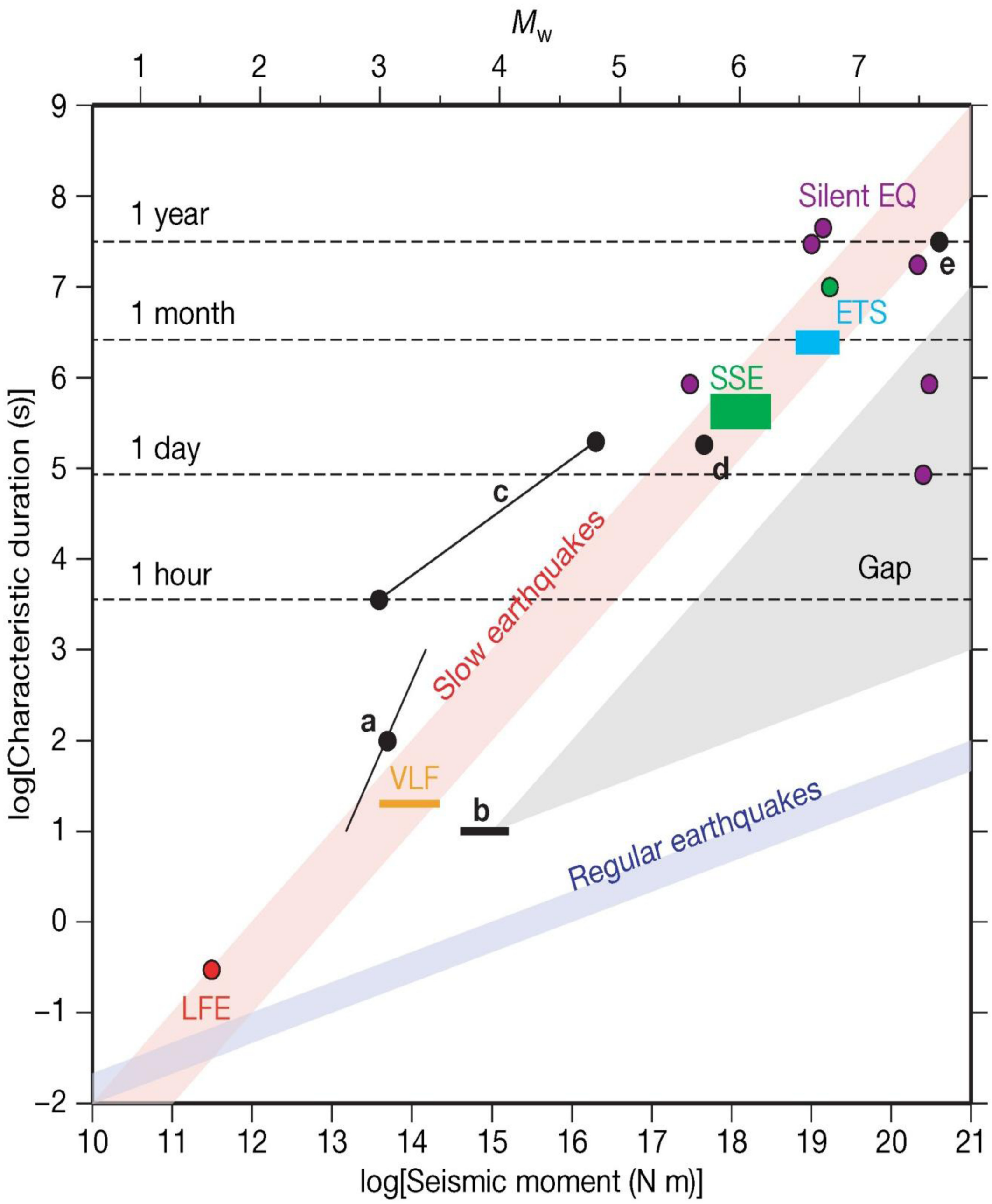

Figure 2.4. Seismic moments (M_0) and durations of various slow earthquakes detected in the world. (From Figure 2 of Ide et al. 2007)

2.3 The slow earthquake family

As mentioned above, diverse types of slow earthquakes have been detected over the world, which reflects variety in fault slip phenomena controlled by different frictional properties (Asano et al., 2015). However, at the early stages, a slow seismic event sometimes had several names because scientists created new words for their observations. Until the 21 Century, the types/names of slow earthquakes were gradually unified. Ide et al. (2007) first proposed that slow earthquakes could be divided into five groups of LFEs, VLFEs, SSEs, ETSs, and silent earthquakes. Subsequently, Peng and Gonberg (2010) classified slow seismic events into the geodetic and seismic groups based on detecting instruments. Each group includes more than one type of slow earthquakes, i.e., the geodetic group comprises SSEs, and the seismic group consists of low-frequency tremors, VLFEs and LFEs (see Figure 2.1). Then, Beroza and Ide (2011) sorted out slow earthquakes and classified them into five main types based on their characteristics, i.e., LFEs, nonvolcanic tremor, SSEs, ETSs, and VLFEs. Recently, Obara and Kato (2016) followed the classification by Peng and Gonberg (2010) to divide slow earthquakes detected in the Nankai Trough into the geodetic and seismic groups, but they replaced LFEs with ETSs (see Figure 2.5). In this section, I adopt the viewpoints of Peng and Gonberg (2010) and Obara and Kato (2016) and propose that four significant relatives of the slow earthquake family should be SSEs, VLFEs, LFEs, and ETSs (Figure 2.6). Brief descriptions of these slow seismic events are given as follows.

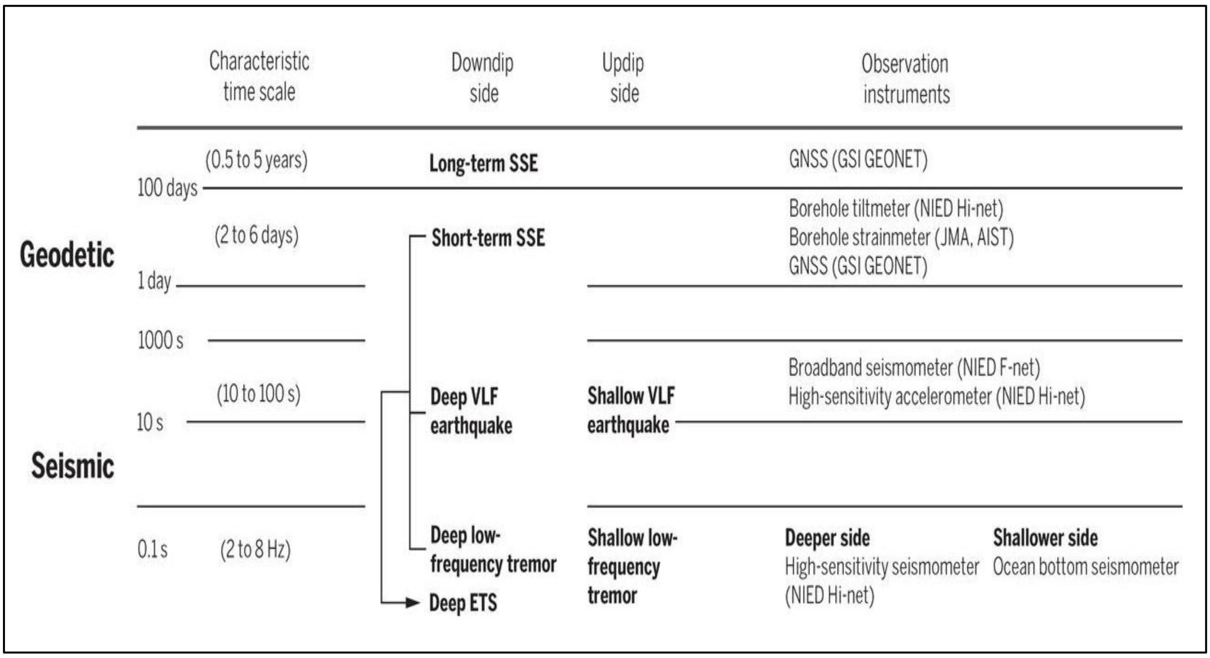

Figure 2.5. Various types of slow earthquakes in the Nankai Trough (From Figure 1 of Obara and Kato, 2016)

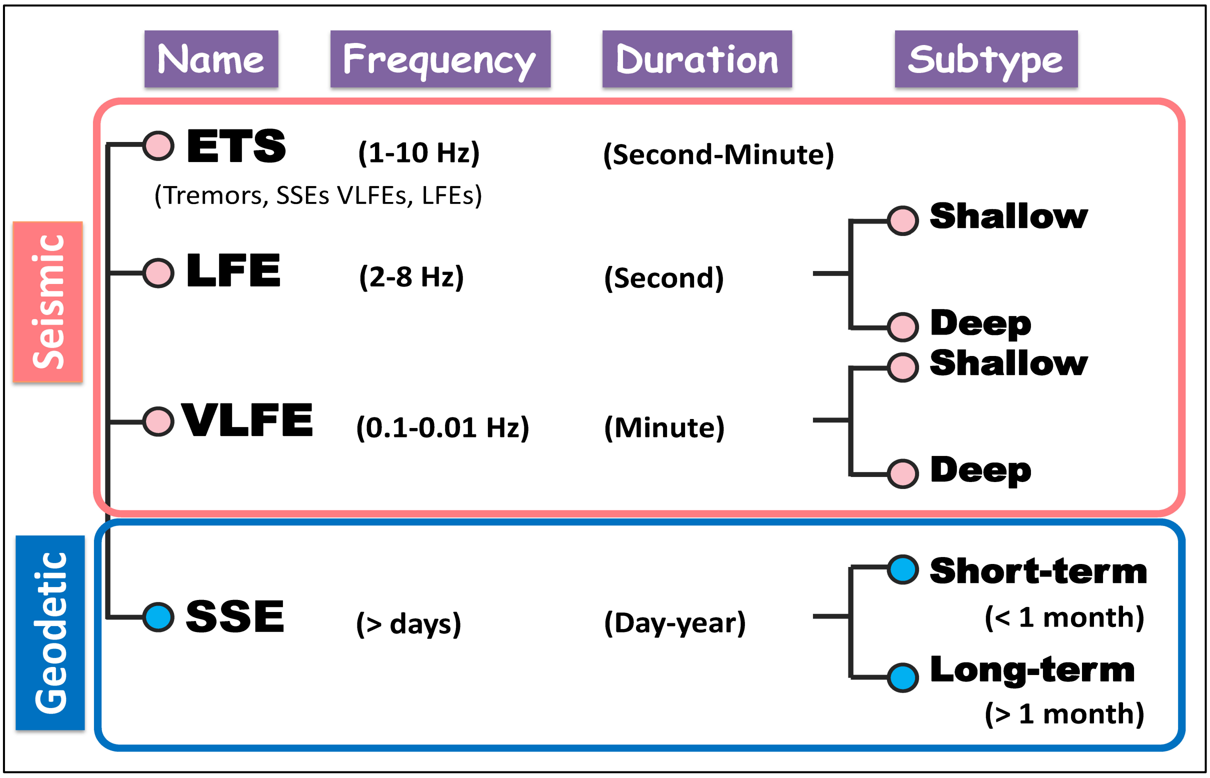

Figure 2.6. Four major types of slow earthquakes proposed by this study.

2.3.1 Slow slip events (SSEs)

The stress release in subduction zones can induce two types of anomalously slow crust deformations, i.e., afterslips of large earthquakes, which occur around asperities that ruptured in the main shock, and slow slip events (SSEs) that occur as slow ruptures at the plate interface (Heki and Kataoka, 2008). SSEs are the exclusive slow seismic event of the geodetic group (Figure 2.6). Because their fault slips are too slow to radiate detectable seismic waves, scientists have been able to detect them only by geodetic sensors such as Global Navigation Satellite System (GNSS) or borehole tiltmeters (Beroza and Ide, 2011). Moreover, based on their duration, these slow events can be further classified into the short-term SSEs lasting from days to weeks and the long-term SSEs from months to years (Figure 2.6).

The name "SSE" was proposed at the end of 20th Century (Hirose et al., 1999), but scientists have already known such anomalous slow crustal movements. For example, silent earthquakes (e.g., Beroza & Jordan 1990; Kawasaki et al., 1995) detected at the early stages may be some type of SSEs judging from little detectable seismic waves and unusually long duration. With the development of space geodesy, more and more SSEs were detected over the world, e.g., in Alaska (e.g., Ohta et al., 2006; Fu and Fremueller, 2013), Cascadia (e.g. Dragert et al., 2001), Mexico (e.g. Lowry et al., 2001, Kostoglodov et al., 2003; Vergnolle et al., 2010), Costa Rica (e.g. Jiang et al., 2012), Chile (e.g. Socquet et al., 2017), New Zealand (e.g., Douglas et al., 2005; Wallace et al., 2016), and Japan (e.g., Hirose et al., 1999; Ozawa et al., 2002, 2004; Hirose and Obara, 2006) (Figure 2.7). These SSEs often occur in subduction zones around the Pacific Ocean (Obara and Kato, 2016) and sometimes show quasi-periodic recurrences (e.g., Heki and Kataoka, 2008; Hirose et al., 2012) and strong links with other slow seismic events (e.g., Hirose et al., 2010; Baba et al., 2018).

In Japan, the best study area to study SSEs, abundant SSEs have been detected in several subduction plate boundaries, such as the Nankai Trough (e.g., Hirose et al., 1999; 2010; Ozawa et al., 2004; Hirose and Obara, 2006; Kobayashi, 2014), the Japan Trench (e.g., the Boso Peninsula, Ozawa et al., 2003, 2007, 2014; Hirose et al., 2012; the Izu-Bonin Arc, Arisa and Heki, 2017), and the Ryukyu subduction zone (Heki and Kataoka, 2008; Nakamura, 2009; Nishimura, 2014; Tu and Heki, 2017; Kano et al., 2018). Additionally, some small SSEs that occurred in an inland plate boundary were also observed in Northen Hokkaido (Ozono et al., 2014; Ikeda et al., 2015).

2.3.2 Very low frequency earthquakes (VLFEs)

Very low-frequency earthquakes (VLFEs) are a type of slow seismic events dominated in the frequency band of 0.1-0.01 Hz with little or no high-frequency contents (Obara and Ito, 2005). These events have a typical duration of ~20s and consist mainly of long-period seismic waves (Ito et al., 2007; Beroza and Ito, 2011). Hence, only high-sensitivity broadband seismometers can detect these signals. Based on different seismogenic processes, VLFEs can be divided into the volcanic type and nonvolcanic type. The volcanic-type VLFEs are related to the fluid or magma transportation (e.g., Arciniega-Ceballos et al., 1999), and the nonvolcanic-type VLFEs are generated by the shear faulting of subduction zones (e.g., Obara et al., 2004b). For the nonvolcanic-type VLFEs, scientists can further classify them into the shallow VLFEs in accretionary prisms near trench axes (e.g., Obara et al., 2004b; Obara and Ito, 2005; Ito and Obara, 2006a, 2006b; Ando et al., 2012; Nakamura and Sunagawa, 2015) and deep VLFEs at the downdip limit of the seismogenic zones that are often accompanied by ETSs, another kind of slow seismic events (e.g., Ito et al., 2007; Ghosh et al., 2015; Baba et al., 2018).

Obara and Ito (2005) first used “VLFEs” to express these anomalous seismic events recorded in broadband seismometers, whose frequency band is much lower than that of low-frequency earthquakes (LFEs). Subsequently, with the development of dense broadband seismic networks, scientists successfully observed plenty of VLFEs. However, unlike the SSEs, VLFEs have only been detected in a few subduction zones, such as the Nankai Trough (e.g., Obara and Ito, 2005; Ito and Obara, 2006a; Asano et al., 2008; Sugioka et al., 2012), the Japan Trench (e.g., Matsuzawa et al., 2015), the offshore of Hokkaido (e.g., Obara et al., 2004b; Asano et al., 2008), the Ryukyu Trench (Ando et al., 2012; Nakamura and Sunagawa, 2015), and the Cascadia subduction zone (e.g., Ghosh et al., 2015) (Figure 2.7).

2.3.3 Low-frequency earthquakes (LFEs)

Low-frequency earthquakes (LFEs) are another slow seismic event with a dominant frequency band of 2–8 Hz (Ide et al., 2007; Aso et al., 2013). Because these events radiate more high frequency seismic waves than VLFEs, scientists usually use short-period seismometers to detect these signals (Beroza and Ito, 2011). Based on their origins, LFEs can be assigned into three major types, i.e., tectonic LFEs on plate boundaries (e.g., Obara, 2002; Shelly et al. 2006), the volcanic LFEs by volcano activities (e.g., Lin et al., 2007), and the intraplate LFEs that are not related to either plate subduction or active volcanoes (e.g., Aso et al., 2013; Aso and Ide, 2014). For the tectonic LFEs, we can further divide them into the shallow LFEs located at the upper segment of subduction zones (e.g., Arai et al., 2016; Nakamura 2017) and deep LFEs at the downdip limit of the seismogenic zones that often synchronize with ETS activities (e.g., Shelly et al. 2006, 2007).

In the 1990s, the Japan Meteorological Agency (JMA) first observed tectonic LFEs from the routine hypocenter determination (Beroza and Ito, 2011). These anomalous seismic events did not have clear P waves and looked like the background noise due to their small amplitudes. Moreover, they appeared to be located in a belt-like region along the Nankai Trough, in which large interplate earthquakes ($M_w > 8$) repeatedly occur (e.g., Ando, 1975). Soon after the 21st Century, JMA recognized these slow events as a new type of earthquakes and started to provide their catalog (e.g., Katsumata and Kamaya, 2003). Simultaneously, Obara (2002) detected abundant nonvolcanic tremors that have occurred in the same region by high-sensitive borehole seismic network (Hi-net) developed by National Research Institute for Earth Science and Disaster Prevention (NIED). At first, seismologists considered that these low-frequency tremors were another type of slow seismic events. However, Shelly et al. (2007) analyzed the characteristics of low-frequency tremors and LFEs in the Nankai Trough and proposed that low-frequency tremors are a swarm type of LFEs. Since then, the boundary between the two slow seismic events becomes vague, but there has been no consensus on this issue so far. This condition causes that some scientists adopt the name ''LFEs'' (e.g., Brown et al. 2009, 2013), but other scientists call them as ''tremors" or "low-frequency tremors'' (e.g., Obana and Kodaira, 2009; Obara and Kato, 2016). Although it is still uncertain whether LFEs and tremors are the same slow seismic event or not, I decide to combine all literature of tremors and LFEs in this study. Based on these data, LFEs and low-frequency tremors have been occurred in several subduction plate boundaries, such as the Nankai Trough (e.g., Obara, 2002, Shelly et al. 2006, 2007; Ito et al., 2007; Obana and Kodaira, 2009; Yamashita et al., 2015), the Ryukyu Trench (e.g., Arai et al., 2016; Nakamura, 2017), the Cascadia subduction zone (e.g., Rogers and Dragart, 2003; Brown et al. 2009), the Aleutian subduction zone (e.g. Brown et al. 2013; Li and Ghosh, 2017), and Middle America (e.g., Brown et al. 2009).

2.3.4 Episodic tremor and slip (ETS)

Episodic tremor and slip (ETS) is the phenomenon that low-frequency tremors and repeating SSEs at the downdip limit of the seismogenic zone are correlated temporally and spatially (see Figure 2.3). According to past studies, such a phenomenon has merely been observed in the Nankai Trough and the Cascadia subduction zone (e.g., Gogers and Dragert, 2003; Obara et al., 2004a). ETSs were discovered first in the Cascadia subduction zone (Gogers and Dragert, 2003). Subsequently, similar phenomena were detected in the Nankai Trough (e.g., Obara et al., 2004a and Hirose and Obara, 2006), but the correlation of slow seismic events extended from the simple case between slow slips and low-frequency tremors to a complicated one involving slow slips, low-frequency tremors, LFEs, and VLFEs.

(e.g., Shelly et al., 2006; Ito et al., 2007). In recent years, Ghosh et al. (2015) confirmed that such an extended correlation has existed between VLFEs and low-frequency tremors in the Cascadia subduction zone. That is, the essential characteristic of ETS is that at least two types of slow seismic events occur simultaneously. Moreover, these slow seismic events sometimes exhibit significant source migrations (e.g., Ghosh et al., 2015; Baba et al., 2018).

2.4 Distribution of slow earthquakes

Considering that various slow seismic events are different manifestations of a single process (Shelly et al., 2007), Obara and Kato (2016) sorted out slow earthquakes detected in the world and plotted their locations. As described in Figure 2.7, slow earthquakes are distributed in subduction zones around the Pacific Ocean, such as Aleutian, Alaska, Cascadia, Mexico, Costa Rica, Chile, New Zealand, Taiwan, and Japan. Among them, the most remarkable area in the slow earthquake studies is the Nankai Trough since all types of slow earthquakes occur in this region (Figure 2.7). The Ryukyu Trench is located to the south of the Nankai Trough. Although the same plate (Philippine Sea Plate) subducts at these two subduction zones, there are significantly differences in the subduction processes due to the different ages of subducting plates (Figure 1.9) (Scholz and Campos, 2012). Likewise, several types of slow seismic events have been detected in the Ryukyu Trench (Figure 2.7). A concise description of the distribution of slow earthquakes in the Nankai Trough and the Ryukyu Trench is given in the following sections.

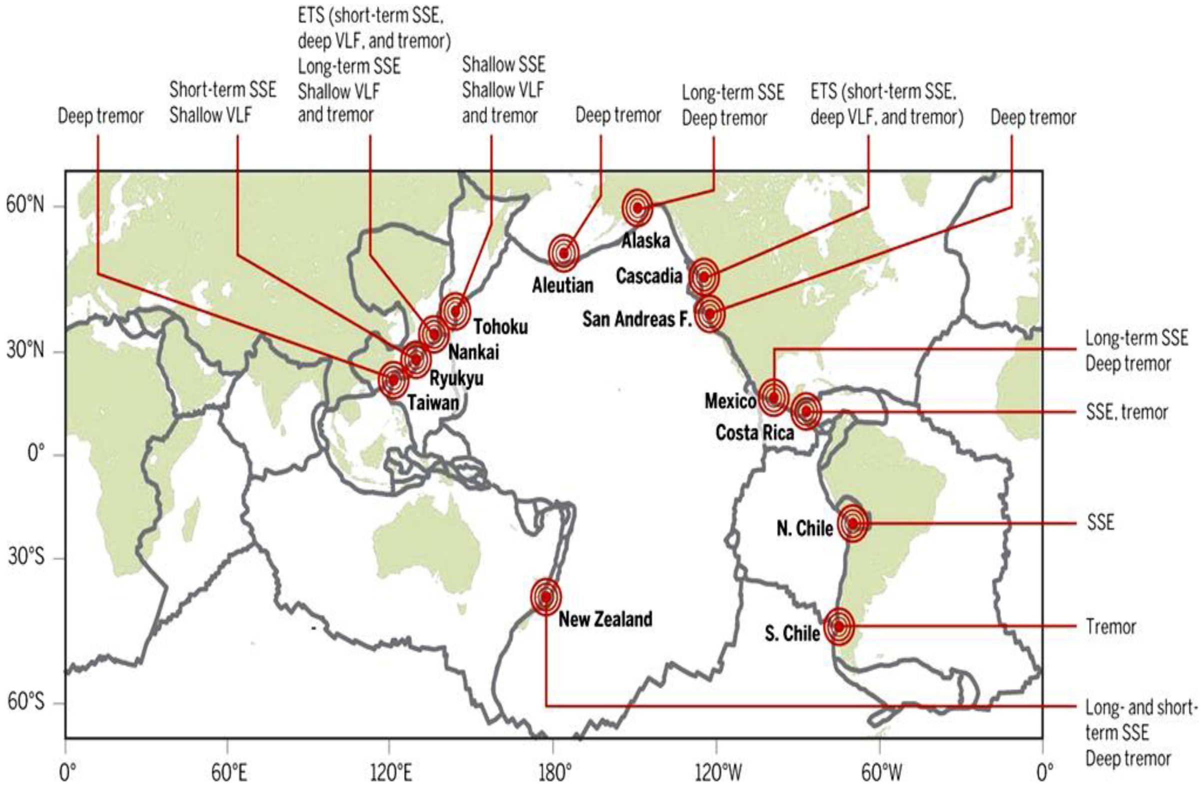

Figure 2.7. Global distribution of different types of slow earthquakes. (From Figure 3 of Obara and Kato, 2016)

2.4.1 Nankai Trough

For nearly two decades, scientists identified various types of slow seismic events in the Nankai Trough, such as long-term SSEs (e.g., Hirose et al., 1999, 2012; Ozawa et al., 2004; Kobayashi, 2010, 2014; Shuto and Ozawa, 2009), short-term SSEs (e.g., Obara et al., 2004a; Hirose and Obara, 2006, 2010), shallow VLFEs (e.g., Obara and Ito, 2005; Ito and Obara, 2006a, 2006b; Asano et al., 2008, 2015; Sugioka et al., 2012), deep VLFEs (e.g., Ito et al., 2007; Baba et al., 2017), shallow LFEs/low-frequency tremors (e.g., Obana and Kodaira, 2009; Yamashita et al., 2015), deep LFEs/low-frequency tremors (e.g., Obara, 2002; Shelly et al., 2006, 2007; Ito et al., 2007), and ETS (e.g., Obara et al., 2004a; Hirose and Obara, 2006, 2010; Ito et al., 2007; Baba et al., 2017; Shelly et al., 2006, 2007). As illustrated in Figure 2.8, the depth ranges of these slow seismic events, form the surface to depth, is shallow VLFEs and shallow LFEs/low-frequency tremors (depths < 10km), long-term SSEs (~30 km), and ETSs (including short-term SSEs, deep LFE/low-frequency tremors, and deep VLFEs) (~40 km). Notably, the asperities of large interplate (megathrust) earthquakes (i.e., locked zones) are coincidentally located in the space between shallow VLFEs and long-term SSEs at depths of ~20 km (Figure 2.8). Accordingly, Obara and Kato (2016) infer that the activity of slow earthquakes might influence the seismogenesis of large interplate earthquakes, and some mechanical links could exist between them.

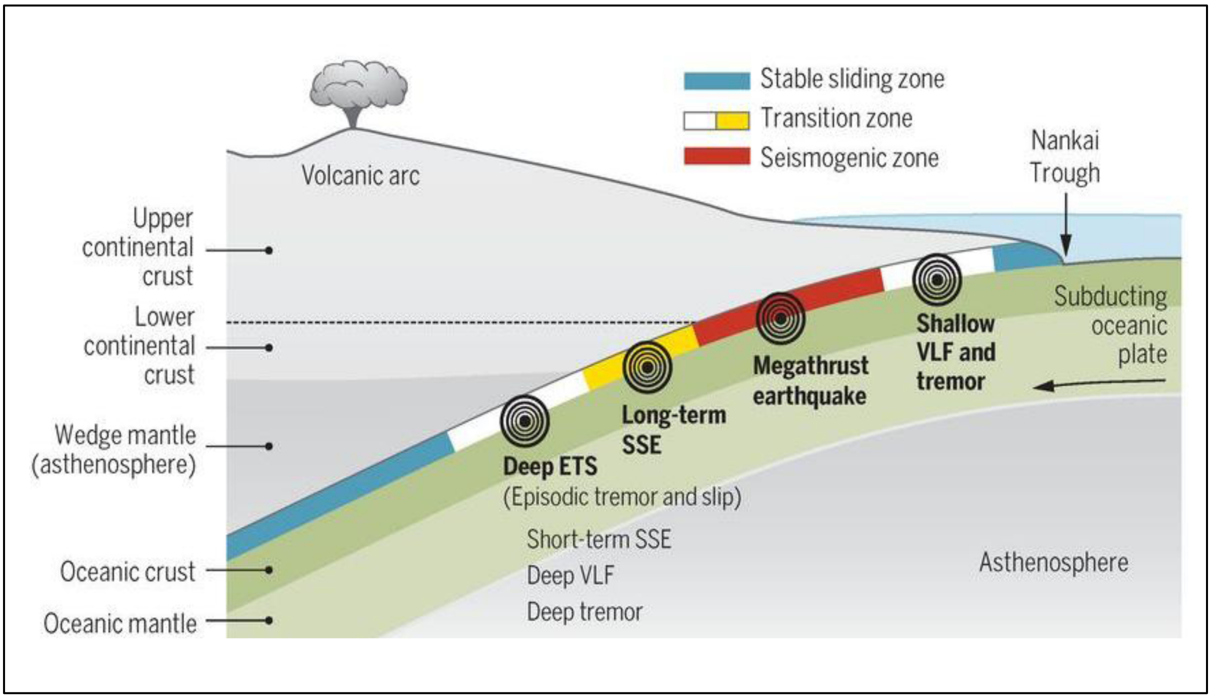

Figure 2.8. Depth range of slow earthquakes and megathrust earthquakes in the Nankai Trough (From Figure 1 of Obara and Kato, 2016)

2.4.2 Ryukyu Trench

The development of slow earthquake research in the Ryukyu Trench started much later than the Nankai Trough because the seismic and geodetic observation stations are sparse here. In the past ten years, scientists strived to overcome this difficulty and successfully detected several types of slow seismic events in the Ryukyu subduction zone, such as long-term SSEs (e.g., Heki and Kataoka, 2008; Nakamura, 2009; Nishimura, 2014, Tu and Heki, 2017; Kano et al., 2018), short-term SSEs (e.g., Nishimura, 2014), shallow VLFEs (e.g., Ando et al., 2012; Nakamura and Sunagawa, 2015), and shallow LFEs (e.g., Arai et al., 2016; Nakamura, 2017). Recently, Arai et al. (2016) analyzed these slow earthquakes and seismic reflection images in this region. They proposed that the depth range of slow earthquakes in the SW Ryukyu Trench should be ~20 km for shallow VLFEs/LFEs and ~30 km for long-term SSEs (Figure 2.9). Notably, the fault zone of the 1771 Yaeyama earthquake, which causes a disastrous tsunami striking Ishigaki and surrounding islands (see detailed contents in Section 1.3.1), is located at the shallowest segment of the Ryukyu subduction zone (see Tsunamigenic zone in Figure 2.9). Moreover, ETSs and other deep slow seismic events have not been observed in this region. Such a distribution is significantly different from that of regular/slow earthquakes in the Nankai Trough. The diagram shown as Figure 2.9 offers a rough concept of slow earthquakes in the Ryukyu subduction zone. However, until now, the location of locked zones (seismogenic zones) and the correlation of these slow seismic events remain vague due to insufficient data of slow earthquakes there. Thus, a detailed and comprehensive study is urgently needed.

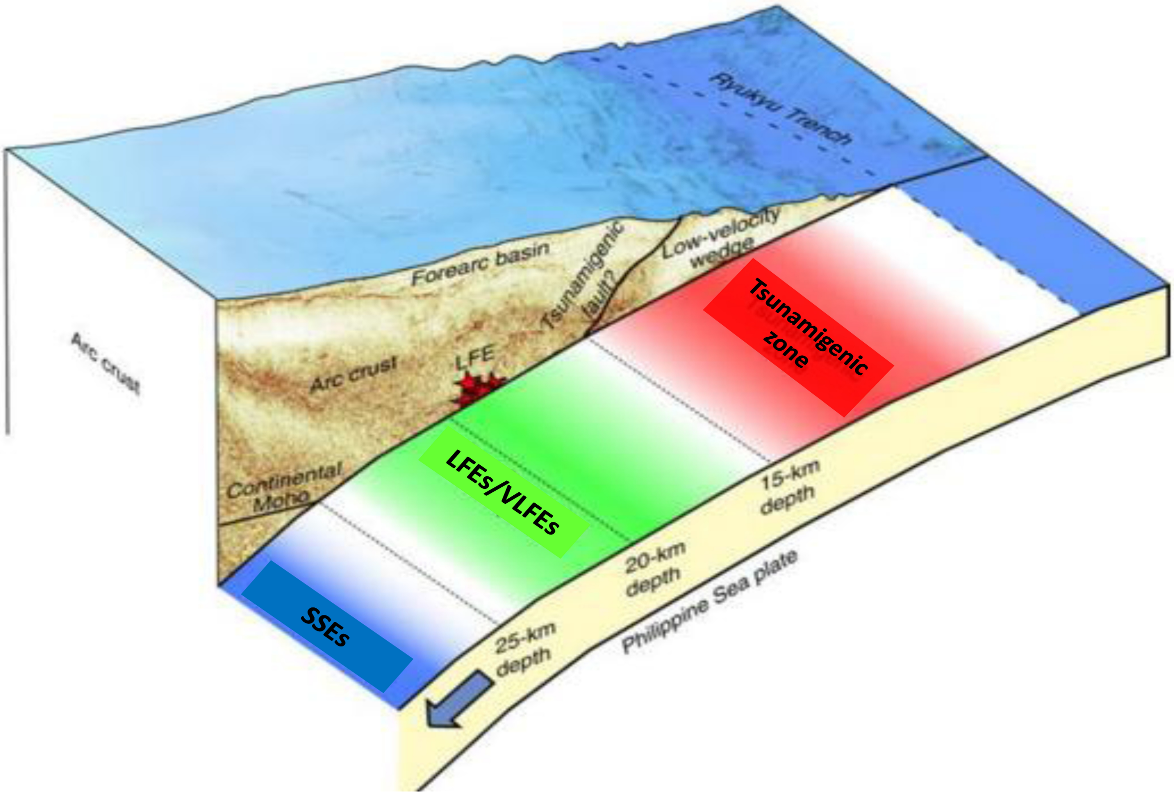

Figure 2.9. Depth range of slow earthquakes and tsunamifenic zone in the Ryukyu Trench (From Figure 4 of Arai et al., 2016)

2.5 Primary objectives of this study

In the Nankai Trough, the locked zones, in which large interplate earthquakes ($M_w \geq 8$) recur regularly, are located in a zone between the shallow VLFEs and long-term SSEs (Figure 2.10) (Obara and Kato, 2016). This result suggests that if we can confirm the relative positions of VLFEs and SSEs, the location of locked zones in the Ryukyu Trench might be determined. Considering this point, I decided to focus on two types of slow seismic events, i.e., SSEs and VLFEs, in this thesis. Since the insufficient database is the fundamental problem for the slow earthquake research in the Ryukyu Trench, I attempted to expand the time span covered by the data at least twice as long as previous studies. Furthermore, the properties, activities, and the correlations between the two types of slow seismic events are to be analyzed in detail. Finally, using the above data, I would discuss the interplate coupling of the Ryukyu subduction zone. I expect that the results of this thesis can help clarify the role of slow earthquakes played for the plate convergence in the Ryukyu Trench. Moreover, I also hope the database of slow earthquakes provided in this thesis can contribute to various kinds of future studies.

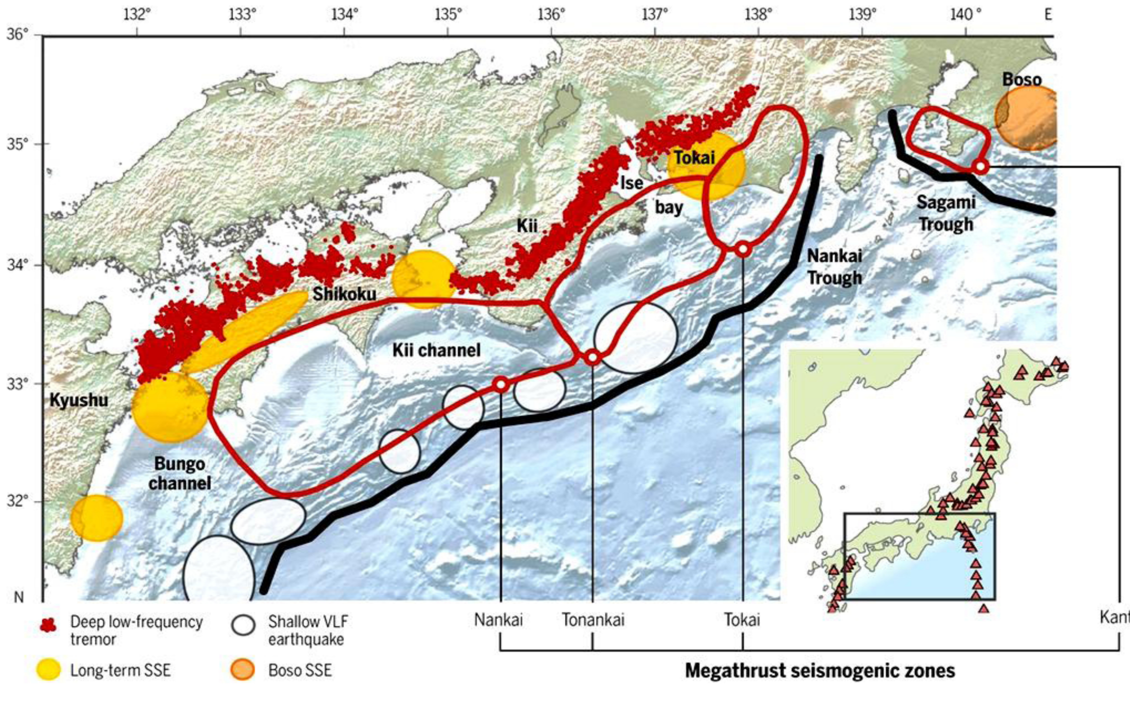

Figure 2.10. Distribution of slow earthquakes in the Nankai Trough. The locked zones (red polygon) are distributed in the region between shallow VLFEs (white circles) and long-term SSEs (yellow circles) (From Figure 2 of Obara and Kato, 2016)

Chapter 3.

Slow Slip Events (SSEs)

The primary contents of this chapter have been published in *Geophysical Research Letters*,

Tu, Y. and K. Heki (2017), Decadal modulation of repeating slow slip event activity in the southwestern Ryukyu Arc possibly driven by rifting episodes at the Okinawa Trough, *Geophys. Res. Lett.*, 44, 9308-9313, doi: 10.1002/2017GL074455.

3.1 Introduction

3.1.1 What are slow slip events (SSEs)?

Slow slip events (SSEs) are a type of slow earthquakes generated by slow fault ruptures at plate interfaces (Heki and Kataoka, 2008). From their durations, these events can be classified into short-term SSEs lasting from days to weeks and long-term SSEs from months to years (Obara and Kato, 2016). Since their fault slips are too slow to generate seismic waves, SSEs are known as geodesic slow earthquakes (Obara and Kato, 2016) and can only be detected by geodetic observations such as Global Navigation Satellite System (GNSS) and tiltmeters.

3.1.2 Where do SSEs occur?

SSEs have been observed in several subduction zones around Japan, such as the Nankai Trough, Southwest Japan (e.g. Hirose at al, 1999, 2010; Ozawa et al., 2002, 2017; Hirose and Obara, 2005, 2006), and the Boso Peninsula, Central Japan (e.g. Ozawa et al., 2003, 2007, 2014; Hirose et al., 2012) (Figure 3.1). In addition, they were also found in other areas over the world, e.g., the Cascadia subduction zone, western Canada (e.g. Dragert et al., 2001; Rogers and Deagert, 2003; Szeliga et al., 2008), Mexico (e.g. Lowry et al., 2001, Kostoglodov et al., 2003; Vergnolle et al., 2010) and New Zealand (e.g. Douglas et al., 2005; Wallace et al., 2016) (Figure 3.1). Since large thrust earthquakes occur repeatedly in these subduction zones, SSEs are considered to have mechanical links to large interplate earthquakes (Obara and Kato, 2016). On the other hand, a few investigations also found SSEs in weakly coupled plate boundaries, such as the Izu-Bonin Arc (Arisa and Heki, 2016) and the Ryukyu subduction zone (Heki and Kataoka, 2008; Nakamura, 2009; Nushimura, 2014). Moreover, Ozono et al. (2014) and Ikeda et al. (2015) also studied small SSEs occurring in an inland convergent plate boundary running NS in Hokkaido, Japan.

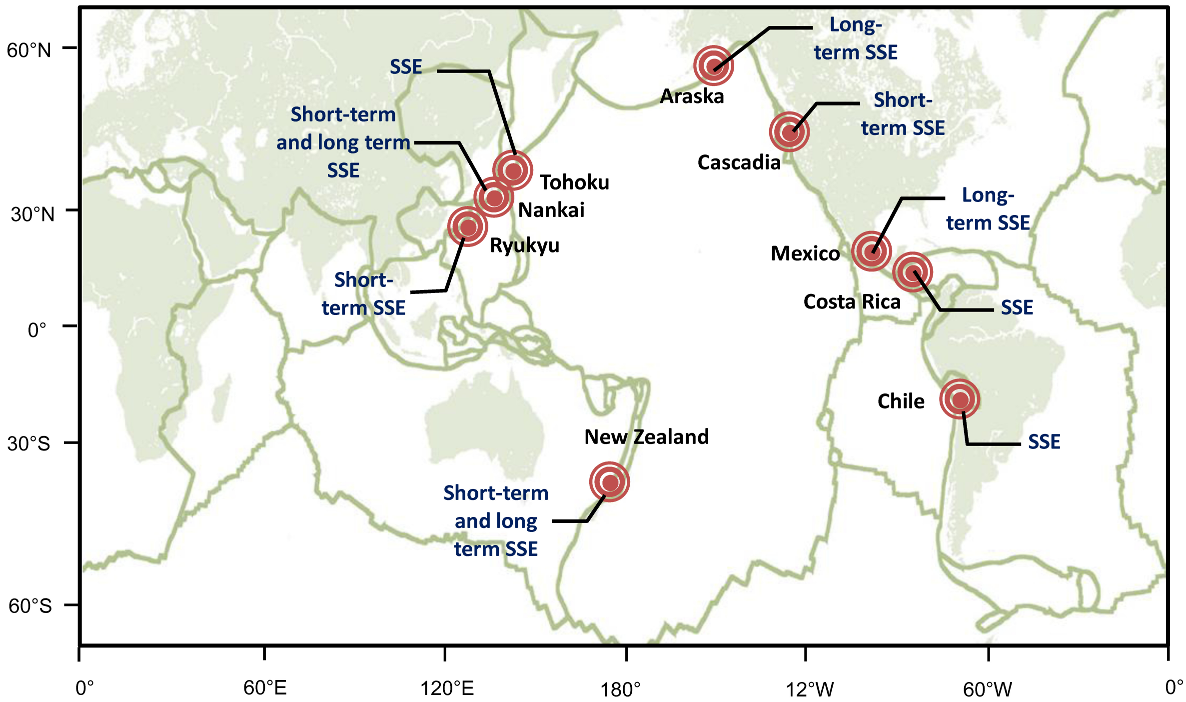

Figure 3.1. Global distribution of slow slip events (SSEs). Most of SSEs occur in coupled plate boundaries around the Pacific Ocean. (Modified from Obara and Kato, 2016.)

3.1.3 SSEs in the Ryukyu Trench

The Ryukyu Trench differs from the Nankai Trough. It is a weakly coupled plate boundary (Uyeda and Kanamori, 1979), and few megathrust earthquakes ($M_w > 8$) rarely occur there

(Ando et al., 2009; Scholz and Campos, 2012). Moreover, active back-arc spreading in the Okinawa Trough makes the Ryukyu Arc moves trench-ward (Figure 3.2a), which causes the fast convergence at the Ryukyu Trench of ~12.5 cm per year (Heki and Kataoka, 2008). In this segment of the Ryukyu Trench, a series of repeating SSEs were found and studied.

Heki and Kataoka (2008) detected SSEs beneath the Iriomote Island in the southwesternmost part of the Ryukyu Arc. These events occur approximately twice per year on the same fault patch. Subsequently, Nakamura (2009) detected a large scale afterslip of a M_w 7.1 thrust earthquake off the eastern coast of Taiwan continuing for ~5 years. Recently, Nishimura (2014) identified ~130 short-term SSEs along the whole Ryukyu subduction zone using a new detection technique based on Akaike's Information Criterion (AIC). The positions of above SSEs are shown in Figure 3.2a.

3.1.4 Purposes of this study

Although Heki and Kataoka (2008) studied repeating SSEs beneath the Iriomote Island in detail, a discussion on the temporal variability of their slip accumulation rate has not been done. Here, I study these SSEs again using more accurate coordinate data with twice as long a time span as in the previous study and focus on the time-variable behavior of slip accumulation rate of SSEs. I expect that the results can clarify what controls the stability of the slip accumulation rate and understand the plate motion of the southwestern Ryukyu subduction zone.

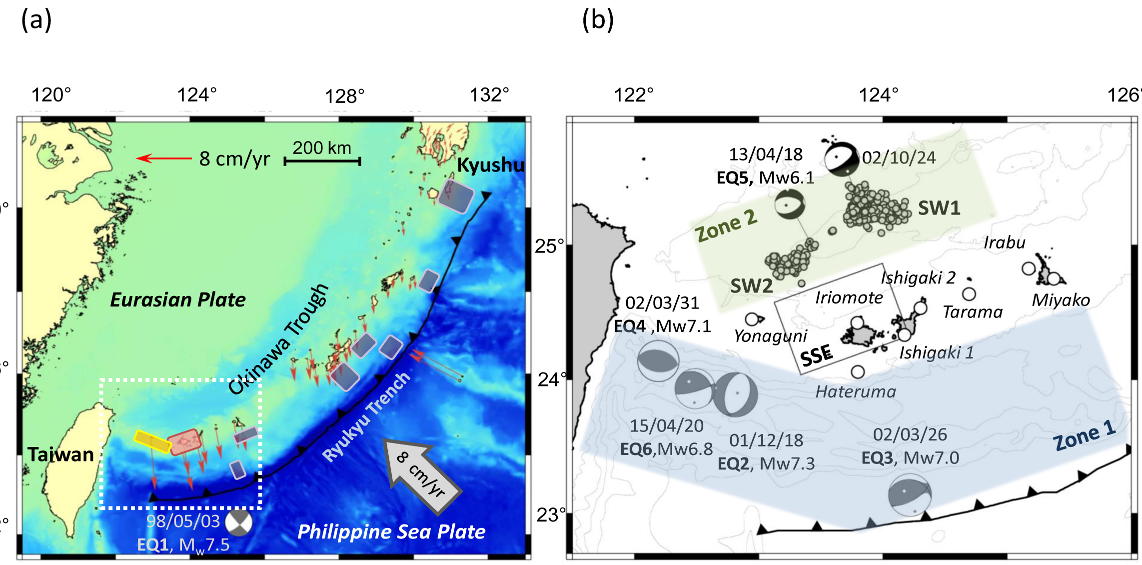

Figure 3.2. (a) Plate tectonic map of the Ryukyu area. The Philippine Sea Plate is subducting beneath the Eurasian Plate along the Ryukyu Trench with a high convergence rate. The Okinawa Trough lie behind the Ryukyu Arc is an active back-arc spreading system. It causes the Ryukyu Arc moves trench-ward as demonstrated by the rapid southward velocities of the GNSS stations. The arrows represent velocities of GNSS stations relative to the Eurasian Plate for the period of 2000-2010. Red, yellow and purple rectangles indicate SSEs detected by Heki and Kataoka (2008), Nakamura (2009), and Nishimura (2014), respectively. **(b)** Distribution of the slow slip events (SSEs) (rectangle), earthquake swarms (gray circles), and six large earthquakes (EQ1-6; EQ1 is shown in 2a). The beach balls along the Ryukyu Trench show the locations and focal mechanisms of five large earthquakes (EQ1-4, and EQ6). The beach balls in the Okinawa Trough display the source mechanisms of two earthquake swarms (SW1 and SW2 including EQ5). The polygons (zone1 and zone2) show the geometric extents of earthquakes illustrated in the Figure 3.12a and 3.12b

3.2 Data and method

3.2.1 Detection of SSEs

GNSS data obtained from 1997 to 2016 at six stations (Figure 3.3) of the GNSS Earth Observation Network System (GEONET) operated by the Geospatial Information Authority (GSI) of Japan were used in this study. I adopted their daily coordinates available as the GSI-F3 solution (Nakagawa et al., 2009), and selected the Miyako station (Figure 3.3) as the reference site based on its large distance from nearby large earthquakes or the Iriomote SSEs (Heki and Kataoka, 2008). These SSEs show the largest signal-to-noise ratio in the movement of the Hateruma station toward N20°W (Figure 3.4a), which is the direction of the Philippine Sea Plate subduction (Heki and Kataoka, 2008).

Offsets generated by antenna changes were removed in advance, and coseismic jumps by nearby earthquakes were marked with dashed lines (see Figures 3.4a and 3.4b). I detected 38 SSEs by visual inspection with assistance from –ΔAIC (Akaike Information Criterion), which is an index showing statistical significance of the SSE onset signatures (Figure 3.4c) (Nishimura, 2014).

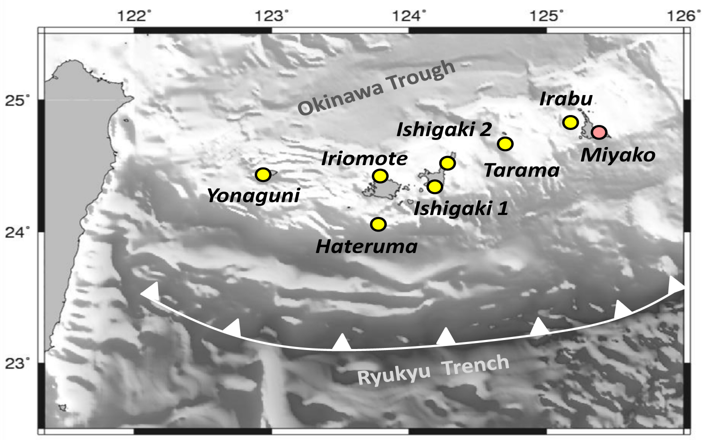

Figure 3.3. GEONET GNSS stations used in this study. The red circle displays the reference site of Miyako.

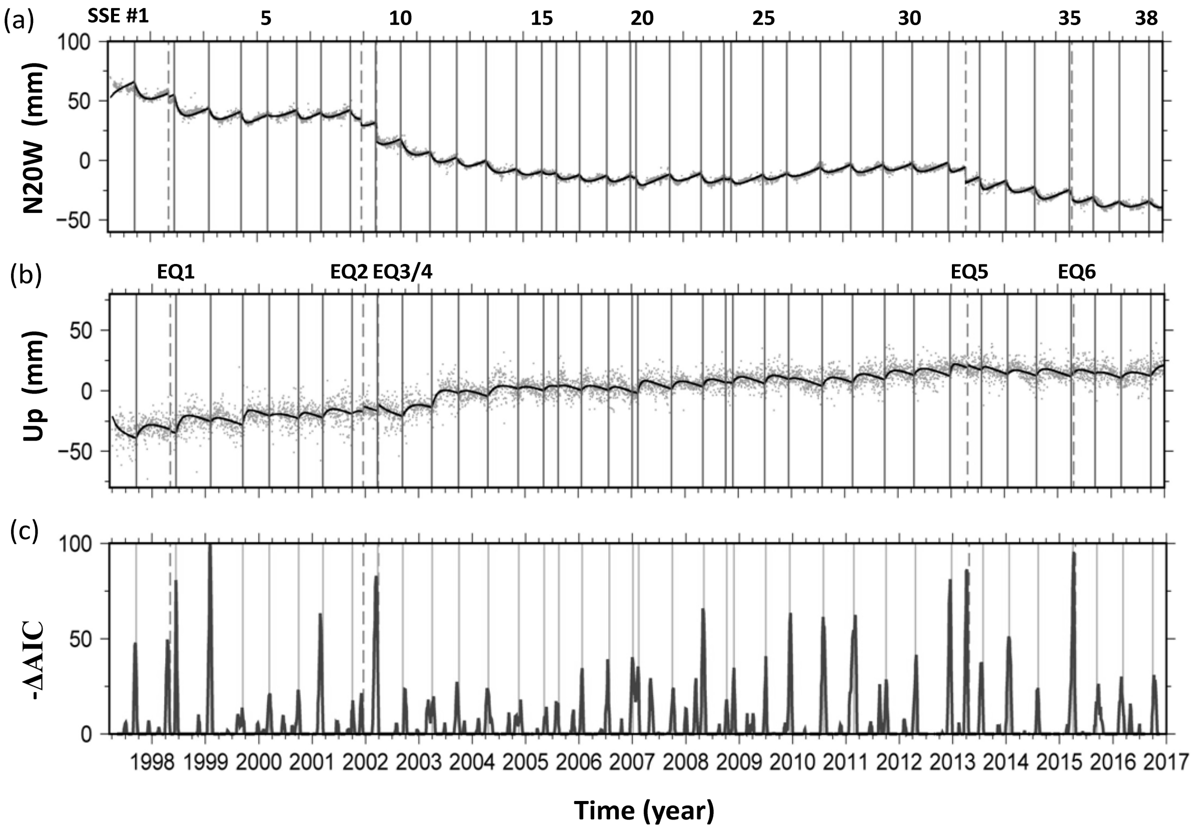

Figure 3.4. (a, b) The change in daily displacements of the Hateruma station relative to Miyako site in the N20W and up directions. Solid vertical lines show the onset times of the 38 SSEs. Their numbers are marked at the top. Dashed lines indicate six large earthquakes (EQ1-6) during the studied period. Locations and focal mechanisms of these earthquakes are shown in Figure 3.2a, b. **(c)** The values of –ΔAIC, which indicates the significance of the trend change (bending) of the N20W component, or the onset of SSEs (Nishimura, 2014).

3.2.2 Model for the time series

To determine three-dimensional (EW, NS, and UD) displacement vectors associated with the SSEs, I used the model as Heki and Kataoka (2008) to estimate the changes of coordinate x in time t as:

$$x = at + b + \sum_{i=1}^{n} X_i \left[1 - \exp \frac{-(t - T_i)}{\tau_i} \right] \quad (T_1 < T_2 < \cdots < T_n < t)$$

(1)

where a is the long-term background trend, and b is the offset. The number of SSEs before the time t is n, and X_i, T_i and τ_i are the final displacement, the onset time, and the time constant of the i'th SSE, respectively. The values of T_i and τ_i here are determined by minimizing the post-fit residual in the Hateruma N20W time series.

As suggested by Heki and Kataoka (2008), a relatively short interval might cause the magnification of the theoretical final displacement X_i. Accordingly, I used the actual final displacement X'_i to replace the theoretical final displacement X_i:

$$X'_i = X_i \left[1 - \exp \frac{-(T_{i+1} - T_i)}{\tau_i} \right]$$

(2)

where X'_i is the cumulative displacement by the i'th event until the onset of the next event.

3.2.3 Estimation of fault parameters

After calculating the three-component displacement vectors at six GNSS stations in all the SSEs, I estimated the slips of the fault patch assuming homogeneous elastic half-space (Okada, 1992). Since these SSEs have similar displacement vectors, we adopted the same geometry of the fault patch as in Heki and Kataoka (2008), which was confirmed to have the smallest post-fit residuals of the displacement vectors. Moreover, the dislocation vectors of dip-slip and strike-slip components were also estimated through the least-squares method from the three-dimensional displacement data. The detailed source parameters of the 38 SSEs are given in Table 3-1.

Table 3-1. Occurrence times, locations, magnitudes and fault parameters of SSEs beneath the Iriomote Island

No.	Date	length (km)	Slip (m)	Moment (e19N·m)	Mw	No.	Date	length (km)	Slip (m)	Moment (e19N·m)	Mw
1	1997.7	160	0.07	3.15	6.93	**21**	2007.7	94	0.041	1.03	6.61
2	1998.4	160	0.087	3.51	6.96	**22**	2008.3	94	0.054	1.34	6.68
3	1999.1	114	0.059	1.79	6.77	**23**	2008.7	160	0.013	0.58	6.44
4	1999.7	94	0.042	1.06	6.62	**24**	2008.9	94	0.025	0.63	6.46
5	2000.2	94	0.038	0.96	6.59	**25**	2009.5	94	0.019	0.48	6.39
6	2000.7	94	0.046	1.15	6.64	**26**	2009.9	94	0.026	0.67	6.48
7	2001.2	94	0.028	0.71	6.5	**27**	2010.5	94	0.033	0.83	6.54
8	2001.7	94	0.041	1.75	6.76	**28**	2011.1	94	0.052	1.3	6.68
9	2002.2	160	0.044	1.88	6.78	**29**	2011.7	94	0.034	0.85	6.55
10	2002.7	160	0.075	3.19	6.94	**30**	2012.3	94	0.048	1.21	6.65
11	2003.2	114	0.050	1.53	6.72	**31**	2012.9	94	0.048	1.2	6.65
12	2003.7	94	0.059	1.79	6.77	**32**	2013.5	114	0.050	1.52	6.73
13	2004.3	94	0.074	2.24	6.83	**33**	2014.0	114	0.071	2.15	6.82
14	2004.8	114	0.045	1.12	6.63	**34**	2014.6	114	0.064	1.93	6.79
15	2005.3	94	0.028	0.71	6.50	**35**	2015.2	114	0.042	1.27	6.67
16	2005.6	94	0.043	1.07	6.62	**36**	2015.7	114	0.039	1.47	6.71
17	2006.0	94	0.045	1.12	6.63	**37**	2016.1	114	0.049	1.46	6.71
18	2006.5	94	0.036	0.91	6.57	**38**	2016.7	96	0.054	1.36	6.69
19	2007.0	94	0.013	0.34	6.29						
20	2007.1	94	0.033	0.82	6.54						

* Location of the center of the SSE fault patch: 24.5°N, 123.8°E, depth 32 km.

** Fault width is 66 km for all SSEs.

*** Strike, Dip, Rake of the fault: 250°, 15° NNE, 116°

3.3 Results

3.3.1 Characteristics of SSEs

The 38 SSEs from 1997 to 2016 occurred regularly with an average interval of ~6 months (Figure 3.5a). Although the recurrent intervals show a strong pick (Figure 3.5a), the occurrence season looks random (Figure 3.5b), which indicates that these SSEs are not controlled by seasonal forcing. The average magnitude (M_w) of these events is ~6.7 (Figure 3.5c). The time constant of ~0.10 years implies that these SSEs just lie on the boundary between the short- and long-term SSEs as defined by Obara and Kato (2016) (Figure 3.5d). These properties are all consistent with Heki and Kataoka (2008).

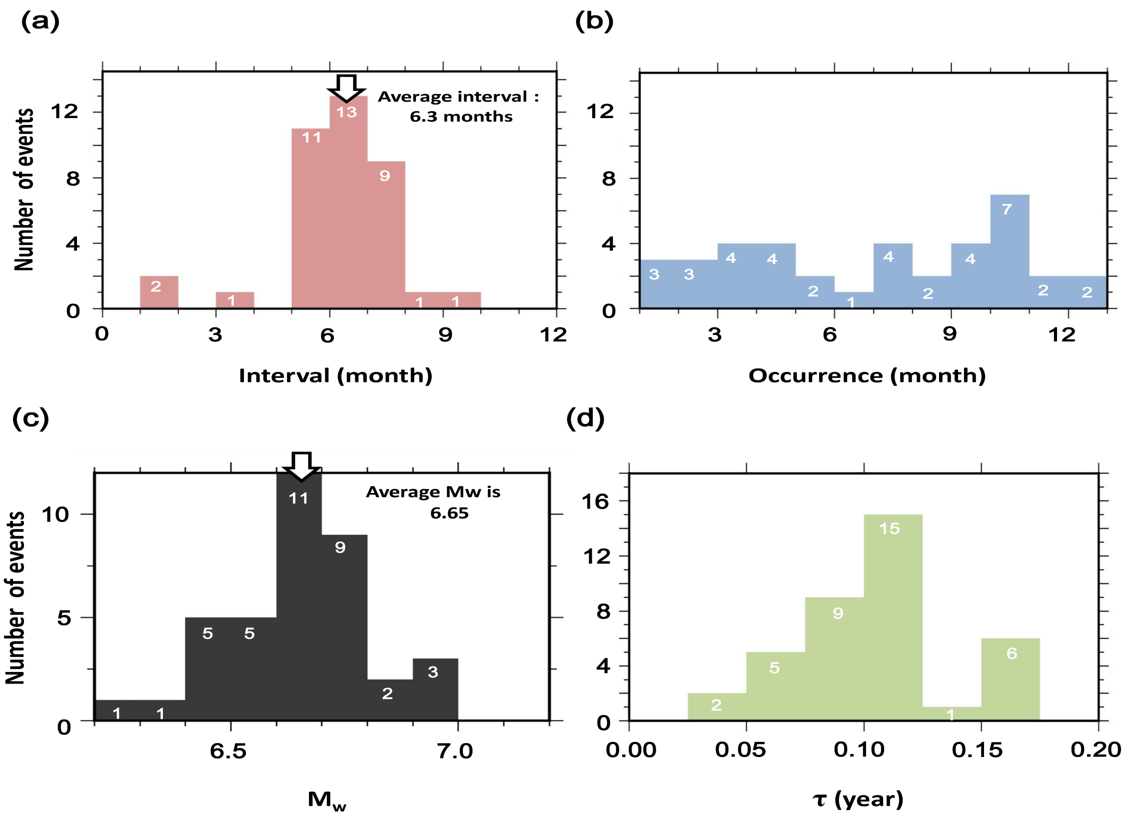

Figure 3.5. (a) The recurrence intervals of the 38 SEEs. The average interval is 6.3 months with the standard deviation of 1.7 months. **(b)** Occurrence months of the SSEs. The

distribution indicates that SSEs are not seasonal. **(c)** The distribution of M_w of the SSEs. Their average is M_w 6.7. **(d)** Time constants of these SSEs.

3.3.2 Fault Parameters of the SSEs

I estimated the fault slip parameters of the 38 SSEs employing the program to calculate surface displacement due to the fault dislocation developed by Okada (1992). Figure 3.6 shows the dislocation vectors and fault parameters estimated for the SSE #18 in July 2006. The fault patch of this event is ~100 km away from the Ryukyu Trench axis and probably lie on the upper surface of the Philippine Sea Plate. Its center is located at ~24.5°N, ~123.8°E at a depth of ~30 km, and the depth of its upper and lower edges are ~20 and ~40 km, respectively. The dimensions of this fault patch are ~90 km in length and ~70 km in width. It strikes in N70E and dips 15 degrees toward NNE.

The 38 SSEs have quite similar horizontal dislocation vectors, which suggests that these ruptures should occur at similar fault patches (Figure 3.7). However, some of them still have slight differences. For example, SSE #1, 2, and 10 display larger horizontal displacements in the Yonaguni Island, which indicates that their fault patches may extend more westward. As suggested by Heki and Kataoka (2008), I assumed two longer fault geometries for these events. Their fault lengths were extended by 20 or 40 km toward the WSW direction to realize better fits to observe displacements. The numbers of SSEs for the three different fault lengths, i.e., long (~160 km in length), middle (~110 km), and short (~90 km) are 6, 10 and 22, respectively. Such differences between SSEs are probably related to the change of fluid distribution or fault friction (Kano et al., 2018), similar to SSEs in the Bungo (e.g., Ozawa et al., 2007b) and Boso areas (Fukuda, 2018).

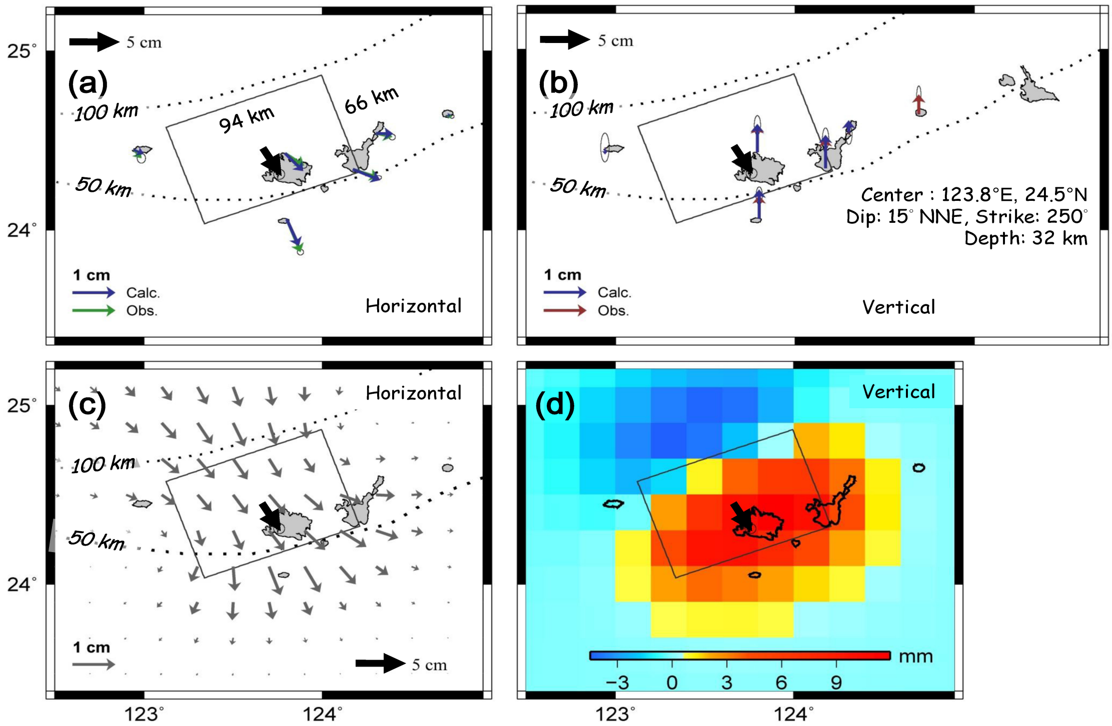

Figure 3.6. (a, b) The estimated fault parameters for the SSE #18 using the observed horizontal (green arrows in (a)) and vertical (red arrows in (b)) displacements. Dotted-line contours show surface depths of the Philippine Sea Plate slab. Blue arrows in (a) and (b) indicate displacements calculated using the fault slips shown by the thick arrows. **(c)** and **(d)** show calculated horizontal and vertical displacements at grid points, respectively.

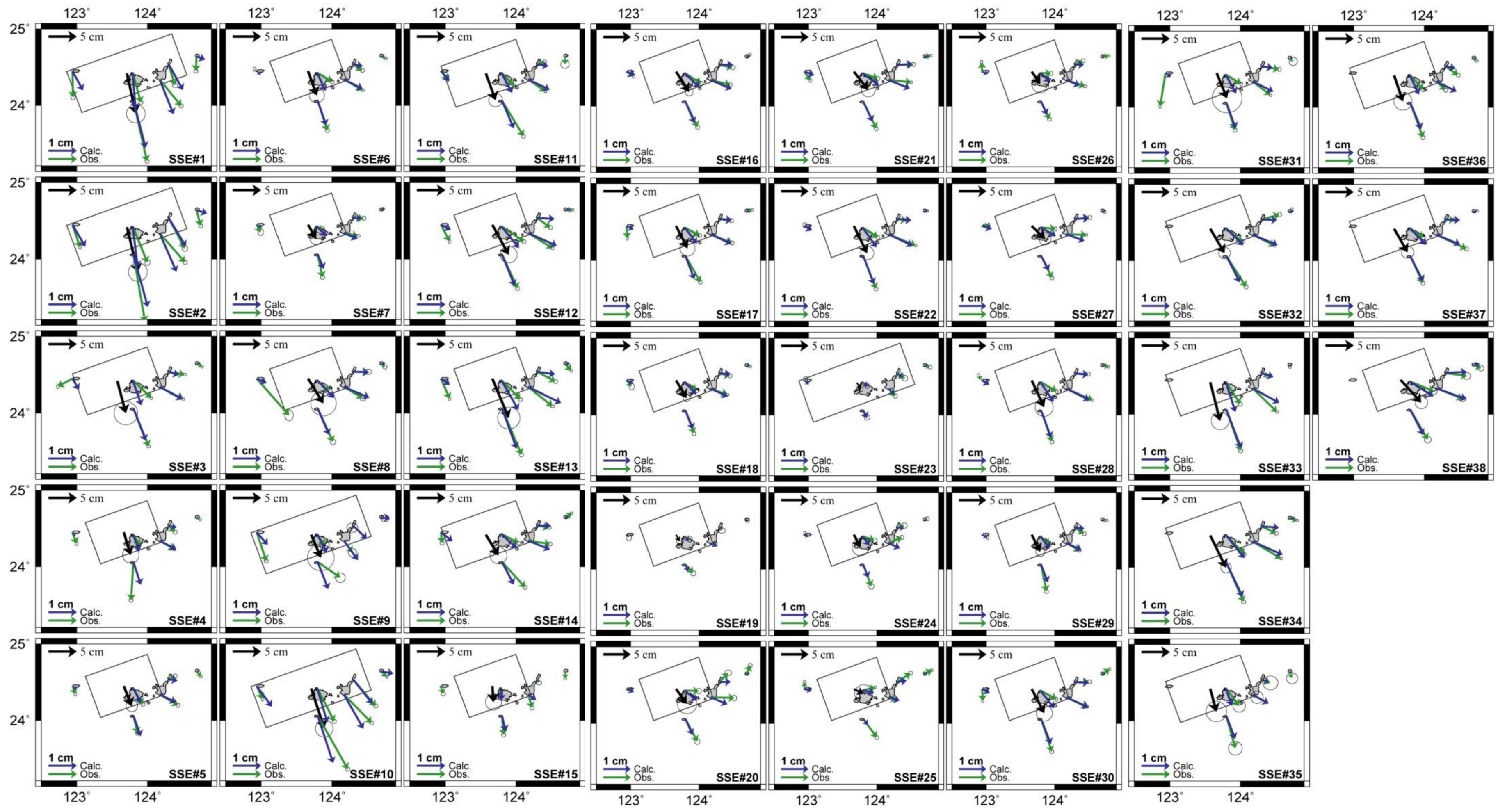

Figure 3.7. Horizontal dislocation vectors (blue/green arrows) and estimated fault slips (black arrows) for the 38 SSEs. Error ellipses show 2δ. I assumed three different fault lengths, i.e., long (e.g. #1, 2, 9, and 10), middle (e.g. #3, 11, and 14), and short (e.g. #4, 5, 6, and 7). The last seven events (Nos. 32-38) were assumed to have middle or short fault length due to the lack of GNSS data of the Yonaguni station caused by the pillar replacement.

3.3.3 Time-predictable recurrence

Heki and Kataoka (2008) inferred that recurrences of SSEs near Iriomote Island were time-predictable from the observation that the lower right corners of the slip accumulation diagram align (Figure 3.8). With the present dataset of the 38 SSEs, such time-predictability seems to hold (Figure 3.9a). To future confirm this, I compared the correlations between slips and recurrence intervals following or preceding the events. The correlation coefficients (0.57 and 0.38) indicate that the slips have a stronger correlation with the intervals following the events. It means that time-predictable recurrence is more likely.

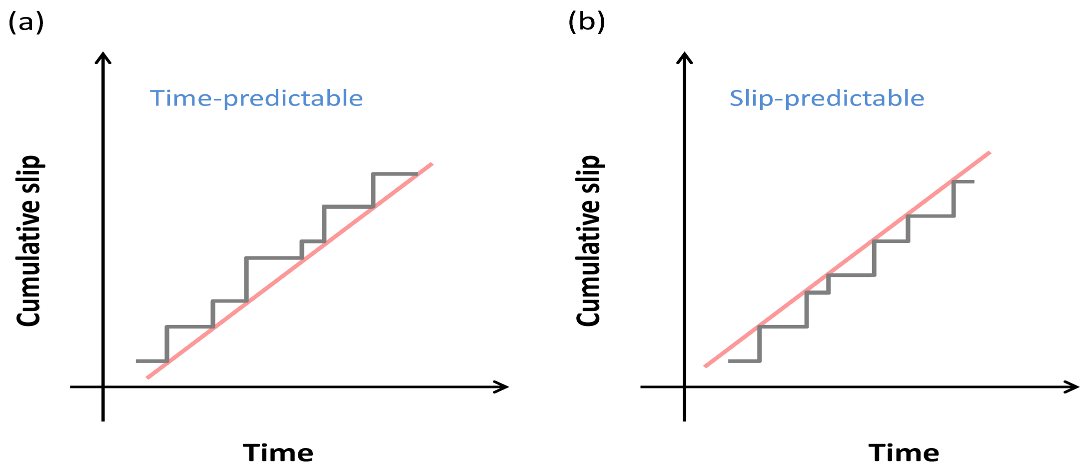

Figure 3.8. (a) Time-predictable recurrences. The lower right corners of the slip accumulation diagram line up. In this case, a stronger correlation exists between slips and recurrence intervals following the events. **(b)** Slip-predictable recurrences. The upper left corners align, and a stronger correlation is expected to exist between slips and recurrence intervals preceding the events. (modified from Heki and Kataoka, 2008.)

3.3.4 Fluctuations of slip accumulation rate

The overall slip accumulation rate (cumulative slip/lapse time) of SSEs from 1997 to 2016 is ~8.6 cm/year, which is significantly lower than ~11 cm/year in 1997-2007 reported by Heki and Kataoka (2008). In addition, the rate fluctuates in time and is hard to fit a single line into the whole time series (Figure 3.9a). The trends during the four periods of 1997-2001, 2003-2007, 2007-2013, and 2013-2016 (slip accumulation is largely linear within these periods) are 9.3 cm/year, 10.9 cm/year, 6.3 cm/year, and 10.2 cm/year, respectively (Figure 3.9a). The detrended cumulative slip provided on Figure 3.9a also clearly indicates two distinct increases in 2002 and 2013 and one gradual slowdown around 2007.

Moreover, I also tried to fit a polynomial into the lower right corners of the slip accumulation diagram (Figure 3.9a). I calculated RMS of each polynomial and found that the degree-6 polynomial is the most appropriate (Figure 3.10). The time derivative of this polynomial was used to represent slopes of the slip accumulation curve in this study (Figure 3.11). Next, I compared the correlation between slopes and two quantities: amount of slips (Figure 3.9b) and recurrence intervals (Figure 3.9c). It is interesting to see a stronger correlation (CC = 0.52) for the slips, which suggests that increased slips cause the rise of the slip accumulation rate rather than decreased recurrence intervals.

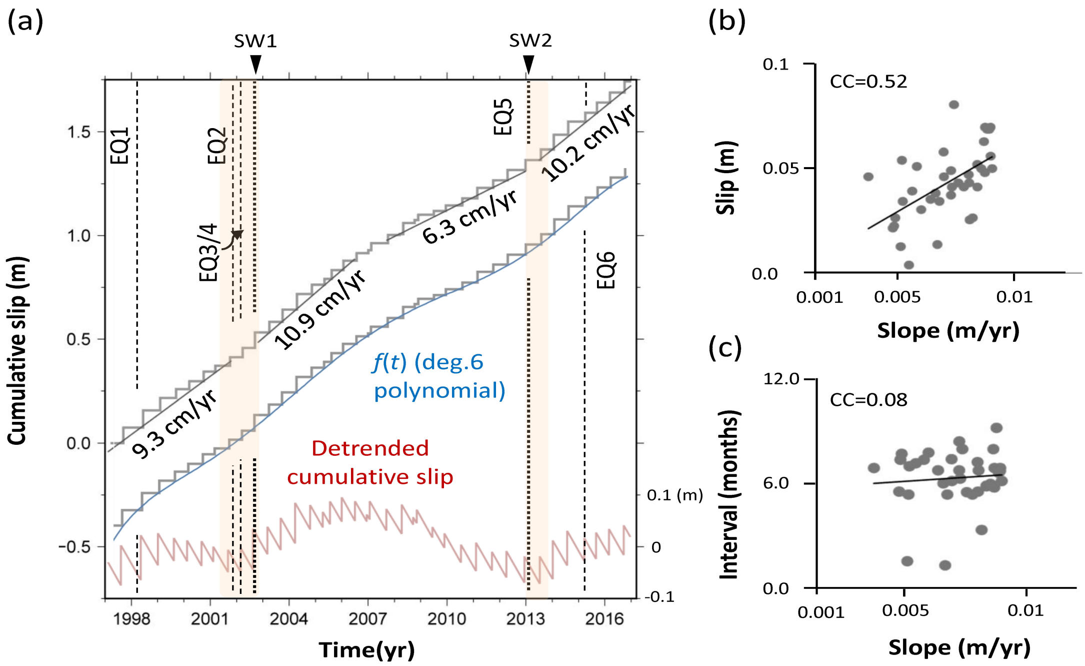

Figure 3.9. (a) Slip accumulation diagram of the 38 SSEs from 1997 to 2016. The upper diagram is fit by four lines with different trends and time periods. It is also modeled with the degree-6 polynomial, whose time derivative *f'(t)* is shown in Figure 3.11. At the bottom of the diagram, the detrended cumulative slip is displayed, which clearly indicates the changes of the trend. Vertical positions of the three curves are arbitrary. Dashed lines and dotted lines with triangles indicate occurrences of large earthquakes (EQ1-6) and earthquake swarms (SW1-2), respectively. The two orange belts in the illustration represent the epochs of the slip accumulation rate increase. (b) The scatter diagram between the slips and *f'(t)* at the SSE onset times. Its correlation coefficient is 0.52, which suggests that the two variables are positively correlated. (c) However, the correlation between the recurrence intervals and *f'(t)* is small. The correlation coefficient is only 0.08.

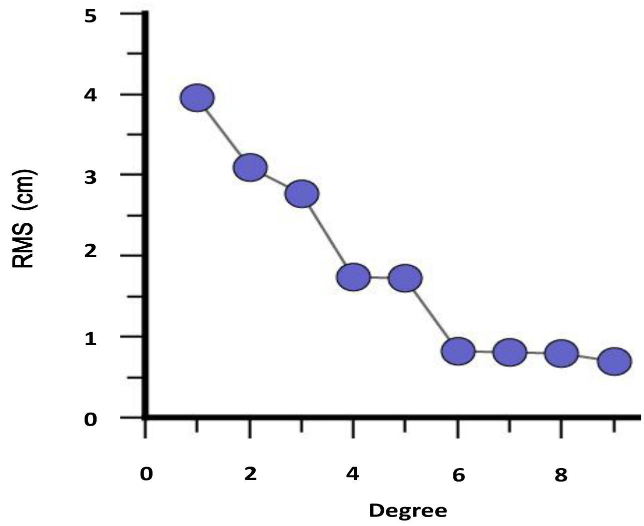

Figure 3.10. The L-curve test was used to determine the most appropriate degree of polynomial to fit the slip accumulation curve of the SSEs. Based on the fast drop of RMS value up to degree 6. Hence, the degree-6 polynomial is inferred to be the most appropriate.

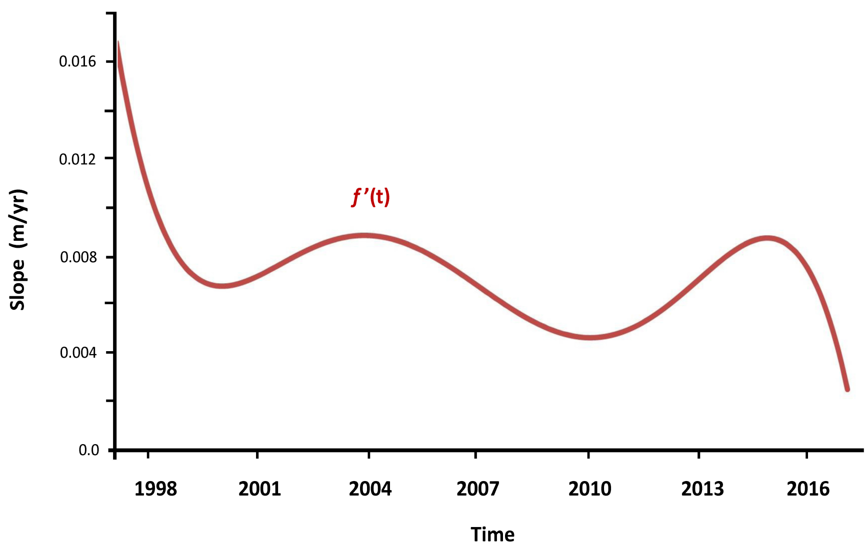

Figure 3.11. The time derivative of the degree-6 polynomial used to model the SSE slip accumulation curve. The time series of *f'(t)* represents slopes of the slip accumulation curve.

3.4 Discussion

3.4.1 Mechanisms of time-variable slip accumulation

Since SSEs release accumulated strain like regular earthquakes, stress disturbances caused by external forces (e.g. large earthquakes) may change their occurrences. Heki and Kataoka (2008) studied the possibility that the static stress perturbation by EQ2-4 (Figure 3.2b) in 2001 and 2002 might have disturbed the regular occurrence of SSEs. However, they considered it unlikely by comparing the stress drop of the average SSE and the Coulomb Failure Stress change (ΔCFS) by EQ2-4 at the SSE fault. Later, Nakamura (2009) proposed the afterslip of EQ4, i.e., the 2002 Hualien earthquake (M_w7.1) east of Taiwan (Figure 3.2b), lasted for 5 years and probably caused the increase of slip accumulation rate. However, no large earthquakes occurred around the second increase of the slip accumulation rate in 2013. Moreover, the activities of small earthquakes ($M_w > 3$) along the Ryukyu Trench did not show significant changes, either (Figure 3.12a). Here, I propose a new mechanism that may ecplain the two increases of the slip accumulation rate, in addition to the afterslip of EQ4 (Nakamura, 2009).

Okinawa Trough, an active back-arc spreading system, is located ~70 km north of the SSE fault patch. During the study period, two earthquake swarms (SW1 and SW2) occurred (Figure 3.12b), possibly suggesting the occurrences of rifting episodes at the trough axis. The first event was active about two days (Oct. 24-25, 2002) and showed a definite stop. The second one started on Apr. 15, 2013 and is followed by a long-duration high seismic activity at the trough. Notably, their occurrences roughly coincide with the increases of the slip accumulation rate in 2002 and 2013 (Figure 3.9a).

Ando et al. (2015) inferred that the SW2 reflects a dike intrusion with the volume of ~0.4 km^3. If I assume a 2-meter tensile opening of a vertical plane with the width 10 km and the length 20 km, a positive ΔCFS of ~9 kPa occurs at the SSE fault. It would be a significant stress change amounting to ~40 % of the stress drop of an SSE but still inadequate to explain the observed increase in the slip accumulation rate from 6.3 cm/year to 10.2 cm/year lasting for several years.

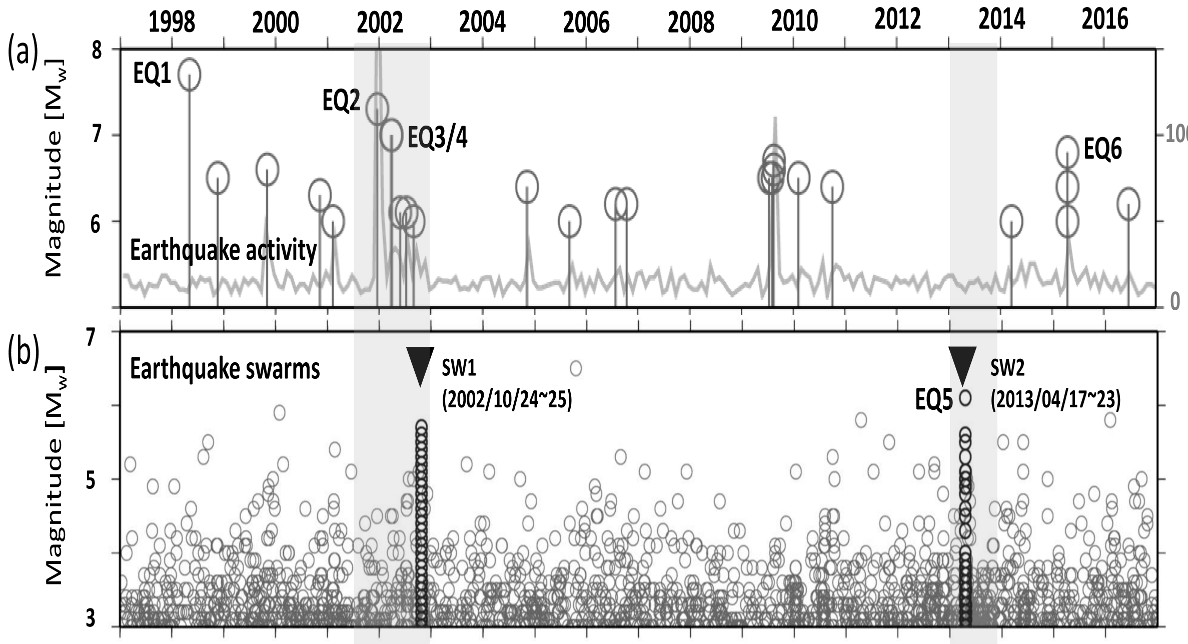

Figure 3.12. (a) Seismicity along the southwestern Ryukyu Trench from 1997 to 2016. Open circles indicate large earthquakes (M_w > 6). The gray curve displays the number of small earthquake (M_w > 3), whose unit is given on the right axis. Gray shaded rectangles represent two epochs when the slip accumulation increased. (b) Earthquake activity (M_w > 3) within the Okinawa Trough. Two triangles indicate earthquake swarms in 2002 and 2013, and EQ5 (M_w 6.1) belongs to the SW2. Geometric ranges of earthquakes shown in (a) and (b) are given in Figure 3.2b.

Iriomote Islands is located above the SSE fault patch in the southwestern Ryukyu Arc (Figure 3.2b). I found that the southward motion of the GNSS station on this island accelerated from 1.4 mm/year to 6.6 mm/year, and from 0.8 mm/year to 10.3 mm/year, when SW1 and SW2 occurred, respectively (Figure 3.13a). Based on the long duration of accelerated periods, I speculate that the two rifting episodes may have been followed by years of post-rifting stress diffusion as seen in NE Iceland after the 1975 Krafla rifting episode (e.g. Foulger et al., 1992). They might have let the block between the Okinawa Trough and the Ryukyu Trench move faster southward over several years after SW1 and SW2, and then have caused the positive trend changes of the slip accumulation curve. The enhanced convergence by SW1 seems to decay in four years or so (Figure 3.13a). It is shorter than the accelerated period lasting over ten years in NE Iceland (Heki et al., 1993). The decay of the second episode is still not obvious at present (Figure 3.13a). In addition to the post-rifting stress diffusion, I consider that the afterslip of EQ4 also has contributed to the increased slip accumulation rate in 2002 as suggested by Nakamura (2009).

Except for the increases mentioned above, one gradual slowdown of the slip accumulation rate is seen around 2007 (Figure 3.9a). Since this event is not accompanied by any corresponding event, I suspect that it reflects the natural decay of the increase that started in 2002. Based on this, another slowdown of the slip rate would appear in the coming years, which is due to the decay of the second acceleration episode in 2013.

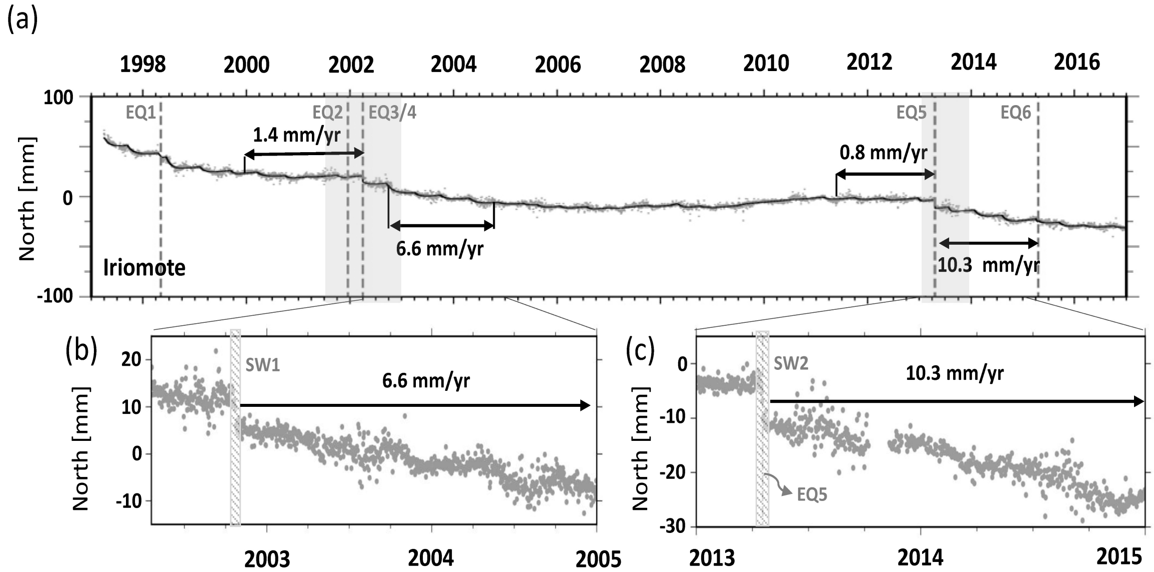

Figure 3.13. (a) Daily north coordinate of the Iriomote station. Southward movements of this island accelerated significantly after SW1 and SW2. Gray shaded rectangles represent two epochs, when the slip accumulation increased. (b) and (c) Enlarge segments of (a) around SW1 and SW2.

3.4.2 Stress increases and the enhancement of slips

In general, transient stress increases caused by external forces would enhance amount of slips and/or the event rate. For example, in the Boso area, Central Japan, the transient stress increase caused by the 2011 Tohoku-oki earthquake encouraged the earlier recurrence of the next SSEs (Hirose et al., 2012). However, in the southwestern Ryukyu Arc, the transient stress increase seems to enhance only amount of slips without making the recurrence intervals shorter (see Figure 3.8b and 3.8c). It is contrary to what I expect that the increased loading would cause the increased event rate. At present, I do not have a reasonable interpretation on this phenomenon, and future studies are necessary.

3.4.3 Coupling ratio of the SSE fault patches

Heki and Kataoka (2008) suggested that SSEs in the SW Ryukyu Arc accommodate most of the plate convergence in the Ryukyu Trench, i.e., the slip accumulation rate of the repeating SSEs was comparable to the plate convergence rate. Hence, there were no long-term stress accumulations that could lead to large interplate earthquakes in the SW Ryukyu subduction zone. With the present dataset, I recalculated the coupling ratio of the SSE fault patch. Considering the average slip for the SSEs of 4.5 cm and the average recurrence interval of six months, I obtain the average slip accumulation rate of ~9 cm/year. It is about 72 % of the plate convergence of 12.5 cm/year in the SW Ryukyu Trench (Heki and Kataoka, 2008). That is, small earthquakes and the stable slips surrounding the SSE fault patches probably contain the rest (~28 %) of the plate convergence.

3.4.4 Comparison with other SSEs

In addition to the SW Ryukyu, SSEs were observed in several regions of Japan, such as the Bungo channel (e.g., Hirose et al., 1999; 2010; Hirose and Obara, 2005), the Kii channel (e.g., Kobayashi, 2014), the Tokai area (e.g., Ozawa et al., 2002; Hirose and Obara, 2006), and the Boso Peninsula (e.g., Ozawa et al., 2003, 2007, 2014; Hirose et al., 2012). Although these SSEs have similar source mechanisms (Beroza and Ito, 2011), they show diverse characteristics. Here, I study properties of series SSEs in different regions and compare them with the Iriomote SSEs. The detail information is provided in Table 3.2.

The Bungo channel separates the Japan islands of Kyushu and Shikoku, SW Japan (Figure

3.14). There the Philippines Sea Plate is subducting beneath SW Japan along the Nankai Trough (Figure 3.14), both long- and short-term SSEs are detected there (e.g., Hirose et al., 1999; Hirose and Obara, 2005). The magnitude (M_w ~6.8) and depth (~30 km) of the Bungo long-term SSEs are similar to those beneath the Iriomote SSEs, although their time constant (~1 year) and the recurrence interval (~6 years) are much longer than the Inriomote events (Hirose and Obara, 2005; Hirose et al., 2012). On the other hand, the short-term SSEs found in the Bungo channel have smaller magnitudes (M_w ~6.0) and shorter durations (< 10 days) (Hirose and Obara, 2005). Their source depths are between 20-45 km (Table 3-2), and fault patches extend northeastward to the Shikoku (Hirose and Obara, 2005).

In the Shikoku region, short-term SSEs possess similar properties to the short-term events in the Bungo channel (Obara et al., 2004; Hirose and Obara, 2005). The fault patches of these short-term SSEs are distributed on a belt-like zone extending more than 600 km (Figure 3.14). Notably, they all have a strong link with deep low-frequency tremor, deep very low frequency earthquakes (VLFEs), and low frequency earthquakes (LFEs) that occurred on the down-dip side of long-term SSE source regions (Obara et al., 2004; Hirose et al., 2010; Hirose and Obara, 2010). The coincidence of these low frequency events is referred to as episodic tremor and slip (ETS)(Hirose and Obara, 2010). Long-term SSEs are rare in Shikoku and distributed beneath the western Shikoku (Figure 3.14). Their magnitudes (M_w~6.5) are smaller than those of the Iriomote SSEs, but they have longer durations up to several months (Kobayashi, 2010; 2014). However, the recurrence intervals of these events are not well understood uncertain because of the small number of the long-term SSEs.

The Kii channel separates the Shikoku Island from the Kii Peninsula of the Kinki District, Honshu (Figure 3.14). It is different from the Bungo channel; short-term SSEs completely disappear in this region, and only one long-term SSE has been observed (Kobayashi, 2014). The magnitude of this event (M_w 6.7) is comparable to that of the Iriomote SSEs, but its duration (1-1.5 years) is much longer (Kobayashi, 2014).

Tokai area is close to the northeastern end of the Nankai Trough, Central Japan (Figure 3.14). Both long-term and short-term SSEs are active in this region (Ozawa et al., 2002; Hirose and Obara, 2006; Suito and Ozawa, 2009). The Tokai long-term SSEs have the largest magnitudes (Mw ~7.0) and long durations (~5 years) and recurrence interval (~ 10 years) among various repeating SSEs in Japan (Suito and Ozawa, 2009). On the other hand, the Tokai short-term SSEs have smaller magnitudes (Mw ~6.0) and shorter durations (2-3 days) (Hirose and Obara, 2006). Their recurrence intervals of ~ 6 months are comparable to the Iriomote events (Hirose and Obara, 2006).

The Boso Peninsula is located in the Kanto District, Central Japan. Its tectonic setting is complicated, i.e. there the Philippines Sea Plate and the Pacific Plate subduct underneath the SW and NE Japan along the Sagami Trough and Japan Trench, respectively (Figure 3.14). Long-term SSEs do not occur in this region; only short-term SSEs have been detected (Ozawa et al., 2003, 2007, 2014; Hirose et al., 2012). The magnitudes of the Boso short-term events (M_w ~6.6) are comparable to those of the Iriomote SSEs, but their recurrence intervals (5-7 years) are much longer (Ozawa et al., 2007; Hirose et al., 2012). A unique point of these repeating short-term SSEs is their relatively short duration, less than 10 days, for their magnitudes (Hirose et al., 2012).

Comparing the long-term SSEs in Japan, I find that the Iriomote SSEs have a short recurrence interval (6 months) and time constants (~0.1 years)(Table 3-2). This may reflect the high plate convergent rate of the SW Ryukyu Trench (Heki and Kataoka, 2008). Their average magnitude (Mw ~6.7) just falls in the middle value, and the source depth of ~30 km is similar to other long-term SSEs (Table 3-2).

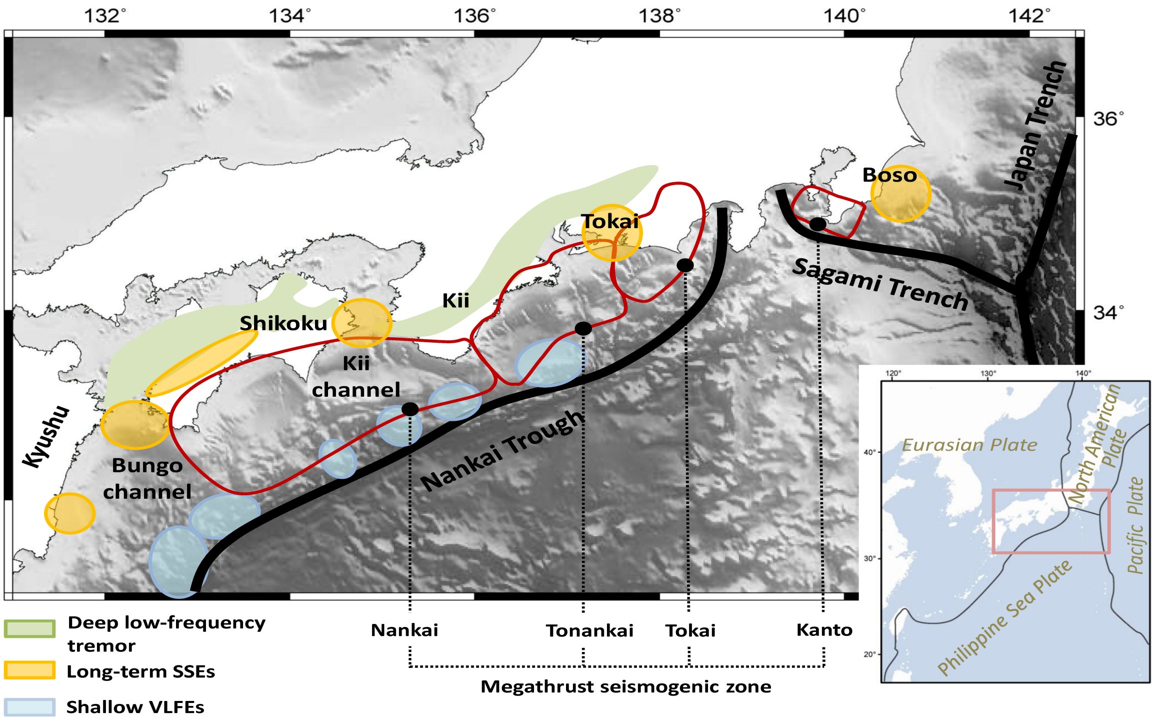

Figure 3.14 Distribution of slow earthquakes and megathrust earthquakes in southwestern Japan. Green zones display the locations of deep low-frequency tremor. Yellow and blue circles are the long-term SSEs and shallow VLFEs, respectively. The regions outlined in red denote seismogenic zones for future megathrust earthquakes. (Modified from Obara and Kato, 2016)

Table 3-2. The properties of SSEs in different regions of Japan, and their relationships with other seismic activities.

	SW Ryukyu	N Ryukyu	Bungo channel	Shikoku	Kii channel	Tokai	Boso
Type	Long-term	Short-term	Long-term Short-term (ETS)	Long-term Short-term (ETS)	Long-term	Long-term Short-term	Short-term
Magnitude (M_w)	(L) ~6.7	(S) 5.6-6.8	(L) ~6.8 (S) 5.8-6.2	(L) ~6.5 (S) ~6.0	(L) 6.7	(L) ~7.1 (S)~6.0	(S) ~6.6
Recurrence Interval	(L) ~6 mos.		(L) ~6 yrs.	(S) ~6 mos.		(L) ~10 yrs. (S) ~6 mos.	(S) 5-7 yrs.
Time constant /duration	(L) ~0.1 yrs.	(S) ~2 weeks	(L) 3 mos-1 yrs. (S) <10 days	(L) several mos. (S) ~1 week	(L) 1-1.5 yrs.	(L) ~5 yrs. (S) 2-3 days	(S) 10 days
Depth (km)	(L) ~30	(S) 10-60	(L) ~30 (S) 20-45	(S) 30-45	(L) 20-30	(L) 20-30 (S) ~35	(S) ~15
Link with other seismic activates	VLFEs		Shallow VLFEs and deep tremor	Deep tremor, DVLFE, LFE		(S) tremors	EQ swarms
Reference	Heki & Kataoka, 2008 Tu & Heki, 2017	Nishimura, 2014	Hirose et al., 1999; 2010 Hirose & Obara, 2005	Obara et al., 2004 Kobayashi, 2010 Hirose & Obara, 2010	Kobayashi, 2014	Ozawa et al., 2002; Hirose and Obara, 2006; Suito and Ozawa, 2009	Ozawa et al., 2003, 2007, 2014; Hirose et al., 2012

(L) Long-term SSE (S) Short-term SSE

3.5 Summary

- From 1997 to 2016, I identified 38 SSEs repeating biannually beneath the Iriomote Island in the southwestern Ryukyu Arc. These events occurred at the same fault patch as those reported by Heki and Kataoka (2008).
- The slip accumulation rate of these SSEs significantly increases in 2002 and 2013, which is consistent with the activations of the back-arc spreading indicated by the earthquakes swarms in the Okinawa Trough.
- The accelerated southward movement of the block between the Okinawa Trough and the Ryukyu Trench caused by post-rifting stress diffusion might induce the increase of the slip accumulation rate of the SSEs.
- The repeating SSEs accommodate about 72% of the plate convergence in the SW Ryukyu subduction zone.

Chapter 4.

Very Low Frequency Earthquakes (VLFEs)

4.1 Introduction

4.1.1 What is a very low frequency earthquake (VLFE)?

Very low-frequency earthquakes (VLFEs) belong to the category of slow earthquakes dominated by the low frequency energy of 0.1-0.01 Hz with little or no high frequency content (Obara and Ito, 2005). In comparison with ordinary (or regular) earthquakes, these events have a longer duration (~20 s) and consist predominantly of long-period waves (Beroza and Ito, 2011). Hence, only high sensitivity broadband seismometers can record such low-frequency signals. Furthermore, VLFEs can be classified into two groups, the volcanic VLFEs related to the fluid or magma transportation (e.g., Arciniega-Ceballos et al., 1999) and the nonvolcanic VLFEs generated by the shear faulting of subduction zones (e.g., Obara et al., 2004b). For the nonvolcanic VLFEs, we still can divide them into shallow VLFEs in accretionary prisms near trench axes (e.g., Obara and Ito, 2005; Ito and Obara, 2006a) and deep VLFEs that occur at the downdip limit of the seismogenic zones often associate with episodic tremor and slips (ETSs, Ito et al., 2007; Ghosh et al., 2015; Baba et al., 2018).

4.1.2 Where do VLFEs occur?

Unlike worldwide distribution of SSEs (Figure 3.1), VLFEs have been observed in a few subduction zones, such as the Nankai Trough (e.g., Obara and Ito, 2005; Ito and Obara, 2006a; Asano et al., 2008), the Japan Trench (e.g., Matsuzawa et al., 2015), the offshore of Hokkaido (e.g., Obara et al., 2004b; Asano et al., 2008), and the Cascadia Subduction Zone (e.g., Ghosh et al., 2015) (Figure 4.1). Because large interplate earthquakes often occur in these subduction zones, VLFEs, like other slow earthquakes, are considered to link with megathrust earthquakes (Obara and Kato, 2016). However, at present, some studies also found that VLFEs occur in weakly coupled plate boundaries, such as the Ryukyu subduction zone (Ando et al., 2012; Nakamura and Sunagawa, 2015) (Figure 4.1).

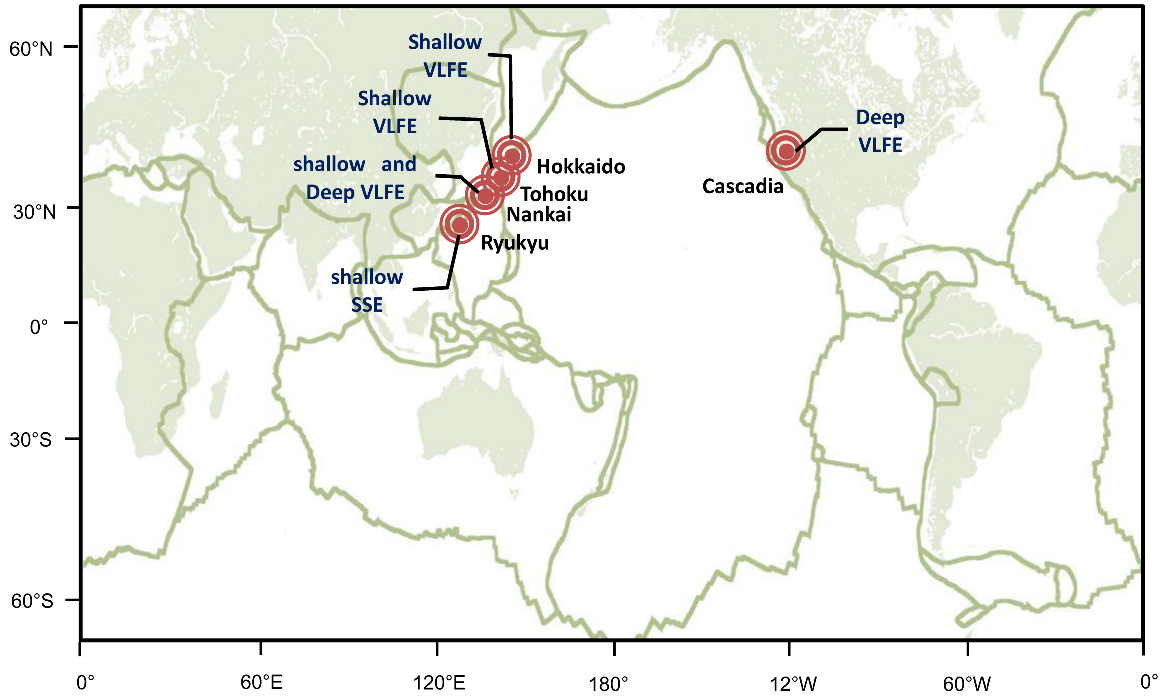

Figure 4.1. Global distribution of nonvolcanic very low frequency earthquakes (VLFEs). (Modified from Obara and Kato, 2016.)

4.1.3 VLFEs in the Ryukyu Trench

Several studies indicated that the Ryukyu subduction zone is a decoupled or weakly coupled plate boundary (e.g., Peterson and Seno, 1984; Scholz and Campos, 2012), but a number of VLFEs were detected in this subduction zone (Ando et al., 2012; Nakamura and Sunagawa, 2015). These VLFEs occurred at depths of < 60km along the Ryukyu trench axis with a thrust fault mechanism. Ando et al. (2012) thus inferred that the VLFEs are distributed within an accretionary prism or on the shallow plate interface of the Ryukyu Subduction Zone. Moreover, Nakamura and Sunagawa (2015) hypothesized that the VLFEs in the southwestern segment of the Ryukyu Subduction zone probably have been activated via repeating SSEs beneath Iriomote Island (Heki and Kataoka, 2008).

4.1.4 Purposes of this study

Ando et al. (2012) studied the properties of VLFEs along the Ryukyu Trench, but their activities are still not clear due to the short span of data sampling (one year). Subsequently, Nakamura and Sunagawa (2015) analyzed long-term (12 years) activities of VLFEs in Ryukyu. However, their study provides neither focal mechanism, nor accurate hypocenters because of unclear onset of long-period first-motion waveform data recorded at sparse seismic stations. To overcome these predicaments, I extend the time span of data sampling to eight years and determine the locations and source mechanisms of VLFEs using a waveform inversion technique (Nakano et al., 2008). In this chapter, I focus on the spatiotemporal variations and characteristic behaviors of VLFEs and try to clarify the relationships between SSEs and VLFEs in the Ryukyu area. I expect that the results can help us understand the generation of slow earthquakes and various slip phenomena on the plate boundaries during the subduction processes. Moreover, I attempt to propose a subduction model for the Ryukyu Trench to compare with the model for the Nankai Trough.

4.2 Data and method

4.2.1 Detection of VLFEs

I analyzed vertical component seismograms in 2005-2012 obtained from ten broadband seismic stations of the F-net by National Research Institute for Earth Science and Disaster Resilience (NIED) of Japan and BATS by Institute of Earth Science (IES) of Taiwan (Figure 4.2). Because the short-period (0.2−1 Hz) noise level is too high to detect VLFE signals, all raw seismic data were bandpass-filtered at 0.02−0.06 Hz (Figure 4.3). After detecting low-frequency signals from the filtered seismograms, I removed teleseismic and local earthquakes referring to earthquake catalogs of Preliminary Determination of earthquakes (PDE, USGS), Japan Meteorological Agency (JMA), and Taiwan Central Weather Bureau (CWB). A few un-cataloged microearthquakes (< M_w 2.5) were also found among the signals, and I deleted them via 1.0 Hz high-pass filtered seismograms. Through these steps, I identified 29,841 VLFEs in the Ryukyu area, whose seismic waves arrived first at one of the seven F-net stations.

Figure 4.4 shows a typical sequence of VLFE activities in Ryukyu recorded at both F-net and BATS broadband seismic stations. Their first arrival times indicate that these events occurred around IGK and YNG stations (Figure 4.2). Moreover, the sequence of VLFEs lasted several hours like an earthquake swarm, which is a primary form of VLFE activities in the Ryukyu area.

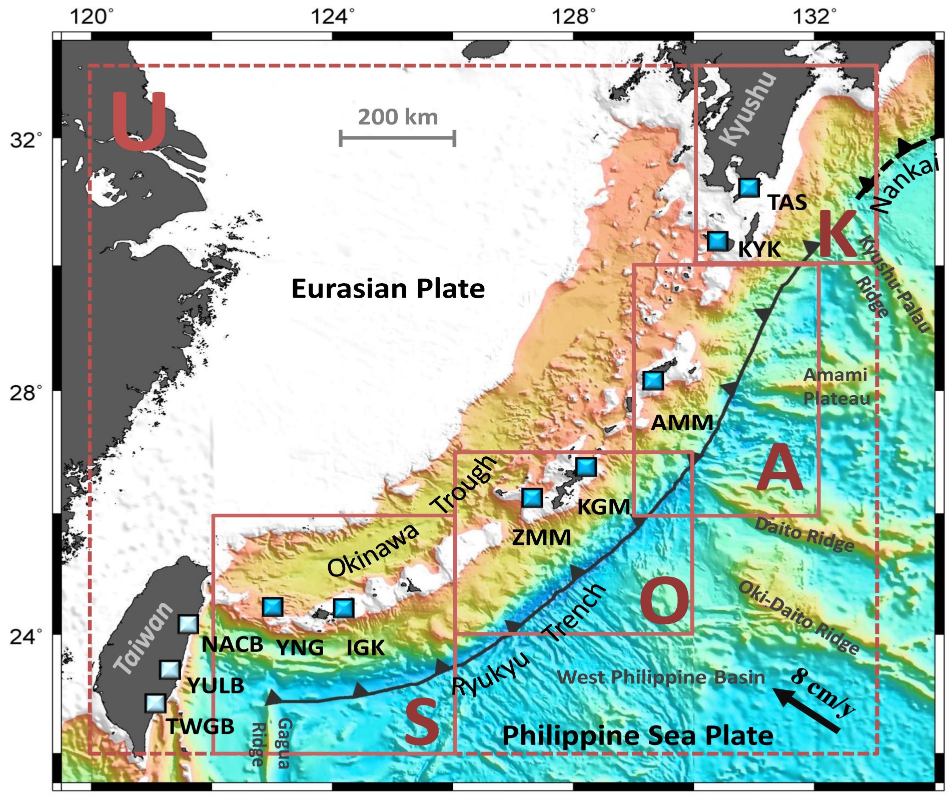

Figure 4.2. Index map of the Ryukyu area. Area U represents the geometric extent of the grid search for the waveform inversion analysis, and the rectangles of S, O, A and K indicate the four sub-areas of Sakishima, Okinawa, Amami, and southern Kyushu, respectively. The blue squares show ten broadband seismic stations of F-net (dark blue) and BATS (light blue) used in this study. The black arrow shows the average convergence rate of ~8 cm/y between the Philippine Sea Plate and Eurasian Plate (Nakamura, 2009). Kyushu-Palau Ridge near the southern Kyushu area (K) is the boundary between the Ryukyu Trench (black solid line) and the Nankai Trough (black dash line). The West Philippine Basin is located at the northwestern Philippine Sea Plate, which is subducting along the Ryukyu trench over 1200 km-long segment bounded by the Kyushu-Palau Ridge in the east and the Gagua Ridge in the west. The West Philippine Basin has a smoothed seafloor around the Sakishima (S) and Okinawa (O) areas, but it becomes uneven in the Amami area (A) where several old oceanic ridges (Oki-Daito Ridge, Daito Ridge, and Amami Plateau) lie or partly subduct at the trench.

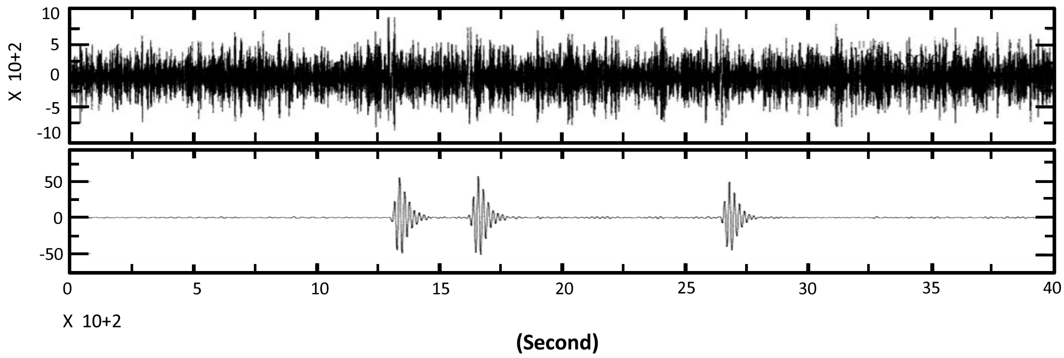

Figure 4.3. Vertical component seismograms of a sequence of VLFEs for a period of 4000s recorded at IGK, SW Ryukyu. The top and bottom diagrams show the raw and bandpass filtered (0.02-0.06 Hz) broadband seismograms, respectively. Three VLFEs are seen at approximately 1300s, 1650s, and 2700s in the filtered seismogram but cannot be identified in the raw seismogram.

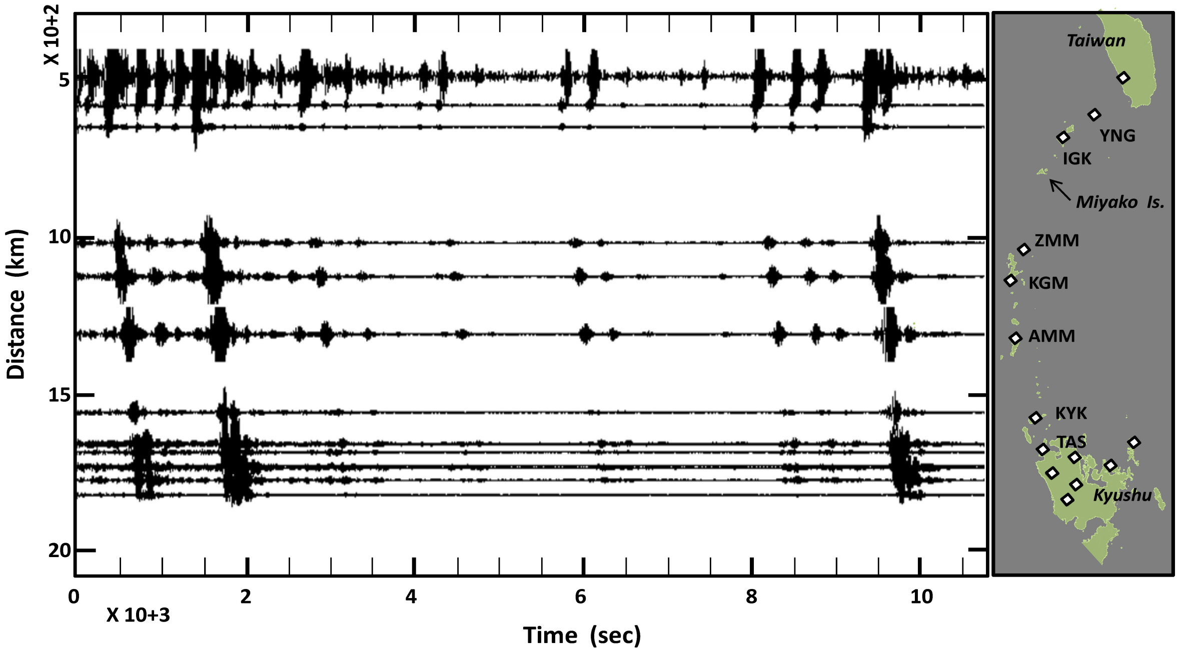

Figure 4.4. Three-hour vertical component seismograms of a sequence of VLFEs obtained from broadband seismic stations of F-net and BATS (diamonds in the right diagram). The bandpass filtered (0.02-0.06 Hz) seismograms are arranged, from top to bottom, based on increasing distance northward from 120°E−20°N (they correspond to the stations shown in the map to the right). The origin time is comparable to (UT) 20:55:00, on Nov. 9, 2007.

4.2.2 Determination of hypocenters and mechanisms

To determine source locations and mechanisms of VLFEs in Ryukyu, I adopted a grid-search moment-tensor inversion program (Nakano et al., 2008). This program can provide a stable solution of hypocenter and focal mechanism using data from a small number of stations. Assuming a double-couple source model, this inversion program locates a target earthquake at a spatial grid point and determines its strike, dip, and rake of the earthquake fault using a 1-D seismic velocity model (AK135, Kennett et al., 1995).

First, I calculated the Green's functions of full waves at each grid point with a horizontal interval of 0.5° and a vertical interval of 10 km in the area U (22°N-33°N and 120°E-133°E). For the waveform inversion analysis, I selected 1,504 VLFEs with a maximum velocity amplitude of > 10 nm/s and a low ambient noise level. After obtaining approximate hypocenters of VLFEs, I reduced the horizontal spacing to 0.2° for estimating more accurate hypocenters in the Sakishima, Okinawa, Amami, and southern Kyushu areas (Figure 4.2). Here, I selected at least two seismic stations for each area to let the epicentral distance of every event < 300 km, i.e., YNG and IGK for the Sakishima area, ZMM and KGM for the Okinawa area, AMM, KGM, and KYK for the Amami area, and KYK and TAS for the S. Kyushu area (Figure 4.2). Such setting of seismic stations is appropriate for the inversion analysis of this study.

Figure 4.5 shows an example for the inversion result of a VLFE on Mar 6, 2005, at 125.4°E−23.8°N with a depth of 30 km. Its moment magnitude (M_w) is 4.0. The best-fit model is a reverse faulting mechanism with a slight strike-slip component. Three-component (EW, NS, and Z) seismograms of YNG and IGK stations were used for the inversion analysis of waveform data of this event.

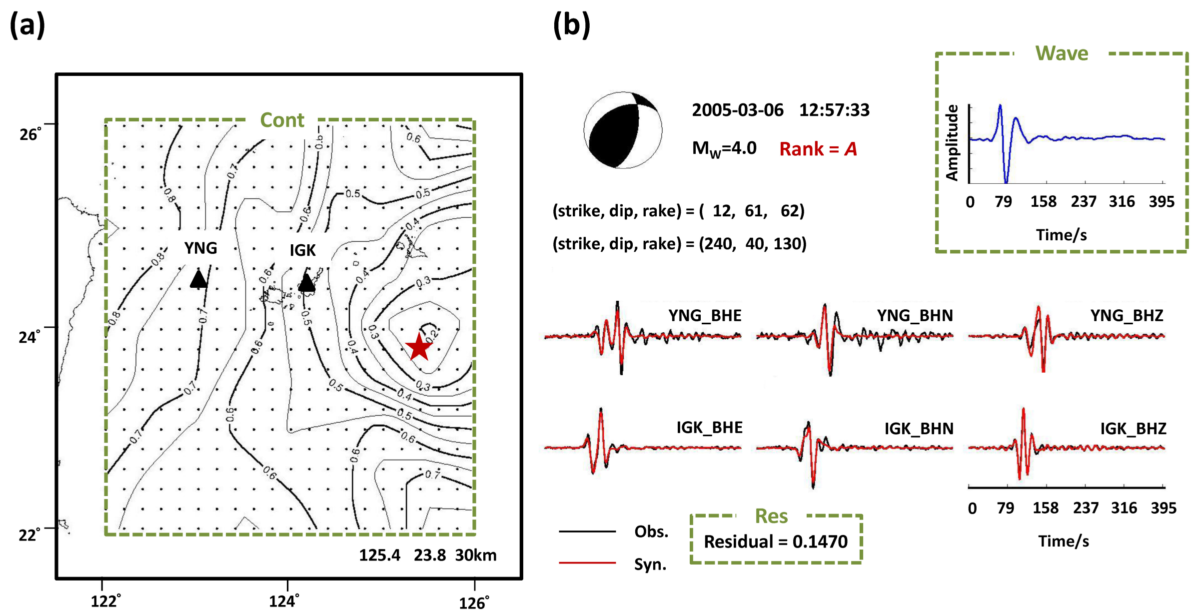

Figure 4.5. (a) The source location (star) of VLFE #30 (see Supplement 1). The contours display the residuals between synthetic and observed waveforms obtained from the hypocenter and CMT grid search. (b) The CMT solution of the VLFE #30. The beach ball at the top shows the best-fit focal mechanism. The obtained waveform at the source is shown at the top right corner. The bottom displays the three-component waveforms of the synthetic (red lines) and observed (black lines) seismograms. The dashed rectangles in green indicate three categories of the residual (Res), waveform at the source (Wave), and shape of residual contours (Cont) for evaluating the reliability of the inversion results. According to Table 4-1 and 4-2, the quality value of this event is 9 and is defined as rank *A*.

4.2.3 Reliability of inversions

After obtaining locations and centroid moment tensor (CMT) solutions of the VLFEs, I evaluated the reliability of inversion results using quality ranks *A* (good), *B* (fair), and *C* (poor) based on three categories, that is, the residual (Res), waveform at the source (Wave), and shape of residual contours (Cont) (Table 4-1; Figure 4.5). I assigned three grades (good=3, fair=2, poor=1) for each category. If the sum of grades is ≥ 8, the inversion results will be defined as rank *A*. However, if the sum falls into 5-7, they will be assigned as rank *B,* and if the sum ≤ 4, assigned as rank *C* (Table 4-2). For example, the VLFE #30 (Figure 4.5) has values of Res=3, Wave=3, and Cont=3, and defined as rank *A* (i.e., Res + Wave + Cont).

Table 4-1. Evaluation points for the inversion results

Point	(1) Residual of waveform matching	(2) Waveform at the source	(3) Shape of residual contours
3 (good)	<0.2	Simple and clear	Circular
2 (fair)	0.2−0.3	Slight noisy	Elliptical
1 (poor)	>0.3	Very noisy	Elongated or unclosed

Table 4-2. The quality ranks of inversion results based on the quality value

	Rank A (good)	Rank B (fair)	Rank C (poor)
Quality value	9, 8	7, 6, 5	4, 3

4.3 Results

4.3.1 Waveform characteristics

I observed 29,841 VLFEs in the Ryukyu area during 2005–2012. To understand differences in waveform characteristics between VLFEs and ordinary earthquakes, I arbitrarily selected a VLFE and an ordinary earthquake that have the same magnitude (M_w 4.6) and are located within a distance of 50 km from each other. Vertical-component seismograms of the two earthquakes were processed with two filters: a band-pass filter of 0.02-0.06 Hz and a high-pass filter of 1 Hz. The bandpass-filtered waveforms of the ordinary earthquake and the VLFE both have low-frequency components (Figure 4.6). However, the high-pass-filtered waveform is ample in the ordinary earthquake but is absent from the VLFE. Moreover, the spectrograms of VLFEs and ordinary earthquakes also display a spectrum swell between 0.03 and 0.15 Hz, whereas another swell of >1 Hz only exists in the ordinary earthquakes (Figure 4.7). It suggests that the VLFEs predominantly consist of long-period waves (0.03-0.15 Hz) without high-frequency content (>1 Hz).

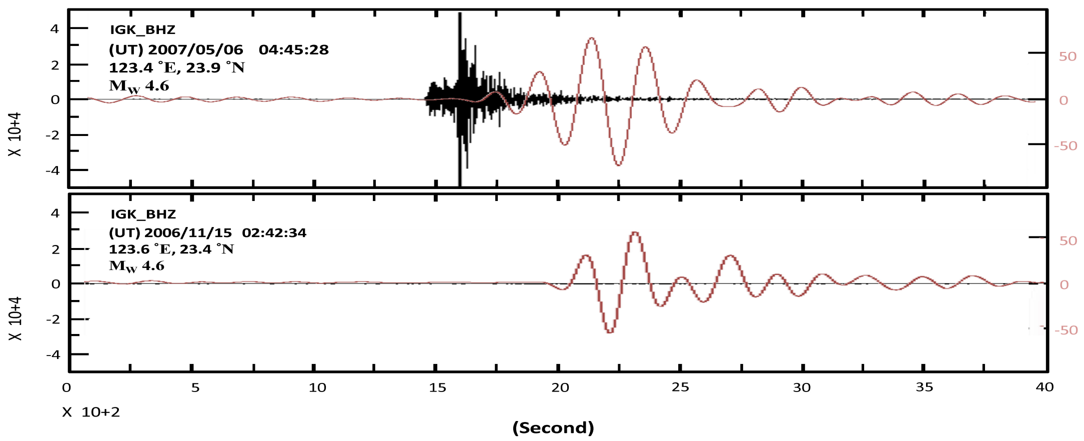

Figure 4.6. Vertical-component waveforms of an ordinary earthquake (upper) and a VLFE

(lower) recorded at IGK. Highpass filtered waveforms at 1 Hz (black) and bandpass filtered waveforms in 0.02-0.06 Hz (red) are shown in the same diagram. The units for the black and red waveforms are given on the left and right axes (nm/s), respectively. The origin time, location, and magnitude (M_w) of the two events are provided at the upper left of each diagram.

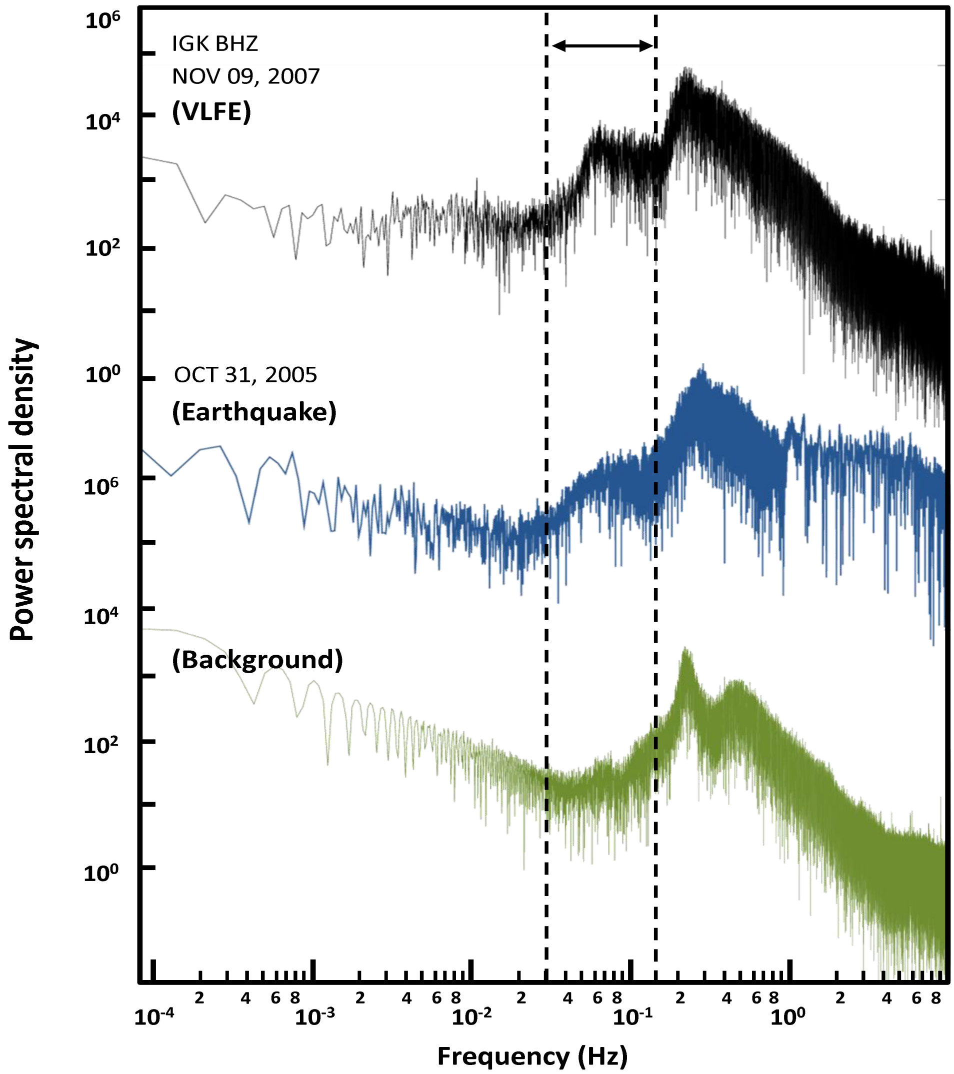

Figure 4.7. Spectra of three-hour vertical-component seismograms of VLFEs (black) depicted in Figure 4.4, an ordinary earthquake (blue), and background noise (green) at IGK station. The two dashed lines define the dominant frequency range (0.03-0.15 Hz) of the VLFEs. The spectrum swell between 0.03 and 0.15 Hz appears in the spectra of VLFEs and ordinary earthquakes, but the other swell of >1 Hz only exists in the spectrum of ordinary earthquakes. Vertical positions of these spectra are arbitrary.

4.3.2 VLFE activities

To analyze activities of the VLFEs, I divided all 29,841 events into four sub-areas of Sakishima, Okinawa, Amami, and southern Kyushu (Figure 4.2) based on the first arrivals of waveforms. For example, if seismic waves of a VLFE arrive first at IGK, this event will be grouped into the Sakishima area. Here, I assigned one or two seismic stations for each area in the present study, i.e., YNG and IGK to Sakishima, ZMM and KGM to Okinawa, AMM to Amami, and KYK and TAS to southern Kyushu (see Figure 4.2).

Figure 4.8 shows the VLFE time series of the four areas. Notably, M_{JMA} 5-7 earthquakes sometimes activate VLFEs or occur together with VLFE activities. For instance, a sequence of VLFEs started one day after an M_{JMA} 5.0 earthquake (see EQ-I in Figure 4.8) on 2 Apr 2006, ~90 km south of IGK in the Sakishima area. Likewise, during an active period of VLFEs on Dec. 2-7 2006, an M_{JMA} 5.0 earthquake (see EQ-II in Figure 4.8) occurred ~100 km southeast of KGM in the Okinawa area. However, every M_{JMA} 5-7-class earthquake not necessarily linked with a VLFE activity. The M_{JMA} 7.2 earthquake (see EQ-III in Figure 4.8) in 2010 is a typical example. This earthquake occurred near the Okinawa Island but did not activate any VLFEs around it. Table 4.3 provides the detail information of ordinary earthquakes that activated VLFEs in the Ryukyu region.

A few teleseismic events can induce VLFEs. For instance, 11 hours after the Sichuan earthquake on May 12, 2008 (M_w 7.9) (see Sichuan in Figure 4.8), VLFEs in southern Kyushu became active and lasted 10 days (May. 12-21, 2008). Similar activations were also seen after the Kuril earthquake of Nov. 15, 2006 (M_w 8.3), and the Tohoku-Oki earthquake of Mar. 11, 2011 (M_w 9.1) (see Kuril and Tohoku in Figure 4.8). However, such a phenomenon has occurred only in southern Kyushu but has never seen in the other areas (Sakishima, Okinawa, and Amami). Supplement 1-F1 provides 24-hour seismograms recorded at all F-net stations after the M_w 8.3 Kuril earthquake occurrence, which displays a typical VLFE activation in the southern Kyushu area.

Figure 4.9 shows the cumulative number of VLFEs for the four areas. I noted that the cumulative curves of the Sakishima, Okinawa and Amami areas increased linearly with time, but that of Southern Kyushu showed a step-like shape, i.e., having relatively quiescent epochs between two active periods. This suggests that the VLFE behaviors of the two groups are probably different. To compare the temporal change of VLFE activities in the four areas, I normalized yearly VLFE counts with the maximum number of each area (Figure 4.10). From 2005 to 2009, the normalized curves of Sakishima, Okinawa, and Amami are quite alike but significantly different from that of Southern Kyushu (Figure 4.10). It means that VLFE activity of the southern Kyushu is distinct from the three other areas. Nevertheless, from 2010 to 2012, the four curves seem to show a similar tendency, which may have occurred coincidentally or due to some unknown reasons. These observations indicate that VLFE activities in the three areas of Sakishima, Okinawa, and Amami along the Ryukyu Trench are somehow tectonically linked but detached from the southern Kyushu area.

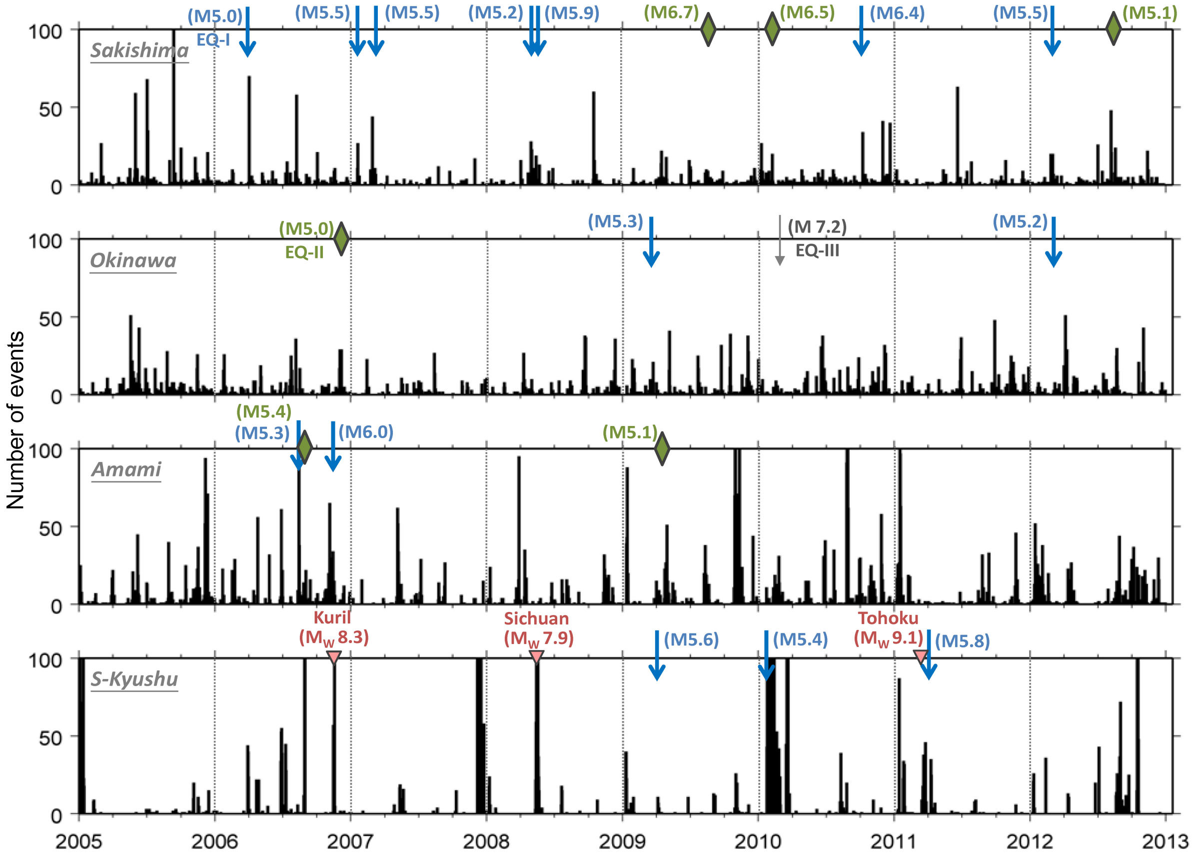

Figure 4.8. Time series of VLFE activities in the Sakishima, Okinawa, Amami, and southern Kyushu areas. Solid bars show the daily count of VLFEs. The blue arrows indicate ordinary earthquakes ($M_{JMA} \geq 5$) that triggered VLFEs, and green diamonds mark local earthquakes that occurred concurrently with VLFE activity. The grey arrow shows an M_{JMA} 7.2 earthquake that did not trigger any VLFEs. The three red inverse triangles indicate teleseismic events that triggered VLFEs in the southern Kyushu area. The source information of 14 local earthquakes (blue arrows) and 3 teleseismic earthquakes (red inverse triangles) are given in Table 4.3

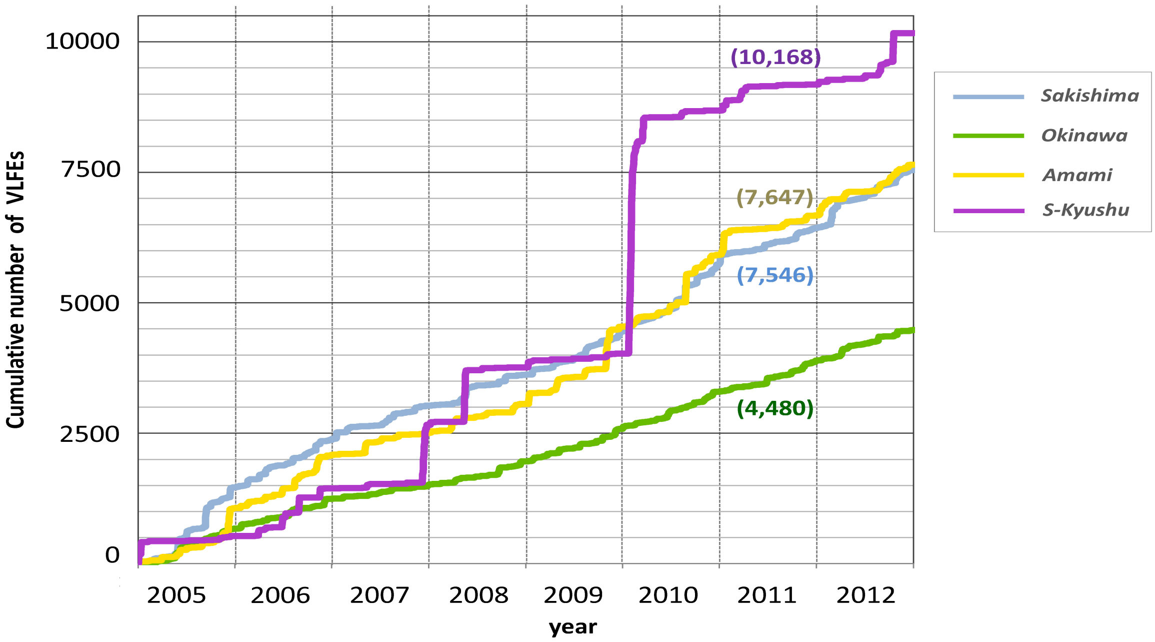

Figure 4.9. Cumulative number of VLFEs for the Sakishima (blue line), Okinawa (green line), Amami (yellow line), and southern Kyushu (purple line) areas.

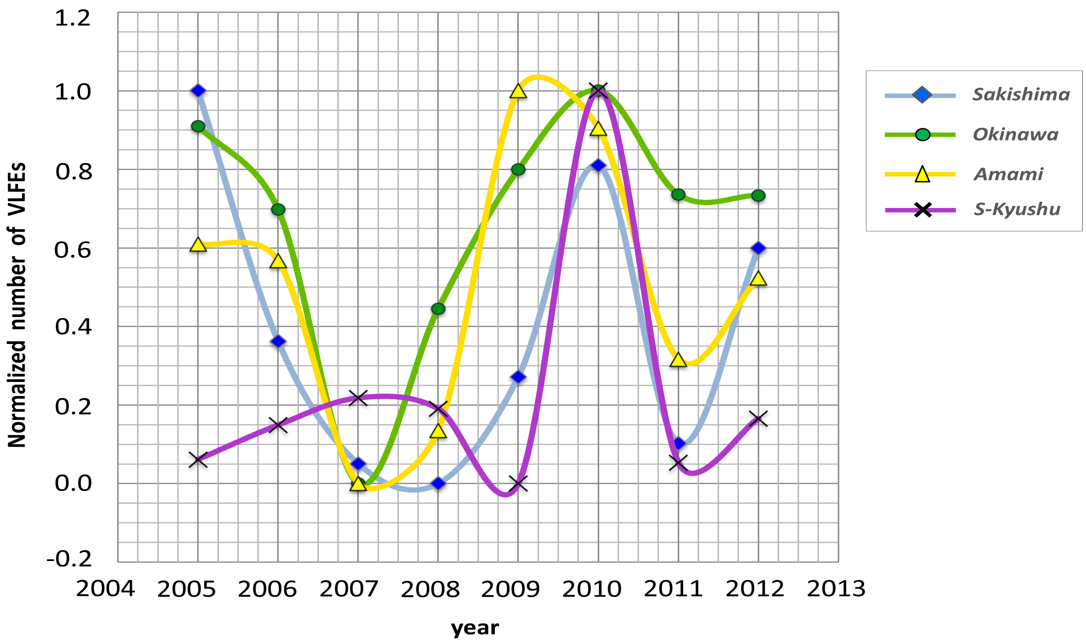

Figure 4.10. Smoothed yearly count of VLFEs normalized by the count (max – min) for each of the Sakishima (blue line), Okinawa (green line), Amami (yellow line), and southern Kyushu (purple line) areas.

Table 4-3. Source information of the 17 earthquakes that triggered VLFEs.

Type	Area	Time (UT)	Lon (°E)	Lat (°N)	Depth (km)	M_{JMA}/M_w	Epicentral distance (km)*
Local	Sakishima	20060402050830	123.91	23.48	36	5.0	70
Local	Sakishima	20070116031035	122.44	23.99	28	5.5	90
Local	Sakishima	20070307225717	122.42	24.03	19	5.5	90
Local	Sakishima	20080427173208	125.07	24.86	32	5.2	200
Local	Sakishima	20080510194200	122.43	23.95	32	5.9	90
Local	Sakishima	20101004132838	125.33	24.21	53	6.4	200
Local	Sakishima	20120227011146	123.36	23.83	30	5.5	10
Local	Okinawa	20090322144546	128.66	26.02	50	5.3	90
Local	Okinawa	20120307061808	127.28	25.53	47	5.2	60
Local	Amami	20060812183917	130.17	28.69	55	5.3	110
Local	Amami	20061117180312	130.15	28.51	30	6.0	90
Local	S-Kyushu	20090405093626	131.89	31.92	28	5.6	160
Local	S-Kyushu	20100125071509	131.15	30.87	49	5.4	180
Local	S-Kyushu	20110409125749	131.83	30.01	61	5.8	150
Teleseismic	Kuril	20061115111413	153.26	46.59	10	M_w 8.3	2500
Teleseismic	Sichuan	20080512062801	103.32	31.00	19	M_w 7.9	2700
Teleseismic	Tohoku	20110311054624	142.37	38.29	29	M_w 9.1	1200

* The epicentral distance from the causative earthquake to the triggered VLFEs

4.3.3 Hypocenters

From 2005 to 2012, I detected a total of 29,841 VLFEs in the Ryukyu area, but only 1,504 events with large amplitudes and low ambient noise levels were applicable for the waveform inversion analysis. Using the moment tensor inversion developed by Nakano et al. (2008), I obtained the locations and CMT solutions of the 1,504 VLFEs. The detailed source parameters of these VLFEs are provided in Supplement 1. The numbers of the VLFEs assigned to ranks *A*, *B*, and *C* are 299, 751, and 454, respectively. However, I deleted 454 events due to their low-quality solutions (quality rank *C* in Table 4.2). Figure 4.11 shows the distribution of the rest 1,050 VLFEs, whose quality ranks are *A* or *B.* These VLFEs are all located along the Ryukyu Trench axis with source depths of 5-60 km (Figure 4.11; Supplement 1). Notably, the VLFEs near YNG and IGK stations (Sakishima area) and those near ZMM and KGM stations (Okinawa area) appear to have well concentrated, while the VLFEs around the AMM station (Amami area) are scattered over the entire area in the fore-arc side bounded by the Ryukyu Trench axis and Okinawa Trough (Figure 4.10). Considering these solutions all have high quality, the scattered distribution in the Amami area is probably related to the location of operational seismic stations, but not caused by low-quality data.

To examine above speculation and clarify the reliability of VLFE locations determined by the waveform inversion method of this study, I attempted to compare hypocenters of ordinary earthquakes determined by F-net and those solved by my approach. For this analysis, I applied the same inversion method to 31 ordinary earthquakes with $M_{JMA} > 4$, which were selected arbitrarily from the Ryukyu region (Figure 4.12). The seismic network, stations, and filter-band used in this analysis were the same as those used for the VLFEs mentioned above. Figure 4.12 displays hypocenters of these ordinary earthquakes obtained from my inversion method and those imported from the F-net earthquake catalog (http://www.fnet.bosai.go.jp/event/joho.php?LANG=ja, accessed on 25 Jan., 2018). As described on the website, the epicenters of the F-net catalog are the same as those of JMA, but the depths, magnitudes, and CMT solutions are determined by the inversion method of F-net. Because JMA has 2-5 times more operational seismic stations than those belonging to F-net, i.e., having a better azimuthal coverage, their hypocenter locations are more reliable in general.

The average differences between the two results for the four areas are summarized in Table 4-4a-c. It is obvious that the differences between my method and the F-net results in the Sakishima and Okinawa areas are: 0.03° ± 0.11° in longitude, 0.06° ± 0.13° in latitude, and -6 km ± 12 km in depth, respectively (Table 4-4a). These differences are as small as ~10 km, suggesting that the hypocenters of VLFEs obtained from my inversion method are sufficiently accurate and reliable in these two areas. In contrary, the differences in Amami (Table 4-4b) and southern Kyushu (Table 4-4c) are 2-5 times larger than those of the Sakishima and Okinawa. Some events have significant discrepancies in the longitudinal direction (~1°), especially around the AMM station (Table 4-4b, Figure 4.12). However, the location errors near the trench axis are relatively small, almost comparable to those in the Sakishima and Okinawa areas (Figure 4.12). These results suggest that the hypocenters of VLFEs in the Amami area are perhaps unstable and need to be dealt carefully as described in the following sections.

4.3.4 Focal mechanisms

The CMT solutions of the 1,050 VLFEs are mostly thrust faults (Supplement 1). In this section, I discuss focal mechanisms of 21 selected VLFEs, whose quality value is 9 (rank is *A*). Despite a limited number of waveforms (two or three seismic stations) used for the inversion analysis, these source mechanisms with rank A are much more reliable than other events due to their highest quality data. As illustrated in Figure 4.11, 85% of the CMT solutions show the thrust faulting mechanisms, and some of them have a little strike-slip component. It suggests that these events are caused by the compressional stresses due to the plate convergence. Since these VLFEs have shallow source depths and thrust-fault mechanisms, they probably occur on splay faults in the accretionary prism or on the plate interface of the Ryukyu subduction zone, which is similar to those observed in the Nankai Trough (Obara and Ito, 2005).

However, three strike-slip faulting mechanisms are also seen south of YNG and ZMM (Figure 4.11). Because several ordinary earthquakes in the two areas all have similar strike-slip mechanisms (Kubo and Fukuyama, 2003; Wu et al., 2010), I infer that these strike-slip VLFEs are one of the typical mechanisms in there. Additionally, these strike-slip events may relate to interactions between the back-arc spreading (Okinawa Trough) and subduction zone system (Ryukyu Trench) (Kubo and Fukuyama, 2003; Wu et al., 2010).

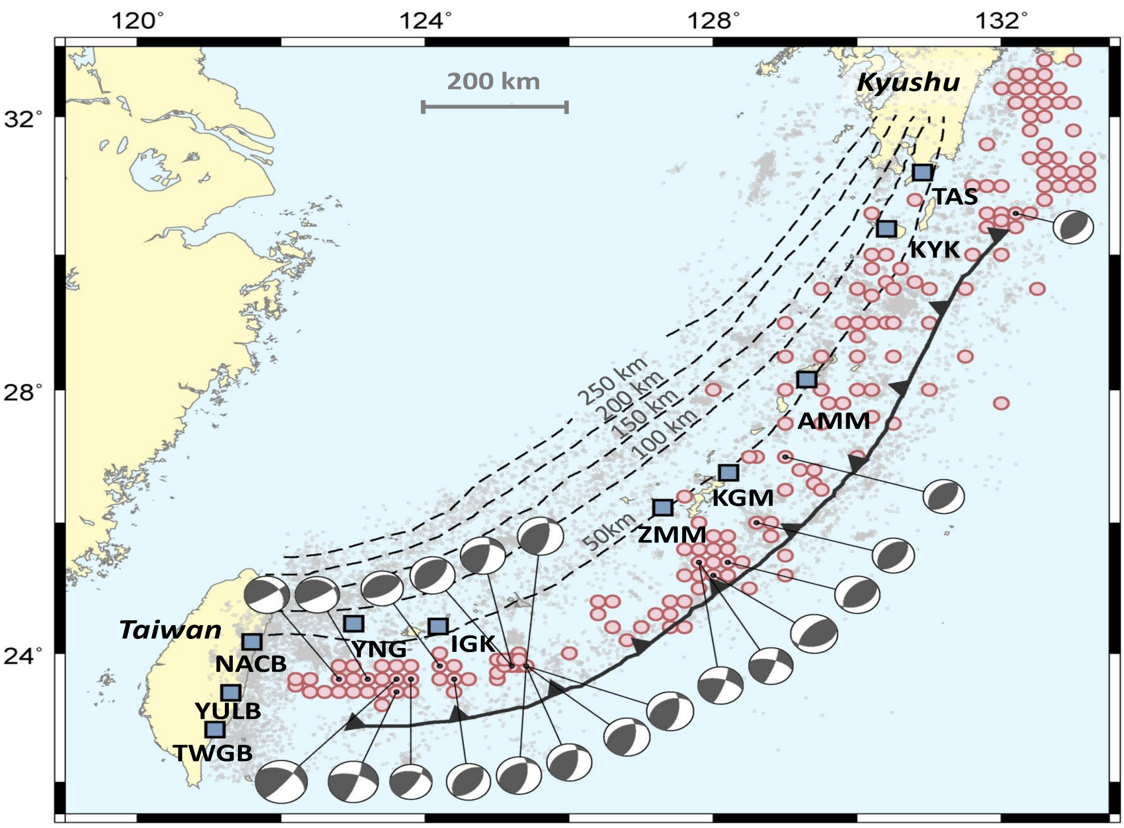

Figure 4.11. Locations and focal mechanisms of the VLFEs in the Ryukyu region. The red

circles depict the epicenter of VLFEs, whose quality ranks are *A* or *B*. The beach balls show the CMT solutions of 21 events possessing the highest quality value 9. The dashed contours display the upper depth of the Philippine Sea Plate (unit in km). The gray dots indicate the epicenters of ordinary earthquakes ($M_{JMA} \geq 3$) in 2000-2015 reported by JMA. The blue squares with a station name aside are the F-net and BATS broadband stations used in the study.

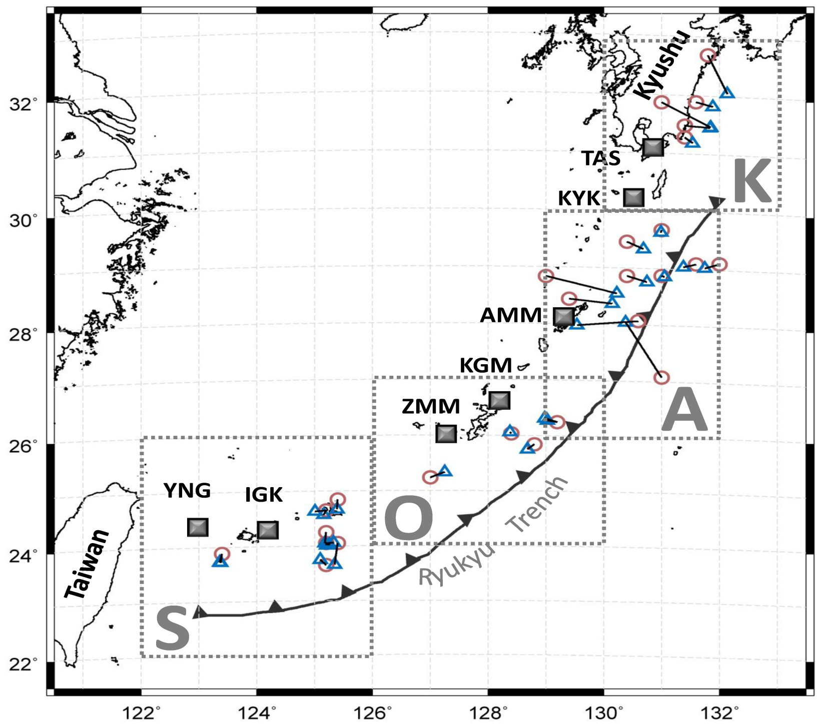

Figure 4.12. Epicenters of the 31 ordinary earthquakes obtained from the inversion method of this study (red circles) and those from the F-net earthquake catalog (blue triangles). The two epicenters (red circles and blue triangles) of the same earthquake are linked with a line. These earthquakes are selected arbitrarily from the four areas of Sakishima (S), Okinawa (O), Amami (A), and southern Kyushu (K). The differences between the two results are negligibly small in the Sakishima and Okinawa areas. However, some events in the Amami and southern Kyushu areas have large discrepancies, especially around AMM.

Table 4-3a. Comparisons of hypocenters and moment magnitudes of 16 ordinary earthquakes in the Sakishima and Okinawa areas determined by F-net and this study.

Time (JST)		F-net				This study				Difference (This study – F-net)			
		Lon	Lat	Depth (km)	M_w	Lon	Lat	Depth (km)	M_w	ΔLon	ΔLat	ΔDepth (km)	ΔM_w
2004/04/28	13:54:22	125.18	24.20	35	4.4	125.2	24.4	20	4.0	0.02	0.20	-15	-0.4
2004/07/22	18:45:13	129.03	26.43	23	6.1	129.2	26.4	5	5.8	0.17	-0.03	-18	-0.3
2007/03/07	01:30:58	123.38	23.84	20	4.3	123.4	24.0	20	4.1	0.02	0.16	0	-0.2
2007/05/03	05:31:43	125.35	23.81	17	4.3	125.4	24.2	30	4.2	0.05	0.39	13	-0.1
2007/05/06	12:45:28	123.36	23.85	20	4.6	123.4	24.0	20	4.4	0.04	0.15	0	-0.2
2009/08/05	09:17:58	125.26	24.17	35	6.1	125.2	24.2	10	6.0	-0.06	0.03	-25	-0.1
2009/08/05	20:26:47	125.21	24.16	35	4.6	125.2	24.2	10	4.4	-0.01	0.04	-25	-0.2
2010/01/17	07:04:52	125.10	23.90	44	4.6	125.2	23.8	50	4.4	0.10	-0.10	6	-0.2
2010/02/27	05:31:25	128.68	25.91	32	7.0	128.8	26.0	20	6.8	0.12	0.09	-12	-0.2
2010/04/26	05:43:58	125.01	24.78	44	4.6	125.2	24.8	50	4.6	0.19	0.02	6	0.0
2010/10/04	22:28:38	125.33	24.21	38	6.2	125.2	24.2	20	6.0	-0.13	-0.01	-18	-0.2
2012/02/28	04:31:49	127.25	25.50	20	5.4	127.0	25.4	30	5.2	-0.25	-0.10	10	-0.2
2013/05/06	06:17:02	125.16	24.72	20	4.4	125.2	24.8	20	4.2	0.04	0.08	0	-0.2
2013/06/13	22:24:45	128.98	26.47	20	5.6	129.2	26.4	5	5.5	0.22	-0.07	-15	-0.1
2014/02/19	19:29:53	128.38	26.22	23	4.5	128.4	26.2	20	4.4	0.02	-0.02	-3	-0.1
2014/09/18	08:18:55	125.39	24.82	47	5.1	125.4	25.0	40	4.7	0.01	0.18	-7	-0.4
									Average	0.03	0.06	-6	-0.2
									std dev.	0.11	0.12	12	0.1

Table 4-3b. Comparisons of hypocenters and moment magnitudes of 10 ordinary earthquakes in the Amami area determined by F-net and this study.

Time (JST)	F-net				This study				Difference (This study –F-net)			
	Lon	Lat	Depth (km)	M_w	Lon	Lat	Depth (km)	M_w	ΔLon	ΔLat	ΔDepth (km)	ΔM_w
2003/04/05 16:49:37	130.99	29.76	26	4.7	131.0	29.8	20	4.7	0.01	0.04	-6	0
2003/08/07 12:57:00	130.38	28.18	23	4.8	131.0	27.2	5	4.6	0.62	-0.98	-18	-0.2
2004/12/29 22:20:25	130.75	28.89	20	5.6	130.4	29.0	10	5.6	-0.35	0.11	-10	0
2006/09/01 07:58:24	130.23	28.69	35	5.5	129.0	29.0	10	5.4	-1.23	0.31	-25	-0.1
2006/11/18 03:03:12	130.15	28.51	35	6.1	129.4	28.6	10	5.9	-0.75	0.09	-25	-0.2
2007/11/22 04:28:42	131.05	28.98	8	4.4	131.0	29.0	5	4.2	-0.05	0.02	-3	-0.2
2009/04/15 13:59:35	131.75	29.13	5	4.4	132.0	29.2	10	4.3	0.25	0.07	5	-0.1
2010/06/26 00:23:16	131.38	29.15	47	4.8	131.6	29.2	40	5.0	0.22	0.05	-7	0.2
2011/12/11 10:22:43	129.54	28.13	29	5.6	130.6	28.2	50	6.0	1.06	0.07	21	0.4
2012/08/06 12:28:21	130.69	29.47	23	5.4	130.4	29.6	10	5.3	-0.29	0.13	-13	-0.1
								Average	-0.05	-0.01	-8	-0.03
								std dev	0.62	0.33	13	0.18

Table 4-3c. Comparisons of hypocenters and moment magnitudes of 5 ordinary earthquakes in the southern Kyushu area determined by F-net and this study

Time (JST)	F-net				This study				Difference (This study –F-net)			
	Lon	Lat	Depth (km)	M_w	Lon	Lat	Depth (km)	M_w	ΔLon	ΔLat	ΔDepth (km)	ΔM_w
2004/04/21 12:20:53	131.84	31.56	29	5.1	131.4	31.6	5	4.8	-0.44	0.04	-24	-0.3
2005/05/31 11:04:14	131.54	31.30	32	5.7	131.4	31.4	30	5.5	-0.14	0.10	-2	-0.2
2009/04/05 18:36:26	131.89	31.92	32	5.8	131.6	32.0	5	5.4	-0.29	0.08	-27	-0.4
2013/03/11 18:34:49	131.85	31.57	35	5.5	131.0	32.0	40	5.2	-0.85	0.43	5	-0.3
2014/08/29 04:14:35	132.14	32.14	17	5.8	131.8	32.8	10	5.9	-0.34	0.66	-7	0.1
								Average	-0.41	0.26	-11	-0.22
								std dev	0.24	0.24	12	0.17

4.3.5 *b*-values

The moment magnitudes (M_w) of the 1,050 VLFEs determined by this study are between 3.2 and 4.7 (Supplement 1). This range is comparable to that of M_w 3.6-4.4 for VLFEs in the Nankai Trough (Ito and Obara, 2006) but slightly larger than M_w 3.4-3.6 for LVFEs in the Japan Trench (Matsuzawa et al., 2015). I calculated *b*-values of VLFEs in the Ryukyu region based on the M_w data. For this estimation, I first divided the 1,050 events into four areas of Sakishima (S), Okinawa (O), Amami (A), and southern Kyushu (K) (Figure 4.13). Subsequently, I adopted the maximum-likelihood method proposed by Utsu (1964) and Aki (1965),

$$b = \log e \,/(M_{mean} - M_c) \tag{4.1}$$,

where M_{mean} and M_{c} are the mean magnitude and the cut-off magnitude of the given sample, respectively. For the Sakishima area (S), I determined the M_c = 3.8 via the cumulative frequency curve of VLFEs (Figure 4.14a). Next, I calculated the average magnitude (M_{mean}) between the maximum magnitude (M_w 4.7) and the M_c (M_w 3.8). Finally, using (4.1), I obtained the *b*-value of 2.3 for the VLFEs in this area. Under this premise, I also estimated the cumulative number of VLFE as 0.4 for $M_w \geq 5.0$ over an eight-year timescale, which suggests that large VLFEs hardly occur in this area or probably the maximum size of VLFE faults is equivalent to M_w 4.8 only. Related parameters for this calculation and *b*-values of the four areas are all provided in Table 4-4.

The *b*-values of VLFEs in the Ryukyu region range from 2.3 to 5.0 (Table 4-4), significantly larger than *b*-values of ordinary earthquakes in tectonic regions (e.g., 0.7-1.1, Utsu, 2001) and for earthquakes swarms in volcanic areas (e.g., 1.5-2.0, McNutt, 2005). To confirm the rationality of high *b*-values of VLFEs in Ryukyu, I estimated *b*-values for ordinary earthquakes of the four areas in 2005-2012 and found that these values all fall in 0.9-1.2 (Table 4-4), comparable to the global average for ordinary earthquakes. Namely, the b-values of VLFEs in the Ryukyu area are intrinsically larger than those of ordinary earthquakes even if they occur in the same tectonic region.

Because the *b*-value reflects the heterogeneity of material (Mogi, 1962; Scholz, 1968), such high b-values of VLFEs in Ryukyu suggest that highly heterogeneous materials may present in the accretionary prism or on subduction plate-boundary interface. Another possible reason for the high *b*-value is the existence of high pore pressure fluid in the VLFE source region (McNutt, 2002; Nakamura and Sunagawa, 2015). In addition to the Ryukyu area, similar anomalously high *b*-values were also seen in the seamount subduction area of southernmost Nicoya, Costa Rica (Ghosh et al., 2008). This phenomenon was interpreted regarding the presence of massive fractured materials or high fluid pressure in the seismic source region (Wang and Bilek, 2014).

4.3.6 Amplitude-magnitude (A-M) relation

Based on the obtained magnitude data, I estimated an empirical relation between amplitudes and moment magnitudes of VLFEs for each area (A-M relation, Table 4-4). This method can help us estimate moment magnitudes for smaller events because only 5% of VLFEs are suitable for my waveform inversion analysis. The CMT solutions of the rest 95% of VLFEs cannot be determined because of their weak and unclear waveforms. For VLFEs in the Sakishima area (S), I obtained the following A-M relation (Figure 4.14b)

$$M_w = 0.42\log A + 3.4 \quad (4.2),$$

where A is the maximum velocity amplitude (nm/s) at the first arrival station. Applying (4.2), the moment magnitudes of all VLFEs in this area can be determined. The A-M relations for another three areas are also provided in Table 4-4. In this calculation, I did not consider traveling effect on seismic wave amplitudes because epicentral distances between VLFEs and seismic stations are all shorter than 2-6 wavelengths (Ando et al., 2012). These empirical relations will be helpful for further VLFE studies, e.g., the triggering caused by tide or tectonic stress changes as observed in ordinary earthquakes (e.g., Thomas et al., 2012; Ide et al., 2016; Scholz, C. H., 2015).

Table 4-4. *b*-values of VLFEs and ordinary earthquakes, and amplitude-magnitude (A-M) relations for the four areas

	VLFE Counts[1]	**M_w**	**M_{mean}**[2]	**M_c**[3]	***b*-value** (VLFEs)	***b*-value** (Ordinary earthquakes)	**A-M relation**[4]
Sakishima (Zone S)	463	3.4−4.7	4.0	3.8	2.3	0.9	$M_w = 0.42\log A+3.4$
Okinawa (Zone O)	280	3.2−4.4	4.1	4.0	5.0	1.1	$M_w = 0.34\log A+3.5$
Amami (Zone A)	165	3.3−4.6	3.9	3.7	2.4	1.1	$M_w = 0.72\log A+3.0$
S-Kyushu (Zone K)	142	3.5−4.6	4.1	3.9	2.5	1.2	$M_w = 0.45\log A+3.3$

1, the number of VLFEs used for the estimation of *b*-value.
2, the mean M_w used in the estimation of *b*-value.
3, the minimum M_w.
4, the amplitude unit is nm/s.

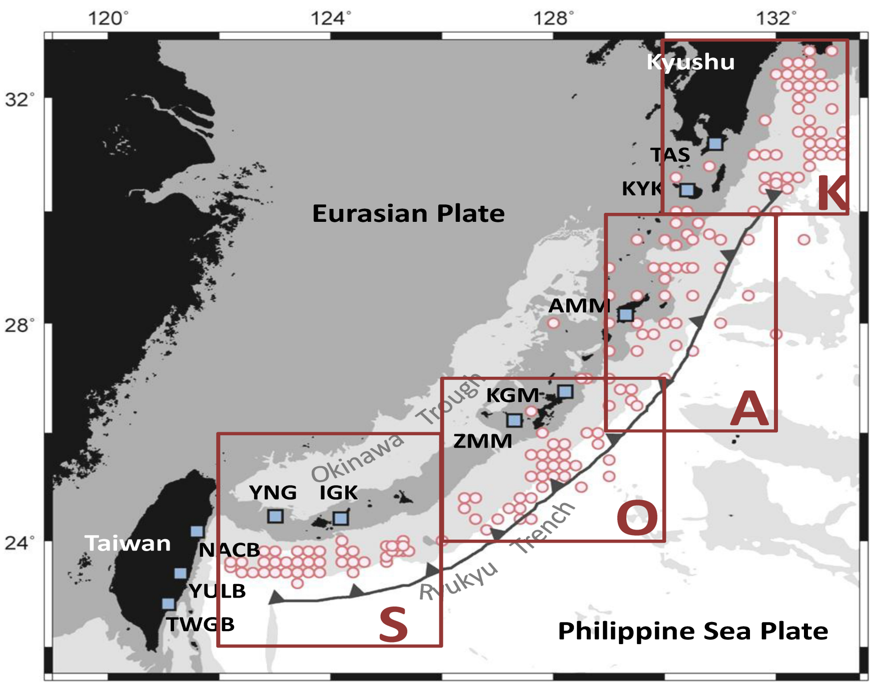

Figure 4.13. Distribution of the 1,050 VLFEs (red circles) detected by the waveform inversion method in the sub-areas of Sakishima (S), Okinawa (O), Amami (A), and southern Kyushu (K).

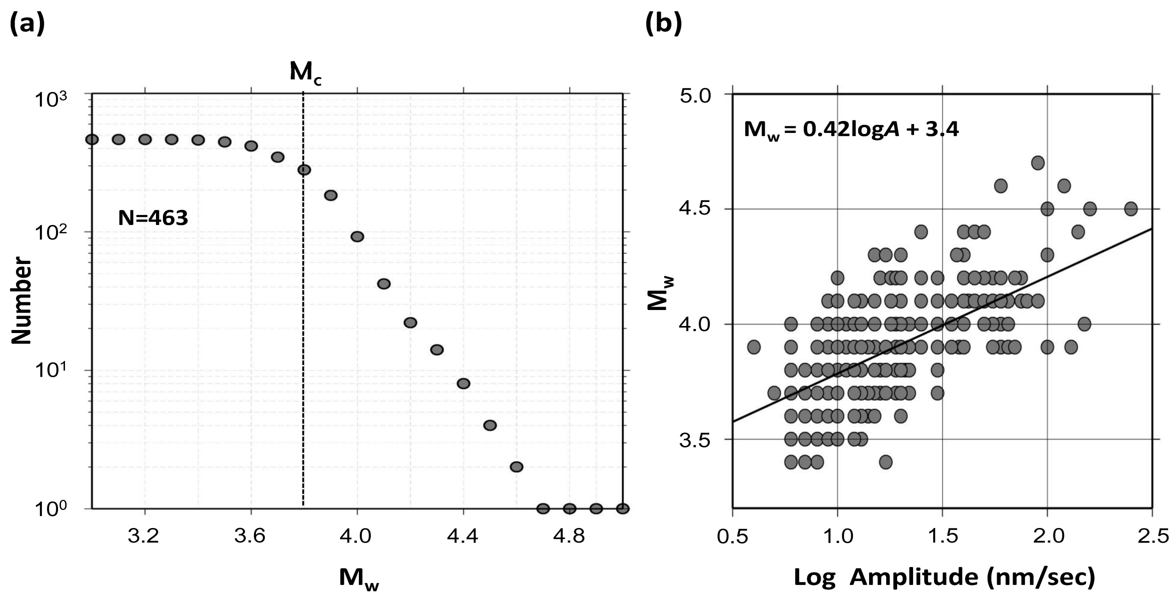

Figure 4.14. (a) Cumulative frequency distribution of VLFEs in the Sakishima area. The total number of VLFEs used for this calculation is 463. This diagram shows that M_c (cut-off magnitude) equals 3.8. (b) The log-amplitude and magnitude relation for VLFEs in the Sakishima area. The maximum amplitude (0.02-0.06 Hz bandpass filtered) of each VLFE recorded at YNG or IGK is plotted in this diagram.

4.4 Discussions

Various slow earthquakes detected on the subduction plate interfaces are considered to have a similar source mechanism (Beroza and Ide, 2011). Hence, different types of slow earthquakes sometimes appear remarkable correlations with each other (Obara and Kato, 2016). For example, in the Bungo Strait, southwest of the Nankai Trough, long-term SSEs activated shallow VLFEs and deep episodic tremor (Hirose et al., 2010; Asano et al., 2015). Likewise, VLFEs triggered by SSEs were also seen in the Ryukyu Trench. Nakamura and Sunagawa (2015) reported that the SSEs near Iriomote Island (hereafter call “Iriomote SSEs”) activated VLFEs around the Ishigaki and Yonaguni Islands in 10-20 days and attributed it to the Coulomb failure stress change (ΔCFS) by the SSEs. However, the relations of the two types of slow earthquakes in the Okinawa and Amami areas have not been clear so far.

4.4.1 Correlations in activity between VLFEs and SSEs

To understand temporal correlations between SSEs and VLFEs in Ryukyu, I used the 29,841 VLFEs and 16 long-term Iriomote SSEs during the period of 2005-2012. Moreover, I adopted short-term SSEs identified by Nishimura (2014) to assist the analysis of the Okinawa and Amami areas. I first divided these selected slow earthquakes into the four areas: Sakishima (S), Okinawa (O), Amami (A), and southern Kyushu (K) as illustrated in Figure 4.15. Next, I compared the occurrence times of SSEs with those of VLFEs within these areas.

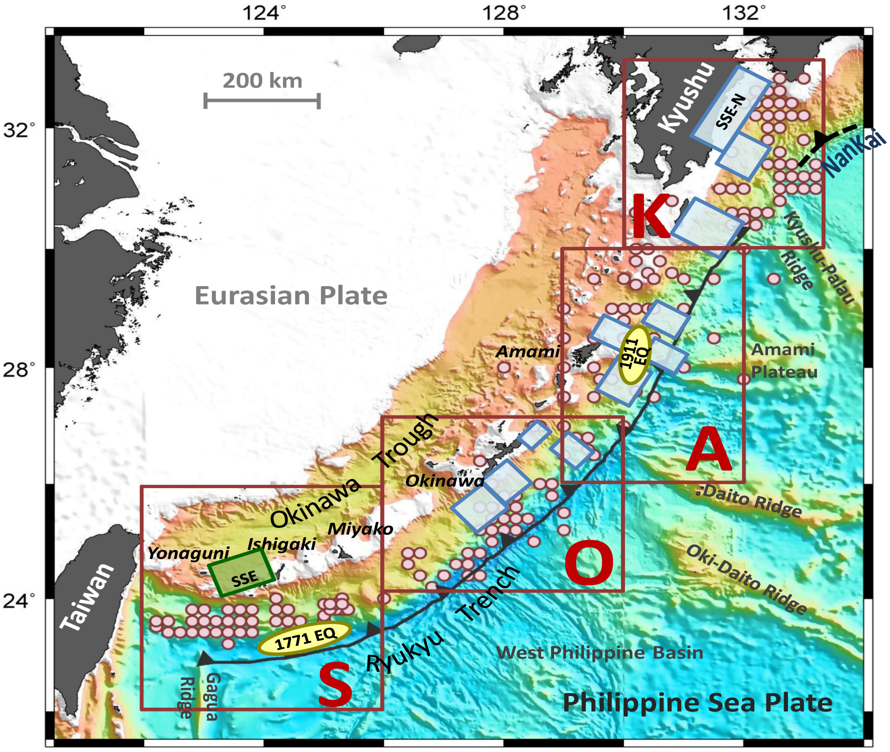

Figure 4.15. Tectonic map in the Ryukyu area and locations of VLFEs (red circles), SSEs (rectangles), and ordinary large (M-8 class) earthquakes (yellow ellipses) in the four areas of Sakishima (S), Okinawa (O), Amami (A), and southern Kyushu (K). The green and blue rectangles are the fault patches of SSEs detected by this study and Nishimura (2014), respectively.

4.4.1.1 Sakishima area

For this area, I selected 3,541 VLFEs whose seismic waves arrive first at IGK, and 16 Iriomote SSEs that were detected in the Sakishima area in this study (Figure 4.15). I analyzed the time series of the two types of slow earthquakes. As described in Figure 4.16, VLFEs occurred actively during the SSEs in progress (e.g., SSEs#15, #16, and #23), but some SSEs were not accompanied by VLFEs (e.g., SSEs#27, #28, and #30). To clarify the puzzling correlations and highlight the VLFE activation, I first separated VLFEs based on the time periods of the 16 SSEs (Figure 4.17). Then, I stacked these SSEs with respect to their onset times. Figure 4.18a displays a stacked count of VLFEs within each of the 16 SSEs. Three significant peaks are seen at 5-30, 60-75, and 120-125 days after the SSE onsets. The first activation of 5-30 days is consistent with the duration of the Iriomote SSEs (0.1-0.15 years, see details in Section 3.3.1). Namely, the VLFEs become more active in general after the SSEs start. In contrast, the peaks of 60-75 and 120-125 days may have occurred coincidentally or be triggered by ordinary earthquakes (Figure 4.17). Moreover, I also noted that the level of VLFE activity was low before the SSEs (Figure 4.18b).

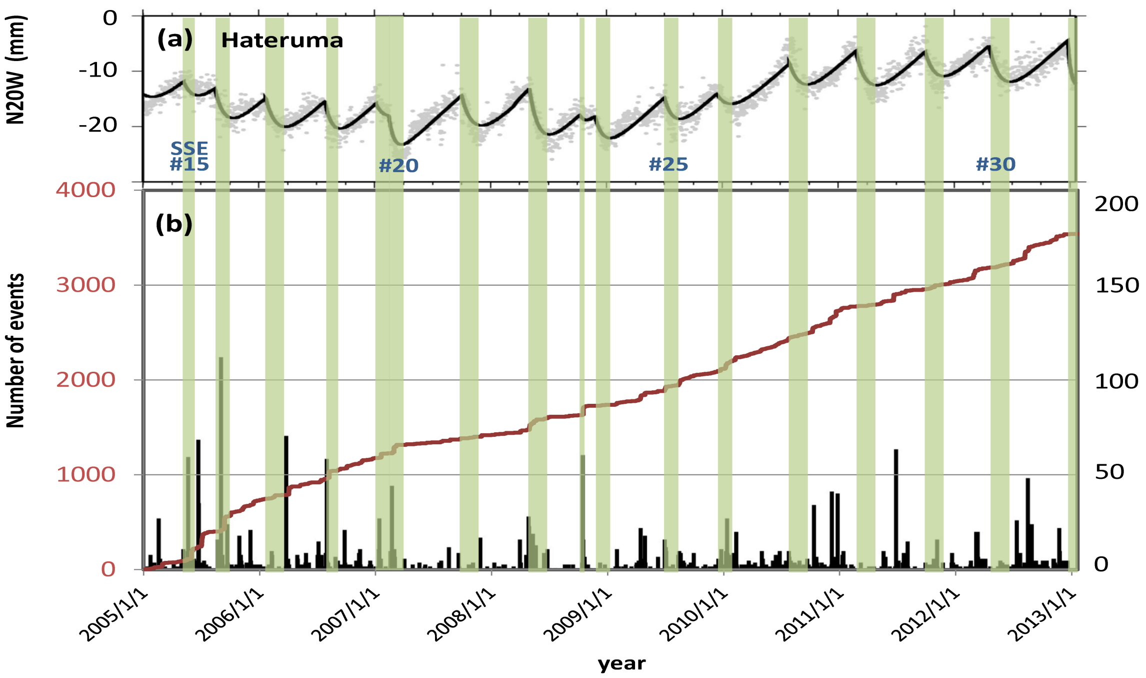

Figure 4.16. (a) The daily GNSS coordinates of the Hateruma site relative to the Miyako site in the N20W direction. The green belts show the active times of the 16 SSEs with a number corresponding to the SSEs in Table 3-1. (b) The daily count of VLFEs (black bars) whose seismic waves arrive first at IGK and its cumulative numbers (red curve). The units of the daily and cumulative numbers are given on the right and left axes, respectively. VLFE activity was high in SSE #15-20, #22-23, #25-26, and #29, but low in SSE #21, #24, #27-28, and #30.

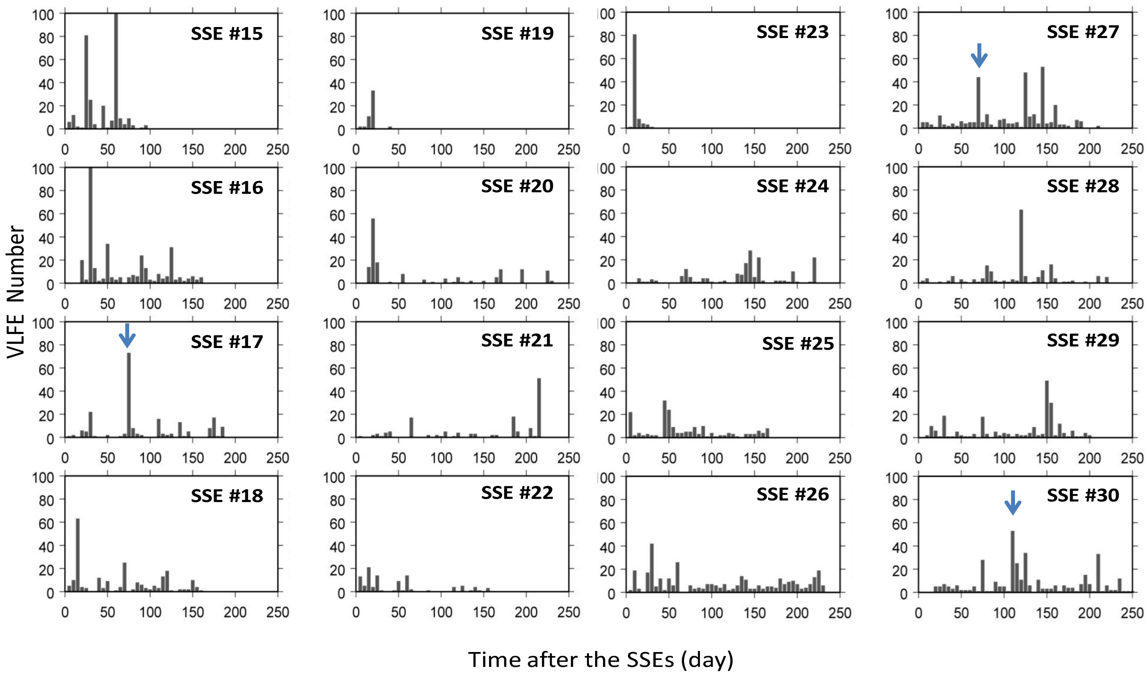

Figure 4.17. The 5-day count of VLFEs within the 16 Iriomote SSEs. The time span of each diagram is from SSEs to their consecutive events. The event numbers at the top right corner refer to the SSEs in Table 3-1. The blue arrows in #17, #27 and #30 indicate VLFEs triggered by local ordinary earthquakes.

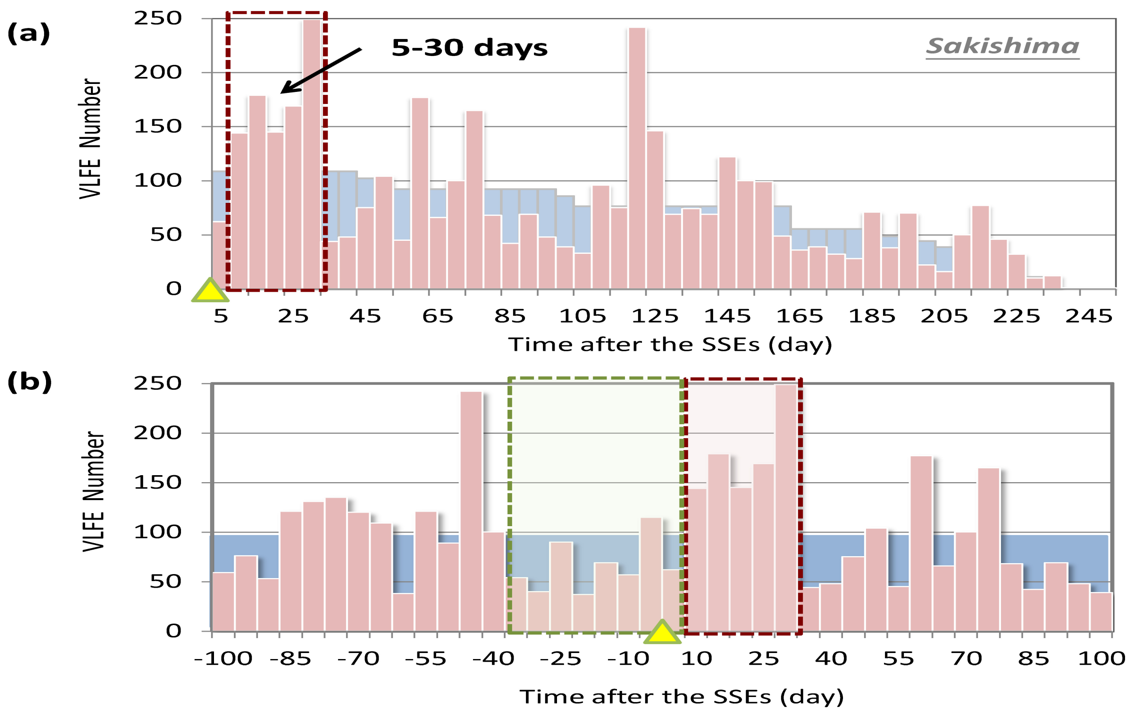

Figure 4.18. (a) Stacked number of VLFEs after the SSEs. The time span is from SSEs to consecutive events, same as Figure 4.17. The red bars, the 5-day count of VLFEs; the blue

bars, the average number of VLFEs with a 5-day interval expected when VLFE occurrences are random; the yellow triangle marks, the onset time of SSEs. The first peak of 5-30 days highlighted by the dashed red rectangle is evidence of the SSE activations. (b) Same as (a), but the time span is 100 days before and after the SSE onsets (yellow triangle). Lower and higher VLFE activity periods are marked by the dashed red and green rectangles, respectively.

4.4.1.2 Okinawa and Amami areas

I applied the same method as used for the Sakishima area to analyze correlations of activities between VLFEs and SSEs in Okinawa and Amami. For the Okinawa area, I compared the occurrence times of 4,480 VLFEs identified in this study and 28 short-term SSEs detected geodetically by Nishimura (2014) (Figure 4.15). As illustrated in Figure 4.19, one significant peak is seen at 0-15 days, which is shorter than that (5-30 days) of the Sakishima area (see Figure 4.18a). One possibility for the short delay time is that the SSE fault patches in the Okinawa area are much closer to the VLFE source region than in the Sakishima area, resulting in higher ΔCFS and triggering VLFEs more quickly.

Likewise, I compared 7,647 VLFEs and 19 short-term SSEs in the Amami area. There are five peaks at 0-5, 75-85, 100-105, 210-220, and 370-375 days (Figure 4.20). The first peak at 0-5 days is probably related to the SSE activation, but other peaks show VLFE activities that may occur coincidentally or be triggered by earthquakes. The reaction time (0-5 days) of VLFE activities here is similar to that in Okinawa but is shorter than that in the Sakishima area. Such short activation time may have been enabled by the shorter distance between SSE faults and VLFE source regions in the both Okinawa and Amami areas than the Sakishima area.

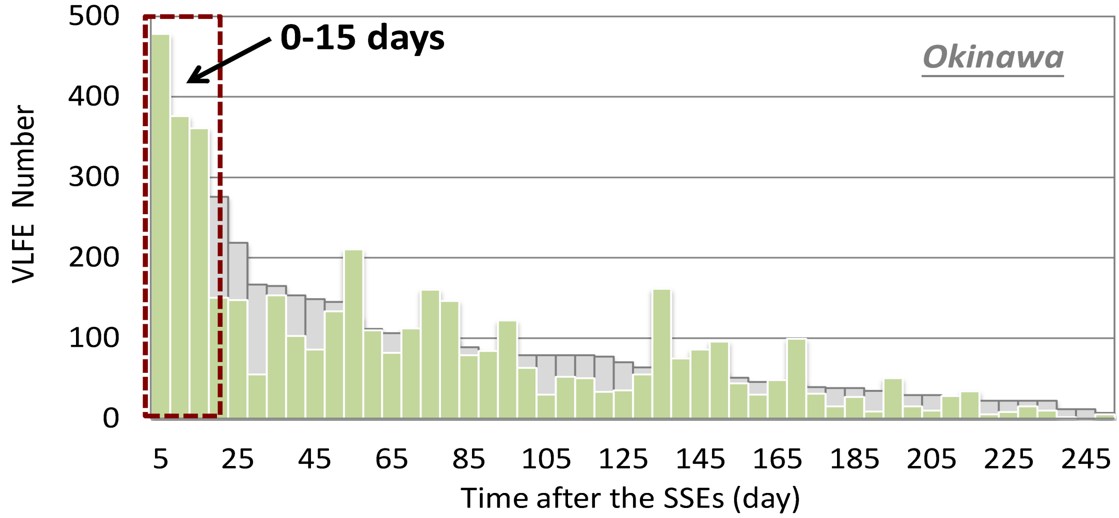

Figure 4.19. Stacked number of VLFEs after the SSE occurrences in the Okinawa area. The green bars display the 5-day counts of VLFEs, and the grey bars show the numbers of VLFEs expected by random occurrences with a 5-day interval. The peak of 0-15 days marked with the red dashed rectangle is related to the activation by SSEs. It is significantly faster than the VLFE activation in the Sakishima area (5-30 days).

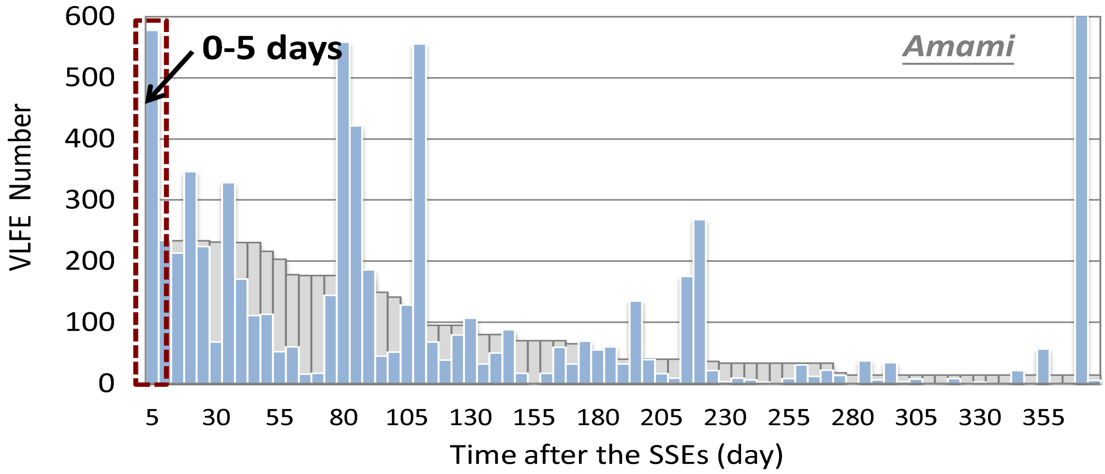

Figure 4.20. Stacked number of VLFEs after the SSEs in the Amami area. The blue bars display the 5-day counts of VLFEs, and the grey bars show the numbers of VLFEs expected by random occurrences with a 5-day interval. Five peaks are seen in this diagram. The first peak marked with a red dashed rectangle is related to the SSE activation, and others are caused by VLFE sequences triggered coincidentally.

4.4.1.3 Southern Kyushu area

The southern Kyushu area differs from the Ryukyu region; it has much more complicated geological structures than other three areas (Figure 4.15). These two subduction systems are bounded via the Kyushu-Palau Ridge, a 2000-km-long remnant of an ancient island arc (Figure 4.15) (Okino et al., 1998; Nishizawa et al., 2017). Across this ridge, the age of the subducting Philippine Sea Plate changes suddenly from 60-70 Ma (Ryukyu Trench) to 15-25 Ma (Nankai Trough) (Figure 4.28) (Okino et al., 1998). This causes that the two adjacent subduction zones have very different subduction processes (Scholz and Campos 2012).

According to previous studies, long-term and short-term SSEs both were detected in this area (e.g., Hirose, et al., 1999; Ozawa et al., 2004; Nishimura, 2014). These SSEs can be divided generally into the Bungo, Hyuga-nada, and Tanega-shima clusters based on their locations (Figure 4.21c). Several studies have mentioned that the Bungo SSEs could activate nearby VLFEs (Hirose et al., 2010; Asano et al., 2015; Baba et al., 2018) and earthquake tremors (Yamashita et al., 2017), but the correlations between VLFEs and the Hyuga-nada and Tanega-shima SSEs are still unknown. Here, I used the same methods as those for the Ryukyu area to analyze the relations among these slow earthquakes.

The Bungo SSEs has moment magnitudes (M_w ~6.8) and source depths (~30 km) similar to the Iriomote SSEs of the Sakishima area, but their duration (~1 year) and the recurrence interval (~6 years) are much longer (Hirose and Obara, 2005; Hirose et al., 2012) (see detail in Table 3-2). From 1996 to 2014, three Bungo SSEs were detected around 1996, 2004, and 2010 (Hirose et al., 1999; Ozawa et al., 2004; Hirose et al., 2010) (Figure 4.21a). Among them, I used the 2010 Bungo SSE for this analysis because it overlaps with my database period from 2005 to 2012. Figure 4.21b displays the time series of VLFEs in the southern Kyushu area and its cumulative curve. It is noted that the VLFEs became very active after the 2010 Bungo SSE. Moreover, the delay time of VLFE activations is about 20-40 days (Figure 4.22a), which is longer than that of the Sakishima area and probably due to a longer distance from the Bungo SSE fault to the VLFE sources.

The Hyuga-nada and Tanega-shima SSEs both are short-term SSEs with an average magnitude (M_w) of ~6.1. From 2005 to 2012, a total of nine events were detected (Nishimura, 2014) (Figure 4.21b). As illustrated in Figure 4.21b, VLFE activity is well correlated with the Tanega-shima SSEs, but the correlation between the VLFEs and Hyuga-nada SSE is not obvious due to the infrequent occurrence of the latter. Figure 4.22b shows the stacked numbers of VLFE time-series with respect to the onset of the nine SSEs. It suggests that these short-term SSEs can activate VLFEs in 0-10 days, which is comparable to the activation period of VLFEs in the Okinawa and Amami areas (Figure 4.19 and 4.20).

Moreover, it is interesting that the activation period (~20 days) of VLFEs caused by the Bungo SSEs is much longer than ~10 days found for the Hyuga-nada and Tanega-shima SSEs (Figure 4.22). Such phenomenon was also seen in the Ryukyu region. In the Sakishima area, the activation period of VLFEs caused by the Iriomote SSEs is ~25 days (Figure 4.18a), which is longer than that in the Okinawa (~15 days) and Amami (~5 days) areas (Figure 4.19 and 4.20). Because the Bungo and Iriomote SSEs both are long-term SSEs having large moment magnitudes (Table 4-5), I suspect that such difference of VLFE activation periods may relate to the size of SSEs. Furthermore, considering that the seismic moment and duration of slow earthquakes are nearly proportional (Ide et al., 2007), the duration of SSEs would also govern the periods of VLFE activities.

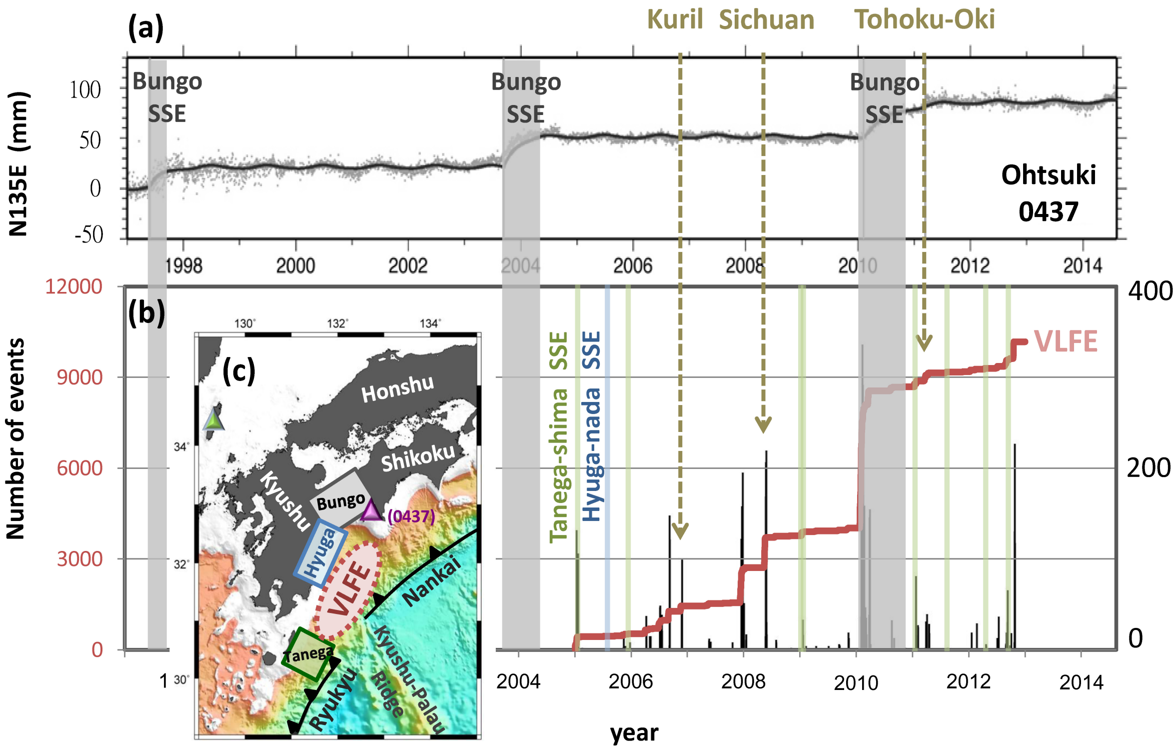

Figure 4.21. (a) Daily position of the Otsuki station (the pink triangle in Figure 4.21c) relative to Tsushima (the green triangle in Figure 4.21c) in the N135E direction. The grey belts show the active time of the three Bungo SSEs. The yellow dashed arrows indicate the occurrence time of three teleseismic events (the 2006 M_w8.3 Kuril, 2008 M_w7.9 Sichuan earthquakes and 2011 M_w9.1 Tohoku-oki earthquakes) that activated VLFEs in the southern Kyushu area. The detail information on these teleseismic earthquakes is given in Table 4.3. (b) The daily (black bars) and cumulated (red line) numbers of VLFEs. Their units are given in right and left axes, respectively. Green and blue vertical lines display the occurring times of Tanega-shima and Hyuga-nada SSEs, respectively (Figure 4.21c). (c) Tectonic map of the Kyushu area and locations of VLFEs (red dashed circle), and SSEs faults of Bungo (grey rectangle), Hyuga-nada (blue rectangle), and Tanega-shima (green rectangle).

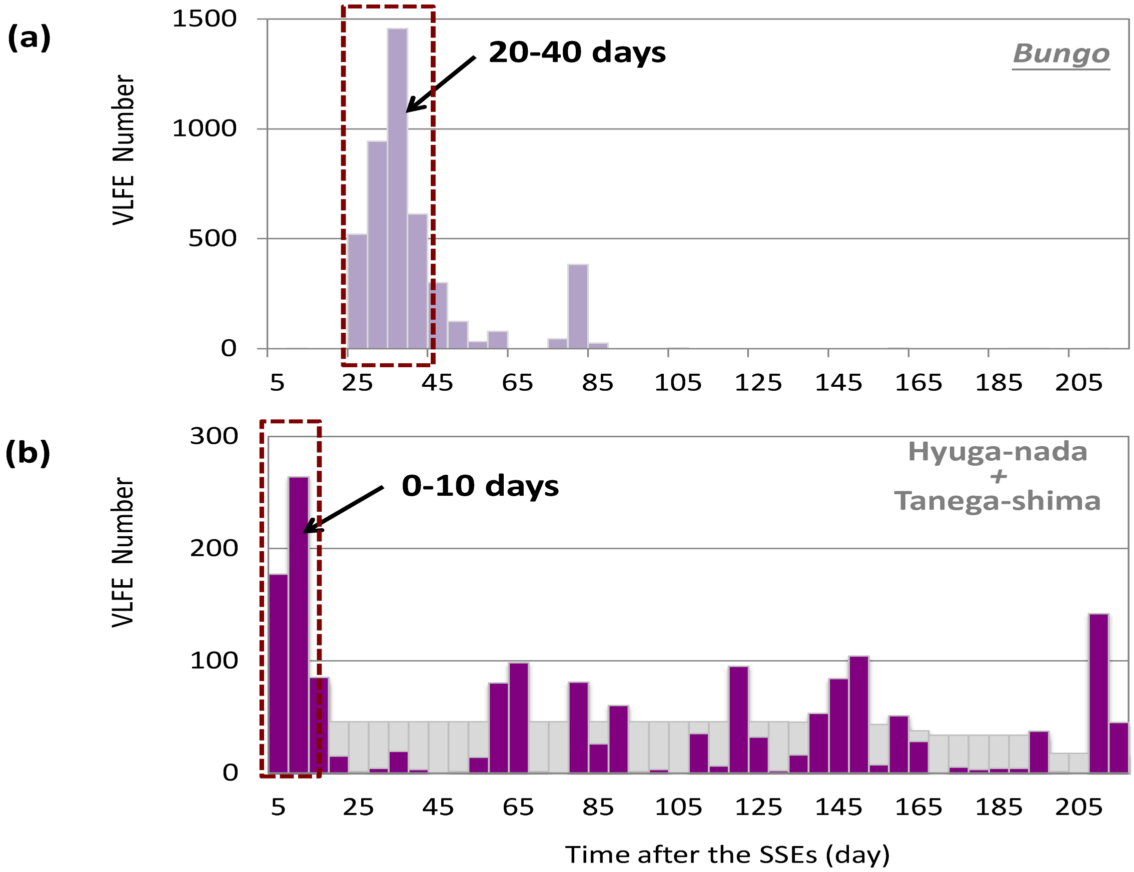

Figure 4.22. Stacked numbers of VLFEs in the southern Kyushu area after (a) the Bungo SSEs and (b) the Tanega-shima and Hyuga-nada SSEs. The color bars display the 5-day counts, and grey bars show the average numbers of VLFEs with a 5-day interval expected assuming their random occurrences. A significant peak appears in 20-40 days in (a), and 0-10 days in (b).

Figure 4-5. VLFE activation periods and related SSE parameters.

Type of SSE	Location	Area	M_w	Duration of SSE	VLFE activation periods
Long-term	Bungo	Southern Kyushu	M_w 6.8	~1 year	~20 days
Long-term	Iriomote	Sakishima	M_w 6.6	1-1.5 mons	~25 days
Short-term	Okinawa	Okinawa	M_w 6.0	Several days	~15 days
Short-term	Tanega-shima / Hyuga-nada	Southern Kyushu	M_w 6.1	Several days	~10 days
Short-term	Amami	Amami	M_w 6.1	Several days	~5 days

4.4.2. Spatial correlations of VLFEs, SSEs, and large (M-8 class) ordinary earthquakes

For the Ryukyu Trench, the most critical issue is whether the locked zones, in which megathrust earthquakes often occur, exist along this subduction zone. Although most studies suggest that no known megathrust earthquakes have occurred there (e.g., Peterson and Seno, 1984; Scholz and Campos 2012), two large earthquakes with $M_w \geq 8$ occurred along the Ryukyu subduction zone in the historical time, i.e., the 1771 Yaeyama earthquake and the 1911 Kikai earthquake (Figure 4.23).

The 1771 Yaeyama earthquake occurred near the Ishigaki Island, southwestern Ryukyu Arc (Figure 4.23). This event accompanied a disastrous tsunami that struck Ishigaki and surrounding islands with the maximum run-up height about 30 meters and caused fatalities of one-third of the populations on the Ishigaki Island (Goto et al., 2012). Although the mechanism of this earthquake is still uncertain, Nakamura (2009b) proposed the event to be an M_w 8.0 tsunami (slow) earthquake occurred near the Ryukyu Trench. Recently, Ando et al., (2018) investigated paleotsunami deposits on the Ishigaki Island and proposed that the 1771 earthquake was an ordinary (not slow) subduction thrust earthquake of $M_w > 8.0$ based on earthquake-induced ground cracks.

The 1911 Kikai earthquake occurred near Amami Island and was felt as far as in Tokyo (> 1000 km) (Usami, 1988) (Figure 4.23). This earthquake generated strong ground shaking that destroyed approximately 400 houses on Kikai Island as well as a tsunami (< 3m) with slight damage to the surrounding islands (Hatori, 1988; Goto, 2013). Several studies considered that the Kikai earthquake was an intraplate earthquake at a depth of ≥ 100 km

($M_w \geq 8$) (e.g., Utsu, 1982; Abe and Kanamori, 1979). However, Goto (2013) relocated its hypocenter using old smoked seismograms and proposed that this event was more likely a great shallow interplate earthquake near the Ryukyu Trench axis.

To understand the positions of the locked zone for megathrust earthquakes in the Ryukyu region, I plotted VLFEs, SSEs, ordinary earthquakes ($M_{JMA} > 3$), and the two possible megathrust events in Figure 4.23. In addition, I drew profiles of all these events along SS', OO', and AA' perpendicular to the trench axis (Figure 4.23). A detail discussion about the spatial correlation of these events is given below.

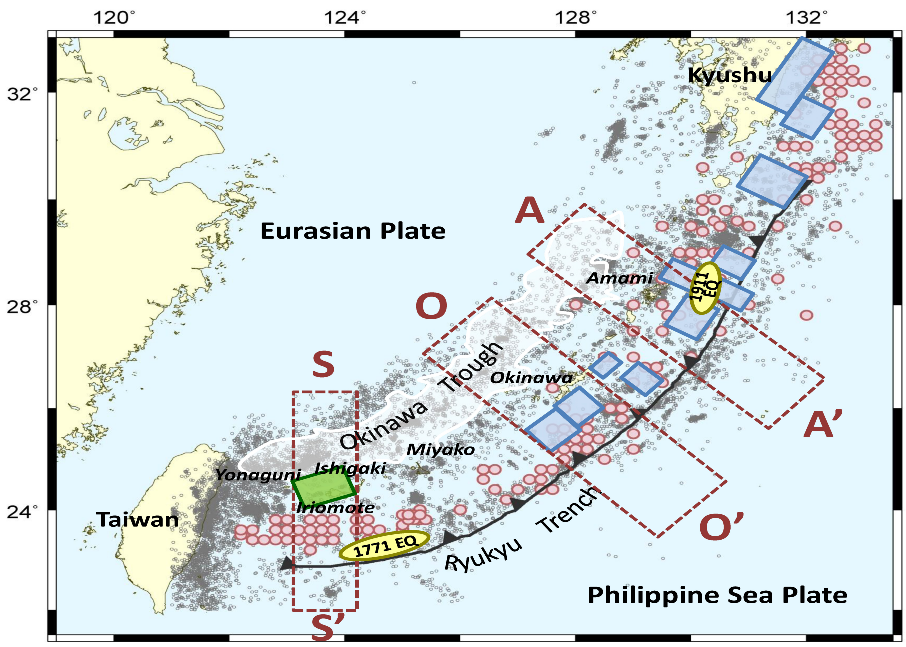

Figure 4.23. Distribution of VLFEs (red circles), SSEs (rectangles), ordinary earthquakes (M_{JMA} >3, gray dots), and two possible megathrust events (yellow ellipses) in the Ryukyu region. The green and blue rectangles are the fault patches of SSEs detected by this study and Nishimura (2014), respectively. The tsunami source ranges of the 1771 earthquake and the 1911 earthquakes are illustrated based on Nakamura (2009b) and Hatori (1988). Seismic profiles of SS', OO', and AA' are shown in Figure 4.24-4.26.

4.4.2.1 Sakishima area

In this area, the seismic events of the 1771 earthquake, VLFEs, and SSEs are distributed in order from the Ryukyu trench to the Okinawa Trough (Figure 4.23). These three types of earthquakes are adjoining but not overlap each other. Figure 4.24 shows the profile of SS', which indicates that the 1771 earthquake fault is located in the shallowest segment of the Ryukyu subduction zone. The VLFEs are concentrated within the area between the 1771 earthquake fault and the Iriomote SSE fault patch. Notably, the updip limit of the Iriomote SSE fault keeps a distance from the trough-ward border of VLFEs (Figure 4.24). This distance may be related to the delayed timing of VLFE activations after the start of SSE. In the Sakishima area, the delay of activated VLFEs is 5-30 days (Figure 4.18), while the delay is only 0-5 days in the Okinawa area (Figure 4.19) and 0-15 days in the Amami area (Figure 4.20) where VLFEs and SSEs are distributed closely or overlapped with each other. It means that the distance between the VLFE and SSE areas may govern the delay of VLFE activities after the SSE onsets.

The locked zones of the Nankai Trough, where megathrust earthquakes repeatedly occur, are located in a particular space between shallow VLFEs and long-term SSEs (Obara and Kato, 2016) (Figure 3.14). However, in the Sakishima area, the space between the VLFEs and SSEs is too narrow to accumulate stress for preparing megathrust earthquakes (Figure 4.24). Accordingly, the locked zone of the Ryukyu subduction zone here should be located between the SSE-VLFE zone and the trench axis, i.e., the location of the 1771 earthquake fault. Such observation is consonant with results raised by Arai et al. (2016) and Nakamura (2017) but significantly different from the seismic distribution in the Nankai Trough.

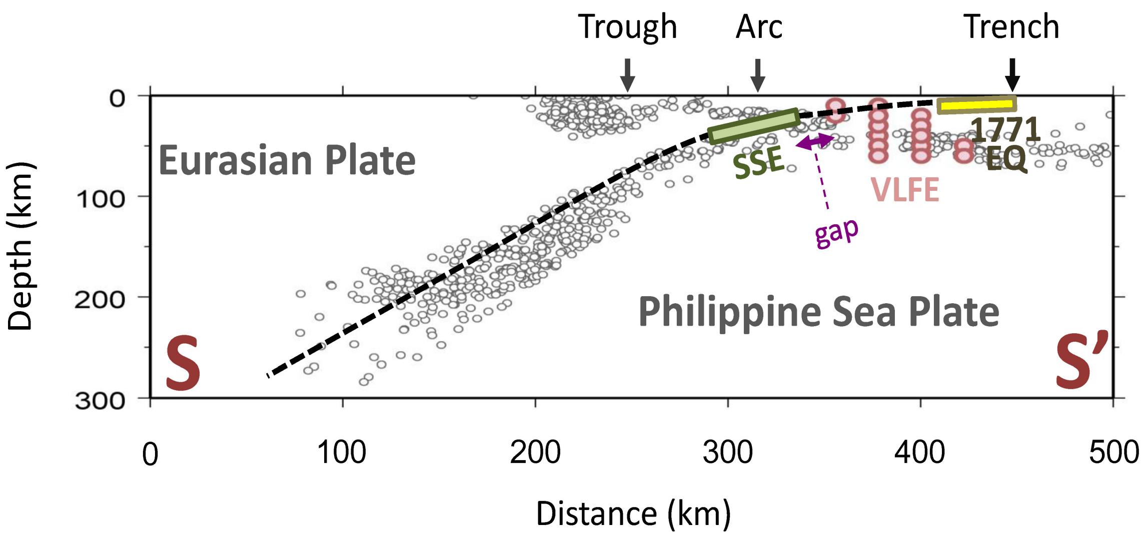

Figure 4.24. Cross-section of profile SS' perpendicular to the trench axis in the Sakishima area. Its geometric extent is shown in Figure 4.23. The red circles are VLFEs detected in this study. The gray circles are small ordinary earthquakes ($M_{JMA} \geq 3$) recorded by JMA. The green rectangle displays the fault patch of long-term SSEs beneath Iriomote Island detected by this study. The yellow rectangle shows the fault zone of the 1771 earthquake estimated by Nakamura (2009b). The black dashed line is the subduction plate boundary between the Philippine Sea Plate and the Eurasian Plate. The solid arrows on the top mark the relative positions of the Ryukyu Arc, Ryukyu Trench, and Okinawa Trough.

4.4.2.2 Okinawa area

Okinawa Island has been the political and cultural center of the Ryukyu Islands over its historical time, but it is remarkable that large earthquakes (M_w >8.0) or tsunamis (>5-10m) had not been recorded in historical documents after the establishment of the Ryukyu Kingdom (15th century). Nevertheless, authentic historical documents of the Kingdom (e.g., "Kyuyo") had recorded details of the 1771 earthquake in Sakishima, 400 km away from Okinawa Island, and several other earthquakes (M < 8) in the Ryukyu region (Usami, 2003;

M. Nakamura, Ryukyu University, http://seis.sci.u-ryukyu.ac.jp/hazard/large-eq/history.html). It means that earthquake phenomena had been a focus of concern and not ignored intentionally in these historical documents. Moreover, geological data also provide another evidence for the lack of large earthquakes (tsunamis) in the Okinawa area. Goto et al. (2010) proposed that tsunami boulders carried by large paleotsunamis during the past 2,300 years have not been found in and around Okinawa Island. Based on the absence of tsunami boulders and historical records on large earthquakes and tsunamis, I suspect that megathrust subduction earthquakes rarely occurred here.

Except for large ordinary earthquakes, both VLFEs and SSEs have been detected in the Okinawa area. The profile of OO' shows the NW-SE section of these earthquakes (Figure 4.25). I found that the VLFEs occur in the shallowest part of the Ryukyu subduction zone close to the trench axis (Figure 4.25). In addition, the SSE fault patch overlaps partly with the VLFE source region (Figure 4.25). This is the reason why the VLFEs in the Okinawa area can be activated immediately after the SSE starts. Due to limited space between the SSE-VLFE zone and the trench axis (Figure 4.25), I infer that the locked zone of the Ryukyu subduction zone in the Okinawa area may be narrow or nearly absent. However, it may be premature to conclude that the Ryukyu Trench is a decoupled plate boundary. For example, Kawana (1990) reported that the coastal terraces on Okinawa Island facing the Pacific Ocean side exhibit the significant landward tilting, which suggests the existence of inter-plate coupling as seen in the Nankai Trough (Ando, 1975). Moreover, Nakamura (2013) reexamined two historical tsunamis of 1768 and 1791 in the Okinawa Island using numerical simulations of tsunami and earthquake shaking. His results also indicated that both events were probably due to M>8 interplate earthquakes near the Ryukyu Trench axis. Namely, further studies are necessary to clarify the coupling in the Okinawa area of the Ryukyu subduction zone.

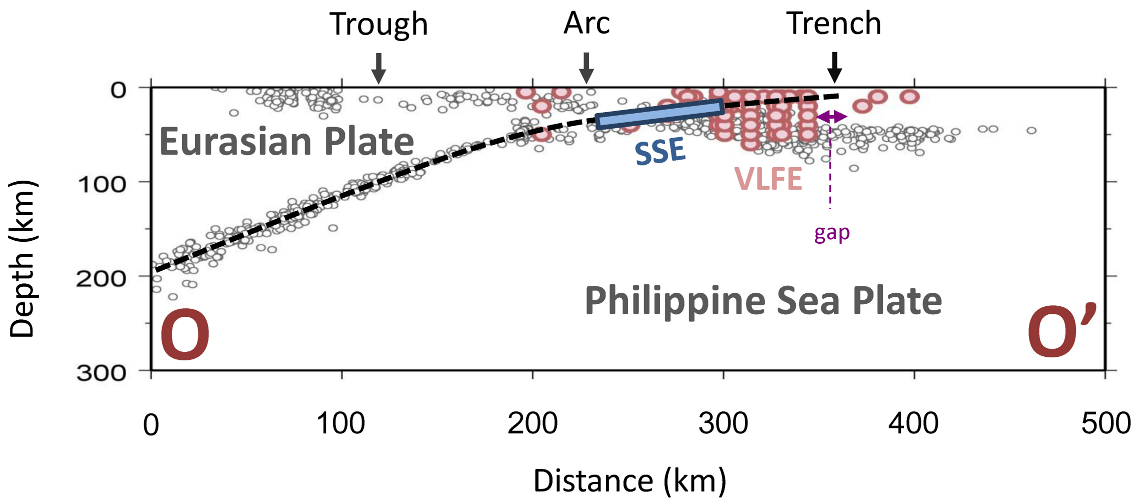

Figure 4.25. Cross-section of the profile OO' in the Okinawa area (Figure 4.23). The red and gray circles are VLFEs and ordinary earthquakes (M_{JMA} >3), respectively. The blue rectangle displays the fault patch of short-term SSEs detected by Nishimura (2014). The black dashed line shows the subduction plate boundary between the Philippine Sea Plate and the Eurasian Plate. The solid arrows on the top mark the relative positions of the Ryukyu Arc, Ryukyu Trench, and Okinawa Trough.

4.4.2.3 Amami area

Slow earthquakes (SSEs and VLFEs) and large ordinary earthquakes (the 1911 Kikai earthquake) both occurred in the Amami area. Notably, the distribution of these earthquakes seems to overlap with each other without a clear boundary (Figure 4.23), which is significantly different from that in the Sakishima and Okinawa areas. The profile AA' indicates that the fault zone of the 1911 earthquake, VLFE source region, and SSE faults are all located in the same area (Figure 4.26). This may be the reason why the SSEs can immediately activate VLFEs. If the SSE and VLFE zones overlap, there is no space between them to accummodate a locked zone for large interplate earthquakes. However, the 1911 Kikai earthquake, possible an interplate megathrust event, is located precisely in this place (Figure 4.23; Figure 4.26).

Although the location and mechanism of the 1911 Kikai earthquake have not been well constrained, I propose two possibilities for its mechanism. If the 1911 earthquake is a megathrust earthquake, the fault zone should be much closer to the trench axis, i.e., it is probably between the SSE-VLFE zone and the Ryukyu trench axis, similar to the 1771 earthquake in the Sakishima area. In contrast, if the location of the 1911 earthquake shown in Figure 4.23 is correct, this event should be an intraplate earthquake, just like an M_w 7.1 (USGS) earthquake that occurred 50 km east of Amami Island at a depth of 20 km on 18 Oct. 1995 (Arai et al., 2017). The 1995 earthquake was determined as a high-dip-angle normal fault in the slab, and it also generated a tsunami (<3m), slightly affecting Amami and Kikai Islands (Satake and Tanioka, 1997; Yamada et al., 1997).

Because the locations of VLFEs in the Amami area have a lower accuracy (see Section 4.3.3), and the sea-mountain (e.g., Daito Ridge and Amami Plateau) subducting also causes complex tectonics here, it is difficult to determine whether or where the locked zone exists in this area. Accordingly, further studies are still necessary.

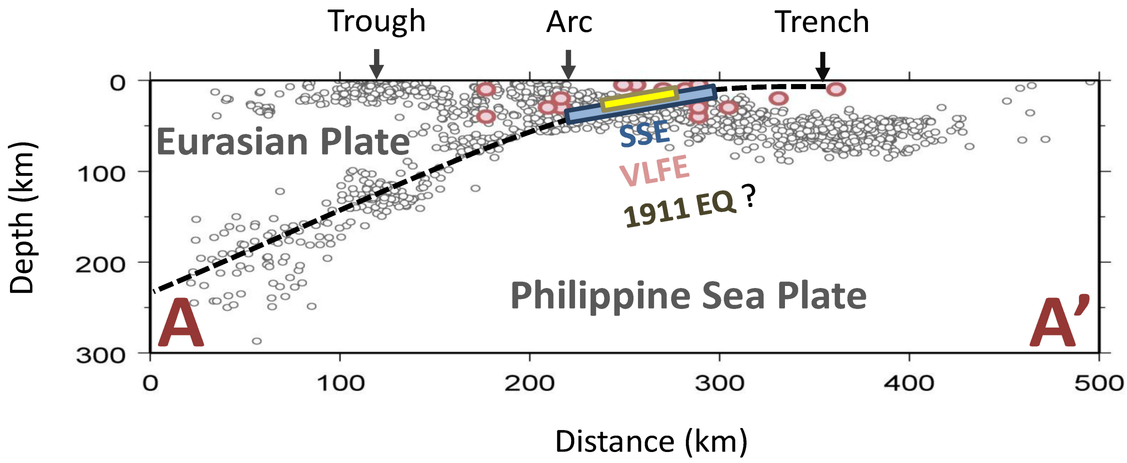

Figure 4.26. Cross-section of profile AA' in the Amami area. Its geometric extent is shown in Figure 4.23. The red and gray circles are VLFEs and ordinary earthquakes (M_{JMA} >3), respectively. The blue rectangle displays the fault patch of short-term SSEs detected by Nishimura (2014). The yellow rectangle describes the fault zone of the 1911 earthquakes suggested by Hatori (1988) and Goto (2013). The black dashed line shows the subduction plate boundary between the Philippine Sea Plate and the Eurasian Plate. Solid arrows on the top mark the relative positions of the Ryukyu Arc, Ryukyu Trench, and Okinawa Trough.

4.4.3 Along-strike variation of earthquake distribution

Based on above discussions, I propose that the Ryukyu subduction zone is coupled at least in the Sakishima area but probably absent in Okinawa. However, it is still uncertain whether the locked zone is present in the Amami area (Figure 4.27). The distribution of seismic events from the surface to depth in Sakishaima is: the megathrust earthquake zone (locked zone, ~10 km), VLFE zone (~20 km), and SSE zone (~30 km), and in Okinawa is: VLFE zone (~20 km) and SSE zone (~30 km) but without locked zones here (Figure 4.27). Notably, such distribution significantly differs from that of the Nankai Trough proposed by Obara and Kato (2016). In the Nankai Trough, the sequence of seismic distribution is: VLFE zone (>10 km), megathrust earthquake zone (10-20 km), SSE zone (~30 km), and episodic tremors and slip (ETS) zone (~40 km)(Figure 3.14). These observations suggest that the two subduction zones have different characteristics although they are related to the Philippine Sea Plate subduction.

For the difference of the seismic distributions between the Sakishima and Okinawa areas and the Nankai Trough, I propose that it may relate to the dip angle of subduction slabs. In the Ryukyu Trench, the age of the Philippine Sea Plate ranges in 50-60 Ma (Muller et al., 2008) (Figure 4.28), and its dip angle is ~20° (Kubo and Fukuyama, 2003; Nishizawa et al., 2017). However, the age and dip angle of the Philippine Sea Plate in the Nankai Trough is 20-30 Ma (Muller et al., 2008) (Figure 4.27) and 10° (Kodaira et al., 2000), respectively. According to a classical model of subduction zones by Uyeda and Kanamori (1979), an old and thick oceanic plate subducts into the mantle with a higher dip angle due to its gravitational force, resulting in a decoupled or weakly coupled plate boundary. In this case, the locked zone becomes narrower and shifts shallower toward the trench axis. This hypothesis is consonant with the narrow locked zone in Sakishima (30 km, Nakamura, 2009) relative to the Nankai Trough (70-100 km, Sagiya and Thatcher, 1999). Similarly, the difference in the seafloor age may cause the diversity of seismic pattern between the Sakishama (50-60 Ma) and Okinawa (60-70 Ma) areas (Figure 4.28). Such a slight difference probably affects stress balance of the upper and lower slab interactions and frictional conditions, causing the absence (Okinawa) or presence (Sakishima) of the locked zone (Figure 4.27).

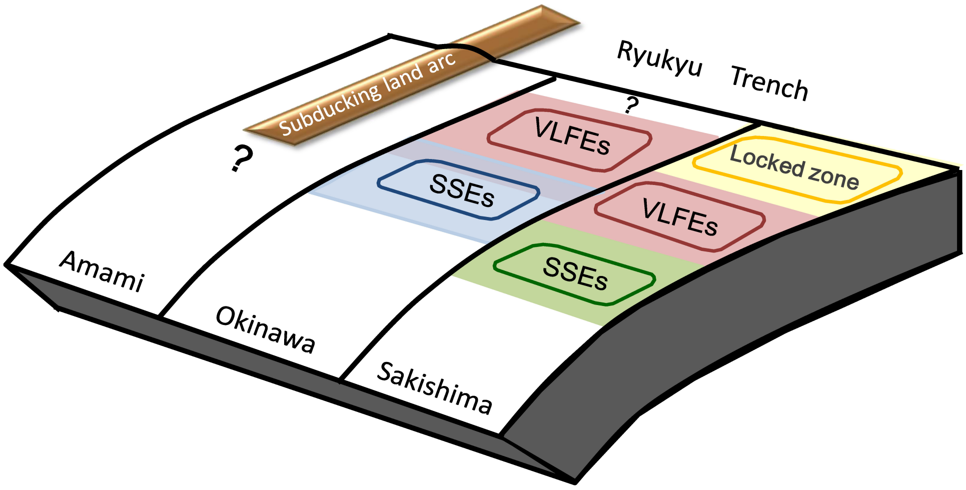

Figure 4.27. The distribution of three seismic zones (Locked, VLFE, and SSEs) in the Sakishima, Okinawa, and Amami areas along the Ryukyu subduction zone. Their scales are arbitrary.

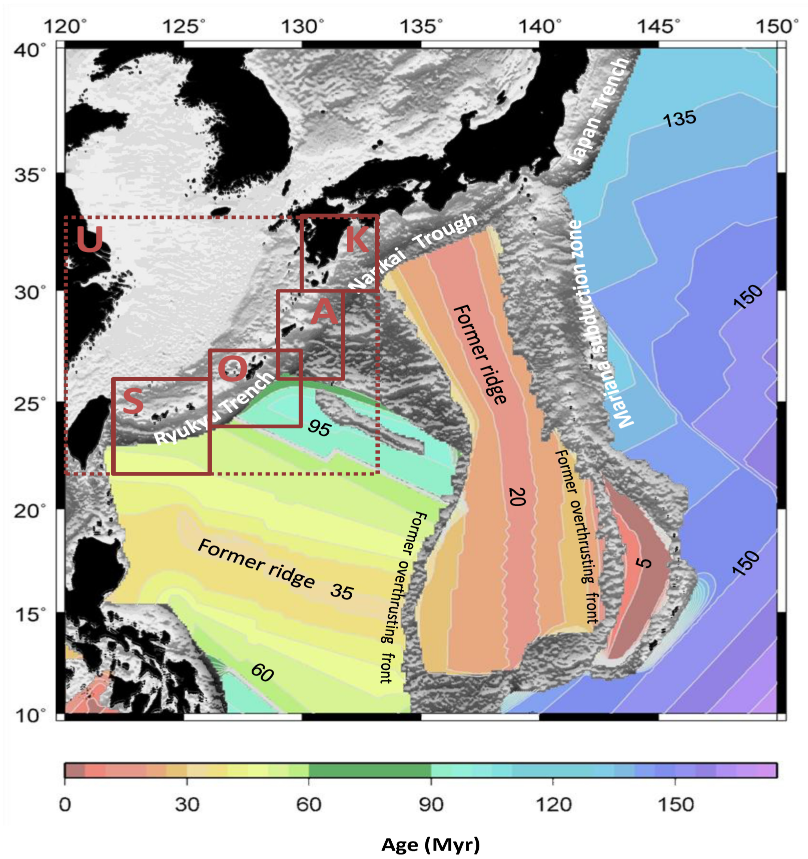

Figure 4.28. The seafloor age of the Philippine Sea Plate and Pacific Plates around Japan. The age data are from Muller et al. (2008). Area U is the extent of this study, and the

rectangles of S, O, A and K indicate the four sub-areas of Sakishima, Okinawa, Amami, and southern Kyushu, respectively.

4.4.4 Migration of VLFE activities

Migration activity is a significant characteristic of slow earthquakes and has been discussed in several studies (e.g., Deep VLFEs, Ghosh et al., 2015; Shallow VLFEs, Asano et al., 2015; Shallow Tremors, Yamashita et al., 2015; ETSs, Hirose and Obara, 2010). In the Ryukyu region, such a phenomenon has been observed in low frequency earthquakes (LFEs) having dominated frequency range of 2-8 Hz (Nakamura, 2017) but has never been reported for VLFEs. To understand the migration activity of VLFEs in Ryukyu, I analyzed the spatiotemporal distribution of the 1,050 VLFEs for the four sub-areas (Figure 4.29a). It is interesting to note that VLFE activities in the Sakishima and southern Kyushu areas occasionally form clusters in time and space, but those in Okinawa and Amami are much scattered and form a random distribution (Figure 4.29b). Because these clustering activities all lasted several days and extended over a distance about 60-100 km, I infer that they are probably the migration of VLFE activities.

To determine the migrating clusters of VLFEs, I assumed that each clustering activity should consist of at least three VLFEs and migrate in one direction to two or more neighboring grid points (> 40 km). Based on this definition, I identified 6 and 3 migrating clusters in the Sakishima and southern Kyushu areas, respectively (Table 4-6 Figure 4.29b). For the Sakishima area, five of the six clusters (S2-S6) migrated westward; only one cluster

(S1) moved from west to east (Table 4-6; Figure 4.30). The migration speeds of these clusters are between 20 and 90 km/day (Table 4-6; Figure 4.30), which are comparable to or higher than those for the Nankai Trough (8-18 km/day, Obara, 2011; 15-20 km/day, Asano et al., 2015) and the Cascadia subduction zone (10-20 km/day, Houston et al., 2011). Notably, these migration clusters all started around the Iriomote SSE fault patches (Figure 4.31), which imply that the Iriomote SSEs may trigger these VLFE migrations.

Sequentially, I compared the occurring times of these six migrating clusters with those of the Iriomote SSEs to examine the above hypothesis. As illustrated in Figure 4.32, the sequences of S1, S3, and S4 just occurred after the SSE onsets and are consistent with the duration of SSE #15, #25, and #29, respectively. It suggests that the Iriomote SSEs triggered these VLFE migrations, similar to the condition between the Bungo SSEs and shallow VLFEs in the Hyuga-nada region (Asano et al., 2015). However, other three sequences (S2, S5, and S6) started before the SSEs (Figure 4.32), i.e., their occurrences may correlate with other external forces, not the Iriomote SSEs. Here, I propose that the migrating cluster of S5 is related to a M_{jma} 5.5 local earthquake because it triggered this VLFE sequence (Figure 4.32), but the causes for the migration clusters of S2 and S6 are still unknown.

For the southern Kyushu area, I detected three migrating clusters of VLFEs in space-time diagram (Figure 4.29b). The detailed information of these VLFE migrations such as the origin time, duration, direction and speed are all provided in Table 4-6. The migrating sequence of K1 lasted about four hours and moved from south to north with an extremely high speed of 240 km/day (see K1 in Figure 4.33). This migrating cluster seems to be isolated from the Bungo, Tanega-shima, and Hyuga-nada SSEs and without any correlations with local or teleseismic earthquakes (Figure 4.34). The sequence of K2 is a VLFE cluster triggered by the 2008 Sichuan earthquake of M_w 7.9, China (Figure 4.34). It started with several VLFEs that occurred simultaneously and then migrated toward the south at a speed of ~20 km/day (see K2 in Figure 4.33). Its duration and travel distance is ~4 days and ~100 km, respectively (Figure 4.33).

The sequence of K3 is the most remarkable cluster, which has a large scale (distance > 200 km) and long duration (~35 days). This migration activity started on 25 Jan 2010 and significantly correlated with the 2010 Bungo SSE (Figure 4.34). These VLFEs first propagated northward gradually with a speed of ~5 km/day (see the 1st migration of K3 in Figure 4.33), but it turned sharply south with a higher speed of ~15 km/day since March (see the 2nd migration of K3 in Figure 4.33). Such a change in the migrating direction was also seen in the shallow low-frequency tremors around the Hyuga-nada area and may be related to nearby un-detected short-term SSEs (Yamashita et al., 2015). Moreover, I also found another short duration sub-migration within the 1st migrating period (see sub-migration of K3 in Figure 4.33), whose VLFEs propagated in the same direction (northward) but with a much higher speed. This phenomenon is comparable to the rapid tremor reversal (RTR) observed in the tremor migration activity near the Hyuga-nada area (Yamashita et al., 2015).

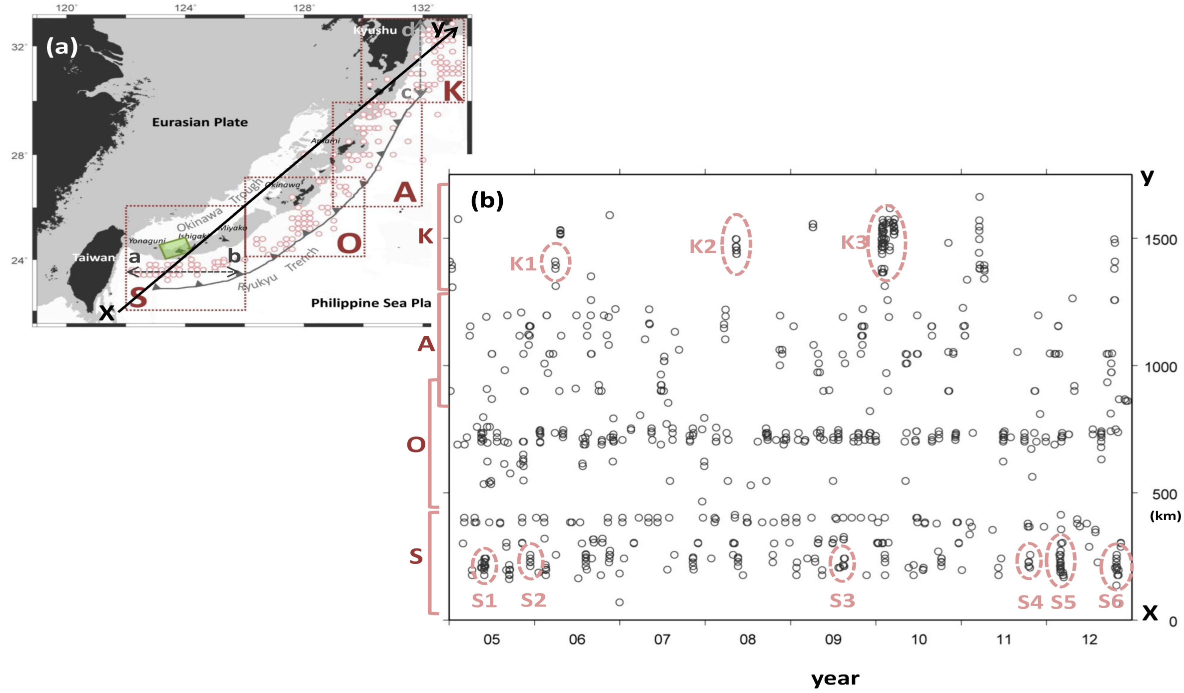

Figure 4.29. (a) Distribution of the 1,050 VLFEs (red circles) in the sub-areas of Sakishima (S), Okinawa (O), Amami (A), and southern Kyushu (K). The green rectangle is the fault patches of Iriomote SSEs detected by this study. (b) Time-space diagram of the 1,050 VLFEs along line X-Y in Figure 4.29a. Red circles mark the migrating clusters of VLFEs detected in this study.

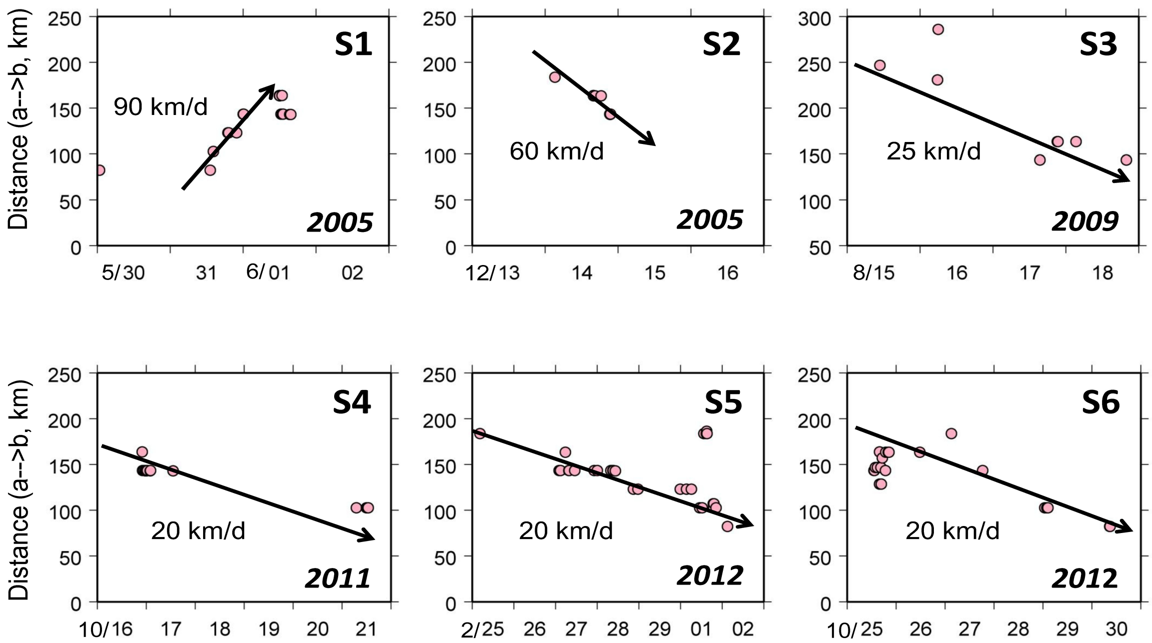

Figure 4.30. Time-space diagrams of six migrating VLFE clusters (S1-S6) in the Sakishima

area along line a-b in Figure 4.29a. The red circles are VLFEs; the black arrows indicate the migrating direction of VLFEs. The migration speed of each case is giving in the diagram.

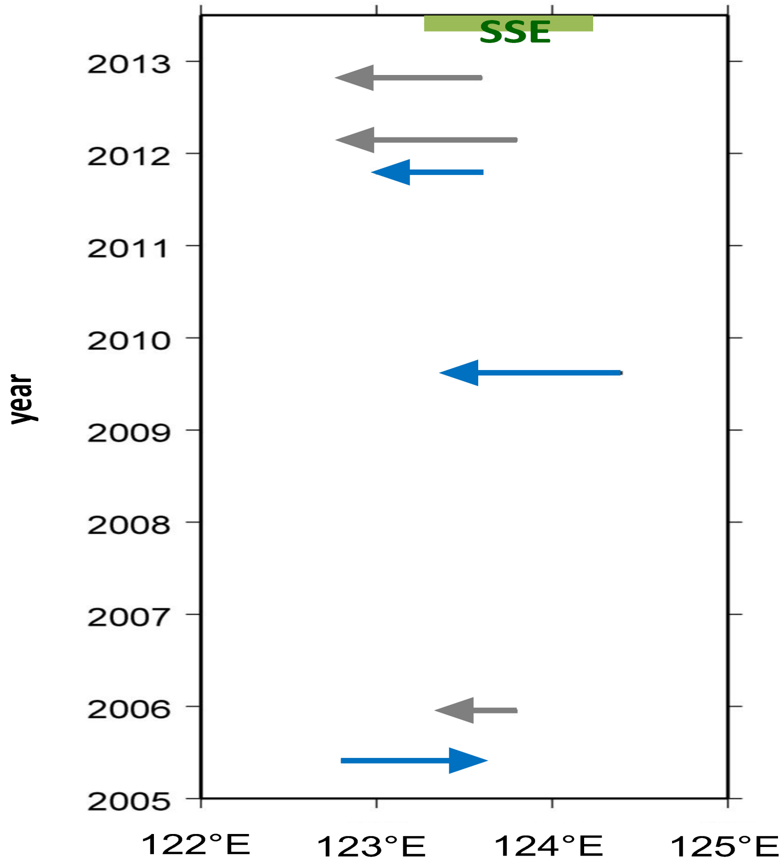

Figure 4.31. Space-time plot of VLFE migrations along the meridian in the Sakishima area. The arrows indicate the location and direction (eastward or westward) for the VLFE migrations. The blue and gray arrows represent VLFE migrations, which are synchronized and unsynchronized with SSEs, respectively. The thick green bar at the top represents an approximate location of the Iriomote SSE fault patch.

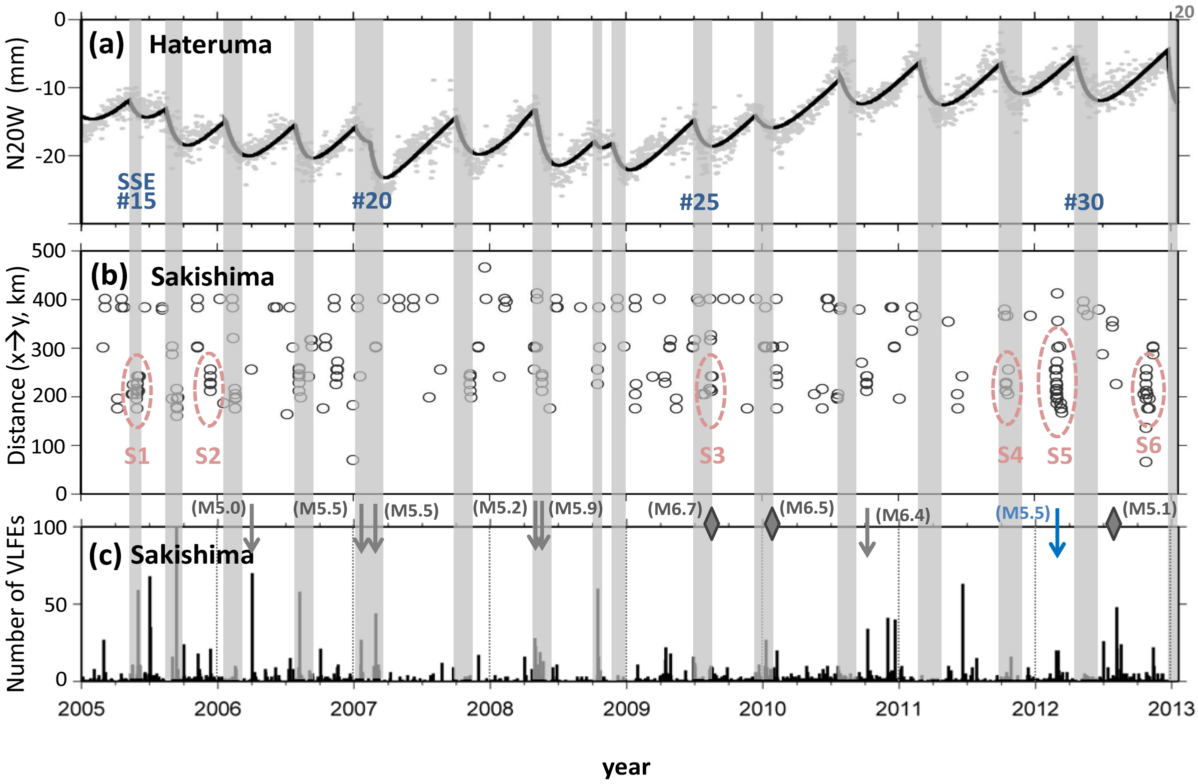

Figure 4.32. (a) The daily GNSS coordinates of the Hateruma site relative to the Miyako site in the N20W direction. The gray belts show the active times of the 16 SSEs with a number below corresponding to the SSEs in Table 3-1. (b) Time-space diagram of VLFEs in the Sakishima area along line X-Y in Figure 4.29a. Dashed red ellipses display the VLFE migrating clusters (S1-S6) detected in this study. The migrating clusters of S1, S3, and S4 are consistent with the activity of SSE#15, #25, and #29, but the clusters of S2, S5, and S6 started before the SSEs. (c) Daily counts (solid bars) of VLFEs for the Sakishima area. The blue arrow indicates an M_{JMA} 5.5 earthquake that probably caused the VLFE migrating cluster of S5. Gray arrows show other local earthquakes ($M_{JMA} \geq 5$) that activated VLFE activities but were not related to the migrations of VLFEs. The diamonds mark local earthquakes that occurred concurrently with VLFE activity.

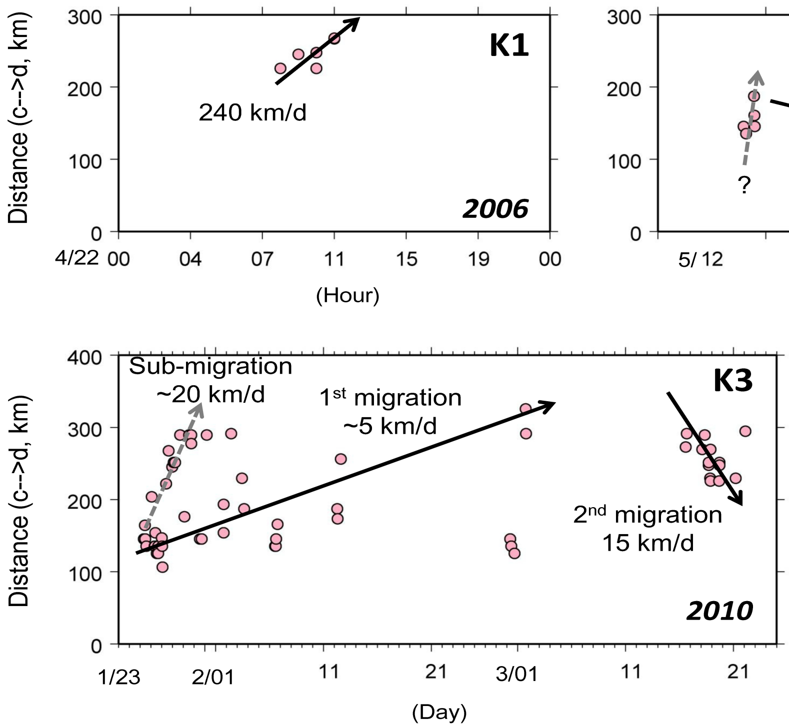

Figure 4.33 Time-space diagrams of three migrating VLFE clusters (K1-K3) in the southern Kyushu area along line c-d in Figure 4.29a. The red circles show VLFEs of these migrating clusters. The solid arrows indicate the migrating VLFE direction. The gray dashed arrows mark the direction of sub-migrations. The migration speed of each case is shown in the diagram.

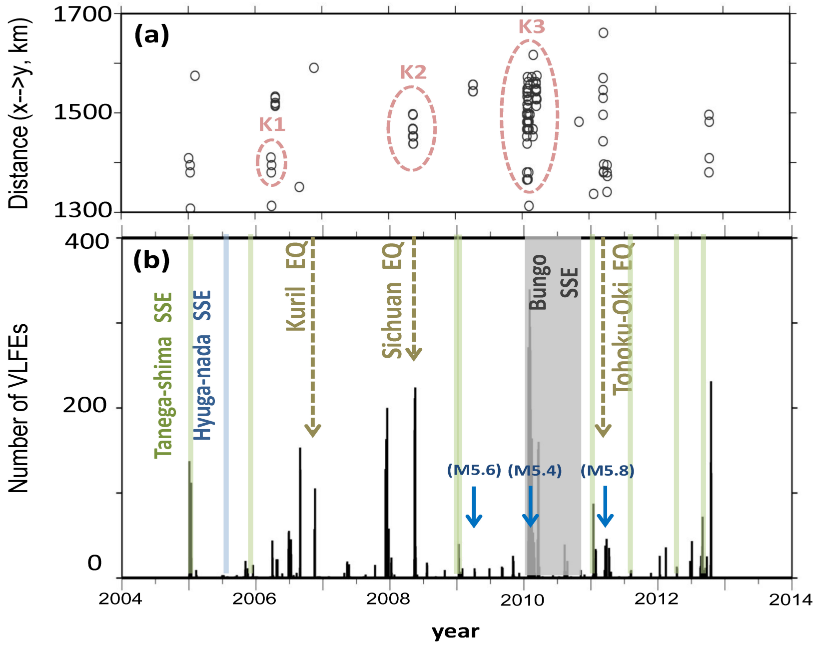

Figure 4.34. (a) Time-space plot of VLFEs in the southern Kyushu area along line X-Y in

Figure 4.29a. Red dashed circles display the VLFE migrating clusters (K1-K3) detected in this study. (b) The daily (black bars) numbers of VLFEs in the southern Kyushu area. Green and blue vertical lines display the occurring times of Tanega-shima and Hyuga-nada SSEs (see their locations in Figure 4.21c). The grey belt shows the active time of the 2010 Bungo SSEs. The dashed yellow arrows indicate the occurrence time of three teleseismic events (the 2006 M_w-8.3 Kuril, 2008 M_w-7.9 Sichuan earthquakes and 2011 M_w-9.1 Tohoku-oki earthquakes) that activated VLFEs in the southern Kyushu area. The blue arrows represent three local earthquakes (M_{JMA} >5) that triggered VLFE activities. The detailed information on these local and teleseismic earthquakes is given in Table 4.3.

Table 4-6. Information of the nine migrating clusters of VLFEs detected in the Sakishima and southern Kyushu areas.

No.	Area	VLFE start	Speed (km/day)	Duration (day)	Direction	Correlative external force
S1	Sakishima	2005/05/30	90	2	W→E	Iriomote SSE#15
S2	Sakishima	2005/12/14	60	2	E→W	?
S3	Sakishima	2009/08/15	25	4	E→W	Iriomote SSE#25
S4	Sakishima	2011/10/16	20	6	E→W	Iriomote SSE#29
S5	Sakishima	2012/02/25	20	7	E→W	Local earthquake
S6	Sakishima	2012/10/25	20	6	E→W	?
K1	S. Kyushu	2006/04/22	240	4hr	S→N	?
K2	S. Kyushu	2008/05/12	20	4	N→S	Sichuan earthquake
K3	S. Kyushu	2010/01/25	5-20	35	S→N N→S	2010 Bungo SSE

4.5 Summary

- From 2005 to 2012, a total of 29,841 VLFEs were identified in the Ryukyu Subduction Zone. Their dominant frequency range is 0.03-0.15 Hz and lack high-frequency content.
- Based on the locations, source depths, and focal mechanisms, these VLFEs are considered as thrust faults that probably occurred along the splay faults in the accretional prism or on the shallow plate interface of the Ryukyu subduction zone.
- High *b*-values (2.3-5.0) of VLFEs in the Ryukyu region suggest that materials in the VLFE source area are highly heterogeneous.
- The VLFEs in Sakishima, Okinawa, and Amami can be activated in 5-30 days, 0-15 days, and 0-5 days, respectively, after the start of nearby SSE activity. Moreover, the VLFE activity in the southern Kyushu is triggered or activated by the Bungo long-tern SSEs, Hyuga-nada and Tanega-shima short-term SSEs, and some large teleseismic earthquakes (e.g., 2006 Kuril earthquake, 2008 Sichuan earthquake, and 2011 Tohoku-Oki earthquake).
- The sources of (slow) earthquakes in Ryukyu Trench are distributed as follows, in Sakishaima: the megathrust earthquakes (locked zone, ~10 km), VLFEs (~20 km), and SSEs (~30 km), and in Okinawa: VLFEs (~20 km) and SSEs (~30 km). However, their distribution in the Amami area is still uncertain due to the complex tectonic setting and inaccurate hypocenters of large earthquakes and VLFEs.

Chapter 5.

Repeating Very Low Frequency Earthquakes (RVLFEs)

5.1 Introduction

5.1.1 Repeating earthquakes (REs)

Repeating earthquakes (REs) are a sequence of earthquakes having similar waveforms, sizes, locations, and focal mechanisms (Rau et al., 2007). These earthquakes maintain their similarity by repeatedly slips at the same fault patch and sometimes possess a reasonably regular interval (Kimura et al., 2006; Tamaribuchi et al., 2010). REs have been documented within the creeping zone of strike-slip plate boundaries, such as the San Andreas Fault, USA (Nadeau et al., 1995) and the Longitudinal Valley Fault, Taiwan (Chen et al., 2009). Moreover, they were also observed in some subduction zones, e.g., the Japan Trench, NE Japan (Matsuzawa et al., 2002), Sagami Trough (Kimura et al., 2006), and the Ryukyu Trench, SW Japan (Tamaribuchi et al., 2010), and might be related to small asperities on the plate interface (Igarashi et al., 2003; Uchida et al., 2003).

Based on the activities and recurrence intervals, Igarashi et al., (2003) classified REs into the continuous type and the burst type. The continuous type events have a constant interval. Large earthquakes rarely disturb their activities, i.e., they directly reflect the stress release of the slab interfaces (Igarashi et al., 2003; Uchida and Matsuzawa, 2013). In contrary, the burst-type events, like earthquake swarms, occur shortly after a large earthquake. Because the source regions of REs are adjoining to the fault patches of megathrust earthquakes, several investigations also used them to determine the extent of locked zones on the slab interface (e.g., Igarashi et al., 2003; Uchida et al., 2003).

5.1.2 Very low frequency earthquakes (VLFEs)

Very low frequency earthquakes (VLFEs) are a type of slow earthquakes dominated in the frequency band of 0.1-0.01 Hz with a little or no high frequency content (Obara and Ito, 2005). In comparison with ordinary earthquakes, VLFEs usually have a longer duration (~20 s) and consist predominantly of long-period waves (Beroza and Ito, 2011). Accordingly, they only can be recorded by high-sensitivity broadband seismometers. Based on the source mechanisms, VLFEs can be divided into the volcanic type and the nonvolcanic type. The volcanic-type VLFEs are related to the fluid or magma transportation caused by volcano activities (e.g., Arciniega-Ceballos et al., 1999), while the nonvolcanic-type VLFEs are generated by the shear faulting of subduction zones (e.g., Obara et al., 2004b).

For the nonvolcanic VLFEs, they usually occur in seismically active plate boundaries, such as the Nankai Trough (e.g., Obara and Ito, 2005) and the Cascadia subduction zone (e.g., Ghosh et al., 2015) (Figure 4.1). Because large interplate earthquakes repeatedly occur there (e.g., Ando, 1975), VLFEs are considered to have certain links to megathrust earthquakes (Obara and Kato, 2016). However, the Ryukyu Trench is different from the subduction zones mentioned above; it is a weakly coupled plate boundary, and probably no megathrust earthquakes have occurred (Peterson and Seno, 1984; Lallemand et al., 2005; Scholz and Campos, 2012). However, some studies reported observations of VLFEs at this trench (Ando et al., 2012; Nakamura and Sunagawa, 2015).

To understand the VLFEs in the Ryukyu area, I followed the study of Ando et al. (2012) to detect 29,841 VLFEs using 8-year broadband seismic data. Furthermore, I analyzed the locations and CMT solutions of 1,504 events obtained from the waveform inversion analysis.

As mentioned in Chapter 4, these VLFEs are all located along the Ryukyu Trench axis with depths of < 60 km, and their focal mechanisms are mostly thrust faults (Figure 4.11; Supplement 1). Hence, these VLFEs might have occurred on the shallow slab interface or in accretionary prisms of the Ryukyu subduction zone (see detail in Section 4.3.3-4.3.4).

5.1.3 Repeating VLFEs (RVLFEs)

In addition to the location and source mechanism, I also investigated the activity of VLFEs for the four subareas of Sakishima (S), Okinawa (O), Amami (A), and southern Kyushu (K) (Figure 5.1a). The related contents and results are provided in Chapter 4. Notably, I found an interesting cluster of VLFEs, south of the Miyako Island (Figure 5.1b). These events are similar to each other in the waveform, location, magnitude, and focal mechanism, and recur in a limited area (approximately 30 km x 10 km) with a roughly regular interval. So far, no similar phenomena have been reported for VLFEs in any subduction zones. Because the characters of these VLFEs are same as those of REs mentioned above, I decided to name the new type of VLFEs as repeating very-low-frequency earthquakes (RVLFEs) to distinguish them from the regular VLFEs described in Chapter 4.

5.1.4 Purposes of this study

Ando et al. (2012) has briefly mentioned this new type of VLFEs, but their properties have been unknown due to the lack of a detailed study. In this chapter, I analyzed their waveform similarities, locations, source mechanisms, and recurrence intervals. Moreover, I discussed the correlations between the RVLFEs and slow slip events (SSEs) and nearby repeating seismic events. I expect that these results can help clarify the mechanism of slow earthquakes and the plate motion of the southwestern Ryukyu subduction zone.

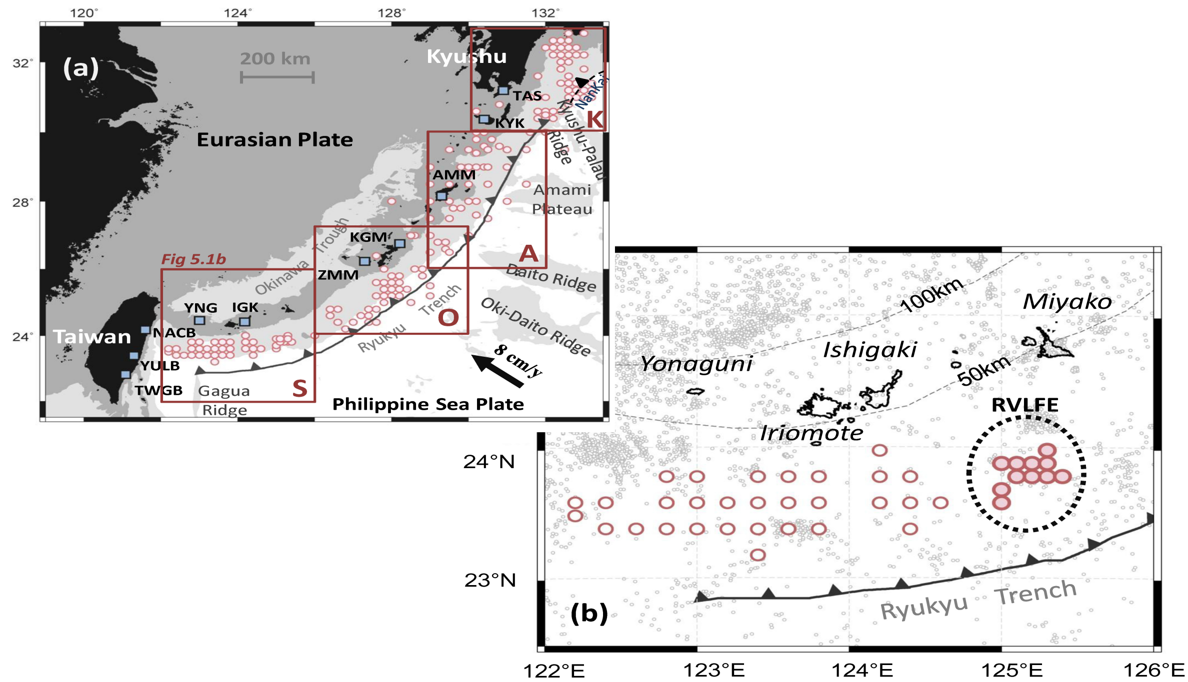

Figure 5.1. (a) Tectonic map in the Ryukyu region and the distribution of VLFEs (red circles) for the four subareas of Sakishima (S), Okinawa (O), Amami (A), and southern Kyushu (K). The blue squares show ten broadband seismic stations of F-net and BATS used for the detection of VLFEs. The Philippine Sea Plate is subducting beneath the Eurasian Plate along the Ryukyu Trench with the average convergence of 8 cm/y (Nakamura, 2009). The Kyushu-Palau Ridge in the southern Kyushu area (K) separates the Ryukyu Trench (black solid line) and the Nankai Trough (black dash line). (b) Seismic distribution of the Sakishima area (S) in Figure 5.1a. Red open circles display the regular VLFEs described in Chapter 4, and red solid circles indicate a new type of VLFEs (hereafter call RVLFEs) detected in this study. Gray dots are ordinary earthquakes ($M_{JMA} \geq 3$) from 2000 to 2015 recorded by JMA. Dashed line contours show the upper surface of the Philippine Sea Plate.

5.2 Data and method

5.2.1 Detections of VLFEs

In this study, I first detected regular VLFEs in the Ryukyu region. I analyzed vertical component seismograms in 2005-2012 recorded at ten broadband seismic stations of the F-net by National Research Institute for Earth Science and Disaster Resilience (NIED) of Japan and BATS (Broadband Array in Taiwan for Seismology) by Institute of Earth Science (IES) of Taiwan (Figure 5.1a). Then, I filtered all seismic data using a bandpass filter of 0.02–0.06 Hz since the short-period (0.2−1 Hz) noise level is too high to identify VLFEs (Beroza and Ide, 2011; Ando et al., 2012). After obtaining low-frequency signals from the filtered seismograms, I deleted local and teleseismic earthquakes based on earthquake catalogs of Preliminary Determination of earthquakes (PDE, USGS), Japan Meteorological Agency (JMA), and Central Weather Bureau (CWB) of Taiwan. Moreover, some un-cataloged microearthquakes (< M_w 2.5) were removed via the 1.0 Hz high-pass filtered seismograms. The above process is same as those used for regular VLFEs described in Section 4.2.1.

5.2.2 Observations of RVLFEs

From 2005 to 2012, a total of 7,546 VLFEs were detected within the Sakishima area, whose seismic waves arriving first at the YNG or IGK stations (Figure 5.1). Among these VLFEs, 97 events were determined as RVLFEs considering their peculiar behaviors and comparable waveforms. Figure 5.2 displays a series of RVLFE activities recorded at broadband seismic stations of F-net and BATS. The first arrival times indicate that these events should occur between IGK and ZMM stations. Unlike the regular VLFEs lasting several hours like earthquake swarms (Figure 4.4), a typical sequence of RVLFE activities contains two or three events within three hours. Sometimes one extra follows but it do not show a regular interval (Figure 5.2). Notably, these events all have similar waveforms and amplitudes (Figure 5.3), and their signals are much more evident than those of regular VLFEs (Ando et al., 2012).

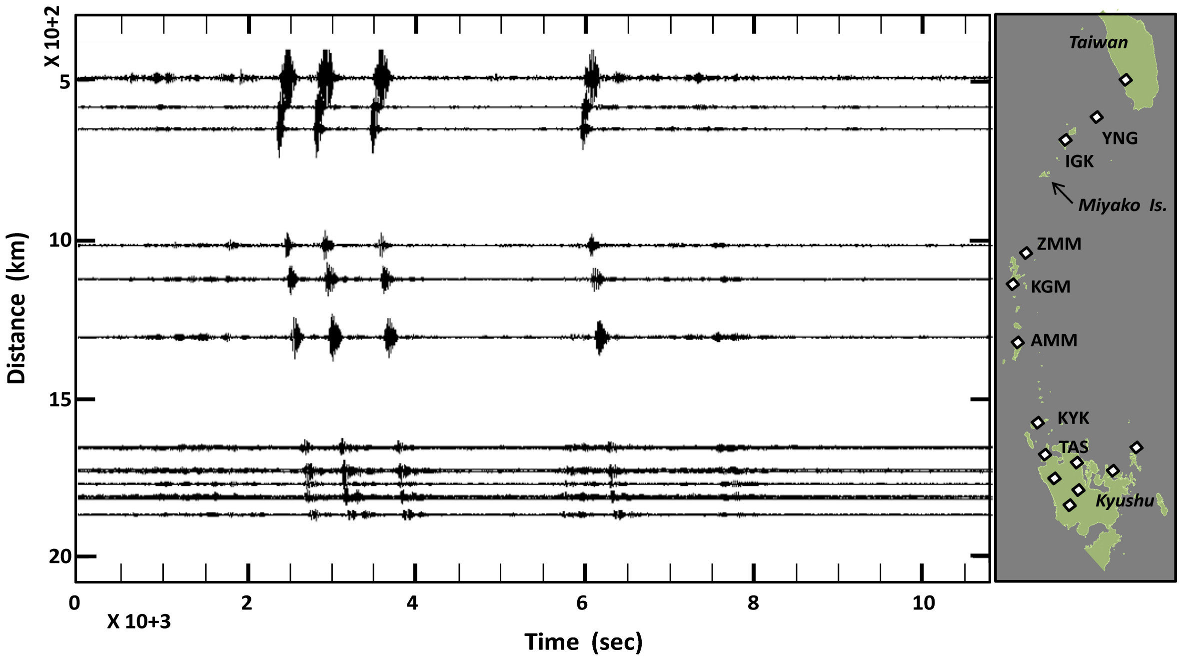

Figure 5.2. Three-hour vertical-component seismograms for four RVLFEs recorded at 14 broadband seismic stations of F-net and BATS (diamonds in the right map). These seismograms, filtered at 0.02-0.06 Hz, are arranged from top to bottom based on increasing distance with a reference point of 120°E–20°N. Each seismogram corresponds to one station shown in the map. This sequence consists of four RVLFEs. Three of the four events occurred sequentially within an hour, and the other one followed 40 minutes later. The origin time of these seismograms is comparable to (UT) 09:00:00, on Mar. 6, 2005.

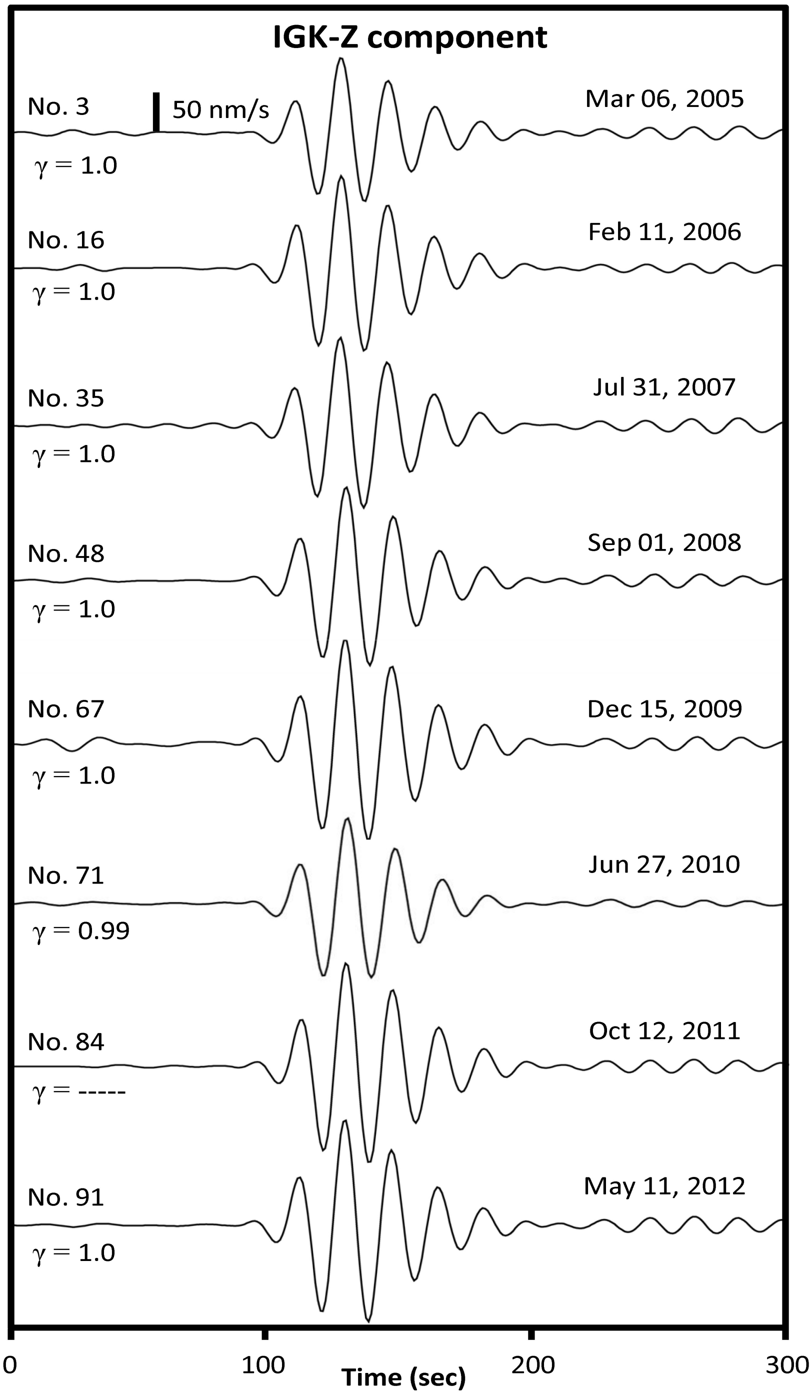

Figure 5.3. Vertical-component waveforms recorded at IGK for eight RVLFEs. The bandpass filtered (0.02-0.06 Hz) seismograms display 300 s-long waveforms starting 50 s before the origin times of these RVLFEs. These events occurred in different time periods but have similar waveforms and amplitudes. The numbers beside the waveforms correspond to the RVLFEs in Supplement 2. Their cross-correlation coefficients (γ) with respect to the master event of No. 84 are also exhibited aside.

5.2.3 Determinations of hypocenters and source mechanisms

I employed the grid-search moment-tension inversion method developed by Nakano et al. (2008) to determine the hypocenters and source mechanisms of RVLFEs. This program locates a target earthquake at a spatial grid point and estimates the strike, dip, and rake of the earthquake fault using a 1-D seismic velocity model (AK135, Kennett et al., 1995). For this analysis, I first calculated the Green's functions of the full waves at each grid point with horizontal and vertical intervals of 0.2° and 10 km, respectively, as shown in Zone S (Figure 5.4a). After obtaining approximate hypocenters, I reduced the horizontal spacing to 0.1° to attain more accurate source locations for the area of 23.2° N−24.6° N and 124.8° E−125.8° E (see Zone M in Figure 5.4a), in which the 97 RVLFEs are concentrated. Figure 5.4 shows one example of the inversion results of an RVLFE (No.84 in Supplement 2). This event is located at a grid of 125.3° E−23.9° N, about 60 km north of the Ryukyu Trench. Its source depth and moment magnitude (M_w) is 20 km and 4.0, respectively. Moreover, the best-estimated model is a thrust fault. The three-component (NS, EW, and Z) seismograms of YNG and IGK were used for the analysis of this event.

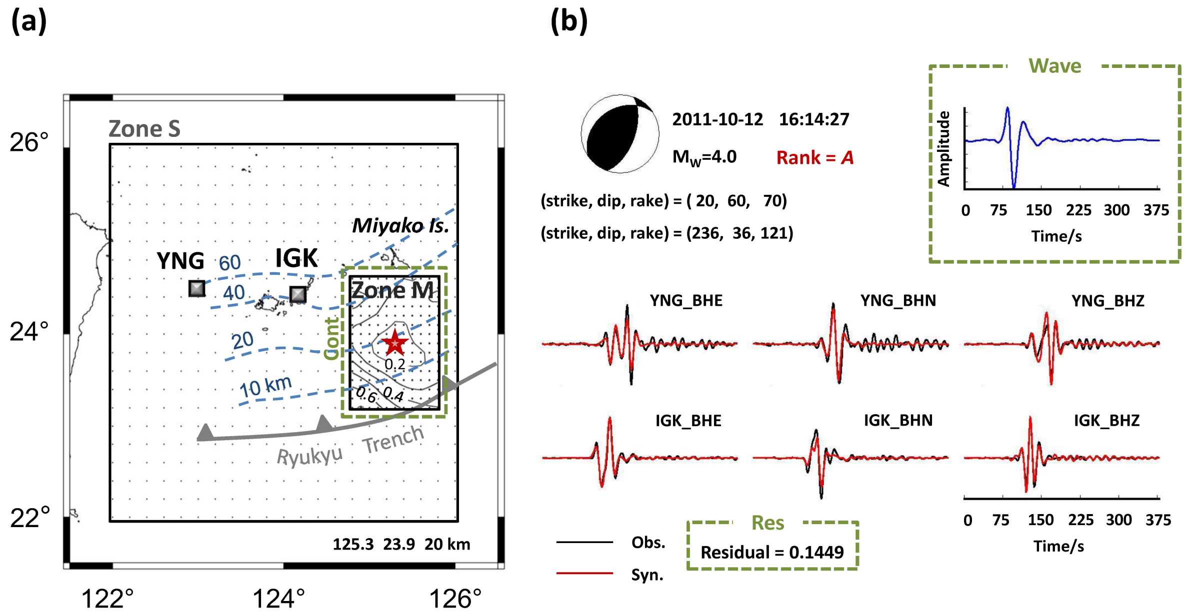

Figure 5.4. (a) The hypocenter (red star) of an RVLFE (No. 84 in Supplement 2) and its residual contours in Zone M. YNG and IGK (grey squares) are the seismic stations of F-net used for the waveform inversion of this event. The grid search of this inversion is performed at the dots with an interval of 0.2° in Zone S and 0.1° in Zone M. The contours within Zone M display the residuals between synthetic and observed waveforms obtained from the hypocenter and CMT grid search. The blue dashed curves show the upper depth of the Philippine Sea Plate (unit of km). (b) The CMT solution of the No. 84 RVLFE. The beach ball displays the best-fit focal mechanism. The obtained waveform (blue curve) at the hypocenter is shown in the top right corner. The bottom displays the three-component waveforms of the synthetic (red curve) and observed (black curve) seismograms. The green dashed rectangles indicate three categories of residual (Res), waveform at the source (Wave), and shape of residual contours (Cont) for evaluating the reliability of the inversion results. The quality value of this event is 8 (see Supplement 2) and is defined as rank *A* based on the criteria described in Table 5-1 and 5-2.

5.2.4 Evaluations of the reliability of the waveform inversion

After obtaining the locations and CMT solutions, I used quality ranks A (good), B (fair), and C (poor) to evaluate the reliability of inversion results based on three criteria, including residual (Res), waveform at the source (Wave), and shape of residual contours (Cont) (Table 5-1; Figure 5.4). Likewise, three grades (good=3, fair=2, poor=1) were assigned to each category. If the grade sum is ≥ 8, the results are defined as rank *A*. If the sum ranges in 5-7, they are assigned to rank *B*, but if the sum ≤ 4, defined as rank *C* (Table 5-2). For instance, the RVLFE of No. 84 (Figure 5.4) has grades of Res=2, Wave=3, and Cont=3. This event is assigned to rank *A* because its grade sum is 8 (i.e., Res + Wave + Cont). This method is same as the one used for the regular VLFEs mentioned in Section 4.2.3, but I adopted a stricter standard on residual here (see Table 5-1) because RVLFEs usually have lower residual values than the regular VLFEs.

Table 5-1. Evaluation points for the inversion results

Point	**(1) Residual of waveform matching**	**(2) Waveform at the source**	**(3) Shape of residual contours**
3 (good)	< 0.13	Simple and clear	Circular
2 (fair)	0.13−0.16	Slight noisy	Elliptical
1 (poor)	> 0.16	Very noisy	Elongated or unclosed

Table 5-2. The quality ranks of inversion results based on the quality value

	Rank A (good)	**Rank B (fair)**	**Rank C (poor)**
Quality value	9, 8	7, 6, 5	4, 3

5.3 Results

5.3.1 Waveform similarity

I observed 97 RVLFEs in 2005-2012 along the southwestern Ryukyu Trench (Figure 5.1b). These events have particular activities and sequences (Figure 5.2), but their dominant frequency range (0.03-0.15 Hz) is same as the regular VLFEs (Figure 5.5). The most remarkable characteristic of RVLFEs is similar waveforms and amplitudes (Figure 5.3). Accordingly, in this section, I attempted to calculate cross-correlation coefficients (γ) for the 97 events to verify their waveform similarity. For this analysis, I first selected the RVLFE of No. 84 as the master event due to its high signal-to-noise ratio. Then, I estimated γ of other 96 RVLFEs with respect to the master event. It is interesting to note that 93 % of RVLFEs (89 events) has $\gamma \geq 0.9$ (Supplement 2), which suggests that these RVLFEs possess high waveform similarity. The remaining seven events, whose $\gamma < 0.9$, are probably related to the higher background noise in waveforms since most of them concurrently have a low-quality rank (Supplement 2).

Nevertheless, a narrow band-pass filter (0.02-0.06 Hz) may have cause the high γ of RVLFEs due to the lack of high-frequency components. To examine this possibility, I extended the upper limit of the band-pass filter from 0.06 to 0.1 Hz and recalculated γ of all RVLFEs. Although high-frequency noise caused by the wider bandpass filter remarkably contaminates the RVLFE signals, I still obtained 70 % of RVLFEs (65 events) having $\gamma \geq 0.9$. It suggests that the high waveform similarity of RVLFEs here is not due to the narrow bandwidth of this filter.

To understand the waveform similarity between RVLFEs and other seismic events, I arbitrarily selected two cases on each regular VLFE, ordinary earthquake, and RVLFE in the Sakishima area (Figure 5.6a). Detailed source parameters of the six events are provided in Table 5-3. Similarly, I calculated the γ for these selected events with respect to the RVLFE of No. 84. The γ values of the two regular VLFEs (see V77 and V1141 in Figure 5.6a) are 0.6 and 0.8, respectively (Table 5-3), significantly lower than the average γ value (0.96) of RVLFEs. It means that the waveforms of RVLFEs are similar to each other but different from those of regular VLFEs even in the same frequency band (Figure 5.6b). Moreover, the γ values of the two ordinary earthquakes (see E1 and E2 in Figure 5.6a) are all < 0.6 as expected (Table 5-3).

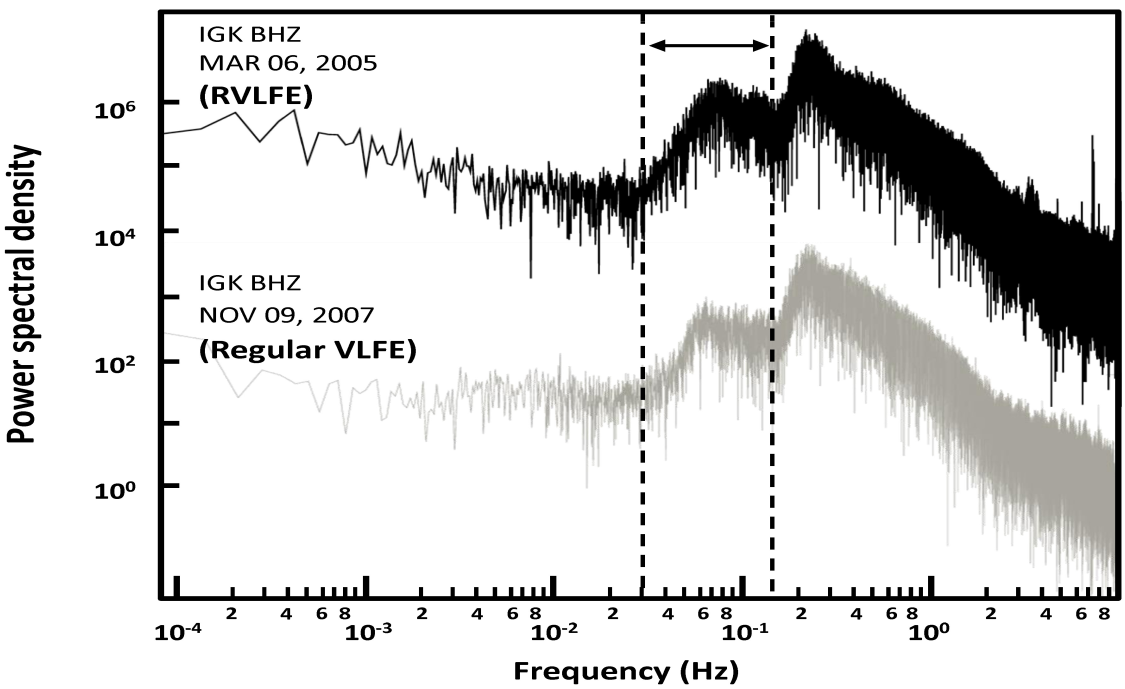

Figure 5.5. Spectra of three-hour vertical-component seismograms of RVLFEs (black line) and regular VLFEs (gray line) recorded at IGK. Their waveforms are shown in Figure 5.2 and Figures 4.4, respectively. The two dashed lines define the dominant frequency range

(0.03-0.15 Hz) of RVLFEs, which is same as that of the regular VLFEs. Vertical positions of these two spectra are arbitrary.

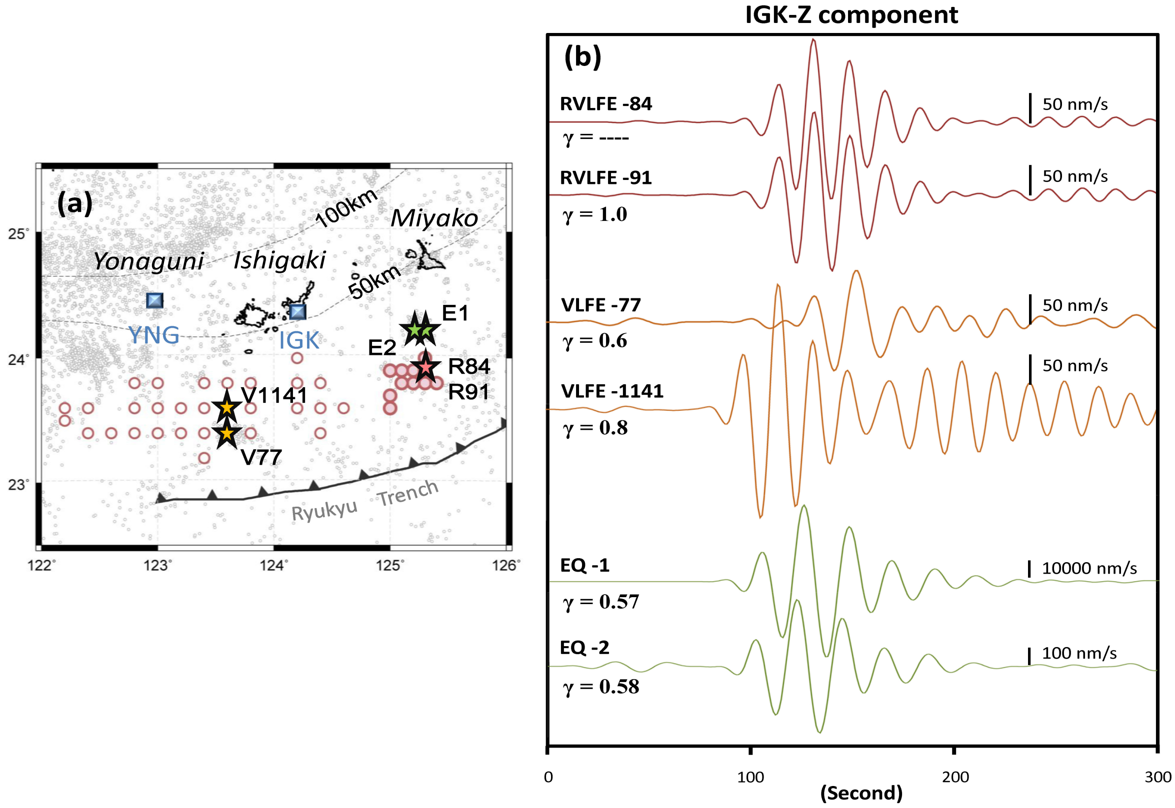

Figure 5.6. (a) Location of the six selected events including two RVLFEs (red stars), two regular VLFEs (yellow stars), and two ordinary earthquakes (green stars) for the comparison of waveform similarity. Their waveforms and source parameters are shown in Figures 5.6b and Table 5-3, respectively. The numbers beside the stars correspond to the events in Table 5-3. The red open circles are regular VLFEs detected in Chapter 4; the red solid circles are RVLFEs observed in this study. The gray dots indicate ordinary earthquakes (M_{JMA} ≥ 3) recorded by JMA. The two blue squares are the broadband seismic stations (YNG and IGK) of F-net in the Sakishima area. Dashed line contours display the upper depth of the Philippine Sea Plate (unit in km). (b) Vertical-component waveforms of the two selected events on each cluster of RVLFEs (red curves), regular VLFEs (yellow curves), and ordinary earthquakes (green curves) recorded at IGK. The bandpass-filtered seismograms (0.02-0.06 Hz) display 300 s-long waveforms starting 50 s before the origin times of these events. The γ below the event number shows the cross-correlation coefficient of this event with respect to the RVLFE of No. 84.

Table 5-3. Source information of the six selected seismic events for the waveform similarity comparison.

Type	Event No.	Time (UT)	Log (°E)	Lat (°N)	Depth (km)	M_w	Strike 1	Dip 1	Rake 1	Strike 2	Dip 2	Rake 2	CCC (γ)
*RVLFE	84	20111012161427	125.3	23.9	20	4.0	20	60	70	236	36	121	---
RVLFE	91	20120511083028	125.3	23.9	20	4.0	20	60	70	236	36	121	1.0
VLFE	77	20050601115254	123.6	23.4	50	4.7	200	80	-30	296	61	-168	0.60
VLFE	1141	20101008163910	123.6	23.6	40	4.6	38	84	50	300	40	170	0.80
EQ	1	20090805001758	125.3	24.2	22	6.5	31	82	76	272	16	151	0.57
EQ	2	20090808054414	125.2	24.2	22	5.0	51	75	78	271	19	128	0.58

* The master event for the calculation of cross-correlation coefficients (γ)

5.3.2 Hypocenters and focal mechanisms

I obtained the locations and CMT solutions of the 97 RVLFEs using the moment tensor inversion program developed by Nakano et al. (2008). The number of these RVLFEs assigned to quality ranks *A, B*, and *C* is 28, 53, and 16, respectively. Detailed source parameters and quality rank of each event are provided in Supplement 2. Figure 5.7a shows the distribution of the 97 RVLFEs. These events are all located in an isolated area (23.6° N−24.0° N and 125.0° E−125.4° E) about 90 km south of the Miyako Island. Their source depths are within 10-30 km (Figure 5.7b), and the moment magnitudes (M_w) range in 3.8-4.2 (Supplement 2). The CMT solutions of all RVLFEs are thrust faults except for one event (Supplement 2). Here, I exhibited source mechanisms of 13 selected RVLFEs, whose quality value is 9 and defined as rank *A.* As illustrated in Figure 5.7a, their CMT solutions all display thrust faulting mechanisms with a slight strike-slip component, which suggests that the occurrence of these RVLFEs may relate to the plate converge of the Ryukyu subduction zone.

Because these RVLFEs have shallow source depths (~20 km) and thrust-fault mechanisms, I suspect that they probably have been occurred in the accretionary prism or on the plate interface of the subduction zone, similar to the regular VLFEs detected along the Ryukyu Trench (see Chapter 4) or shallow VLFEs observed in the Nankai Trough (e.g., Obara and Ito, 2005). The source region of RVLFEs seems to fall precisely on the slab interface of the Ryukyu subduction zone (Figure 5.7b). However, if I assume the shallower dip nodal planes as slip planes (Supplement 2), the average dip angle will be 37°. It is significantly higher than the subduction slope (~20°) of the Philippine Sea Plate in the Ryukyu area (Kubo and Fukuyama, 2003; Nishizawa et al., 2017). Namely, the RVLFEs more likely occur in the accretionary prism rather than on the slab interface of the Ryukyu subduction zone.

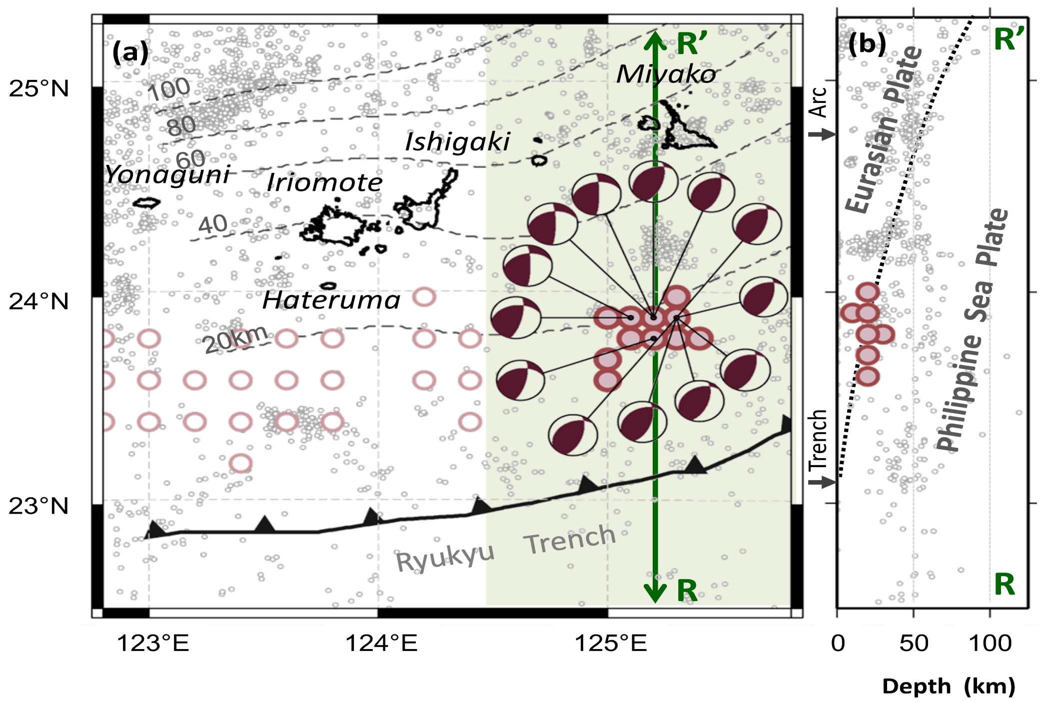

Figure 5.7. (a) Locations and focal mechanisms of RVLFEs. The red solid circles depict the epicenter of the 97 RVLFEs. Beach balls display the CMT solutions of 13 selected events

whose quality value of 9 (rank A). Red open circles indicate the regular VLFEs detected in Chapter 4. The grey dots show the epicenters of ordinary earthquakes with $M_{JMA} \geq 3$ in 2000-2015 reported by JMA. Dashed line contours (unit in km) display the surface depth of the Philippine Sea Plate. The green area shows the geometric extent of profile RR', whose cross-section is displayed in Figure 5.7b. (b) The cross-section of profile RR' in Figure 5.7a. The red solid circles are RVLFEs detected in this study. The black dotted line shows the subduction plate boundary between the Philippine Sea Plate and Eurasian Plate. The solid arrows in the left mark the relative positions of the Ryukyu Trench and the Ryukyu Arc.

5.3.3 Location errors

To examine the reliability of RVLFE hypocenter locations estimated by the waveform inversion of this study, I compared hypocenters of ordinary earthquakes determined by F-net and those solved by my method. For this analysis, I applied the same inversion method to six ordinary earthquakes with $M_{JMA} > 4$, which were selected arbitrarily from Zone M (Figure 5.8). The seismic network, stations, and filter-band used in this analysis were same as those adopted for the RVLFEs mentioned in Section 5.2.3. Figure 5.8 illustrates epicenters of the six ordinary earthquakes obtained from my inversion method and those given in the F-net earthquake catalog. As mentioned in Chapter 4, the earthquake epicenters of F-net catalog are the same as those of JMA, while their depths, magnitudes, and CMT solutions are determined by the own inversion method of F-net. In general, the epicenters of JMA are more reliable than those of F-net because JMA has more seismic stations (2-5 times) with a better azimuthal converge for the hypocenter positioning. The average differences of the two results between the F-net and my inversion method are 0.09° ± 0.10° in longitude, 0.09° ± 0.10° in latitude, and -9 km ± 15 km in depth (Table 5-4). It is evident that these differences are all smaller than 0.1° (i.e., 10 km), suggesting that the hypocenters of RVLFEs estimated by this study are accurate and reliable.

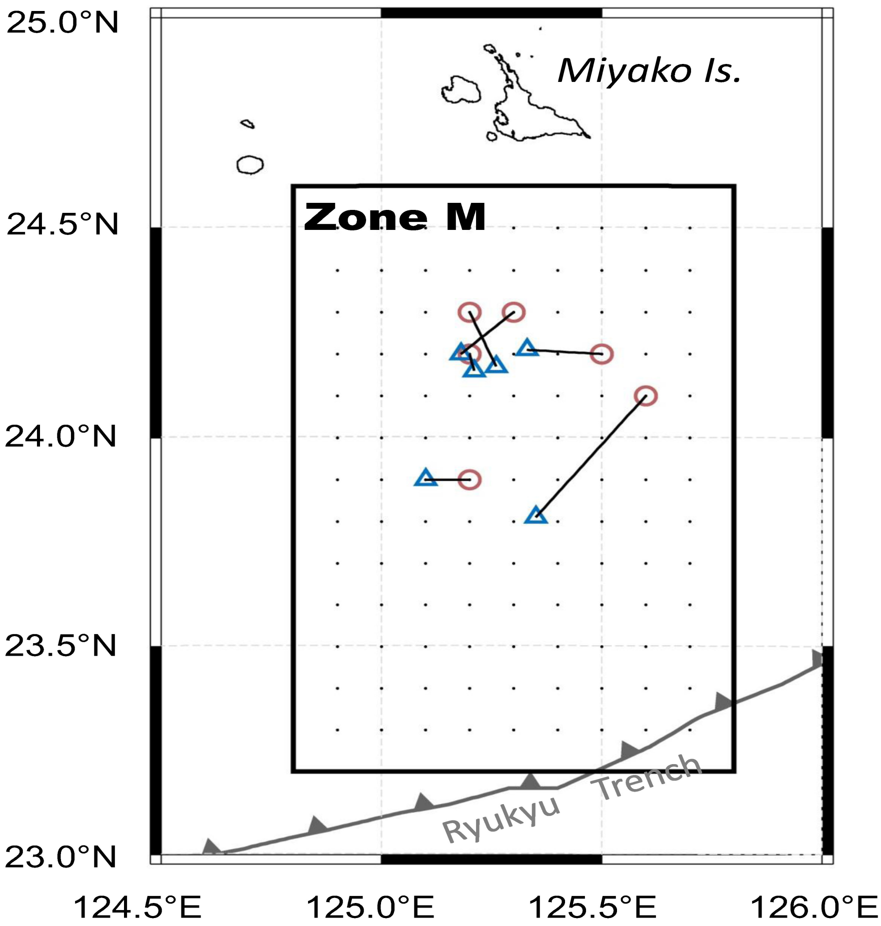

Figure 5.8. Epicenters of the 6 ordinary earthquakes ($M_{JMA} \geq 4$) obtained from the inversion method of this study (red circles) and those from the F-net earthquake catalog (blue triangles). The two epicenters (red circles and blue triangles) of the same earthquake are linked with a line. These earthquakes are arbitrarily selected from Zone M. The source information of the six earthquakes and the differences between the two results are given in Table 5-4.

Table 5-4. Comparison of hypocenters and moment magnitudes of 6 ordinary earthquakes south of the Miyako Island determined by F-net and in this study.

Time (JST)		F-net				This study				Difference (This study – F-net)			
		Lon	Lat	Depth (km)	M_w	Lon	Lat	Depth (km)	M_w	ΔLon	ΔLat	ΔDepth (km)	ΔM_w
2004/04/28	13:54:22	125.18	24.20	35	4.4	125.3	24.3	20	4.1	0.12	0.1	-15	-0.3
2007/05/03	05:31:43	125.35	23.81	17	4.3	125.6	24.1	30	4.2	0.25	0.29	13	-0.1
2009/08/05	09:17:58	125.26	24.17	35	6.1	125.2	24.3	10	5.9	-0.06	0.13	-25	-0.2
2009/08/05	20:26:47	125.21	24.16	35	4.6	125.2	24.2	10	4.4	-0.01	0.04	-25	-0.2
2010/01/17	07:04:52	125.10	23.90	44	4.6	125.2	23.9	50	4.3	0.10	0	6	-0.3
2010/10/04	22:28:38	125.33	24.21	38	6.2	125.5	24.2	30	5.9	0.17	-0.01	-8	-0.3
									Average	0.09	0.09	-9	-0.2
									std dev.	0.10	0.10	14	0.07

5.3.4 Recurrence intervals

A remarkable feature of RVLFEs is the time interval (t) between two successive events. As illustrated in Figure 5.9, the recurrence intervals of the 97 events display a tri-modal (or bimodal) distribution, which consists of an exponential distribution for t < 10 days (Type-1), a dome-like distribution (Type-2) for t = 10-100 days, and a pulse-like distribution (Type-3) for t > 100 days. The Type-1 cluster includes 52 intervals (53 RVLFEs) and exhibits an exponential attenuation with time (Figure 5.9). More than 77 % intervals (40 intervals) are less than one day (Figure 5.9), which suggests that these RVLFEs occurred intensively as a series within a short period. Because a typical sequence of VLFEs is usually composed of two or three events that occur within three hours (see Figure 5.2), these 52 intervals of the Type-1 may reflect the time spacing of each RVLFE in the same sequences.

The Type-2 cluster, made up of 37 intervals, displays a normal distribution with a mean of 50 ± 20 days (Figure 5.9). Unlike the Type-1 cluster, these intervals of the Type-2 exhibit the recurrence interval of the RVLFE sequences. It means that the RVLFEs recur approximately every two months, but their durations are less than ten days in general. Although several statistical models, such as Weibull, gamma, lognormal, and Brown Passage Time distributions, have been proposed for earthquake intervals (e.g., Utsu, 2003), it is still difficult to obtain a best-fit model for the Type-2 cluster at this stage due to the insufficient number of RVLFEs. However, I infer that the distribution of the Type-2 intervals may be close to the lognormal model, similar to repeating micro-earthquakes in the San Andreas Fault because both of them possess identical characteristics including both short- and long-term recurrences (Nadeau et al., 1995).

The Type-3 cluster contains seven intervals whose t >100 days (Figure 5.9). These intervals are different from Type-1 and Type-2; they exhibit the quiescent epochs of RVLFE activities, i.e., the RVLFEs cannot be detected during these periods. The absence of seismic data, overlapping signals by teleseismic waves, and the variation of creeping rate around the RVLFE fault all have potentials of generating such unusual long-term quiescence. However, until now, the causes of the long-term quiescence are uncertain, and further studies are necessary.

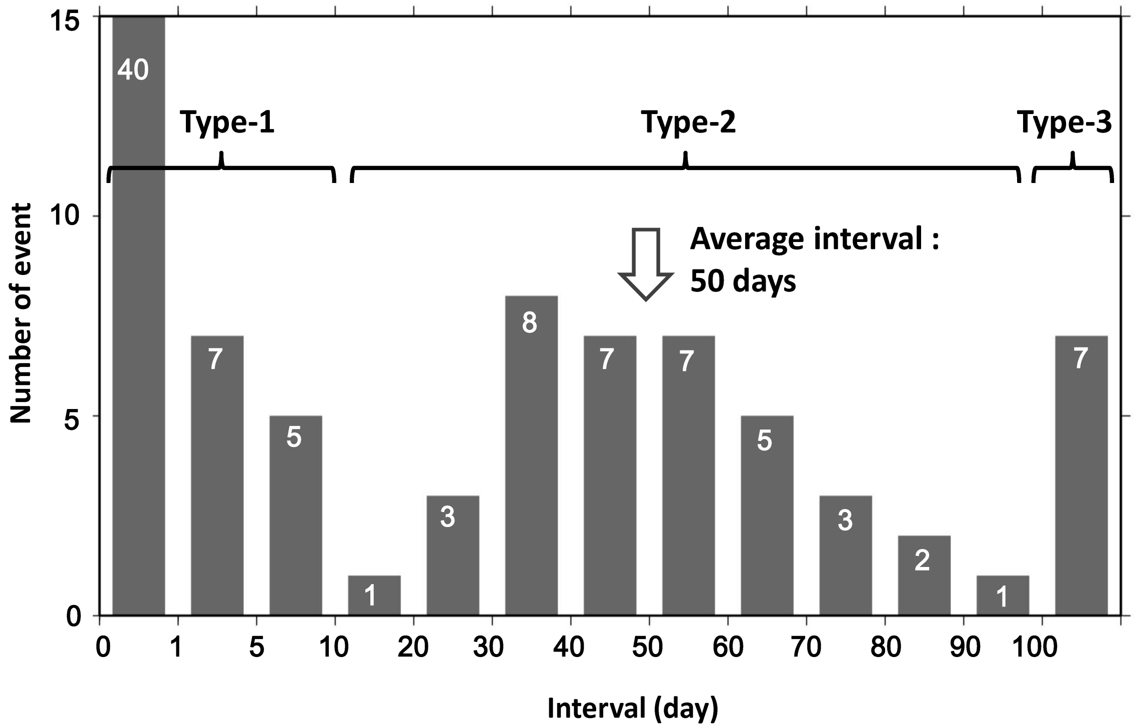

Figure 5.9. The distribution of recurrence intervals of the 97 RVLFEs. Type-1 includes more than half of RVLFEs and reflects the within-sequence recurrence intervals of RVLFEs. Type-2 exhibits the between-sequence time intervals of RVLFEs with the average of 50 (± 20) days. Type-3 reflects the occurrences of long-term quiescence (t >100 days) without RVLFE activities.

5.3.5 Mainshock-aftershock relations

Because the within-sequence recurrence intervals of RVLFEs show significant exponential attenuation with time (see Type-1 in Figure 5.9), some primary-secondary relations may exist between RVLFEs in the same sequences. To examine this hypothesis, I divided the 97 RVLFEs into 45 sequences and assigned the numbers (from 1st to 4th events) for RVLFEs in each sequence (Supplement 2). For this analysis, the 1st event was defined as having no any other events that occur within the previous ten days, and the 2nd event should occur following the 1st event within ten days. Likewise, the 3rd and 4th events needed to occur within ten days after the previous one. The number of 1st, 2nd, 3rd, and 4th events here is 45, 31, 16, and 5, respectively.

Based on this data, I found that the average M_w of the 1st events was slightly larger than that of the 2nd, 3rd, and 4th events (Table 5-5) with the average difference (ΔM_w) of -0.05 ± 0.13 (Figure 5.10). Moreover, the average intervals between the 1st and 2nd events and between the 2nd and 3rd events were 0.2 ± 0.4 h and 1.5 ± 3.0 h, respectively. These observations suggest that the 1st events have larger sizes and shorter recurrence intervals than other subsequent events, i.e., the mainshock-aftershock relation may exist within these RVLFEs.

Table 5-5. The average magnitudes (M_w) of the 1st, 2nd, 3rd and 4th RVLFE events in the same sequences.

	1st events	**2nd events**	**3rd events**	**4th events**
Average M_w	4.02	4.00	3.95	3.96

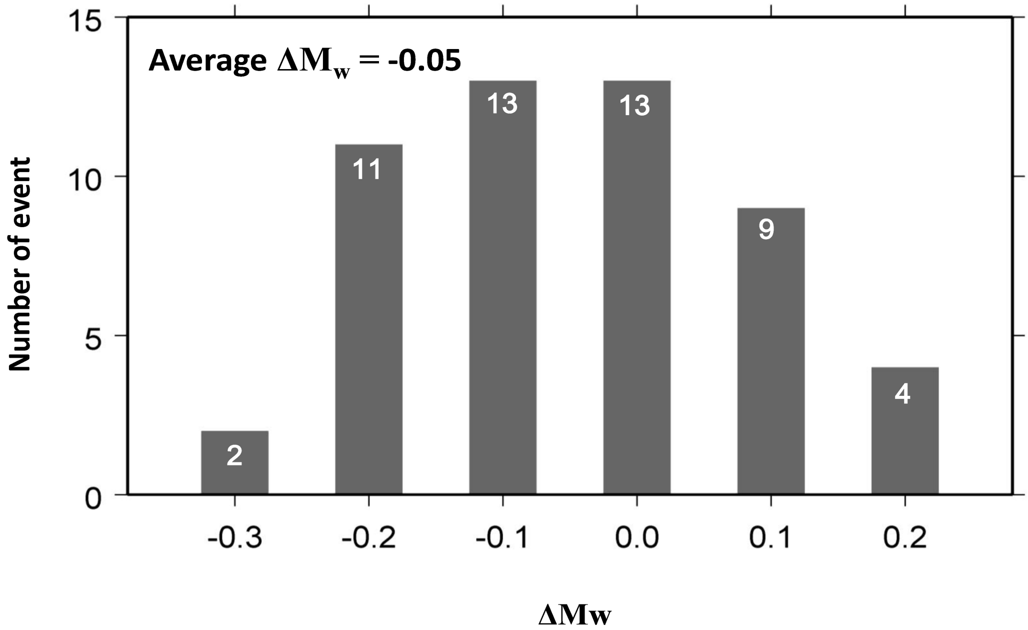

Figure 5.10. The magnitude difference (ΔM_w) between the 1st RVLFEs and subsequence RVLFEs within the same sequence.

5.3.6 *b*-values

The moment magnitudes (M_w) of RVLFEs determined by this study range from 3.8 to 4.2 (Supplement 2), which is much more centralized than those of M_w 3.4-4.7 of regular VLFEs in the Sakishima area (Table 4-4). It means that the RVLFEs have comparable sizes in addition to similar waveforms. To calculate the *b*-value of RVLFEs, I substituted the M_w data into the maximum-likelihood method proposed by Utsu (1965) and Aki (1965),

$$b = \log e \,/ (M_{mean} - M_c) \quad (5.1),$$

where M_{mean} and M_c are the mean magnitude and the cut-off magnitude for the given sample, respectively. For this estimation, I first determined the M_c = 3.8 by the cumulative frequency curve of RVLFEs (Figure 5.11). Then, I calculated the average magnitude (M_{mean})

between the maximum value (M_w 4.2) and the M_c (M_w 3.8). Finally, through (5.1), I obtained the *b*-value of 2.2 for the RVLFEs south of Miyako Island. Related parameters for this calculation are provided in Table 5-6.

As mentioned in Section 4.3.5, the *b*-value of regular VLFEs and ordinary earthquakes in the Sakishima area is 2.3 and 0.9, respectively. It is interesting to note that the *b*-value of RVLFEs is comparable to that of regular VLFEs but significantly higher than the *b*-value of ordinary earthquakes even in the same tectonic region (Table 5-6). Since the *b*-value is deemed to be an indicator of the heterogeneity of material (Mogi, 1962; Scholz, 1968), the high *b*-values of RVLFEs and VLFEs suggest that highly heterogeneous materials may exist in their source regions. In addition, the presence of high pore pressure fluid is another possibility for such high *b*-values (McNutt, 2002; Nakamura and Sunagawa, 2015).

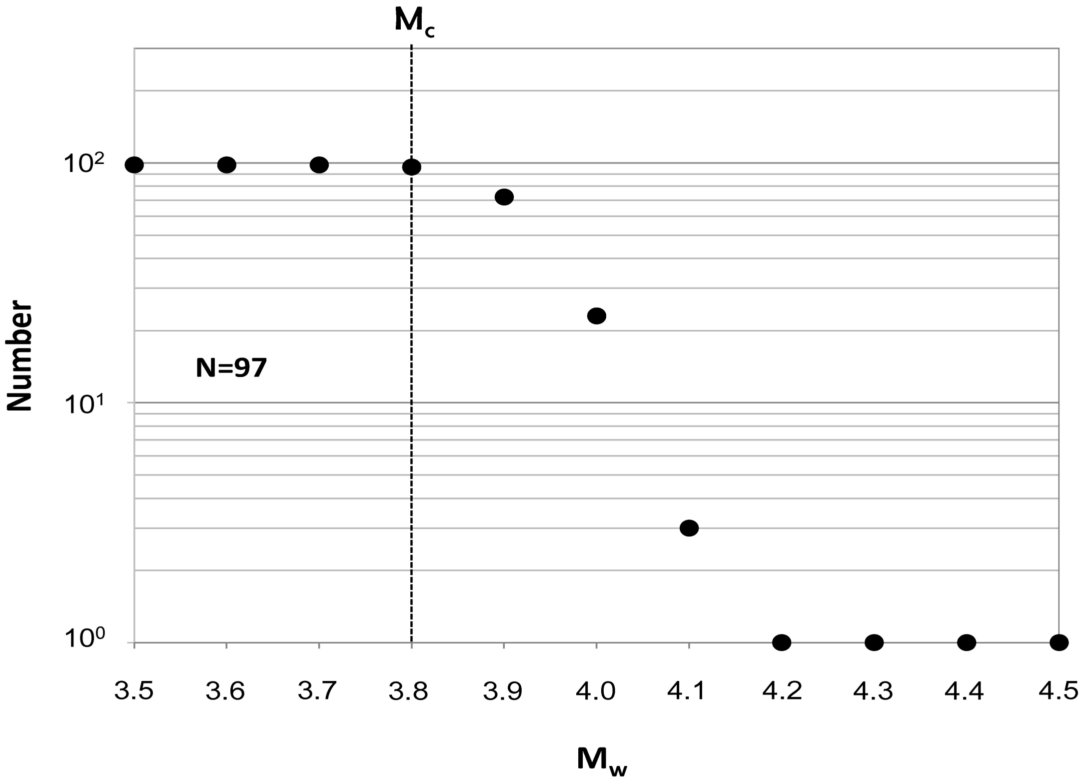

Figure 5.11. Cumulative frequency distribution of RVLFEs. The total number of RVLFEs used for this calculation is 97. This diagram shows that M_c (cut-off magnitude) equals 3.8.

Table 5-6. Parameters for the calculation and *b*-values of RVLFEs, regular VLFEs, and ordinary earthquakes within the Sakishima area.

	Counts[1]	M_w	M_{mean}[2]	M_c[3]	***b*-value** (RVLFEs)	***b*-value** (Regular VLFEs)	***b*-value** (Ordinary earthquakes)
RVLFE	97	3.8–4.2	4.0	3.8	2.2	2.3	0.9

1, the number of RVLFEs
2, the mean M_w used in the estimation of *b*-value.
3, the minimum M_w.

5.4 Discussions

5.4.1 Spatial correlations between RVLFEs and other repeating seismic events

From 2005 to 2012, I detected a total of 97 RVLFEs south of the Miyako Island. These events have similar waveforms (γ >0.9) (Figure 5.3), magnitudes (M_w 3.8−4.2) (Supplement 2), and source mechanisms (thrust fault) (Figure 5.7) and recur in a limited area (23.6° N−24.0° N and 125.0° E−125.4° E) (Figure 5.1b) with an average interval of ~50 days (Figure 5.9). Because their characteristics are the same as those of repeating ordinary earthquakes (REs) in the creeping zone of plate boundaries (e.g., Nadeau et al., 1995; Matsuzawa et al., 2002), I infer that these RVLFEs may be a type of REs but possess different frequency contents. Namely, it is likely that RVLFEs are due to regular ruptures on the same fault patch.

Figure 5.12a shows the distribution of RVLFEs and other seismic events in the Sakishima area, southwestern Ryukyu Trench. It is interesting to note that several repeating seismic events exist together in this region. For example, slow slip events (SSEs) beneath the Iriomote Island detected in Chapter 3 are located approximately 150 km northwest of the RVLFEs. These SSEs occur at the same fault patch with an average interval of ~6 months. According to Heki and Kataoka (2008), the Iriomote SSEs are probably related to an ex-asperity on the plate interface, where the coupling between the upper and lower slabs is stronger than the surrounding area. Moreover, Tamaribuchi et al. (2010) identified two clusters of REs near the Miyako Island (see RE-1 and RE-2 in Figure 5.12a). The RE-1 sequence is located about 15 km north of RVLFEs, which consists of M6-class earthquakes with an average interval of ~22 years. The RE-2 sequence is composed of M5-class earthquakes north of the Miyako Island repeating in 6-year intervals. Because the source depths of the two RE sequences fall precisely on the upper surface of the Philippine Sea Plate (Figure 5.12b), Tamaribuchi et al. (2010) considered that these REs have occurred on the subduction plate interface. That is, they are similar to REs observed in the Japan Trench (e.g., Matsuzawa et al., 2002) or in the Sagami Trough (Kimura et al., 2006), generated by repeating ruptures of small asperities on the plate boundary (Igarashi et al., 2003) (Figure 5.13).

In addition to the repeating seismic events mentioned above, the 1771 Yaeyama earthquake also occurred within the Sakishima area (Figure 5.12a). This earthquake was accompanied by a destructive tsunami that struck Ishigaki and surrounding islands with the maximum run-up height of 30 m and caused fatalities of one-third of the populations on the Ishigaki Island (Goto et al., 2012). For the mechanism of this event, Imamura et al. (2001; 2008) suggested an extensive submarine landslide triggered by an M7-class intraplate earthquake, but Nakamura (2009b) inferred it to be an M_w 8.0 tsunami (slow) earthquake near the Ryukyu Trench axis (Figure 5.12a). Lately, Ando et al. (2018) studied paleotsunami deposits on Ishigaki Island and proposed that this earthquake might be an ordinary subduction thrust earthquake of M_w > 8.0 based on earthquake-induced ground cracks observed in the soil bed underlying the Yaeyama tsunami sediments. This result indicates that the 1771 earthquake is probably a megathrust earthquake ($M_w \geq 8.0$) generated by slips of large asperities on the subduction plate interface in the southwestern Ryukyu Trench (Figure 5.13).

The 1771 earthquake, RVLFEs, and REs are distributed in order from the Ryukyu Trench to the Okinawa Trough (Figure 5.12a). To understand their spatial relations, I drew a cross-section for these seismic events along the profile RR' in Figure 5.12a. As displayed in Figure 5.12b, the fault zone of the 1771 earthquake estimated by Nakamura (2009b) is located at the shallowest segment of the Ryukyu subduction zone close to the trench axis. Notably, its downdip edge is adjoining the trench-ward border of RVLFEs, and the two RE clusters are also located outside the 1771 earthquake fault (Figure 5.12b). This phenomenon suggests that repeating seismic events do not occur within large asperities, in which megathrust earthquakes have occurred, but often appear at their periphery. Such a spatial correlation is consistent with that of REs in the Japan Trench (e.g., Igarashi et al., 2003; Uchida et al., 2003; Matsuzawa et al., 2004) and can be used for the determination of the range of locked zones (Igarashi et al., 2003).

In the Nankai Trough, the locked zone is located within a particular space between the shallow VLFEs and long-term SSEs (Obara and Kato, 2016) (Figure 3.14). However, in the Sakishima area, southwestern Ryukyu Trench, the space between the regular VLFEs and the Iriomote SSEs is too small to accumulate stress for megathrust earthquakes (Figure 5.12b). Accordingly, the locked zone here should be placed between the regular VLFEs and the Ryukyu Trench axis, i.e., the location of the 1771 earthquake fault (Figure 5.13). The above hypothesis is described in detail in Section 4.4.2.1, but it cannot tell if the locked zones exist around the Miyako Island because of the lack of long-term SSEs in this region (Figure 5.12a). To clarify this issue, I reexamined the possible positions of locked zones near the Miyako Island by the spatial correlation between RVLFEs, REs, and the 1771 earthquake determined in this chapter. I note that the RE clusters are all distributed in the downdip area of RVLFE sources (Figure 5.12), which suggests that the locked zones may not exist within this space because the fault patches of REs should be surrounded by stable slide areas to maintain their sizes and intervals (Igarashi et al., 2003). It means that the locked zone in the Miyako area should be located between the RVLFEs and the trench axis, i.e., the source region of the 1771 earthquake (Figure 5.13), similar to the locked zone in the Ishigaki area.

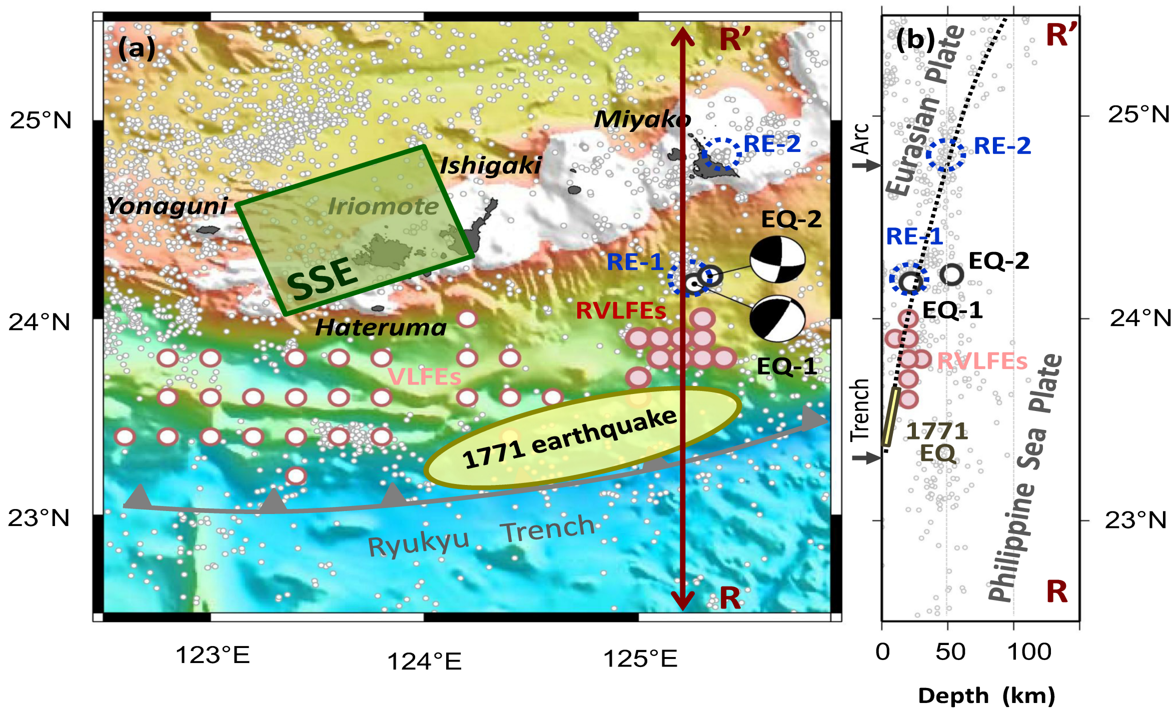

Figure 5.12. (a) Distribution of RVLFEs (red solid circles), regular VLFEs (red open circles), ordinary earthquakes (M_{JMA} ≥3; grey dots), REs (blue dashed circles), Iriomote SSEs (green rectangle), and the fault zone of the 1771 Yaeyama earthquake (yellow ellipse) in the Sakishima area. The sources of REs and the fault patch of the 1771 earthquake are depicted based on the results of Tamaribuchi et al. (2010) and Nakamura (2009b), respectively. The black circles show epicenters of two earthquakes (M_w > 6) that occurred during the time window of this study. Their focal mechanisms are expressed with the beach balls. (b) The cross-section of profile RR' in (a). Its geometric extent is 124.5°E−126.0°E and 23.5°N−25.5°N. The black dotted line shows the subduction plate boundary between the Philippine Sea

Plate and Eurasian Plate. The red circles display RVLFEs, and yellow rectangle shows the fault zone of the 1771 earthquake estimated by Nakamura (2009b). The gray and black circles are small ordinary earthquakes (M_{JMA} ≥3) recorded by JMA and two M6-class earthquakes, respectively. The blue dashed circles are two REs sequences determined by Tamaribuchi et al. (2010). Solid arrows in the left exhibit the relative positions of the Ryukyu Trench and the Ryukyu Arc.

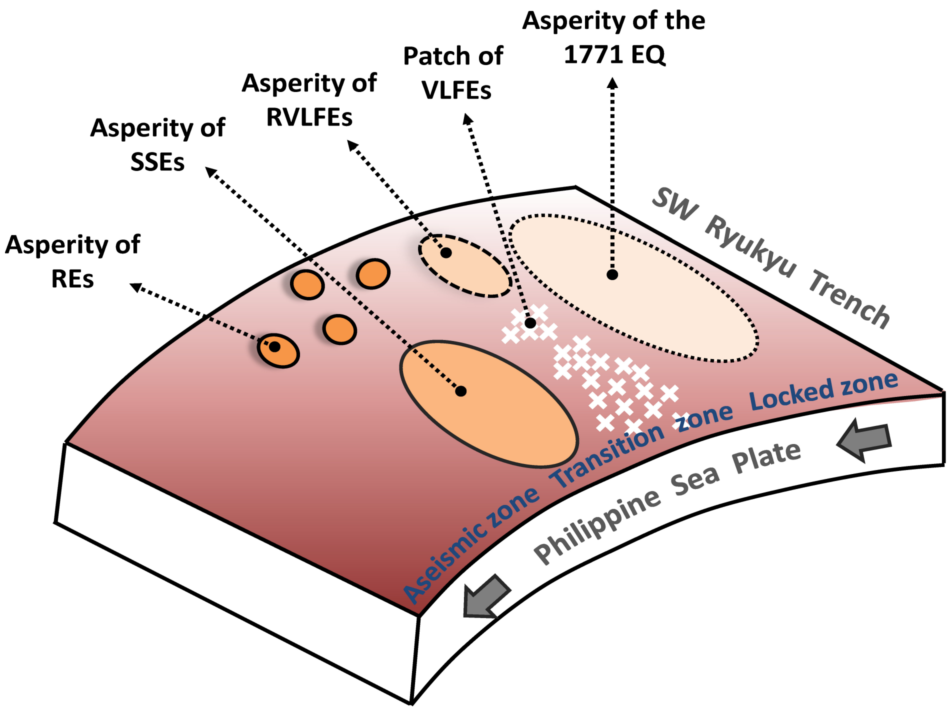

Figure 5.13. Schematic diagram showing the distribution of asperities for the 1771 earthquake, RVLFEs, SSEs, and REs on the subduction plate interface along the SW Ryukyu Trench. The sizes of asperities are arbitrary.

5.4.2 Activity correlations between RVLFEs and SSEs

Different types of slow earthquakes sometimes exhibit remarkable correlations between their activities (Obara and Kato, 2016). For example, in the Bungo Strait, southwestern Japan, long-term SSEs significantly activated VLFEs (e.g., Asano et al., 2015; Baba et al., 2018) and low-frequency tremors (e.g., Hirose et al., 2010; Yamashita et al., 2015). Similarly, VLFEs triggered by SSEs were also seen in the Ryukyu area. Nakamura and Sunagawa (2015) first mentioned that SSEs beneath Iriomote Island activated VLFEs around the Ishigaki and Yonaguni Islands due to the Coulomb failure stress change (ΔCFS) by the SSEs. Moreover, in Chapter 4, I compared the occurrence times of SSEs with those of VLFEs along the Ryukyu Trench and found that the VLFEs in the Sakishima, Okinawa, and Amami area could be activated by nearby SSEs for 5-30 days, 0-15 days, and 0-5 days, respectively (see detail in Section 4.4.1).

Although the correlations between SSEs and VLFEs in the Sakishima area have already been confirmed, the relations of SSEs and RVLFEs have not been clear. To understand whether the RVLFEs have similar activation as nearby regular (unrepeating) VLFEs, I analyzed the time series of the 97 RVLFEs and 16 Iriomote SSEs in 2005-2012. As illustrated in Figure 5.14, several RVLFE sequences coincided with SSEs (e.g., SSEs#17, #19, #23, #24, #25, #26, and #30), but some SSEs were not accompanied by any RVLFE activities (e.g., SSEs#15, #16, #18, #21, and #28). To clarify such ambiguous correlation and highlight the RVLFE activation, I divided these RVLFEs based on the periods of the 16 SSEs (Figure 5.15). Further, I stacked these SSEs with respect to their starting times. Figure 5.16 shows the stacked numbers of RVLFEs within the 16 SSEs. Two significant peaks are seen at 5-15 days and 135 days, respectively. Here, I suspect that the first activation of 5-15 days is related to the SSE activities because it accords with the time constant of 0.1-year of the Iriomote SSEs (see detail in Section 3.3.1). Contrarily, the causes of the second peak (135 days) are still unknown, probably due to coincidental occurrences or the triggering by some external forces. Although RVLFEs appear to be more active after the SSE start, it is premature to conclude that the Iriomote SSEs really can activate the RVLFEs because the event count of RVLFEs (97) is too few to offer a statistically meaningful discussion. After all, it is still possible that the existence of these peaks is just by chance, and further studies are necessary.

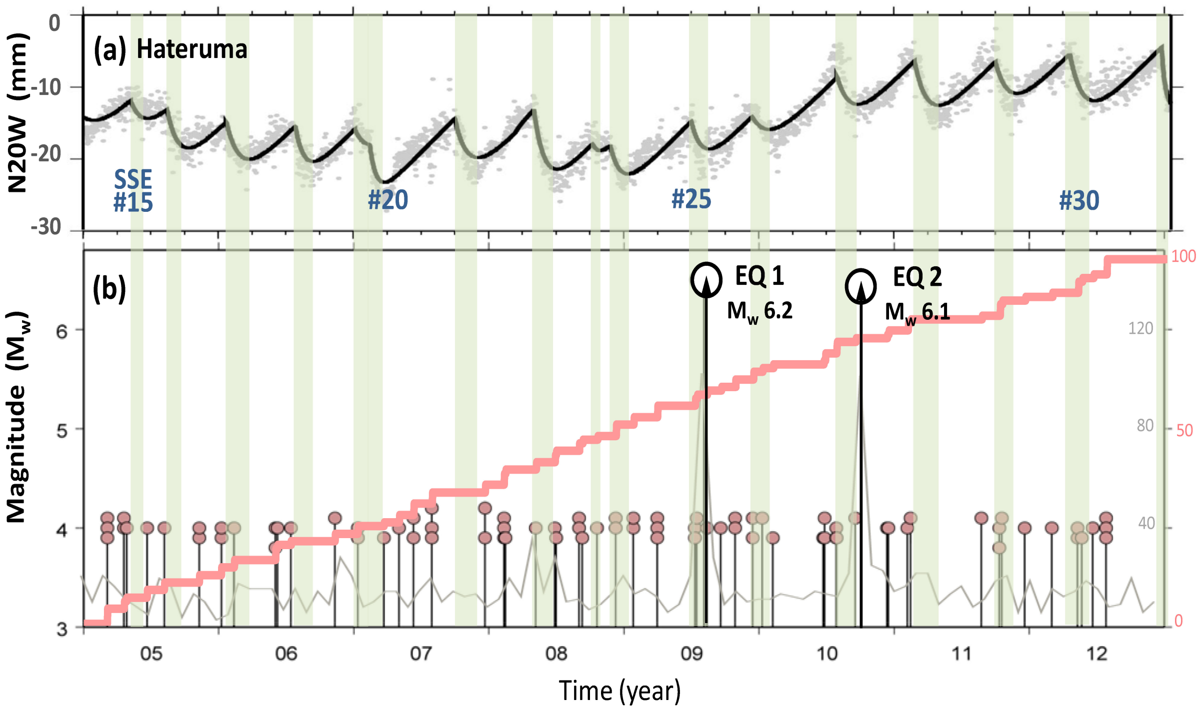

Figure 5.14. (a) The daily GNSS coordinates of the Hateruma station relative to the Miyako station in the N20W direction. The green belts show the active times of the 16 SSEs with a number corresponding to the SSEs in Table 3-1. Their fault patches are shown in Figure 5.12a. (b) The time series of RVLFEs (red circles) and its cumulative numbers (red curve). The units on the right and left axes are the cumulative numbers (red) and magnitudes (black),

respectively. The black circles denote two major earthquakes that occurred in the time windows of this study. Their locations and focal mechanisms are exhibited in Figure 5.12a. The gray curve at the bottom indicates the background seismicity variation within the distance of 100 km from the RVLFE source region, whose unit is given on the right inner axis (grey).

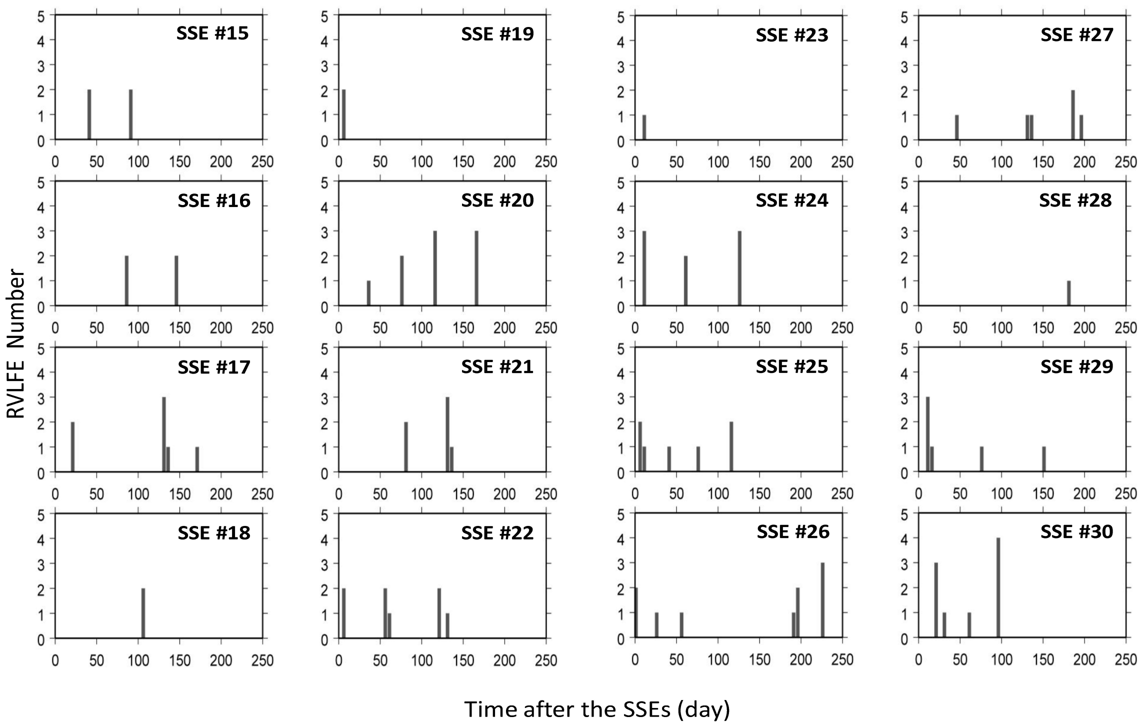

Figure 5.15. The 5-day count of RVLFEs within the 16 Iriomote SSEs. The time span of each diagram is from SSEs to their subsequent events. The event numbers at the top right corner refer to the SSEs in Table 3-1.

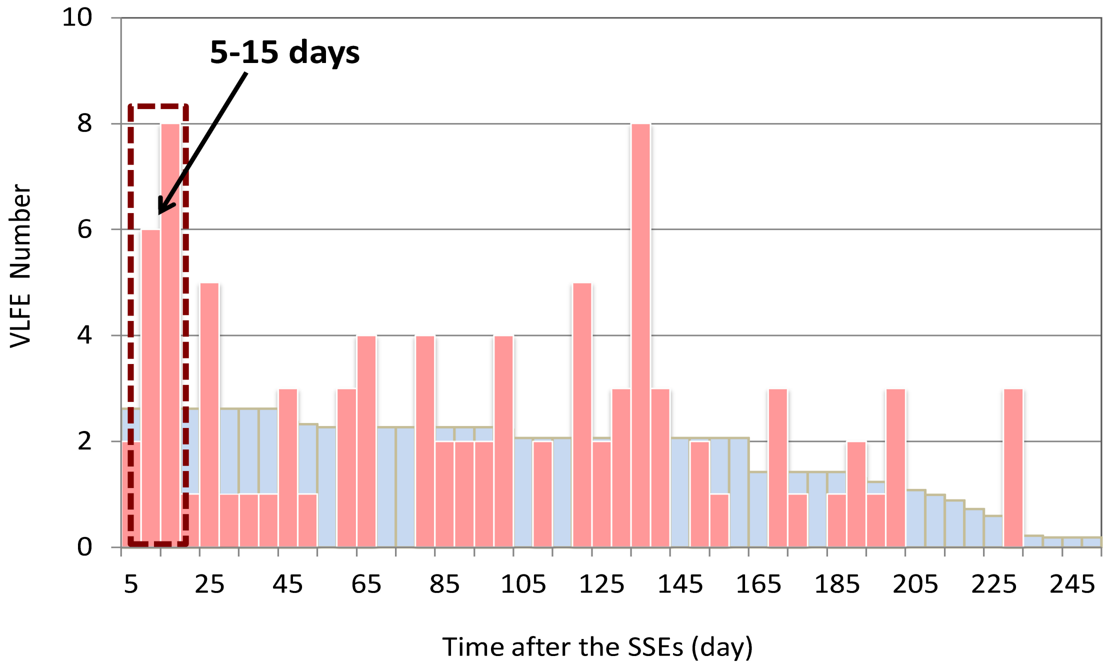

Figure 5.16. Stacked numbers of RVLFEs after the SSE start. The time span is from SSEs to consecutive events, same as Figure 5.15. The red bars display the counts of VLFEs with 5-day interval, and the blue bars show the numbers of VLFEs expected by random occurrences. Two significant peaks at 5-15 days and 135 days are seen in this diagram. The first peak of 5-15 days highlighted by the dashed red rectangle is evidence of the SSE activations.

5.4.3 Burst type or continuation type

REs can be classified into burst and continuation types based on their pattern of recurrence intervals (Igarashi et al., 2003). The burst-type REs, similar to earthquake swarms, only occur after a large earthquake (Igarashi et al., 2003). These REs last less than three years in general (Yamashita et al., 2012) and are located around large asperities on the subduction plate interface, in which megathrust earthquakes often occur (Igarashi et al., 2003). The continuation type of REs is different from the burst type; it has a similar interval and lasts longer than the burst-type events (i.e., > 3 years) (Igarashi et al., 2003). Large earthquakes rarely trigger their activities (Igarashi et al., 2003) but sometimes temporarily vary their slip rate (e.g., Uchida et al., 2003, Matsuzawa et al., 2004), which indicates that the continuation-type REs may directly reflect the stress accumulation caused by plate motions.

The 97 RVLFEs south of Miyako Island have regular interseismic intervals (~50 days) (Figure 5.9) and last over eight years (from 2005 to 2012). It suggests that these events probably belong to the continuation type. However, these RVLFEs simultaneously possess the burst-type characteristics as well. For example, the source area of RVLFEs is adjoining the fault patch of the 1771 earthquake (Figure 5.12). In addition, the RVLFEs within the same sequences also exhibit a significant mainshock-aftershock relationship (see detail in Section 5.3.5).

To clarify RVLFEs are the continuation type or the burst type, I analyzed the activity correlations between the RVLFEs and nearby large ordinary earthquakes in this section. From 2005 to 2012, only two moderate-class earthquakes (M_w >6) occurred around the Miyako Island (see EQ-1 and EQ-2 in Figure 5.12). The EQ-1, about 15 km north of the RVLFEs, is a repeating seismic event of the RE-1 sequence with an average interval of 22 years (Tamaribuchi et al., 2010). However, the EQ-2, around 30 km north of RVLFEs, is a typical intraplate earthquake located within the Philippine Sea Plate (see EQ-2 in Figure 5.12b). The occurrence times of the two earthquakes and the 97 RVLFEs are shown in Figure 5.14b. It is interesting to note that the two M6-class earthquakes did not trigger any RVLFE sequences, and the accumulation curve of RVLFEs maintains a stable and linear increase even around the EQ-1 and EQ-2 (Figure 5.14b). Moreover, the background seismicity in an area approximately 100 km x 100 km near the RVLFE sources did not synchronize with RVLFE activities either (Figure 5.14b). These observations suggest that nearby earthquakes would not trigger RVLFE activities, that is, the RVLFEs are likely to be the continuation-type repeating events rather than the burst type.

5.4.4 Fault zone and seismic slip rate

Although the 97 RVLFEs detected in this study are placed in an area of approximately 50 x 50 km^2 (Figure 5.12a), the epicenters of more than 70 % of RVLFEs concentrate at three grid points, and the rest of these events are scattered over eight neighboring points (Figure 5.17a). The solutions of RVLFEs at the three points possess higher quality ranks (mostly A) (Figure 5.17b). Thus, I infer that these scattered events might have occurred at the same three points, but their epicenters were erroneously located at surrounding grid dots. It means that a reliable source region of the 97 RVLFEs may only lie in the three horizontal blocks, i.e., the range of 30 km x 10 km. According to this observation, I assumed the above geometric range as the fault zone of RVLFEs here to estimate the seismic slip rate as described below.

Under this assumption, I roughly calculated the slip rate of RVLFEs based on the following relation,

$$\dot{d} = \mu^{-1} S^{-1} \dot{M} \tag{5.2}$$

where $\dot{d}$ is the slip rate, μ is the rigidity, S is the source area, and $\dot{M}$ is the moment release rate. For this estimation, I first determined $\dot{M}$ = 1.6 x 10^{16} Nm/year based on the sum of seismic moments (M_0) of the 97 RVLFEs in 2005-2012 (see M_0 in Supplement 2). Subsequently, I adopted the rigidity in sediments of an accretionary prism of 1.6−6.4 x 10^9 Pa assessed by Ito and Obara (2006b) because these RVLFEs were probably located within the accretionary prism of the Ryukyu subduction zone (see related contents in Section 5.3.2). Nevertheless, these RVLFEs still have a possibility to have occurred on the shallow slab interface. Considering this point, I additionally employed the rigidity along megathrust faults in subduction zones at depths 5-40 km as 1–12 x 10^9 Pa estimated by Bilek and Lay (1999) using results from the analysis of earthquake source time functions (see Figure 3 in Bilek and Lay, 1999). Applying these parameters, I obtained the slip rate of RVLFEs of 8-33 mm/year in accretionary prisms (the rigidity of 1.6−6.4 x 10^9 Pa) and 4-53 mm/year on the slab interface (the rigidity of 1–12 x 10^9 Pa), respectively. It means that if the fault is located within the accretionary prisms, the slip of RVLFEs contains about 6-26 % of the relative plate convergence in the southwestern Ryukyu subduction zone (125 mm/year) (Heki and Kataoka, 2008). However, if the fault lies on the plate surface, the RVLFEs represent 3-42 % of the relative plate motion. Although this estimation highly depends on the assumed fault size and rigidity, the above result indicates that RVLFEs accommodate plate convergence substantially smaller than the time-average plate convergence rate, regardless of my assumption of faults being on the subduction slab interface or in the accretionary prism. Such a slip rate of repeating seismic events lower than the plate convergence was also seen in the Tohoku area (Uchida et al., 2003), and it might reflect the existence of high coupling regions on the subduction plate boundary (Uchida and Matsuzawa, 2011).

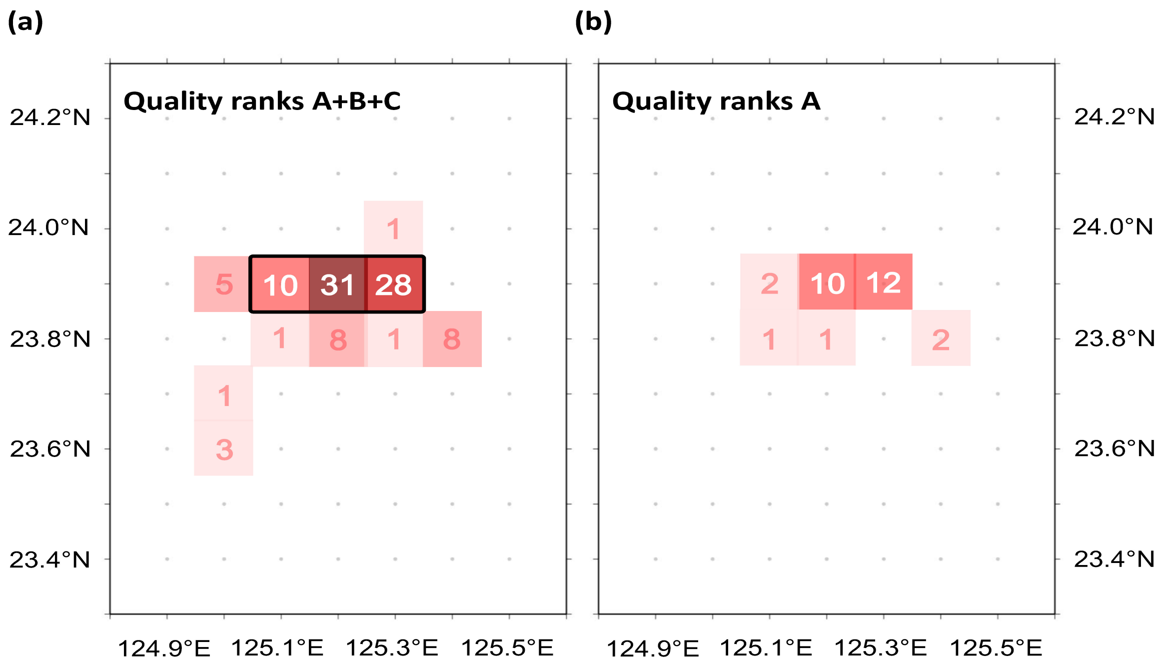

Figure 5.17 (a) The horizontal distribution of the 97 RVLFEs. The number within each color block displays the count of RVLFEs at the grid point. Most of the RVLFEs are concentrated on the three grids at 125.1°E–125.3°E and 23.9°N. (b) The horizontal distribution of the 28 RVLFEs with quality rank A.

5.5 Summary

- From 2005 to 2012, I detected 97 RVLFEs south of Miyako Island. These events have similar waveforms (γ>0.9), magnitudes (Mw 3.8−4.2), and source mechanisms (thrust fault) and repeatedly occurred in a small area of approximately 30 km x 10 km with an average interval of ~50 days.
- The characteristics of RVLFEs are the same as repeating earthquakes (REs) in the creeping zone of the plate boundary but possess different frequency contents.
- These RVLFEs, probably belonging to the continuation-type repeating seismic events, cannot be triggered by nearby ordinary earthquakes. However, the long-term SSEs beneath the Iriomote Island, ~150 km northwest of RVLFEs, may activate RVLFEs in 5-15 days after their onsets.
- The slip released by the RVLFEs in one year is about 6-26 % (in accretionary prisms) and 3-42 % (on the slab interface) of the average plate convergence rate in the southwestern Ryukyu subduction zone.

Chapter 6.

Conclusions

In this study, I detected slow slip events (SSEs) and very low frequency earthquakes (VLFEs) in the Ryukyu area using GEONET GNSS data and board-band seismic data of F-net and BATS. I made a detailed analysis to clarify their properties, activities, and relations between them. Furthermore, I applied these data to explain the most contentious issue of the Ryukyu subduction zone, i.e., whether the upper and lower plates are coupled or decoupled. The main conclusions of this thesis are summarized as follows:

6.1 Slow slip events (SSEs)

1) A total of 38 SSEs were identified in this study from 1997 to 2016. These events occurred at the same fault patch and repeated biannually beneath the Iriomote Island in the southwestern Ryukyu Arc.
2) The slip accumulation rate of these SSEs changes in time and significantly increases in 2002 and 2013, which coincides with the activation of the back-arc spreading as indicated by the earthquakes swarms in the Okinawa Trough.
3) The accelerated southward movement of the block between the Okinawa Trough and the Ryukyu Trench due to post-rifting stress diffusion might cause the increase of the slip accumulation rate of the Iriomote SSEs.
4) Based on the slip rate, the Iriomote SSEs might accommodate ~72% of the plate convergence of the southwestern Ryukyu subduction sone

6.2 Very low frequency earthquake (VLFEs)

1) From 2005 to 2012, I detected 29,841 VLFEs in the Ryukyu subduction zone, whose

dominant frequency range falls within 0.03-0.15 Hz without significant high-frequency content. These events are all located near the Ryukyu Trench axis and have shallow thrust-faulting mechanisms, similar to VLFEs in the Nankai Trough reported by Obara and Ito (2005).

2) Based on the location and focal mechanism, I infer that these VLFEs probably occurred along the splay faults in the accretional prism or on the shallow plate interface of the Ryukyu subduction zone.

3) The high *b*-value (2.3-5.0) is a remarkable characteristic of VLFEs in the Ryukyu area, which suggests that highly heterogeneous materials or high pore pressure fluid exist near the VLFE source region.

4) Nearby SSEs and local earthquakes often influence VLFE activities. In the Sakishima, Okinawa, and Amami areas, VLFEs are found to be activated in 5-30 days, 0-15 days, and 0-5 days, respectively, after the start of SSEs. However, in the southern Kyushu area, both long-term (Bungo) and short-term (Hyuga-nada and Tanega-shima) SSEs and some teleseismic earthquakes (e.g., 2011 Tohoku-Oki earthquake) are found to trigger or activate the VLFEs.

6.3 Repeating very low frequency earthquakes (RVLFEs)

1) Among the VLFEs in the Sakishima area, I observed 97 repeating events (RVLFEs), south of the Miyako Island, having similar waveforms, amplitudes, locations, magnitudes, and source mechanisms. These events recurred in the same area with an average interval of ~50 days.

2) Nearby ordinary earthquakes cannot trigger the RVLFE activity, but the Iriomote SSEs probably activate the RVLFEs in 5-15 days after their onsets.

3) The cumulative seismic slip by the RVLFEs accommodated about 6-26 % (in accretionary prisms) and 3-42 % (on the slab interface) of the time-averaged plate convergence there.

6.4 Duration and magnitudes of the SSEs and VLFEs in the Ryukyu subduction zone

1) The average magnitude (M_w) and duration of the Iriomote SSEs and the VLFEs in Ryukyu both are consistent with the scaling law proposed for slow earthquakes by Ide et al. (2007) (Figure 6.1).

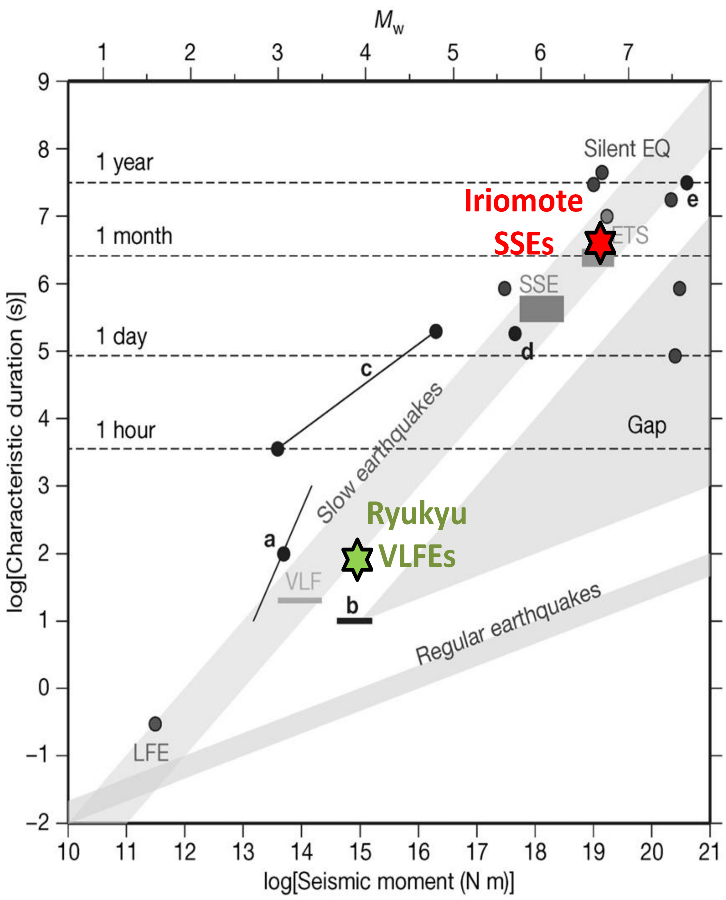

Figure 6.1. Magnitude (M_w) and duration for the Iriomote SSEs (red star) and the VLFEs in

the Ryukyu area (green star) compared with the general scaling law of slow earthquakes (passed to Figure 2 of Ide et al. 2007)

6.5 Ryukyu subduction zone

Integrating the locations of SSEs, VLFEs, and two suspect megathrust earthquakes (M_w >8) in the Ryukyu area, I propose that both slow and ordinary earthquakes occur in the Ryukyu Trench at following depths:

- Sakishaima: the megathrust earthquakes (locked zone, ~10 km), VLFEs (~20 km), and SSEs (~30 km).
- Okinawa: VLFEs (~20 km) and SSEs (~30 km).
- Amami: Still uncertain due to the complex tectonic setting and inaccurate hypocenters of large earthquakes and VLFEs.

References

Abe, K.and Kanamori, H. (1979), Temporal variation of the activity of intermediate and deep focus earthquakes, *J. Geophys. Res.*, Solid Earth, 84(B7), 3589-3595.

Aki, K. (1965), Maximum likelihood estimate of b in the formula log (N) = a − bM and its confidence limits, *Bull. Earthq*. Res. Inst. Tokyo Univ., 43, 237-239.

Ando, M., (1975), Source mechanisms and tectonic significance of historical earthquakes along the Nankai Trough, *Tectonophysics*, 27, 119-145.

Ando, M., M. Nakamura, T. Matsumoto, M. Furukawa, K. Tadokoro M. Furumoto (2009), Is the Ryukyu subduction zone in Japan coupled or decoupled? —The necessity of seafloor crustal deformation observation, *Earth, Planets and Space*, *61,* 1031-1039, doi: 10.1186/BF03352954.

Ando, M., Y. Tu, H. Kumagai, Y. Yamanaka, C.- H. Lin (2012), Very low frequency earthquakes along the Ryukyu subduction zone, Very low frequency earthquakes along the Ryukyu subduction zone, *Geophys. Res. Lett.*, *39*, doi:10.1029/2011GL050559

Ando, M., R. Ikuta, Y. Tu, H. Y. Chen, and C. H. Lin (2015), The Apr 2013 earthquake swarm and dyke intrusion in the Okinawa trough, paper presented at *the Japan Geoscience Union Meeting,* Chiba, Japan, 27 May, 2015.

Ando, M., A. Kitamura, Y. Tu, Y. Ohashi, T. Imai, M. Nakamura, R. Ikuta, Y. Miyairi, Y. Yokoyama, and M. Shishikura (2018), Source of high tsunamis along the southernmost Ryukyu trench inferred from tsunami stratigraphy, *Tectonophysics.* 722, 265-276, doi:10.1016/j.tecto.2017.11.007.

Arai R., T. Takahashi, S. Kodaira, Y. Kaiho, A. Nakanishi, G. Fujie, Y. Nakamura, Y. Yamamoto, Y. Ishihara, S. Miura and Y. Kaneda (2016), Structure of the tsunamigenic plate boundary and low-frequency earthquakes in the southern Ryukyu Trench, *Nat. Commun,* 7:12255, doi: 10.1038/ncomms12255

Arai R., T. Takahashi, S. Kodaira, T. Yamada, T. Takahashi, S. Miura, Y. Kaneda, A. Nishizawa, M. Oikawa (2017), Subduction of thick oceanic plateau and high-angle normal-fault earthquakes intersecting the slab, *Geophys. Res. Lett.*, doi: 10.1002/2017GL073789

Arciniega-Ceballos, A., B. A. Chouet, and P. Dawson (1999), Very long period signals associated with vulcanian explosions at Popocatépetl volcano, Mexico, *Geophys. Res. Lett.*, 26, 3013–3016, doi:10.1029/1999GL005390.

Arisa, D. and K. Heki (2017), Space geodetic observations of repeating slow slip events beneath the Bonin Islands, Geophys. J. Int., 210, 1494-1502, doi:10.1093/gji/ggx2582017

Asano, Y., K. Obara and Y. Ito (2008), Spatiotemporal distribution of very-low frequency earthquakes in Tokachi-oki near the junction of the Kuril and Japan trenches revealed by using array signal processing, *Earth, Planets Space*, 60, 871-875

Asano, Y., K. Obara, T. Matsuzawa, H. Hirose, and Y. Ito (2015), Possible shallow slow slip events in Hyuga-nada, Nankai subduction zone, inferred from migration of very low frequency earthquakes, *Geophys. Res. Lett.*, 42, 331–338, doi:10.1002/2014GL062165.

Aso, N., K. Ohta, and S. Ide (2013), Tectonic, volcanic, and semi-volcanic deep low-frequency earthquakes in western Japan, *Tectonophysics, 600*, 27–40, doi:10.1016/j.tecto.2012.12.015

Baba, S., A. Takeo, K. Obara, A. Kato, T. Maeda and T. Matsuzawa (2018), Temporal Activity Modulation of Deep Very Low Frequency Earthquakes in Shikoku, Southwest Japan, *Geophys. Res. Lett.*, *45,* 733-738, doi:10.1002/2017GL076122

Beroza, G.C. and T.H. Jordan (1990), Searching for slow and silent earthquakes using free oscillations, *J. Geophys. Res.*, 95, 2485-2510

Beroza, C. G., and S. Ide (2011), Slow Earthquakes and Nonvolcanic Tremor, *Ann. Rev. Earth Planet. Sci., 39,* 271-296*,* doi: 10.1146/annurev-earth-040809-152531.

Bilek, S.L. and T. Lay (1999), Rigidity variations with depth along interplate megathrust faults in subduction zones, *Nature*, 400, 443-446, doi:10.1038/22739

Brown, J. R., G. C. Beroza, S. Ide, K. Ohta, D. R. Shelly, S. Y. Schwartz, W. Rabbel, M. Thorwart, and H. Kao (2009), Deep low-frequency earthquakes in tremor localize to the plate interface in multiple subduction zones, *Geophys. Res. Lett., 36*, L19306, doi:10.1029/2009GL04002.

Brown, J. R., S. G. Prejean, G. C. Beroza, J. Gomberg, and P. J. Haeussler (2013), Deep low-frequency earthquakes in tectonic tremor along the Alaska-Aleutian subduction zone, *J. Geophys. Res., 118*, 1079–1090, doi:10.1029/2012JB009459.

Chen, H.-Y., R. Ikuta, C.-H. Lin, Y.-J. Hsu, T. Kohmi, C.-C. Wang, S.-B. Yu, Y. Tu, T. Tsujii, and M. Ando (2018), Back-arc opening in the western end of the Okinawa Trough revealed from GNSS/Acoustic measurements, Geophys. Res. Lett. doi: 10.1002/2017GL075724

Chen, K. H., R.-J. Rau and J.-C. Hu (2009), Variability of repeating earthquake behavior along the Longitudinal Valley fault zone of eastern Taiwan, *J. Geophys. Res.,* 114, doi:10.1029/2007JB005518

Deschamps, A., and S. Lallemand (2002), The West Philippine Basin: An Eocene to early Oligocene back arc basin opened between two opposed subduction zones, *J. Geophys. Res.*, 107(B12), 2322, doi:10.1029/2001JB001706.

Dragert, H., K. Wang, and T. S. James (2001), A silent slip event on the deeper Cascadia subduction interface, *Science, 292*, 1525–1528, doi: 10.1126/science.1060152.

Douglas, A., J. Beavan, L. Wallace, and J. Townend (2005), Slow slip on the northern Hikurangi subduction interface, New Zealand, *Geophys. Res. Lett., 32,* doi:10.1029/2005GL023607

Dziewonski, A.M. and D.L. Anderson (1981), Preliminary reference Earth model, *Phys. Earth Planet. Interiors*, 25, 297–356.

Foulger, G.R., C.-H. Jahn, G. Seeber, P. Einarsson, B.R. Julian and K. Heki (1992), Post-rifting stress relaxation at the divergent plate boundary in Northeast Iceland, *Nature, 358,* 488-490, doi:10.1038/358488a0.

Fu, Y. and J. T. Freymueller (2013), Repeated large Slow Slip Events at the southcentral Alaska subduction zone, *Earth and Planetary Science Letters, 375,* 303-311, doi.org/10.1016/j.epsl.2013.05.049

Fukuda, J. (2018), Variability of the space-time evolution of slow slip events off the Boso Peninsula, central Japan, from 1996 to 2014, *J. Geophys. Res.,* 123, 732–760, doi:10.1002/2017JB014709

Ghosh, A., A. V. Newman, A.M. Thomas, G. T. Farmer (2008), Interface locking along the subduction megathrust from microseismicity near Nicoya, Costa Rica*, Geoph. Res. Lett.*, 35, L01301, doi:10.1029/2007GL03161.

Ghosh, A., E. Huesca-Pérez, E. Brodsky and Y. Ito (2015), Very low frequency earthquakes in Cascadia migrate with tremor, *Geophys. Res. Lett.*, 42, doi:10.1002/2015GL063286.

Goto, K., K. Miyazawa, A. Adaniya, S. Kaikihana, Y. Kumagai, A. Shimabukuro, N. Shimabukuro, Y. Masaki, S, Matsushima, and K. Miyagi (2012), The reconsideration of the 1771 Meiwa tsunami runup heights II- The whole Sakishima area, *Tsunami Engineering Report*, 29, 129-146.

Goto K. (2013), Re-evaluation of hypocenter of the 1911 great earthquake around Kikai-jima, Japan, *J. Seismol. Soc. Jpn. (Zisin)*, 65, 231–242, doi:10.4294/Zisin.65.231

Hatori, T. (1988), Tsunami Magnitudes and Source Areas along the Ryukyu Islands, *Zisin* (II), 41, pp. 541-547 (in Japanese with English abstract)

Heki, K., G.R. Foulger, B.R. Julian and C.-H. Jahn (1993), Plate dynamics near divergent boundaries: geophysical implications of postrifting crustal deformation in NE Iceland, *J. Geophys. Res., 98,* 14279-14297, doi: 10.1029/93JB00781.

Heki, K., S. Miyazaki and H. Tsuji (1997), Silent fault slip following an interplate thrust earthquake at the Japan Trench, *Nature, 386,* 595–598

Heki, K. and Y. Tamura (1997), Short term afterslip in the 1994 Sanriku-Haruka-Oki earthquake, *Geophys. Res. Lett., 24*, 3285-3288,

Heki, K., and T. Kataoka (2008), On the biannually repeating slow-slip events at the Ryukyu Trench, southwestern Japan, *J. Geophys. Res.*, *113,* B11402, doi:10.1029/2008JB005739.

Hirose, H., K. Hirahara, F. Kimata, N. Fujii, and S. Miyazaki (1999), A slow thrust slip event following the two 1996 Hyuganada earthquakes beneath the Bungo Channel, southwest Japan, *Geophys. Res. Lett., 26*, 3237-3240, doi: 10.1029/1999GL010999.

Hirose, H., and K. Obara (2005), Repeating short- and long-term slow slip events with deep tremor activity, *Earth Planets Space*, 57, 961–972, doi:10.1186/BF03351875.

Hirose, H. and K. Obara (2006), Short-term slow slip and correlated tremor episodes in the Tokai region, central Japan, *Geophys. Res. Lett., 33,* doi:10.1029/2006GL026579.

Hirose, H., Y. Asano, K. Obara, T. Kimura, T. Matsuzawa, S. Tanaka, and T. Maeda (2010), Slow earthquakes linked along dip in the Nankai subduction zone, *Science*, *330*, doi: 1502. 10.1126/science.1197102.

Hirose, H and K. Obara (2010), Recurrence behavior of short-term slow slip and correlated nonvolcanic tremor episodes in the western Shikoku, southwest Japan, *J. Geophys. Res., 115,* DOI: 10.1029/2008JB006050.

Hirose, H., H. Kimura, B. Enescu, and S. Aoi (2012), Recurrent slow slip event likely hastened by the 2011 Tohoku earthquake, *Proc. Nat. Acad. Sci., 109,* 15157-15161, doi: 10.1073/pnas.1202709109.

Houston, H., B. G. Delbridge, A. G. Wech and K. C. Creager (2011), Rapid tremor reversals in Cascadia generated by a weakened plate interface, *Nature Geoscience,* 4(6), 404.

Hsu, Y. J., M. Ando, S. B. Yu, and M. Simons (2012), The potential for a very large earthquake along the southernmost Ryukyu subduction zone, *Geophys. Res. Lett.,* 39, doi:10.1029/2012GL052764

Ide, S., G. C. Beroza, D. R. Shelly, and T. Uchide (2007), A scaling law for slow earthquakes, *Nature*, 447, 76–79, doi:10.1038/nature05780

Ide, S., Yabe, S., and Tanaka, Y. (2016), Earthquake potential revealed by tidal influence on earthquake size-frequency statistics, *Nature*, 9(11), 834-837, doi:10.1038/ngeo2796

Igarashi, T., T. Matsuzawa and A. Hasegawa (2003), Repeating earthquakes and interplate aseismic slip in the northeastern Japan subduction zone, *J. Geophys. Res, 108*, doi:10.1029/2002JB001920

Ikeda, S., H. Heki, and K. kimura (2015), Shallow repeating slow-slip-events along the convergent block boundary in northern Hokkaido, Japan, paper presented at *the Fall Meeting of American Geophysical Union,* San Francisco, USA, 14 Dec, 2015.

Ito, Y. and K. Obara (2006a), Dynamic deformation of the accretionary prism excites very low frequency earthquakes, *Geophys. Res. Lett.*, 33, doi:10.1029/2005GL025270

Ito, Y., and K. Obara (2006b), Very low frequency earthquakes within accretionary prisms are very low stress-drop earthquakes, *Geophys. Res. Lett.*, 33, L09302, doi:10.1029/2006GL025883.

Ito, Y., K. Obara, K. Shiomi, S. Sekine, and H. Hirose (2007), Slow earthquakes coincident with episodic tremors and slow slip events, *Science, 315*, 503–506, doi:10.1126/science.1134454

Imamura, F., I. Yoshida, and A. Moore (2001), Numerical study of the 1771 Meiwa tsunami at Ishigaki Island, Okinawa and the movement of the tsunami stones, *Proc. Coastal Eng. Jpn. Soc. Civ. Eng.*, 48, 346–350 (in Japanese).

Imamura, F., K. Goto, S. Ohkubo (2008), A numerical model for the transport of a boulder by tsunami, *J. Geophys. Res*., 113, C01008, doi:10.1029/2007JC004170.

Iwasa, Y. and K. Heki (2018), Repeating rifting episodes and uplift of the southwestern Ryukyu Arc, Paper presented at the 2018 Japan Geoscience Union Meeting, Makuhari, Chiba, Japan, SSS09-12.

Jiang Y., S. Wdowinski, T. H. Dixon, M. Hackl, M. Protti and V. Gonzalez (2012), Slow slip events in costa rica detected by continuous gps observations, 2002–2011. *Geochemistry, Geophysics, Geosystems, 13*, doi.org/10.1029/2012GC004058.

Kanamori, H. (1972), Mechanism of tsunami earthquakes, *Phys. Earth Planet. Int.*, 6, 346-359, doi:10.1016/0031-9201(72)90058-1

Kanamori, H., and G.S. Stewart (1979) A slow earthquake, *Phys. Earth Planet. Int.*, *18*, 167-175.

Kanamori, H. and M. Kikuchi (1993), The 1992 Nicaragua earthquake: A slow tsunami earthquake associated with subducted sediments, *Nature, 361*, 714–716.

Kano, M., J. Fukuda, S. Miyazaki and M. Nakamura (2018), Spatio-temporal evolution of recurrent slow slip events along the southern Ryukyu subduction zone, Japan, from 2010 to 2013, *J. Geophys. Res.*, doi: 10.1029/2018JB016072

Kao, H. (1998), Can great earthquakes occur in the southernmost Ryukyu arc-Taiwan region?, *Terr. Amos. Oceanic Sci*., 9, 487–508.

Katsumata, A. and Kamaya, N. (2003), Low-frequency continuous tremor around the Moho discontinuity away from volcanoes in the southwest Japan, *Geophys. Res. Lett., 30*: doi: 10.1029/2002GL015981.

Kawana, T. (1990), The notch with characteristics of coral reef, *Coral reef in Japan*, 1, pp. 66-82. (in Japanese)

Kawasaki, I., Y. Asai, Y. Tamura, T. Sagiya, N. Mikami, Y. Okada, M. Sakata, and M. Kasahara (1995), The 1992 Sanriku-oki, Japan, ultra-slow earthquake, *J. Phy. Earth*, *43*, 105–116.

Kawasaki, I. (2004), Silent earthquakes occurring in a stable-unstable transition zone and impications for earthquake prediction, *Earth Planets Space, 56,* 813 – 821.

Kennett, N., E. Engdahl and R. Buland (1995), Constraints on seismic velocities in the Earth from travel times, *Journal Geoph Int.*, 122, 108-124.

Kimura, H., K. Kasahara, T. Igarashi, and N. Hirata (2006), Repeating earthquake activities associated with the Philippine Sea plate subduction in Kanto district, central Japan: A new plate configuration revealed by interplate aseismic slips, *Tectonophysics,* 417, 101–118, doi:10.1016/j.tecto.2005.06.013

Kobayashi, A. (2010), A small scale long-term slow slip occurred in the western Shikoku in 2005, J. *Seismol. Soc. Jpn. (Zisin)*, *63*, 97–100, doi:10.4294/zisin.63.97. (in Japanese with English figure captions)

Kobayashi, A. (2014), A long-term slow slip event from 1996 to 1997 in the Kii Channel, Japan, *Earth, Planets and Space*, *66,* doi:org/10.1186/1880-5981-66-9.

Kodaira, S., N. Takahashi, J. Park, K. Mochizuki, M. Shinohara, S. Kimura (2000), Western Nanaki Trough seismogenic zone: Result from wide-angle Ocean-Bottom Seimographic survey, *J. Geophys. Res.*, 105, 5887-5905

Kostoglodov, V., S. K. Singh, J. A. Santiago, S. I. Franco, K. M. Larson, A. R. Lowry, and R. Bilham (2003), A large silent earthquake in the Guerrero seismic gap, Mexico, *Geophys. Res. Lett., 30*, 1807, doi:10.1029/2003GL017219.

Kubo, A., and E. Fukuyama (2003), Stress field along the Ryukyu Arc and the Okinawa Trough inferred from moment tensors of shallow earthquakes, *Earth and Planetary Science Letters*, 210(1), 305-316, doi: 10.1016/S0012-821X(03)00132-8

Lallemand, S., A. Heuret, and D. Boutelier (2005), On the relationships between slab dip, back-arc stress, upper plate absolute motion, and crustal nature in subduction zones, Geochem. Geophys. Geosyst., 6, Q09006, doi:10.1029/2005GC000917.

Li, B., and A. Ghosh (2017), Near-continuous tremor and low-frequency earthquake activities in the Alaska-Aleutian subduction zone revealed by a mini seismic array, Geophys. Res. Lett., 44, doi:10.1002/2016GL072088

Lin, C.H., L.W. Hsu, M.Y. Ho, T.C. Shin, K.J. Chen and Y.H. Yeh (2007), Low-frequency submarine volcanic swarms at the southernwestern end of the Okinawa Trough, *Geophys. Res. Lett.*, *34*, L06310, doi:10.1029/2006GL029207.

Lin, J.-Y., J.-C . Sibuet, S.-K. Hsu, W.-N. Wu (2014), Could a Sumatra-like megathrust earthquake occur in the south Ryukyu subduction zone? Earth Planets Space 66, 1–8.

Lowry, A. R., K. M. Larson, V. Kostoglodov, and R. Bilham (2001), Transient fault slip in Guerrero, southern Mexico, *Geophys. Res. Lett., 28,* 3753–3756, doi: 10.1029/2001GL013238.

Matsuzawa, T., T. Igarashi and A. Hasegawa (2002), Characteristic small-earthquake sequence off Sanriku, northeastern Honshu, Japan, *Geophys. Res. Lett.,* 29, DOI: 10.1029/2001GL014632

Matsuzawa, T., N. Uchida, T. Igarashi, T. Okada and A. Hasegawa (2004), Repeating earthquakes and quasi-static slip on the plate boundary east off northern Honshu, Japan, *Earth Planet. Sci., 56,* 803-811

Matsuzawa, T., Y. Asano and K. Obara (2015), Very low frequency earthquakes off the Pacific coast of Tohoku, Japan, *Geophys. Res. Lett.,* 42, DOI: 10.1002/2015GL063959

McNutt, S. R. (2002), Volcano seismology and monitoring for eruptions, *Int. Geophys. Ser.*, 81(A), 383–406.

McNutt, S. R. (2005), A Review of Volcanic Seismology. *Annual Reviews of Earth and Planetary Sciences*, 33, 461-491 doi: 10.1146/annurev.earth.33.092203.122459

Mogi, K. (1962) Magnitude-Frequency Relationship for Elastic Shocks Accompanying Fractures of Various Materials and Some Related Problems in Earthquakes. *Bull. Earthq*. Res. Inst. Tokyo Univ., 40, 831-853.

Muller, R.D., M. Sdrolias, C. Gaina, and W.R. Roest (2008), Age, spreading rates and spreading symmetry of the world's ocean crust, Geochem. Geophys. Geosyst., 9, Q04006, doi: 10.1029/2007GC001743

Nadeau, R. M., W. Foxall, and T. V. McEvilly (1995) Clustering and Periodic Recurrence of Microearthquakes on the San Andreas Fault at Parkfield, California, *Science*, *27*, 503-507, doi: 10.1126/science.267.5197.503

Nakagawa, H., T. Toyofuku, K. Kotani, B. Miyahara, C. Iwashita, S. Kawamoto, Y. Hatanaka, H. Munekane, M. Ishimoto, T. Yutsudo, N. Ishikura, and Y. Sugawara (2009), Development and validation of GEONET new analysis strategy, *J. Geogr. Surv. Inst., 118*, 1–8 (in Japanese).

Nakamura, M. (2009), Aseismic crustal movement in southern Ryukyu Trench, southwest Japan, *Geophys. Res. Lett.*, *36,* doi: 10.1029/2009GL040357.

Nakamura, M. (2009b), Fault model of the 1771 Yaeyama earthquake along the Ryukyu Trench estimated from the devastating tsunami, *Geophys. Res. Let,* 36, L19307, Doi.org/10.1029/2009GL039730

Nakamura, M., M. Nakamura, K. Tadokoro, T. Okuda, M. Ando, T. Watanabe, S. Sugimoto, M. Furukawa (2010), Interplate coupling along the central Ryukyu Trench inferred from GPS/acoustic seafloor geodetic observation, Abstract T51D-2085, Presented at 2010 Fall Meeting, AGU, San Francisco, CA, 13–17 Dec.

Nakamura, M. (2013), The 1768 and 1791 Okinawa tsunamis in the Ryukyu Trench region, *American Geophysical Union Fall meeting*, San Francisco.

Nakamura, M. and N. Sunagawa (2015), Activation of very low frequency earthquakes by slow slip events in the Ryukyu Trench, *Geophys. Res. Lett.,* 42, doi: 10.1002/2014GL062929

Nakamura, M. (2017), Distribution of low-frequency earthquakes accompanying the very low frequency earthquakes along the Ryukyu Trench, *Earth Planet. Sci.,* doi:10.1186/s40623-017-0632-4

Nakano, M., H. Kumagai, and H. Inoue (2008), Waveform inversion in the frequency domain for the simultaneous determination of earthquake source mechanism and moment function, *Geophys. J. Int.*, *173*, 1000-1011, doi: 10.1111/j.1365-246X.2008.03783.x

Nakano, M., T. Hori, E. Araki, S. Kodaira and S. Ide (2018), Shallow very-low-frequency earthquakes accompany slow slip events in the Nankai subduction zone, Nature communication, 9, doi: 10.1038/s41467-018-03431-5

Nishimura, S., M. Hashimoto, and M. Ando (2004), A rigid block rotation model for the GPS derived velocity field along the Ryukyu arc, *Phys. Earth Planet. Inter.*, 142, 185-203, doi:10.1016/j.pepi.2003.12.014.

Nishimura, T. (2014), Short-term slow slip events along the Ryukyu Trench, southwestern Japan, observed by continuous GNSS, *Prog. Earth Planet. Sci.,* doi: 10.1186/s40645-014-0022-5.

Nishizawa A., K. Kaneda, Y. Katagiri, and M. Oikawa (2014), Wide-angle refraction experiments in the Daito Ridges region at the northwestern end of the Philippine Sea plate, *Earth Planets Space,* 66*,* doi:10.1186/1880-5981-66-25

Nishizawa A., K. Kaneda, M. Oikawa, D. Horiuchi, Y. Fujioka, and C. Okada (2017), Variations in seismic velocity distribution along the Ryukyu (Nansei-Shoto) Trench subduction zone at the northwestern end of the Philippine Sea plate, *Earth Planets Space.,* 69(1), doi: 10.1186/s40623-017-0674-7

Okino, K., Y.Ohara, S. Kasuga, Y. Kato, (1999). The Philippine Sea: new survey results reveal the structure and the history of the marginal basin. *Geophys. Res. Lett.* 26, 2287-2290.

Obana, K., S. Kodaira (2009), Low-frequency tremors associated with reverse faults in a shallow accretionary prism, *Earth Planets Sci. Lett., 287*, 168-174, 10.1016/j.epsl.2009.08.005

Obara, K. (2002), Nonvolcanic deep tremor associated with subduction in southwest Japan. *Science, 296*, 1679-1981, doi: 10.1126/science.1070378

Obara, K., H. Hirose, F. Yamamizu, and K. kasahara (2004a), Episodic slow slip events accompanied by non-volcanic tremors in southwest Japan subduction zone, *Geophys. Res. Lett, 31,*doi: 10.1029/2004GL020848.

Obara, K., Y. Haryu, Y. Ito, and K. Shiomi (2004b), Low frequency events occurred during the sequence of aftershock activity of the 2003 Tokachi-Oki earthquake; a dynamic process of the tectonic erosion by subducted seamount, *Earth Planets Space*, 56, 347–351

Obara, K. and Y. Ito (2005), Very low frequency earthquakes excited by the 2004 off the Kii peninsula earthquakes: A dynamic deformation process in the large accretionary prism, *Earth, planets and space,* 57, 321-326, doi:10.1186/BF03352570

Obara, K. (2011), Characteristics and interactions between non-volcanic tremor and related slow earthquakes in the Nankai subduction zone, southwest Japan, *Journal of Geodynamics*, *52(3-4)*, 229-248.

Obara, K., and A. Kato (2016), Connecting slow earthquakes to huge earthquakes, *Science, 353*, 253-257,doi: 10.1126/science.aaf1512.

Ohta, Y., J. Freymueller, S. Hreinsdottir and H. Suito (2006), A large slow slip event and the depth of the seismogenic zone in the south central Alaska subduction zone, *Earth Planet. Sci. Lett., 247*, 108-116, doi: 10.1016/j.epsl.2006.05.013

Ohzono, M., H. Takahashi, and M. Ichiyanagi (2014), An intraplate slow earthquake observed by a dense GPS network in Hokkaido, northernmost Japan, *Geophys. J. Int*., *200*, 144-148, doi: 10.1093/gji/ggu380.

Okada, Y. (1992), Internal deformation due to shear and tensile faults in a half-space, *Bull.*

Seism. So. Am., *82*, 1018-1040.

Okino, K., S. Kasuga, and Y. Ohara (1998), A new scenario of the Parece Vela Basin genesis, *s, Mar. Geophys. Res.*, *20*(1), 21-40

Ozawa, S., M. Murakami, M. Kaidzu, T. Tada, T. Sagiya, Y. Hatanaka, H. Yarai, and T. Nishimura (2002), Detection and monitoring of ongoing aseismic slip in the Tokai Region central Japan, *Science*, *298*, 1009–1012, doi:10.1126/science.1076780.

Ozawa, S., S. Miyazaki, Y. Hatanaka, T. Imakiire, M. Kaidzu, and M. Murakami (2003), Characteristic silent earthquakes in the eastern part of the Boso Peninsula, central Japan, *Geophys. Res. Lett.*, *30,* 1283, doi:10.1029/2002GL016665.

Ozawa, S., Y. Hatanaka, M. Kaidzu, M. Murakami, T. Imakiire, and Y. Ishigaki (2004), Aseismic slip and low-frequency earthquakes in the Bungo channel, southwestern Japan, *Geophys. Res. Lett.*, 31, L07609, doi:10.1029/2003GL019381

Ozawa, S., H. Suito, and M. Tobita (2007), Occurrence of quasi-periodic slow-slip off the east coast of the Boso Peninsula, central Japan, *Earth, Planets and Space*, *59,* 1241–1245, doi:10.1186/BF03352072.

Ozawa, S., H. Suito, T. Imakiire and M. Murakmi (2007b), Spatiotemporal evolution of aseismic interplate slip between 1996 and 1998 and between 2002 and 2004, in Bungo channel, southwest Japan, *J. Geophys. Res.*, 112, B05409, doi:10.1029/2006JB004643.

Ozawa, S. (2014), Shortening of recurrence interval of Boso slow slip events in Japan, *Geophys. Res. Lett.*, *41*, 2762–2768, doi: 10.1002/2014GL060072.

Ozawa, S. (2017), Long-term slow slip events along the Nankai trough subduction zone after the 2011 Tohoku earthquake in Japan, *Earth, Planets and Space*, *69,* doi: 10.1186/s40623-017-0640-4.

Peng, Z. and J. Gomberg (2010). An integrated perspective of the continuum between earthquakes and slow-slip phenomena, *Nature Geosci.*, *3*, 599–607, doi: 10.1038/ngeo940

Peterson, E. T. and T. Seno (1984), Factors affecting seismic moment release rates in subduction zones, *J. Geophys. Res.*, *89*, 10233-10248, doi: 10.1029/JB089iB12p10233.

Rau, R.-J., K. H. Chen and K.-E. Ching (2007), Repeating earthquakes and seismic potential along the northern Longitudinal Valley fault of eastern Taiwan, *Geophys. Res. Lett.*, *34*, doi: 10.1029/2007GL031622

Rogers, G., and H. Dragert (2003), Episodic tremor and slip on the Cascadia subduction zone: the chatter of silent slip, *Science*, *300*, 1942-1943, doi: 10.1126/science.1084783

Sagiya, T. and W. Thatcher (1999), Coseismic slip resolution along a plate boundary megathrust: The Nankai Trough, southwest Japan, *J. Geophys. Res*., 104, 1111-1129,

Satake, K., and Y. Tanioka (1997), Fault Parameters and Tsunami Generation of the 1995 Amami-Oshima-Kinkai Earthquake, *Journal of Geography (Chigaku Zasshi)*, *106*(4), 546-556.

Scholz, C. H. (1968). The frequency-magnitude relation of microfracturing in rock and its relation to earthquakes. *Bull. Seism. So. Am.*, 58(1), 399-415.

Scholz, C. H., and J. Campos (2012), The seismic coupling of subduction zones revisited, *J. Geophys. Res.*, *117,* doi: 10.1029/2011JB009003.

Scholz, C. H. (2015). On the stress dependence of the earthquake b value, *Geophys. Res. Lett.*, 42(5), 1399-1402.

Shelly, D. R., G. C. Beroza, S. Ide, and S. Nakamula (2006), Low-frequency earthquakes in Shikoku, Japan, and their relationship to episodic slip and tremor, *Nature, 442*, 188 – 191, doi:10.1038/nature04931.

Shelly, D. R., G. C. Beroza, and S. Ide (2007), Non-volcanic tremor and low-frequency earthquake swarms, *Nature, 446*, 305 – 307, doi:10.1038/nature05666.

Shibazaki, B. and Y. Iio (2003), On the physical mechanism of silent slip events along the deeper part of the seismogenic zone, Geophys. Res. Lett., 30, 2003GL017047, doi:10.1029/2003GL017047.

Sibuet, J.-C., J. Letouzey, F. Barbier, J. Charvet, J.-P. Foucher, T. W. C. Hilde, M. Kimura, L.-Y. Chiao, B. Marsset, C. Muller, and J.-F. Stephan (1987), Backarc extension in the Okinawa Trough, *J. Geophys. Res.*, 92, 14,041-14,063.

Socquet, J., Piña Valdes, J. Jara, F. Cotton, A. Walpersdorf, N. Cotte, S. Specht, F. Ortega, D. Carrizo and E. Norabuena (2017). An 8-month slow slip event triggers progressive nucleation of the 2014 Chile megathrust, *Geophys. Res. Lett., 44*, doi: 10.1002/2017GL073023.

Stern, R.J. (2002), Subduction zones, *Rev. Geophys,* 40, doi:10.1029/2001RG000108.

Sugioka, H., T. Okamoto, T. Nakamura, Y. Ishihara, A. Ito, K. Obana, K. Nakahigashi, M. Shinohara, and Y. Fukao (2012), Tsunamigenic potential of the shallow subduction plate boundary inferred from slow seismic slip, *Nat. Geosci.*, *5*, 414–418, doi:10.1038/NGEO1466.

Suito, H. and S. Ozawa (2009), Transient crustal deformation in the TokaiDistrict -The Tokai Slow Slip Event and Postseismic deformation caused by the 2004 off southeast Kii

Peninsula earthquake, *J. Seismol. Soc. Jpn.*, *2(61)*, 113–135. (in Japanese with English abstract)

Szeliga, W., T. Melbourne, M. Santillan, and M. Miller (2008), GPS constraints on 34 slow slip events within the Cascadia subduction zone, 1997–2005, *J. Geophys. Res.*, *113,* doi: 10.1029/2007JB004948

Tamaribuchi K., Y. Yamada, Y. Ishigaki, Y. Takagi, M. Nakamura, K. Maeda and M. Okada (2010), Characteristic earthquake sequence near Miyakojima Island, Ryukyu Arc, Japan, *J. Seismol. Soc. Jpn.*, 2(62), 193–207. (in Japanese with English abstract)

Thomas, A. M., R. Bürgmann, D. R. Shelly, N. M. Beeler, and M. L. Rudolph (2012), Tidal triggering of low frequency earthquakes near Parkfield, California: Implications for fault mechanics within the brittle-ductile transition, *J. Geophys. Res.*, 117, doi: 10.1029/2011JB009036

Tu, Y. and K. Heki (2017), Decadal modulation of repeating slow slip event activity in the southwestern Ryukyu Arc possibly driven by rifting episodes at the Okinawa Trough, *Geophys. Res. Lett.*, 44, 9308-9313, doi: 10.1002/2017GL074455

Uchida, N., T. Matsuzawa and T. Igarashi (2003), Interplate quasi-static slip off Sanriku, NE Japan, estimated from repeating earthquakes, *Geophys. Res. Lett.*, *15*, doi: 10.1029/2003GL017452

Uchida, N., and T. Matsuzawa (2011), Coupling coefficient, hierarchical structure, and earthquake cycle for the source area of the 2011 off the Pacific coast of Tohoku earthquake inferred from small repeating earthquake data, *Earth Planets Space*, 63, 675–679, doi:10.5047/eps.2011.07.006.

Uchida, N. and T. Matsuzawa (2013), Pre- and postseismic slow slip surrounding the 2011 Tohoku-oki earthquake rupture, *Earth, planets and space,* 374, 81-91

Usami, T. (2003), Materials for Comprehensive List of Destructive Earthquakes in Japan, pp. 605, *Univ. Tokyo Press*, Tokyo.

Utsu, T. (1965), A method for determining the value of b in a formula log n = a – bM showing the magnitude-frequency relation for earthquakes, *Geophys. Bull.*, Hokkaido Univ., Hokkaido, Japan, 13, 99-103 (in Japanese).

Utsu, T. (1982), Catalog of Large Earthquakes in the Region of Japan from 1885 through 1980, *Bulletin of the Earthquake Research Institute*, University of Tokyo, 57, 401-463 (in Japanese).

Utsu, T. (2001), Seismology 3rd Ed., (Kyoritsu Shuppan, Tokyo), pp. 376, (in Japanese).

Uyeda, S., and H. Kanamori (1979), Back-Arc Opening and the Mode of Subduction, *J. Geophys. Res., 84*, 1049-1061, doi: 10.1029/JB084iB03p01049.

Vergnolle, M., A. Walpersdorf, V. Kostoglodov, P. Tregoning, J. A. Santiago, N. Cotte, S. I. Franco (2010), Slow slip events in Mexico revised from the processing of 11 year GPS observations, *Geophys. Res. Lett.*, *115*, doi: 10.1029/2009JB006852.

Wallace, L. M., S. C. Webb, Y. Ito, K. Mochizuki, R. Hino, S. Henrys, S. Y. Schwartz, and A. F. Sheehan (2016), Slow slip near the trench at the Hikurangi subduction zone, New Zealand, *Science*, *352*, 701-704, doi: 10.1126/science.aaf2349

Wang, K., and S. L. Bilek (2014), Invited review paper: Fault creep caused by subduction of rough seafloor relief, *Tectonophysics*, 610, 1–24.

Wu, W. N., H. Kao, S. K. Hsu, C. L. Lo, and H. W. Chen, (2010). Spatial variation of the crustal stress field along the Ryukyu-Taiwan-Luzon convergent boundary. *J. Geophys. Res.*, 115(B11), doi: 10.1029/2009JB007080

Yamada, T., R. Hino, A. Nishizawa, H. Shiobara, T. Sato, K. Goto, ... & H. Shimamura, (1997), Aftershock observation of the 1995 Amami-Oshima-Kinkai Earthquake using ocean bottom seismometers, *Journal of Geography (Chigaku Zasshi)*, 106(4), 514-524.

Yamano, H., H. Kayane, N. Yonekura (2001), Anatomy of a modern coral reef flat: A recorder of storms and uplift in the late Holocene, *Journal of Sedimentary Research*, 71, 295–304, doi:10.1306/082900710295.

Yamano, H., O. Abe, E. Matsumoto, H. Kayanne, N. Yonekura and P. Blanchond (2003), Influence of wave energy on Holocene coral reef development: an example from Ishigaki Island, Ryukyu Islands, Japan, *Sedimentary Geology*, 159, 27-41, doi: 10.1016/S0037-0738(03)00093-9

Yamashita, Y., H. Shimizu, and K. Goto (2012), Small repeating earthquake activity, interplate quasi-static slip, and interplate coupling in the Hyuga-nada, southwestern Japan subduction zone, *Geophys. Res. Lett.*, 39, L08304, doi:10.1029/2012GL051476.

Yamashita, Y., H. Yakiwara, Y. Asano, H. Shimizu, K. Uchida, S. Hirano, ... and M. Kamizono (2015), Migrating tremor off southern Kyushu as evidence for slow slip of a shallow subduction interface, *Science*, 348(6235), 676-679.

Supplementary 1

The catalog of VLFEs in 2005-2012

Table S1. Occurrence times, locations, magnitudes and source parameters of the 1504 VLFEs along the Ryukyu trench.

No.	Time	Log	Lat	Mw	Deep (km)	Strike$_1$	Dip$_1$	Rake$_1$	Strike$_2$	Dip$_2$	Rake$_2$	Quality value	Quality rank
1	20050103064550	133.8	31.6	4.1	50	60	80	-30	156	61	-168	4	C
2	20050103073820	134.0	31.6	4.3	30	60	80	-70	176	22	-153	3	C
3	20050103105409	133.4	31.2	4.4	60	55	81	30	320	60	170	3	C
4	20050103144749	132.4	30.6	3.9	20	225	81	330	320	60	190	5	B
5	20050106232344	128.0	28.0	3.8	40	40	80	170	132	80	10	5	B
6	20050111174646	132.6	30.4	4.0	10	45	53	286	200	40	250	4	C
7	20050112135909	132.2	30.6	4.1	10	25	53	106	180	40	70	5	B
8	20050112153820	132.0	30.6	4.0	10	40	60	130	161	46	42	5	B
9	20050112160000	132.2	30.6	4.0	10	25	53	106	180	40	70	5	B
10	20050113153119	130.6	30.6	3.9	60	20	80	190	288	80	350	4	C
11	20050113172500	134.0	32.0	4.3	10	238	75	-103	100	20	-50	4	C
12	20050113182500	132.8	30.2	4.1	5	280	40	-70	75	53	-106	4	C
13	20050114060605	131.6	30.0	3.7	20	39	48	138	160	60	50	5	B
14	20050130073049	133.2	31.2	4.2	60	60	80	170	152	80	10	4	C
15	20050130111730	130.8	30.8	3.8	5	15	53	74	220	40	110	4	C
16	20050206171341	127.8	25.2	3.8	30	20	80	190	288	80	350	5	B
17	20050208052730	132.6	32.6	3.9	30	8	80	170	100	80	10	5	B
18	20050208060614	132.4	32.0	3.7	5	260	50	90	80	40	90	4	C
19	20050301105211	124.2	23.8	3.8	20	240	30	90	60	60	90	8	A
20	20050301105756	124.2	23.8	3.8	20	240	30	90	60	60	90	8	A
21	20050301111059	124.2	23.8	3.9	20	240	30	90	60	60	90	8	A
22	20050301111926	124.2	23.8	3.7	20	240	30	90	60	60	90	8	A
23	20050301112531	124.2	23.8	3.7	20	260	20	110	59	71	83	8	A
24	20050301113045	124.2	23.8	3.7	20	240	30	90	60	60	90	7	B
25	20050301120344	124.2	23.8	3.8	20	240	30	-90	60	60	-90	8	A
26	20050301134123	124.2	23.8	3.5	20	240	30	90	60	60	90	5	B
27	20050301170134	124.2	23.8	3.7	20	240	30	90	60	60	90	7	B
28	20050306123858	125.2	23.8	4.1	20	260	40	150	14	71	54	8	A
29	20050306124629	125.4	23.8	4	30	12	61	62	240	40	130	8	A
30	20050306125733	125.4	23.8	4	30	12	61	62	240	40	130	9	A
31	20050306133848	125.4	23.8	4	30	12	61	62	240	40	130	8	A
32	20050308161309	127.8	25.2	4.1	30	20	80	190	288	80	350	5	B
33	20050318083419	127.4	26.2	4.2	40	297	0	147	60	90	90	3	C
34	20050318114204	128.2	25.2	4	10	215	53	-106	60	40	-70	4	C
35	20050318165241	128.0	25.4	4	10	200	60	230	79	48	318	5	B
36	20050325002519	128.2	25.4	3.8	40	192	80	-170	100	80	-10	4	C
37	20050329123710	130.0	29.0	4.2	10	20	10	90	200	80	90	4	C
38	20050329124249	130.0	29.0	4.1	20	20	90	-90	194	0	-96	4	C
39	20050330211409	129.5	28.5	4	40	300	20	10	201	87	110	4	C
40	20050330230909	130.0	29.0	3.8	20	35	81	30	300	60	170	7	B
41	20050401053234	130.0	29.0	4.3	20	20	90	-90	194	0	-96	4	C
42	20050401103910	130.5	29.0	3.6	5	62	41	15	320	80	130	5	B
43	20050409071211	122.8	23.6	3.8	20	60	80	50	318	41	165	7	B
44	20050409124836	122.8	23.4	3.8	40	60	80	210	324	61	348	5	B
45	20050409141656	122.8	23.6	3.9	40	58	84	50	320	40	170	8	A
46	20050413065000	127.2	25.0	4.1	60	254	71	54	140	40	150	3	C
47	20050420034835	125.2	23.8	4	20	240	20	110	39	71	83	6	B
48	20050420040628	125.4	23.8	4.1	30	12	61	62	240	40	130	9	A
49	20050420143230	126.8	24.8	3.6	5	320	20	230	182	75	283	4	C
50	20050427174542	125.2	23.8	4	20	260	40	150	14	71	54	8	A
51	20050430073935	128.2	25.8	3.6	20	40	60	90	220	30	90	6	B
52	20050518043500	123.0	23.6	3.8	40	58	84	50	320	40	170	7	B
53	20050519132406	127.8	25.4	4.1	40	20	80	190	288	80	350	8	A
54	20050519153416	128.0	25.6	4	10	240	40	-90	60	50	-90	5	B
55	20050519180226	127.8	25.6	3.6	20	279	48	318	40	60	230	5	B
56	20050519181910	128.0	25.6	3.9	40	20	80	30	284	61	168	5	B
57	20050519184540	128.0	25.4	4.1	50	12	80	10	280	80	170	5	B
58	20050519203453	128.2	25.4	3.8	20	200	60	50	79	45	138	5	B
59	20050519214319	128.0	25.6	3.9	20	200	80	10	108	80	170	3	C
60	20050521171632	123.0	23.6	3.8	40	58	84	80	320	40	170	7	B
61	20050521172724	123.0	23.8	3.6	20	220	60	-10	315	81	-150	6	B
62	20050526040842	129.0	25.2	3.9	10	80	60	150	156	64	34	5	B
63	20050526045343	128.0	25.4	3.9	10	268	80	350	0	80	190	3	C
64	20050526065013	128.0	25.2	3.9	20	12	80	10	280	80	170	7	B
65	20050526071605	128.2	25.4	4.1	40	12	80	10	280	80	170	6	B
66	20050527051541	128.2	25.4	3.8	10	200	60	50	79	48	138	8	A
67	20050529103441	126.4	24.6	3.8	10	260	60	-70	44	36	-121	5	B
68	20050530003909	122.8	23.6	4	40	240	80	-30	336	61	-168	8	A
69	20050531130948	122.8	23.4	3.9	40	60	80	210	324	61	348	6	B
70	20050531141149	123.0	23.6	3.6	40	60	80	230	318	41	345	6	B
71	20050531185719	123.2	23.6	3.8	60	304	22	153	60	80	70	8	A
72	20050531190914	123.2	23.6	3.7	60	222	84	310	320	40	190	7	B
73	20050531214629	123.2	23.6	3.7	60	222	84	130	320	40	10	4	C
74	20050531215142	123.2	23.6	3.9	40	38	84	50	300	40	170	5	B
75	20050531235759	123.4	23.4	4.1	50	40	80	50	298	41	165	9	A

76	20050601000529	123.4	23.4	3.8	50	40	80	50	298	41	165	9	A
77	20050601115254	123.6	23.4	4.7	50	200	80	-30	296	61	-168	9	A
78	20050601120041	123.6	23.6	4.4	40	38	84	50	300	40	170	8	A
79	20050601122549	123.4	23.4	4	60	38	84	50	300	40	170	9	A
80	20050601122917	123.4	23.4	4	50	40	80	30	304	61	168	9	A
81	20050601124506	123.6	23.4	4.3	40	205	81	330	300	60	190	8	A
82	20050601125732	123.4	23.4	3.9	50	35	81	-150	300	60	-10	7	B
83	20050601130629	123.4	23.4	4.1	60	38	84	50	300	40	170	8	A
84	20050601152103	123.4	23.6	4.2	40	40	80	50	296	41	165	9	A
85	20050601153640	123.4	23.6	4	20	276	36	121	60	60	70	9	A
86	20050605034024	129.0	27.0	3.9	10	40	50	90	220	40	90	3	C
87	20050605221457	123.4	23.4	4	60	40	80	50	298	41	165	7	B
88	20050605222408	123.6	23.6	4.1	20	240	30	-90	60	60	-90	7	B
89	20050606000140	123.6	23.6	3.8	20	276	36	121	60	60	70	4	C
90	20050606004954	123.4	23.4	3.8	50	276	36	121	60	60	70	4	C
91	20050606220246	123.6	23.6	3.6	20	276	36	121	60	60	70	7	B
92	20050607042552	123.6	23.6	3.6	20	280	40	110	75	53	74	6	B
93	20050608054559	129.6	26.6	3.9	10	268	80	350	0	80	190	4	C
94	20050609025804	131.0	29.0	3.7	20	40	80	-10	132	80	-170	5	B
95	20050611213919	129.4	26.6	3.7	10	245	53	106	40	40	70	5	B
96	20050612184440	128.2	25.8	3.6	20	240	40	70	85	53	106	7	B
97	20050612184825	128.2	25.8	3.6	20	240	40	70	85	53	106	7	B
98	20050613134000	127.4	24.6	4.3	5	296	22	-153	180	80	-70	5	B
99	20050613152316	127.6	25.6	4	30	60	80	10	326	80	170	8	A
100	20050621032500	126.6	24.4	3.6	10	16	61	-168	280	80	-30	6	B
101	20050621104929	125.2	23.8	4	20	260	40	150	14	71	54	8	A
102	20050621110512	125.2	23.8	4	20	40	60	90	220	30	90	8	A
103	20050623065757	128.2	25.8	3.6	20	260	40	90	80	50	90	5	B
104	20050629100140	126.4	24.6	4.3	40	60	80	-10	152	80	-170	5	B
105	20050629150808	126.4	24.8	4.1	30	300	40	-30	54	71	-126	5	B
106	20050702200956	128.6	27.0	3.7	40	300	20	170	39	87	70	4	C
107	20050702201825	128.6	27.0	3.7	10	40	70	90	220	20	90	5	B
108	20050702211205	130.0	28.0	3.6	30	34	64	326	140	60	210	7	B
109	20050702212052	130.0	28.0	3.5	30	34	64	146	140	60	30	7	B
110	20050703053007	130.0	28.0	3.7	20	40	60	-30	146	64	-146	7	B
111	20050703054752	129.5	28.5	3.6	10	46	64	34	300	60	150	4	C
112	20050704071130	123.2	22.4	4.2	5	20	60	-70	164	36	-121	3	C
113	20050713091043	130.5	29.0	3.6	5	64	61	348	160	80	210	4	C
114	20050715085500	132.0	25.5	4	30	280	20	170	19	87	70	4	C
115	20050724064113	128.0	25.4	4.1	10	200	60	50	79	48	138	6	B
116	20050724065019	127.8	25.4	3.9	20	20	80	190	288	80	350	4	C
117	20050724065618	127.8	25.4	4	30	20	80	10	288	80	170	6	B
118	20050724071741	127.8	25.4	3.7	30	20	80	190	288	80	350	4	C
119	20050724072306	127.8	25.4	3.8	30	20	80	190	288	80	350	6	B
120	20050724074516	128.2	25.4	4	20	192	80	-170	100	80	-10	5	B
121	20050807180609	125.0	24.0	3.9	10	62	75	103	200	20	50	7	B
122	20050807181213	125.2	23.8	3.9	20	20	60	70	236	36	121	7	B
123	20050812073549	129.6	25.6	4.1	50	80	60	150	186	64	34	4	C
124	20050814093500	130.0	25.4	3.9	60	194	71	-126	80	40	-30	3	C
125	20050817235230	129.2	26.2	3.9	30	300	60	-90	120	30	-90	3	C
126	20050822221404	130.0	25.4	3.9	5	20	90	90	194	0	64	3	C
127	20050825203943	127.4	24.4	4.3	5	300	20	210	182	80	287	6	B
128	20050826000712	127.8	25.4	3.9	30	20	80	10	288	80	170	6	B
129	20050826001642	128.0	25.2	4.1	30	200	80	210	104	61	348	4	C
130	20050826010703	127.8	25.4	3.8	20	200	80	190	108	80	360	5	B
131	20050827101000	130.0	27.0	3.3	5	1	48	42	240	60	130	5	B
132	20050831093339	129.0	28.0	3.8	30	360	20	50	222	75	103	4	C
133	20050902051925	122.8	23.6	3.9	20	60	80	50	318	41	165	9	A
134	20050902174401	124.2	23.6	3.5	20	240	40	110	35	53	74	7	B
135	20050902175301	124.4	23.6	3.7	20	220	40	70	65	53	106	6	B
136	20050907063140	131.5	28.5	3.8	5	62	80	287	180	20	210	5	B
137	20050909051142	127.6	25.6	3.9	20	299	48	318	60	60	230	6	B
138	20050915121628	122.2	23.6	3.5	10	272	61	62	140	40	130	5	B
139	20050915132025	122.4	23.4	3.4	10	254	71	54	140	40	150	7	B
140	20050915205248	122.8	23.8	3.4	30	80	80	230	338	41	345	3	C
141	20050915205500	122.8	23.8	3.4	20	78	84	50	340	40	170	6	B
142	20050915212945	122.8	23.8	3.6	20	50	80	50	338	41	165	7	B
143	20050916002004	122.8	23.6	3.6	30	240	80	-10	332	80	-170	7	B
144	20050916064929	122.8	23.6	3.7	40	58	84	50	320	40	170	6	B
145	20050916070546	122.8	23.4	3.8	30	60	80	30	324	61	168	8	A
146	20050918233008	123.2	23.4	3.7	30	200	80	-10	292	80	-170	5	B
147	20050919050232	127.0	24.4	4.1	5	300	20	210	182	80	287	5	B
148	20050925204617	124.6	26.0	4.4	30	0	40	90	180	50	90	3	C
149	20051029005204	130.0	29.0	3.8	20	32	80	10	300	80	170	7	B
150	20051101153730	127.4	24.4	4	5	340	30	-90	160	60	-90	6	B
151	20051105000410	132.8	31.2	4.0	10	259	71	-97	100	20	-70	4	C
152	20051105002030	130.2	30.0	3.6	10	320	20	30	202	80	107	5	B
153	20051109075447	124.4	23.6	3.7	20	240	40	110	35	53	74	8	A
154	20051109075930	124.2	23.8	3.5	20	240	30	-90	60	60	-90	7	B
155	20051109081122	124.2	23.8	3.9	20	240	30	-90	60	60	-90	8	A
156	20051109091019	124.2	23.8	3.8	20	240	30	90	60	60	90	8	A
157	20051109091518	124.2	23.8	3.6	20	240	30	-90	60	60	-90	7	B

158	20051109132820	124.2	23.8	3.8	20	240	30	-90	60	60	-90	7	B
159	20051109134749	124.2	23.8	3.9	20	240	30	-90	60	60	-90	7	B
160	20051109135113	124.2	23.8	3.7	20	240	30	90	60	60	90	8	A
161	20051109151721	124.2	23.8	3.6	20	240	30	90	60	60	90	8	A
162	20051109152125	124.2	23.8	3.8	20	240	30	90	60	60	90	8	A
163	20051109233207	125.2	23.8	3.9	20	260	40	150	14	71	54	8	A
164	20051109233829	125.4	23.8	4	30	12	61	62	240	40	130	9	A
165	20051113171809	127.8	25.4	4	20	279	48	318	40	60	230	5	B
166	20051114161820	127.6	24.8	3.2	5	260	80	150	356	61	12	7	B
167	20051114164000	127.4	24.8	3.9	5	258	41	165	0	80	50	7	B
168	20051114165640	127.4	24.6	3.9	5	296	22	-153	180	80	-70	5	B
169	20051114170341	127.4	24.6	4.2	5	296	22	27	180	80	110	8	A
170	20051114170730	127.4	24.6	4	5	296	22	-153	180	80	-70	7	B
171	20051115095450	130.0	28.0	3.6	30	40	80	150	136	61	12	6	B
172	20051115095954	130.0	28.0	3.8	30	34	64	146	140	60	30	6	B
173	20051115114410	127.2	24.6	3.5	5	0	40	-30	114	71	-126	5	B
174	20051115123219	127.8	25.2	4.1	40	28	80	350	120	80	190	4	C
175	20051115130631	127.0	24.2	4.2	10	280	20	170	19	87	70	4	C
176	20051115133609	127.4	24.6	4.1	5	320	20	230	182	75	283	4	C
177	20051115172230	126.8	24.2	3.9	5	260	20	-20	18	80	-109	5	B
178	20051116165106	127.8	25.4	4	20	26	64	-146	280	60	-30	5	B
179	20051118171148	129.0	27.0	3.8	10	40	50	90	220	40	90	7	B
180	20051119185032	129.0	27.0	3.8	10	40	50	-90	220	40	-90	6	B
181	20051202175730	131.5	28.5	3.9	5	62	80	107	180	20	30	3	C
182	20051206172640	130.0	29.5	3.7	20	296	22	-153	180	80	-70	3	C
183	20051206183229	130.0	29.5	4	20	296	22	-153	180	60	-70	4	C
184	20051206204410	129.5	29.5	4	10	360	20	110	159	71	83	5	B
185	20051206213421	130.0	28.5	3.5	5	260	60	10	165	51	150	4	C
186	20051207051320	130.0	29.0	4	20	20	90	-90	194	0	-96	4	C
187	20051207052313	130.0	28.5	3.6	5	248	80	170	340	80	10	5	B
188	20051207071002	130.5	29.0	3.8	10	60	80	-10	152	80	-170	4	C
189	20051207074400	130.5	29.0	4	5	64	61	168	160	80	30	4	C
190	20051207094414	130.5	29.0	3.7	10	60	80	10	328	80	170	4	C
191	20051207133454	130.0	29.0	3.7	20	316	22	27	200	80	110	4	C
192	20051209234945	130.5	29.0	3.8	10	60	80	170	152	80	10	7	B
193	20051210124502	130.0	29.5	4.1	20	300	20	210	182	80	287	6	B
194	20051210125356	130.0	29.0	3.8	20	316	22	27	200	80	110	5	B
195	20051210130758	130.5	29.0	3.6	5	320	60	130	81	48	42	5	B
196	20051211021100	130.0	29.0	4.2	10	0	20	250	201	71	277	5	B
197	20051211043315	130.0	29.0	4.1	20	20	90	-90	194	0	-96	4	C
198	20051211224916	130.5	29.0	4.1	10	60	80	-10	152	80	-170	5	B
199	20051212171000	130.5	29.0	4	20	202	64	130	300	40	10	3	C
200	20051213114820	130.5	29.0	3.7	10	60	80	-10	152	80	-170	4	C
201	20051213125319	130.5	29.0	4	10	60	80	-10	152	80	-170	3	C
202	20051214030607	123.8	23.6	4	20	240	30	-90	60	60	-90	3	C
203	20051214030910	123.8	23.6	3.9	20	280	40	130	52	61	62	5	B
204	20051214043104	123.8	23.6	3.6	20	276	36	121	60	60	70	4	C
205	20051214052559	123.8	23.6	3.7	20	300	40	150	54	71	54	4	C
206	20051214133628	123.8	23.8	3.8	20	240	30	-90	60	60	-90	3	C
207	20051214134958	123.8	23.8	3.6	20	260	20	-70	59	71	-97	3	C
208	20051214155306	123.6	23.6	4.5	40	36	84	50	300	40	170	9	A
209	20051214155530	123.6	23.4	4.3	50	200	80	-30	296	61	-168	7	B
210	20051214162621	123.6	23.6	4.1	40	35	81	-150	300	60	-10	8	A
211	20051214170232	123.6	23.6	3.9	40	202	84	130	300	40	10	4	C
212	20051214182509	123.6	23.6	4.2	20	280	20	150	38	80	73	7	B
213	20051214192108	123.4	23.4	3.8	50	40	80	50	298	41	165	4	C
214	20051214204050	123.4	23.6	4	20	284	22	333	40	80	250	4	C
215	20051214211434	123.4	23.4	4.1	60	40	80	230	298	41	345	7	B
216	20051214212134	123.4	23.6	4.2	50	38	84	-130	300	40	-10	8	A
217	20051214212820	123.4	23.4	4	50	40	80	50	298	41	165	5	B
218	20051215002140	123.4	23.4	3.9	50	40	80	230	298	41	345	4	C
219	20051215003000	123.4	23.8	3.8	10	284	22	333	40	80	250	4	C
220	20051215153912	130.5	29.0	4	10	60	80	-10	152	80	-170	6	B
221	20060108075941	125.4	23.8	4	30	12	61	62	240	40	130	9	A
222	20060108080640	125.4	23.8	4	30	12	61	62	240	40	130	9	A
223	20060118100156	123.0	23.4	3.9	30	200	80	10	108	80	170	7	B
224	20060120071130	124.0	22.6	4.1	60	20	20	-90	200	70	-90	3	C
225	20060123094723	128.0	25.8	4.1	10	256	36	121	40	60	70	6	B
226	20060124232000	128.0	25.8	3.8	10	40	60	90	220	30	90	4	C
227	20060124232546	128.2	25.4	3.8	10	215	53	74	60	40	110	5	B
228	20060125002703	128.0	25.6	3.7	10	260	40	-70	55	53	-106	6	B
229	20060125032106	128.0	25.8	4	20	40	60	90	220	30	90	5	B
230	20060125033037	128.2	25.6	3.9	10	240	40	110	35	53	74	5	B
231	20060125044140	127.8	25.4	4.1	40	20	80	190	288	80	350	6	B
232	20060125045000	128.0	25.6	3.8	20	260	40	-50	32	61	-118	4	C
233	20060125091905	127.8	25.4	3.9	30	20	80	190	288	50	350	5	B
234	20060125094732	127.8	25.4	3.8	30	20	80	30	284	61	168	4	C
235	20060125095801	128.0	25.0	4.3	50	20	80	-10	112	80	-170	7	B
236	20060125100346	127.8	25.4	3.9	30	20	80	30	284	61	168	6	B
237	20060126005453	128.0	25.6	4.1	5	268	80	170	0	80	10	5	B
238	20060126042230	127.8	25.0	4.1	50	32	80	10	300	80	170	4	C
239	20060126044410	127.8	25.6	3.9	20	279	48	316	40	60	230	4	C

240	20060127040830	128.0	25.4	4	20	220	80	10	128	80	170	3	C
241	20060211094229	125.4	23.8	4	30	12	61	62	240	40	130	9	A
242	20060212131129	125.2	23.8	3.9	20	260	40	150	14	71	54	9	A
243	20060213001319	129.5	28.0	3.6	30	40	80	190	308	80	350	5	B
244	20060213214019	124.6	23.6	3.7	30	20	80	50	278	41	165	5	B
245	20060215050134	124.2	24.0	3.5	10	300	20	-10	39	87	-110	4	C
246	20060216062742	129.0	28.0	3.6	5	280	20	170	19	87	70	4	C
247	20060217185921	123.2	23.6	4	40	299	48	318	60	60	230	5	B
248	20060218041543	122.8	23.6	3.8	40	58	84	50	320	40	170	8	A
249	20060218045050	122.8	23.4	3.9	40	60	80	30	324	61	168	8	A
250	20060218054319	122.8	23.4	3.9	40	60	80	30	324	61	168	8	A
251	20060218071735	122.8	23.6	3.9	40	58	84	50	320	40	170	9	A
252	20060218101122	123.0	23.6	3.7	40	58	84	50	320	40	170	7	B
253	20060218125234	122.8	23.8	3.7	20	240	80	-30	336	61	-168	4	C
254	20060219040445	123.6	24.0	4	5	254	71	-126	140	40	-30	4	C
255	20060219041133	123.2	23.4	3.9	20	12	80	10	280	80	170	7	B
256	20060222071050	131.5	28.5	3.8	5	62	80	107	180	20	30	6	B
257	20060222110221	129.0	28.0	3.6	30	360	20	230	222	75	283	4	C
258	20060223092410	131.5	28.5	3.7	5	62	80	287	180	20	210	6	B
259	20060227161306	129.0	28.0	3.7	30	20	20	250	221	71	277	5	B
260	20060306181721	130.0	28.0	3.6	30	34	64	148	140	60	30	6	B
261	20060307034135	130.0	28.0	3.6	30	48	80	170	140	80	10	6	B
262	20060321221530	130.0	28.0	3.9	20	34	64	146	140	60	30	5	B
263	20060329154730	131.0	31.5	4	10	358	41	345	100	80	230	3	C
264	20060329155311	130.5	29.5	4.1	40	12	80	10	280	80	170	4	C
265	20060329183934	128.2	25.4	4.2	50	12	80	10	280	80	170	5	B
266	20060330152959	132.0	31.0	3.8	20	240	80	-30	336	61	-168	7	B
267	20060331182935	132.0	30.6	3.6	5	40	40	-90	220	50	-90	7	B
268	20060401024044	132.2	30.6	3.5	5	45	53	106	200	40	70	8	A
269	20060401024709	130.8	30.8	3.6	40	235	81	-150	140	60	-10	5	B
270	20060401032139	130.8	30.8	3.7	40	240	80	30	144	61	168	4	C
271	20060403043953	123.8	23.6	3.9	20	280	40	130	52	61	62	7	B
272	20060403044218	123.8	23.6	3.7	20	280	40	130	52	61	62	8	A
273	20060403051705	123.8	23.6	3.7	20	280	40	-50	52	61	-118	6	B
274	20060414054109	129.6	26.8	3.8	10	360	40	210	246	71	306	4	C
275	20060414062037	129.2	27.0	4	20	240	80	130	342	41	15	3	C
276	20060417090133	129.0	27.0	3.8	10	240	40	110	35	53	74	5	B
277	20060418042309	126.6	24.6	4.3	10	240	40	110	35	53	74	4	C
278	20060418074640	126.4	24.0	4.4	20	260	40	150	34	71	54	3	C
279	20060422091410	132.4	32.0	4.5	10	20	60	-70	164	36	-121	6	B
280	20060422100910	132.2	32.2	4.3	30	20	80	170	112	80	10	6	B
281	20060422110230	132.4	32.2	4.0	20	200	80	-30	296	61	-168	8	A
282	20060422113044	132.4	32.0	3.8	20	25	81	330	120	60	190	7	B
283	20060422121533	132.0	32.4	4.2	30	8	80	350	100	80	190	6	B
284	20060422125229	132.2	32.4	3.6	30	8	80	350	100	80	190	5	B
285	20060425120434	130.0	29.0	3.8	40	20	80	-50	122	41	-165	5	B
286	20060425133509	129.5	29.0	3.5	5	180	80	-10	272	80	-170	4	C
287	20060426232456	122.2	23.6	3.4	30	260	80	210	164	61	348	4	C
288	20060503044640	128.2	25.4	4.1	20	200	80	10	108	80	170	6	B
289	20060503054603	128.0	25.4	4.1	30	192	80	-170	100	80	-10	9	A
290	20060503060559	128.2	25.4	4.3	30	192	80	10	100	80	170	5	B
291	20060503061726	128.0	25.4	4	60	15	81	-150	280	60	-10	6	B
292	20060503062814	128.0	25.6	3.9	40	20	80	230	278	41	345	8	A
293	20060504095011	128.2	25.6	3.6	20	259	48	138	20	60	50	5	B
294	20060516011412	129.5	27.0	3.8	30	300	40	-90	120	50	-90	4	C
295	20060521084140	130.0	25.6	4.3	10	300	30	90	120	60	90	3	C
296	20060526010000	122.8	23.6	3.5	10	200	20	-10	299	87	-110	3	C
297	20060603055500	125.2	23.8	3.8	20	260	40	150	14	71	54	8	A
298	20060603061320	125.2	23.8	4	20	40	60	90	220	30	90	9	A
299	20060603074427	125.2	23.8	4	20	40	60	90	220	30	90	9	A
300	20060604102754	127.8	25.2	3.8	20	26	64	-146	280	60	-30	4	C
301	20060609033829	125.2	23.8	4	20	260	40	150	14	71	54	9	A
302	20060613160000	124.8	26.0	4.1	20	344	36	-121	200	60	-70	3	C
303	20060626130809	129.5	26.5	3.4	10	245	53	106	40	40	70	6	B
304	20060629074658	131.5	28.5	4	5	62	80	107	180	20	30	7	B
305	20060707193010	122.8	23.8	3.9	5	340	40	30	226	71	126	4	C
306	20060707200807	122.5	23.4	3.9	30	60	80	30	324	61	168	5	B
307	20060711071952	128.0	25.4	4.2	10	40	40	-90	220	50	-90	3	C
308	20060714092730	123.0	24.6	3.4	5	236	61	12	140	80	150	4	C
309	20060714123545	124.2	23.8	4.2	40	40	60	-50	161	48	138	3	C
310	20060715204946	125.2	23.8	3.9	20	18	75	77	240	20	130	6	B
311	20060723030702	124.2	23.8	3.5	20	260	20	130	38	75	77	6	B
312	20060723031103	124.2	23.8	3.6	20	240	30	90	60	60	90	7	B
313	20060723031504	124.2	23.8	3.6	20	260	20	130	38	75	77	7	B
314	20060723032702	124.2	23.8	3.7	20	240	30	90	60	60	90	8	A
315	20060723034819	124.2	23.8	3.7	20	60	60	110	204	36	59	8	A
316	20060723040544	124.2	23.8	3.6	20	240	30	-90	60	60	-90	8	A
317	20060725040640	128.2	25.6	4	20	240	40	-70	35	53	-106	3	C
318	20060725175151	127.2	24.8	4	5	260	60	150	6	64	34	5	B
319	20060726051441	127.4	24.4	4.3	5	280	20	10	181	87	110	4	C
320	20060726071858	127.8	25.6	3.7	10	20	80	10	288	80	170	5	B
321	20060726080235	127.2	24.6	4	5	296	22	27	180	80	110	6	B

322	20060726101749	127.8	25.4	3.8	40	32	80	-170	300	80	-10	4	C
323	20060730185058	127.8	25.2	4.1	40	20	80	190	288	80	350	6	B
324	20060805235614	127.8	25.4	3.9	20	20	80	10	288	80	170	4	C
325	20060806005614	127.8	25.4	4.1	40	20	80	10	288	80	170	4	C
326	20060806005910	127.8	25.4	4	40	20	80	10	288	80	170	7	B
327	20060806023623	128.0	25.4	4.2	20	200	80	190	108	80	350	9	A
328	20060806025336	127.8	25.4	4.2	20	259	48	138	20	60	50	3	C
329	20060806031354	128.0	25.4	4	20	200	60	50	79	45	138	7	B
330	20060806031600	127.8	25.4	3.8	30	20	80	30	284	61	168	4	C
331	20060806155844	127.8	25.2	4	40	20	80	-10	112	80	-170	7	B
332	20060806160238	127.8	25.4	4	40	20	80	190	288	80	350	6	B
333	20060807120640	128.0	25.4	3.9	10	200	60	230	79	48	318	4	C
334	20060808062205	123.6	23.6	4.3	40	38	84	50	300	40	170	8	A
335	20060808065050	123.6	23.8	4.1	10	284	22	153	40	80	70	4	C
336	20060808080415	123.4	23.4	4	40	40	80	230	298	41	345	7	B
337	20060808081555	123.4	23.8	3.9	10	284	22	153	40	80	70	6	B
338	20060808082230	123.6	23.8	4	20	220	20	70	61	71	97	6	B
339	20060808085049	123.4	23.8	3.9	10	280	20	130	58	75	77	7	B
340	20060808090103	123.4	23.8	4	10	284	22	333	40	80	250	6	B
341	20060808090441	123.4	23.8	3.9	10	280	20	-50	58	75	-103	8	A
342	20060808090935	123.4	23.8	4	10	284	22	333	40	80	250	6	B
343	20060808093947	123.4	23.6	4	20	40	80	230	298	41	345	8	A
344	20060808094414	123.4	23.4	4.1	50	40	80	230	298	41	345	6	B
345	20060808095320	123.4	23.4	3.9	40	40	80	230	298	41	345	6	B
346	20060808101539	123.4	23.8	3.8	10	280	20	-50	58	75	-103	6	B
347	20060808103410	123.4	23.4	3.9	50	40	80	50	298	41	165	7	B
348	20060808122257	123.8	23.6	3.9	20	280	40	150	34	71	54	8	B
349	20060808125633	123.6	23.6	4.2	40	38	84	50	300	40	170	8	B
350	20060808130338	123.6	23.6	4.2	40	38	84	50	300	40	170	9	A
351	20060812213140	126.0	24.2	4.1	50	40	80	50	298	41	165	4	C
352	20060813124228	123.2	23.4	4	30	200	80	190	108	80	350	9	A
353	20060813130122	123.2	23.4	4.1	30	192	80	10	100	80	170	9	A
354	20060814041320	131.5	29.0	4.3	20	62	75	103	200	20	50	3	C
355	20060814042403	130.0	29.5	4.3	40	260	80	-10	352	80	-170	4	C
356	20060814071801	130.0	29.0	4.1	20	20	90	90	194	0	84	5	B
357	20060814090140	130.0	29.5	3.9	40	6	71	306	120	40	210	5	B
358	20060814123524	130.0	29.0	3.9	20	22	75	283	160	20	230	6	B
359	20060814145439	130.0	29.0	4.1	40	20	80	90	200	10	90	5	B
360	20060817184947	128.2	25.4	4	40	12	80	10	280	80	170	6	B
361	20060817231719	128.2	25.4	3.9	30	192	80	10	100	80	170	4	C
362	20060829192724	131.5	28.5	3.7	5	62	80	107	180	20	30	6	B
363	20060830234820	134.0	31.6	3.9	20	45	81	150	140	60	10	3	C
364	20060831055037	130.2	30.6	4.0	50	188	80	350	280	80	190	5	B
365	20060831204523	132.2	30.4	4.0	10	245	81	330	340	60	190	4	C
366	20060831205937	131.8	30.4	3.7	5	240	60	150	346	54	34	5	B
367	20060831212044	130.0	28.0	3.6	20	40	60	150	146	64	34	6	B
368	20060831214109	130.0	28.0	3.5	20	40	60	-50	161	48	-138	6	B
369	20060831215400	130.0	28.0	3.7	30	34	64	146	140	60	30	7	B
370	20060831215656	130.0	28.0	3.5	20	40	60	130	161	48	42	5	B
371	20060902044832	130.0	28.0	3.5	30	34	64	325	140	60	210	5	B
372	20060903030529	123.8	23.4	4.1	30	20	80	30	284	61	168	8	A
373	20060909180918	124.4	23.8	3.7	20	280	40	150	34	71	54	9	A
374	20060911013844	124.4	23.8	3.7	20	280	40	150	34	71	54	9	A
375	20060912104801	123.4	23.8	4.3	10	338	80	-107	220	20	-30	3	C
376	20060912105813	124.4	23.6	3.6	20	279	48	138	40	60	50	8	A
377	20060916051500	125.6	23.8	4.5	20	245	53	106	40	40	70	3	C
378	20060919035820	123.8	24.4	4.5	30	280	80	-70	36	22	-153	3	C
379	20060919211410	125.8	23.4	4	20	188	80	170	280	80	10	4	C
380	20060929232516	130.5	27.0	3.6	5	0	60	70	216	36	121	4	C
381	20060930104813	128.0	28.0	3.8	40	40	80	190	308	80	350	4	C
382	20061003004739	129.6	26.6	3.9	10	254	64	146	350	60	30	6	B
383	20061003051245	129.0	27.0	3.7	10	40	50	-90	220	40	-90	5	B
384	20061003231106	129.0	27.0	3.7	10	240	40	-70	35	53	-106	4	C
385	20061003232959	129.0	27.0	3.7	10	40	50	90	220	40	90	5	B
386	20061012101536	122.8	23.4	3.9	40	55	81	-150	320	60	-10	9	A
387	20061012103113	122.8	23.4	3.9	40	60	80	30	324	61	168	9	A
388	20061014171847	129.0	27.0	3.7	10	240	40	110	35	53	74	6	B
389	20061014173915	129.0	27.0	3.7	10	240	40	110	35	53	74	6	B
390	20061015235528	127.8	25.2	4	40	20	80	190	288	80	350	8	A
391	20061016000556	127.8	25.4	4.1	40	20	80	190	288	80	350	7	B
392	20061016103129	128.0	25.2	3.9	20	12	80	10	280	80	170	7	B
393	20061016121535	127.8	25.4	4.1	30	20	80	190	288	80	350	7	B
394	20061016122336	128.0	25.2	4.1	30	200	80	30	104	61	168	8	A
395	20061017110441	124.4	23.6	4.1	20	32	80	-170	300	80	-10	9	A
396	20061018153508	124.6	23.6	3.7	20	280	40	150	34	71	54	7	B
397	20061019150140	124.4	23.6	3.5	20	256	36	301	40	60	250	7	B
398	20061025171600	131.5	28.5	3.9	5	62	80	107	180	20	30	6	B
399	20061025172500	131.5	28.5	3.4	5	62	80	107	180	20	30	6	B
400	20061025174500	131.5	28.5	3.8	5	62	80	107	180	20	30	6	B
401	20061106103439	130.5	28.5	3.5	5	76	61	-168	340	80	-30	5	B
402	20061106104352	130.5	28.5	3.5	5	50	80	190	348	80	350	5	B
403	20061111114031	125.2	23.8	4.1	20	260	40	150	14	71	54	9	A

404	20061111114500	125.4	23.8	4.1	30	12	61	62	240	40	130	7	B
405	20061114023842	130.0	28.5	3.7	5	256	61	12	160	80	150	5	B
406	20061114034602	130.5	29.5	3.9	40	20	60	150	126	64	34	5	B
407	20061115024234	123.6	23.4	4.6	40	200	80	-30	296	61	-168	9	A
408	20061116190355	133.2	32.8	4.1	60	40	80	-70	156	22	-153	4	C
409	20061117132736	123.8	23.4	3.7	20	279	48	318	40	60	230	5	B
410	20061117133909	123.8	23.6	3.6	20	280	40	130	52	61	62	6	B
411	20061118040158	123.6	23.6	4.4	20	202	84	310	300	40	190	8	A
412	20061118042701	123.8	23.6	3.8	20	280	40	130	52	61	62	7	B
413	20061118043028	123.8	23.6	4	20	276	36	121	60	60	70	8	A
414	20061119121320	132.6	32.8	4.0	30	0	60	-30	106	64	-146	5	B
415	20061120041239	123.8	23.6	3.7	20	280	40	130	52	61	62	6	B
416	20061120043036	123.8	23.8	3.9	10	280	20	130	58	75	77	5	B
417	20061120044500	123.8	23.8	3.7	10	260	20	110	59	71	83	6	B
418	20061120052910	123.8	23.6	3.9	20	276	36	121	60	60	70	9	A
419	20061120053710	123.8	23.6	3.7	20	280	40	130	52	61	62	8	A
420	20061122154527	127.8	25.2	3.9	30	32	80	10	300	80	170	3	C
421	20061122155329	127.8	25.4	3.9	30	20	80	190	288	80	350	4	C
422	20061122173659	128.0	25.4	3.8	20	20	80	10	288	80	170	5	B
423	20061122175029	128.0	25.4	3.8	10	200	60	230	79	48	318	5	B
424	20061202135857	127.2	24.2	4.3	5	320	20	230	182	75	283	4	C
425	20061202142259	127.4	24.6	4	5	260	60	-30	6	64	-146	5	B
426	20061202144142	127.4	24.6	3.8	5	296	22	-153	180	80	-70	4	C
427	20061203132823	128.0	25.4	4.1	20	12	80	-170	280	80	-10	9	A
428	20061203134852	128.0	25.2	4.1	30	20	80	10	288	80	170	7	B
429	20061204134509	128.6	25.8	3.6	10	200	80	30	104	61	168	7	B
430	20061204164426	127.8	25.4	4.2	20	26	80	170	120	80	10	6	B
431	20061204180133	128.0	25.6	4	10	200	60	210	94	64	326	7	B
432	20061206162339	127.8	25.4	4	40	40	80	210	304	61	348	6	B
433	20061212043904	130.5	29.5	4	30	15	81	30	280	60	170	3	C
434	20061213124145	130.4	30.0	4.0	5	0	80	110	116	22	27	7	B
435	20061231133410	122.2	22.6	3.7	10	248	80	350	340	80	190	6	B
436	20061231135550	122.4	23.6	3.7	5	226	64	-146	120	60	-30	5	B
437	20061231211050	122.2	22.4	3.6	10	248	80	350	340	80	190	4	C
438	20070112055350	125.2	23.8	3.9	20	260	40	150	14	71	54	8	A
439	20070112060028	125.4	23.8	4	30	12	61	62	240	40	130	9	A
440	20070112095502	128.0	25.2	4.1	10	220	60	70	76	36	121	5	B
441	20070119000316	123.6	23.6	4.5	40	38	84	50	300	40	170	7	B
442	20070119003426	123.6	23.6	4.1	40	202	84	130	300	40	10	6	B
443	20070208213944	126.0	24.6	4.2	50	60	80	10	328	80	170	4	C
444	20070213101556	126.0	24.6	4.1	5	40	50	-90	220	40	-90	4	C
445	20070213102936	128.2	26.0	4	5	266	64	-146	160	60	-30	4	C
446	20070218012611	128.2	25.6	4.1	10	240	40	-70	35	53	-106	6	B
447	20070218021436	128.2	25.6	4.1	20	259	48	138	20	60	50	6	B
448	20070218024346	128.4	25.4	3.6	10	56	36	121	200	60	70	5	B
449	20070228190833	123.8	23.6	3.8	20	240	30	90	60	60	90	4	C
450	20070228192640	123.8	23.6	3.7	20	276	36	121	60	60	70	4	C
451	20070302152117	124.2	23.8	3.6	20	284	22	153	40	80	70	5	B
452	20070302154957	124.4	23.6	3.9	20	220	40	70	65	53	106	6	B
453	20070302155742	124.2	23.8	3.7	20	240	30	90	60	60	90	5	B
454	20070317151108	129.0	25.0	4	10	80	60	-30	186	64	-146	4	C
455	20070323140746	125.4	23.8	3.9	30	12	61	62	240	40	130	8	A
456	20070329005726	128.6	26.0	3.7	20	40	50	90	220	40	90	8	A
457	20070419160132	129.8	29.0	4.2	60	200	80	30	104	61	168	6	B
458	20070425053138	122.6	24.2	4.2	60	200	20	30	82	80	107	4	C
459	20070503013303	125.2	23.8	4	20	260	40	150	14	71	54	6	B
460	20070503013608	125.2	23.8	4	20	264	22	333	20	80	250	3	C
461	20070503014118	125.4	23.8	4	30	12	61	62	240	40	130	8	A
462	20070504221639	130.0	29.8	4.1	50	0	60	-30	106	64	-146	3	C
463	20070505231416	130.4	29.6	4.1	50	12	80	10	280	80	170	4	C
464	20070506164614	130.0	29.6	4.5	60	202	84	310	300	40	190	3	C
465	20070507032850	129.8	29.8	4.6	60	6	71	126	120	40	30	5	B
466	20070507040506	130.6	29.8	4.3	30	15	81	30	280	60	170	5	B
467	20070509153259	130.2	29.4	3.9	10	360	20	90	180	70	90	7	B
468	20070509160249	130.2	29.4	3.8	10	360	20	90	180	70	90	5	B
469	20070517051005	128.4	25.4	4.2	10	56	36	121	200	60	70	6	B
470	20070517053352	128.2	25.4	4.3	30	12	80	10	280	80	170	5	B
471	20070517061954	128.0	25.8	3.8	10	40	60	90	220	30	90	4	C
472	20070517062530	128.0	25.8	3.6	10	40	60	-90	220	30	-90	5	B
473	20070517064313	128.0	25.8	3.8	10	40	70	-90	220	20	-90	5	B
474	20070517065738	128.2	25.4	3.7	20	215	53	74	60	40	110	5	B
475	20070519201728	129.0	25.4	4.1	10	74	64	326	180	60	210	4	C
476	20070520044347	129.2	25.2	4	10	59	48	318	180	60	230	4	C
477	20070520051725	129.0	25.2	4.1	10	74	64	326	180	60	210	4	C
478	20070520052936	128.0	25.2	4.4	40	20	80	10	288	80	170	7	B
479	20070524085513	126.0	24.8	4.4	50	300	40	-30	54	71	-126	3	C
480	20070601074748	128.4	25.6	4	20	259	48	318	20	60	230	4	C
481	20070611114039	125.2	23.8	4.1	40	260	40	150	14	71	54	7	B
482	20070611114556	125.4	23.8	3.9	30	12	61	62	240	40	130	8	A
483	20070611120309	125.2	23.8	3.9	20	40	60	90	220	30	90	8	A
484	20070620121748	126.4	24.8	3.9	20	299	48	138	60	60	50	4	C
485	20070623151455	129.6	26.6	3.9	10	245	53	286	40	40	250	4	C

486	20070623161139	129.6	26.6	4	10	245	53	286	40	40	250	4	C
487	20070626011908	127.8	25.2	4.1	30	20	80	10	288	80	170	5	B
488	20070626111511	129.0	27.0	3.9	10	0	40	230	228	61	298	7	B
489	20070626113344	129.8	27.0	4.2	30	60	80	-10	152	80	-170	7	B
490	20070626221216	129.6	26.6	4	10	245	53	286	40	40	250	5	B
491	20070628022910	129.2	26.8	3.6	5	85	81	150	180	60	10	5	B
492	20070628023146	129.6	26.6	3.8	10	245	53	106	40	40	70	6	B
493	20070628024238	126.0	26.6	4.1	5	278	75	-103	140	20	-50	3	C
494	20070708031416	129.0	27.0	3.6	5	260	80	150	356	61	12	5	B
495	20070709103930	129.8	27.8	3.4	20	40	60	130	161	48	42	5	B
496	20070710084538	129.8	27.8	3.6	20	42	75	103	180	20	50	7	B
497	20070710204919	130.2	27.6	3.9	20	20	40	-90	200	50	-90	5	B
498	20070720074119	128.2	26.0	3.7	5	266	64	-146	160	60	-30	5	B
499	20070723110843	123.2	23.4	3.9	20	60	60	30	314	64	146	5	B
500	20070727195232	128.6	27.0	3.6	10	0	60	50	239	48	138	4	C
501	20070727195809	128.4	27.0	4	50	340	40	30	226	71	126	6	B
502	20070731065125	125.4	23.8	4.1	30	12	61	62	240	40	130	9	A
503	20070731065636	125.4	23.8	4	30	12	61	62	240	40	130	9	A
504	20070731070752	125.4	23.8	4	30	12	61	62	240	40	130	8	A
505	20070803130309	126.4	24.8	4.2	40	60	80	170	152	80	10	7	B
506	20070814095540	128.0	25.2	4.1	30	26	64	-146	280	60	-30	5	B
507	20070815155839	128.4	25.4	4	10	56	36	301	200	60	250	6	B
508	20070815161127	128.2	25.4	4	20	194	71	54	80	40	150	6	B
509	20070822170706	123.8	23.6	3.7	20	280	40	150	34	71	54	8	A
510	20070822171951	123.8	23.6	3.9	20	280	40	130	52	61	62	7	B
511	20070822172140	123.8	23.6	3.5	20	280	40	-50	52	61	-118	3	C
512	20070825121740	130.2	29.0	3.8	5	40	20	-70	199	71	-97	6	B
513	20070905234614	129.0	25.0	3.9	10	80	60	150	186	64	34	4	C
514	20070911033010	130.2	28.0	3.6	30	34	64	146	140	60	30	6	B
515	20070911033840	130.2	28.0	3.7	30	40	60	-30	146	64	-146	6	B
516	20070911034259	130.2	28.0	3.6	30	40	60	150	146	64	34	5	B
517	20071027213556	128.2	25.2	3.7	10	200	60	50	79	48	138	7	B
518	20071028033809	128.0	25.2	4.1	10	220	60	70	76	36	121	8	A
519	20071028034510	128.0	25.2	3.9	20	214	71	54	100	40	150	6	B
520	20071028041023	127.8	25.4	3.9	20	20	80	30	284	61	168	8	A
521	20071028042657	127.8	25.4	3.8	30	20	80	210	284	61	348	8	A
522	20071109180505	128.4	25.4	4.1	10	56	36	121	200	60	70	7	B
523	20071109180844	128.2	25.2	4.1	40	12	80	-170	280	80	-10	6	B
524	20071109210012	123.6	23.4	4.3	40	200	80	-30	296	61	-168	4	C
525	20071109210612	123.4	23.4	3.9	60	38	84	50	300	40	170	4	C
526	20071109211736	123.6	23.4	4.4	50	200	80	-10	292	80	-170	8	A
527	20071109230752	123.6	23.4	3.8	40	280	40	150	34	71	54	3	C
528	20071109232935	123.6	23.6	4.5	40	40	80	50	298	41	165	8	A
529	20071110002625	123.6	23.6	3.7	20	276	36	121	60	60	70	3	C
530	20071110003000	123.6	23.6	3.9	20	276	36	121	60	60	70	4	C
531	20071110010756	123.6	23.6	3.9	30	276	36	301	60	60	250	5	B
532	20071110042245	123.4	23.4	4	50	40	80	50	298	41	165	6	B
533	20071110043909	123.4	23.4	4.2	50	40	80	50	298	41	165	7	B
534	20071110061212	123.4	23.8	3.9	10	284	22	333	40	80	250	4	C
535	20071110062004	123.4	23.4	4.1	50	40	80	230	298	41	345	5	B
536	20071110065128	123.4	23.8	4	10	284	22	153	40	80	70	5	B
537	20071110155639	128.2	25.4	4.1	20	240	50	-90	60	40	-90	3	C
538	20071112050052	128.2	24.6	3.8	5	280	20	30	162	80	107	3	C
539	20071112050517	128.2	25.4	3.9	20	215	53	74	60	40	110	8	A
540	20071113171812	123.2	23.4	4	30	200	80	190	108	80	350	6	B
541	20071201093702	124.4	23.6	3.7	20	220	40	70	65	53	106	7	B
542	20071201094326	124.2	23.8	3.8	20	260	20	-50	38	75	-103	5	B
543	20071201094657	124.2	23.8	3.7	20	240	30	90	60	60	90	5	B
544	20071201100708	124.2	23.8	3.8	20	240	30	-90	60	60	-90	8	A
545	20071201101647	124.4	23.6	3.8	20	40	50	90	220	40	90	8	A
546	20071201102026	124.2	23.8	3.7	20	240	30	-90	60	60	-90	6	B
547	20071201110203	124.2	23.8	3.7	20	240	30	90	60	60	90	8	A
548	20071201110939	124.4	23.6	3.8	20	40	50	90	220	40	90	9	A
549	20071201120325	124.2	23.8	3.7	20	240	30	90	60	60	90	8	A
550	20071201121448	124.2	23.8	3.7	20	240	30	-90	60	60	-90	7	B
551	20071219004229	126.0	24.0	4.3	5	260	20	-30	18	80	-107	7	B
552	20071219013648	127.6	26.4	4	50	238	75	-103	100	20	-50	6	B
553	20071222002454	125.4	23.8	4.2	30	12	61	62	240	40	130	7	B
554	20071222002833	125.4	23.8	4	30	12	61	62	240	40	130	6	B
555	20071228212319	127.2	24.6	4.1	5	340	20	70	181	71	97	6	B
556	20071228213049	128.0	26.6	4.1	5	240	10	-90	60	80	-90	5	B
557	20071228215339	127.4	24.6	4.2	5	340	20	70	181	71	97	7	B
558	20080107142544	130.8	30.8	3.7	60	260	40	10	162	84	130	4	C
559	20080108023137	132.8	31.6	4	60	225	81	330	320	60	190	4	C
560	20080108024430	132.2	30.2	3.6	5	60	60	-50	181	48	-138	4	C
561	20080125044730	130.4	30.8	3.2	10	280	60	-50	41	48	-138	3	C
562	20080127053547	123.8	23.4	4.1	40	20	80	30	284	61	168	7	B
563	20080210053530	132.0	27.8	4.2	20	40	80	210	304	61	348	4	C
564	20080210054715	130.4	27.6	3.7	20	4	36	59	220	60	110	4	C
565	20080211033518	125.2	23.8	4.1	20	260	40	150	14	71	54	9	A
566	20080211034135	125.4	23.8	4	30	12	61	62	240	40	130	9	A
567	20080211035345	125.2	23.8	3.9	20	40	60	90	220	30	90	9	A

568	20080215103429	125.2	24.0	3.9	20	258	41	165	0	80	50	6	B
569	20080216114538	127.8	25.4	3.8	20	279	48	138	40	60	50	6	B
570	20080216115230	126.2	24.0	4.5	5	20	20	90	200	70	90	4	C
571	20080217124124	127.8	25.4	3.9	10	26	64	34	280	60	150	4	C
572	20080217130725	127.6	26.5	4.2	5	300	40	30	186	71	126	5	B
573	20080217133627	127.8	25.4	3.9	20	279	48	318	40	60	230	7	B
574	20080217145617	128.0	25.4	3.9	10	215	53	74	60	40	110	6	B
575	20080321101614	130.2	29.4	3.9	20	182	84	130	280	40	10	5	B
576	20080321141849	130.2	28.6	3.7	5	80	80	30	344	61	168	4	C
577	20080321154846	130.0	29.4	4	20	0	40	-70	155	53	-106	4	C
578	20080321155424	130.4	29.0	3.8	5	64	61	168	160	80	30	5	B
579	20080327212803	130.0	28.8	3.7	5	320	40	150	74	71	54	6	B
580	20080328020624	130.2	28.8	3.6	5	252	80	-170	160	80	-10	4	C
581	20080328083741	130.2	29.8	4.5	50	268	80	170	0	80	10	5	B
582	20080328084358	130.8	29.6	4.2	50	20	80	190	288	80	350	5	B
583	20080328091530	130.2	30.0	4.4	60	268	80	170	0	80	10	3	C
584	20080402143709	128.2	25.4	4.2	10	212	61	-118	80	40	-50	9	A
585	20080407101339	126.4	24.8	4.1	40	60	80	170	152	80	10	7	B
586	20080407191249	126.4	24.8	4.1	40	60	80	190	328	80	350	7	B
587	20080409055149	128.0	25.2	4.3	20	200	80	30	104	61	168	7	B
588	20080429001826	123.8	23.6	3.8	20	280	40	130	52	61	62	5	B
589	20080429162637	123.8	23.6	3.7	20	276	36	121	60	60	70	6	B
590	20080501185054	124.2	23.8	3.6	20	240	30	90	60	60	90	8	A
591	20080501194259	124.4	23.6	3.9	20	40	50	90	220	40	90	9	A
592	20080501202158	124.2	23.8	3.8	20	256	36	301	40	60	250	8	A
593	20080506041752	124.2	23.8	3.8	20	240	30	90	60	60	90	8	A
594	20080506042255	124.2	23.8	3.7	20	240	30	90	60	60	90	7	B
595	20080506044703	124.2	23.8	3.8	20	240	30	-90	60	60	-90	8	A
596	20080506052123	124.2	23.8	3.7	20	240	30	90	60	60	90	8	A
597	20080507055345	125.4	24.0	4	20	258	41	165	0	80	50	5	B
598	20080507055957	125.4	23.8	4.1	30	12	61	62	240	40	130	8	A
599	20080512190353	132.6	31.2	4.1	10	20	50	-90	200	40	-90	7	B
600	20080512193659	132.8	31	4.1	10	40	60	-90	220	30	-90	5	B
601	20080512211922	132.6	31.6	4.1	30	40	80	-10	132	80	-170	5	B
602	20080512212649	132.4	31.4	4	10	46	71	306	160	40	210	6	B
603	20080512213022	132.6	31.2	4	10	15	53	-106	220	40	-70	6	B
604	20080512233002	130.8	30.8	3.8	5	15	53	-106	220	40	-70	4	C
605	20080512233814	130.8	30.8	3.8	5	15	53	-106	220	40	-70	4	C
606	20080513061108	132.4	30	3.9	10	68	61	118	200	40	50	3	C
607	20080513061829	131.2	30.6	4.1	60	80	80	30	344	61	168	3	C
608	20080513120739	132.6	31	4	10	15	53	-106	220	40	-70	5	B
609	20080513121453	132.6	31.2	4.1	10	40	60	110	184	36	59	5	B
610	20080513125922	132.6	31.2	4	10	15	53	-106	220	40	-70	6	B
611	20080513130430	132.6	31.2	4.2	10	40	-70	184	36	-121	-90	7	B
612	20080513213546	132.6	31	4	10	40	60	-90	220	30	-90	5	B
613	20080514000751	132.6	31.2	4.2	10	20	50	90	200	40	90	7	B
614	20080514022200	132.6	31	3.9	10	15	53	74	220	40	110	6	B
615	20080514043430	132.8	31.4	4	20	341	48	-138	220	60	-50	5	B
616	20080514071005	132.8	31	3.8	10	40	60	90	220	30	90	4	C
617	20080514073209	132.6	31	4	10	15	53	-106	220	40	-70	6	B
618	20080514114337	133.2	31	3.9	20	15	53	74	220	40	110	5	B
619	20080514134434	132.6	30.8	4	10	40	60	90	220	30	90	7	B
620	20080514215928	132.6	30.8	4	10	40	60	90	220	30	90	7	B
621	20080515000948	132.6	31	4.2	10	40	60	-90	220	30	-90	7	B
622	20080515052038	132.6	30.8	3.9	10	15	53	-106	220	40	-70	6	B
623	20080515104819	132.6	30.8	4.2	10	40	60	-90	220	30	-90	8	A
624	20080516093623	131.8	30.6	3.5	5	60	40	-50	192	61	-118	4	C
625	20080517050355	133	31	4.1	10	260	40	-70	55	53	-106	4	C
626	20080518082705	132.4	30	4	10	80	80	-30	176	61	-168	3	C
627	20080520233517	123.4	23.8	3.8	20	260	20	-70	59	71	-97	5	B
628	20080521060205	123.6	23.6	3.8	20	276	36	121	60	60	70	8	A
629	20080521063119	129.6	27.8	3.5	10	42	80	107	160	20	30	4	C
630	20080521084529	123.6	23.6	3.9	20	276	36	121	60	60	70	9	A
631	20080521090835	123.4	23.4	3.9	50	40	80	50	298	41	165	8	A
632	20080521093213	123.4	23.6	4	40	40	80	50	298	41	165	9	A
633	20080521104911	123.4	23.4	3.9	50	40	80	50	298	41	165	9	A
634	20080521105227	123.4	23.4	3.9	50	40	80	50	298	41	165	9	A
635	20080521105500	123.4	23.6	3.9	20	300	40	-30	54	71	-126	8	A
636	20080611064111	122.8	23.4	4.1	40	60	80	30	324	61	168	7	B
637	20080626102734	124.2	24.8	3.5	10	236	61	12	140	80	150	4	C
638	20080627071123	125.2	23.8	4	20	40	60	90	220	30	90	6	B
639	20080627073005	125.4	23.8	4	30	12	61	62	240	40	130	9	A
640	20080627111525	124.4	23.6	3.8	20	40	50	90	220	40	90	4	C
641	20080627112837	124.2	23.8	3.7	20	240	30	-90	60	60	-90	4	C
642	20080701010637	125.2	23.8	3.9	30	260	40	150	14	71	54	8	A
643	20080714075539	126.2	24.8	3.9	20	299	48	318	60	60	230	5	B
644	20080722170624	129.8	29.0	4.2	60	200	80	30	104	61	168	4	C
645	20080804041659	130.2	28.8	4	5	76	61	12	340	80	150	4	C
646	20080813034906	127.8	25.4	4.1	30	20	80	190	288	80	350	6	B
647	20080813041610	127.8	25.4	3.9	30	20	60	210	284	61	348	7	B
648	20080901171242	125.2	23.8	4.1	30	260	40	150	14	71	54	9	A
649	20080901192611	125.2	23.8	4	20	40	60	90	220	30	90	9	A

650	20080910061233	125.2	23.8	4	20	258	41	165	0	80	50	4	C
651	20080918054810	128.2	25.4	3.8	10	215	53	74	60	40	110	9	A
652	20080918180550	128.2	25.4	4.1	20	40	50	-90	220	40	-90	5	B
653	20080918183039	128.4	25.4	4	10	56	36	121	200	60	70	7	B
654	20080918192703	128.0	25.6	4	30	15	81	30	280	60	170	6	B
655	20080918194931	128.2	25.4	4	20	259	48	318	20	60	230	7	B
656	20080918203958	128.2	25.4	3.8	20	215	53	74	60	40	110	6	B
657	20080919020459	126.4	24.8	4	20	299	48	318	60	60	230	5	B
658	20080923210535	127.8	25.2	4.1	30	32	80	-170	300	80	-10	4	C
659	20080923211220	128.0	25.4	4	10	215	53	-106	60	40	-70	6	B
660	20080923220818	128.2	25.2	4	20	200	60	30	104	61	168	5	B
661	20080924001929	128.2	25.4	3.9	20	215	53	-106	60	40	-70	5	B
662	20080924003504	128.0	25.4	4.1	20	26	64	-146	280	60	-30	6	B
663	20080924004106	128.0	25.2	4.2	10	212	61	62	80	40	130	7	B
664	20080924005419	128.2	25.2	3.8	10	194	71	54	80	40	150	6	B
665	20081016110312	123.8	23.6	3.7	20	280	40	130	52	61	62	7	B
666	20081016113233	123.6	23.4	4.4	50	200	80	-30	296	61	-168	9	A
667	20081020164607	125.2	23.8	4.1	30	260	40	150	14	71	54	8	A
668	20081022162629	124.2	23.8	3.7	20	240	30	90	60	60	90	7	B
669	20081031174628	128.0	25.2	4.3	10	220	60	70	76	36	121	7	B
670	20081101163959	124.4	23.4	3.5	10	206	64	-146	100	60	-30	3	C
671	20081113183426	132.0	27.8	4.1	20	40	80	30	304	61	168	4	C
672	20081114003916	130.2	28.0	3.9	30	40	60	150	146	64	34	5	B
673	20081114004740	130.2	28.0	4.1	30	40	60	150	146	64	34	5	B
674	20081115062404	129.6	27.8	3.5	10	42	75	103	180	20	50	6	B
675	20081116151213	132.0	27.8	3.7	10	40	80	30	304	61	168	5	B
676	20081120094842	129.6	27.8	3.9	10	21	71	277	180	20	250	4	C
677	20081120095140	129.6	27.8	3.4	20	46	71	126	160	40	30	4	C
678	20081120154642	129.8	28.0	3.4	20	14	64	326	120	60	210	3	C
679	20081120155109	130.4	28.0	4	40	40	60	-30	146	64	-146	4	C
680	20081125113016	130.2	28.0	3.6	30	40	60	130	161	48	42	7	B
681	20081125113920	130.0	28.0	3.7	20	26	71	306	140	40	210	6	B
682	20081202195921	127.8	25.2	3.9	30	20	80	190	288	80	350	7	B
683	20081203181530	128.0	25.2	4.1	10	212	61	62	80	40	130	8	A
684	20081203185052	128.0	25.2	4.2	30	200	80	30	104	61	168	7	B
685	20081203190438	128.0	25.2	4.1	20	200	80	230	98	41	345	4	C
686	20081209131015	125.2	23.8	4.1	20	40	60	90	220	30	90	9	A
687	20081209131841	125.4	23.8	4.1	30	12	61	62	240	40	130	9	A
688	20081209134558	125.2	23.8	4	20	240	20	110	39	71	83	6	B
689	20081211154016	128.4	25.4	4	10	56	36	121	200	60	70	4	C
690	20081211154230	128.0	25.6	3.7	40	20	80	30	284	61	168	3	C
691	20081211160314	128.2	25.4	3.8	20	245	53	106	40	40	70	5	B
692	20081212104511	128.0	25.4	4	50	20	80	30	284	61	168	7	B
693	20081212204957	128.0	25.2	3.9	10	220	60	250	76	36	301	7	B
694	20081227035623	124.4	23.6	3.7	20	240	40	110	35	83	74	6	B
695	20090112164550	131.5	30.5	4.3	30	280	40	150	34	71	54	3	C
696	20090112165729	130.0	29.5	4.2	20	182	84	130	280	40	10	4	C
697	20090113004205	130.0	29.0	4.3	40	280	20	170	19	87	70	4	C
698	20090113035342	130.5	29.0	3.8	10	240	80	190	148	80	350	5	B
699	20090113080759	130.0	29.0	3.9	20	300	20	190	201	87	290	3	C
700	20090113161037	129.0	28.5	3.6	5	199	87	-110	100	20	-10	4	C
701	20090113170633	129.0	27.0	3.8	10	240	40	-70	35	53	-106	4	C
702	20090114174322	131.6	30.0	3.9	20	215	53	74	60	40	110	4	C
703	20090115040228	129.0	27.0	3.8	10	40	50	-90	220	40	-90	4	C
704	20090125212556	123.0	23.6	3.7	50	60	80	50	318	41	165	8	A
705	20090125234017	123.0	23.6	3.7	40	58	84	50	320	40	170	8	A
706	20090126000736	123.0	23.6	3.7	40	60	80	50	318	41	165	7	B
707	20090126003739	123.0	23.6	3.8	40	60	80	230	318	41	345	4	C
708	20090126013658	122.8	23.4	3.9	40	60	80	30	324	61	168	7	B
709	20090126101620	123.0	23.6	3.7	40	58	84	50	320	40	170	8	A
710	20090126155347	125.2	23.8	4	20	260	40	150	14	71	54	9	A
711	20090126160213	125.4	23.8	4.1	30	12	61	62	240	40	130	9	A
712	20090128151800	128.2	25.4	3.6	10	215	53	-106	60	40	-70	4	C
713	20090128160519	123.6	23.4	4.5	40	200	80	-30	296	61	-168	9	A
714	20090129060224	128.2	25.4	3.9	10	240	50	90	60	40	90	4	C
715	20090201210123	128.0	25.2	4	10	212	61	-118	80	40	-50	5	B
716	20090201232129	128.0	25.2	4	30	195	81	30	100	60	170	8	A
717	20090202030210	128.2	25.4	4	20	215	53	74	60	40	110	4	C
718	20090203063859	128.2	25.4	3.8	10	240	40	90	60	50	90	6	B
719	20090301065539	127.8	25.4	3.8	20	20	80	190	288	80	350	5	B
720	20090303224203	128.0	25.2	3.6	10	212	61	-118	80	40	-50	5	B
721	20090304070254	128.0	25.2	3.9	10	212	61	-118	80	40	-50	6	B
722	20090313075448	123.8	23.4	4	30	20	80	30	284	61	168	8	A
723	20090316072730	126.2	24.8	4.4	10	260	20	130	38	75	77	3	C
724	20090316121601	126.4	24.8	4	40	60	80	10	328	80	170	3	C
725	20090325144410	127.2	26.6	4.2	40	240	80	-10	332	80	-170	3	C
726	20090331090046	125.4	23.8	4.1	20	20	60	70	236	36	121	9	A
727	20090331090645	125.4	23.8	4	20	258	41	165	0	80	50	8	A
728	20090331092229	125.4	23.8	3.9	30	12	61	62	240	40	130	9	A
729	20090406213236	132.6	32.2	4.4	20	200	80	150	296	61	12	8	A
730	20090406213910	132.6	32.2	4.3	30	200	80	150	296	61	12	5	B
731	20090406214320	132.8	32.2	4.2	20	194	64	326	300	60	210	5	B

732	20090407004243	132.6	32.2	4	20	200	80	150	296	61	12	7	B
733	20090407024106	132.8	32.2	3.8	20	200	80	-30	296	61	-168	7	B
734	20090409122444	130.0	28.5	3.4	20	199	87	-110	100	20	-10	5	B
735	20090412185139	126.0	24.6	3.9	50	60	80	10	328	80	170	3	C
736	20090414135511	123.8	23.4	3.8	20	279	48	138	40	60	50	6	B
737	20090416004234	123.4	23.6	4	50	38	84	50	300	40	170	9	A
738	20090423035622	128.2	25.4	3.7	10	40	40	90	220	50	90	6	B
739	20090426162459	129.5	27.5	3.7	20	260	30	90	80	60	90	5	B
740	20090427043730	131.5	28.0	3.4	40	40	80	30	304	61	168	3	C
741	20090427054906	130.0	28.0	3.7	30	26	71	126	140	40	30	4	C
742	20090428053605	130.0	28.0	3.6	40	22	84	310	120	40	190	5	B
743	20090428073345	124.4	23.6	3.5	20	220	40	70	65	53	106	5	B
744	20090428074149	124.4	23.6	3.7	20	200	40	70	65	53	106	7	B
745	20090428105146	124.2	23.8	3.7	20	240	30	-90	60	60	-90	7	B
746	20090428110300	124.4	23.6	3.9	20	40	50	90	220	40	90	9	A
747	20090430082416	124.4	23.8	3.7	20	260	20	130	38	75	77	6	B
748	20090501042610	129.0	28.5	3.7	40	268	80	170	0	80	10	5	B
749	20090505024550	132.5	28.0	3.8	5	280	20	130	58	75	77	4	C
750	20090505140412	129.5	27.5	3.5	10	240	20	90	60	70	90	5	B
751	20090507031118	128.0	25.4	4.2	10	215	53	74	60	40	110	7	B
752	20090507031755	128.0	25.4	4	10	215	53	-106	60	40	-70	6	B
753	20090507042928	128.0	25.2	3.9	10	220	60	70	76	36	121	3	C
754	20090507154513	128.2	25.4	3.9	20	240	40	110	35	53	74	6	B
755	20090507164241	128.2	25.4	3.9	20	259	48	138	20	60	50	5	B
756	20090508011423	128.0	25.4	4	30	15	81	30	280	60	170	4	C
757	20090508011853	128.0	25.4	4.1	30	12	80	10	280	80	170	5	B
758	20090508014920	128.2	25.6	4	20	240	40	110	35	53	74	5	B
759	20090515153432	122.8	23.6	3.9	30	60	80	30	324	61	168	5	B
760	20090515170806	122.8	23.4	3.7	40	60	80	30	324	61	168	8	A
761	20090521163404	129.0	27.0	3.7	10	240	40	-70	35	53	-106	6	B
762	20090521165505	129.0	27.0	3.8	10	240	40	-70	35	53	-106	6	B
763	20090521200456	129.0	27.0	3.6	10	240	40	-70	35	53	-106	5	B
764	20090522025156	128.0	25.2	3.7	10	212	61	62	60	40	130	6	B
765	20090610153050	125.6	22.6	4.3	40	320	60	-90	140	30	-90	3	C
766	20090614014230	129.2	26.8	3.5	20	40	60	110	184	36	59	7	B
767	20090629204927	124.4	23.6	3.7	20	40	50	90	220	40	90	7	B
768	20090629205304	124.4	23.6	3.6	20	220	40	70	65	53	106	7	B
769	20090629210700	124.0	23.4	3.7	20	215	53	74	60	40	110	4	C
770	20090629211606	124.2	23.8	3.7	20	240	30	90	60	60	90	6	B
771	20090629213021	124.2	23.8	3.8	20	240	30	-90	60	60	-90	7	B
772	20090629222521	124.2	23.8	3.8	30	320	20	10	221	87	110	8	A
773	20090629223352	124.2	23.8	3.6	30	320	20	10	221	87	110	8	A
774	20090629223809	124.4	23.6	3.6	20	240	40	90	60	50	90	6	B
775	20090701174853	126.4	24.8	3.7	20	298	48	138	60	60	50	5	B
776	20090702001213	128.0	25.4	3.9	10	215	53	-106	60	40	-70	6	B
777	20090702012456	128.0	25.2	3.8	10	212	61	62	80	40	130	5	B
778	20090703030320	124.4	23.8	3.5	20	300	20	10	201	87	110	5	B
779	20090711050335	125.4	23.8	4	20	12	61	62	240	40	130	8	A
780	20090711051533	125.4	23.8	4	20	12	61	62	240	40	130	8	A
781	20090716144536	125.2	24.0	4.2	10	360	80	250	244	22	333	8	A
782	20090723155628	128.0	25.6	3.7	10	220	40	70	65	53	106	5	B
783	20090723162426	128.2	25.4	3.8	10	200	60	230	79	48	318	8	A
784	20090723163026	128.2	25.4	3.8	20	200	60	230	79	48	318	4	C
785	20090723164238	128.2	25.6	3.9	20	260	40	130	32	61	62	5	B
786	20090723173621	128.0	25.6	3.7	20	260	40	-50	32	61	-118	7	B
787	20090723182519	128.2	25.4	3.7	20	215	53	74	60	40	110	6	B
788	20090723194535	128.0	25.2	3.9	30	20	80	10	288	80	170	6	B
789	20090724025201	123.0	23.6	3.9	60	300	20	130	78	75	77	7	B
790	20090724025631	123.0	23.6	3.9	60	300	20	-50	78	75	-103	6	B
791	20090724080554	128.0	25.4	3.9	10	200	60	50	79	48	138	5	B
792	20090731162054	123.0	23.6	3.7	40	58	84	-130	320	40	-10	6	B
793	20090808073447	129.0	29.0	3.8	20	261	71	277	60	20	250	3	C
794	20090811195820	130.0	30.0	4.3	5	41	87	110	140	20	10	3	C
795	20090811230921	129.5	28.5	4.4	30	280	20	-10	19	87	-110	5	B
796	20090812013510	123.2	23.6	3.8	20	299	48	138	60	60	50	6	B
797	20090812013909	123.2	23.6	3.9	30	299	48	318	60	60	230	5	B
798	20090812085340	131.0	29.5	4	5	60	60	-50	161	48	-138	4	C
799	20090812171200	130.5	29.5	4	40	20	80	210	284	61	348	5	B
800	20090813042016	125.4	23.8	4.2	20	15	53	74	220	40	110	8	A
801	20090814160602	123.2	23.6	3.8	60	222	84	130	320	40	10	7	B
802	20090814161039	123.2	23.6	3.6	60	222	84	310	320	40	190	7	B
803	20090815002049	123.2	23.6	3.9	60	304	22	153	60	80	70	7	B
804	20090815104606	124.4	23.8	3.6	20	280	20	170	19	87	70	6	B
805	20090816054336	124.2	24.0	3.4	10	300	20	-10	39	87	-110	6	B
806	20090816055755	124.8	23.4	3.9	30	260	60	150	6	64	34	8	A
807	20090817152221	123.4	23.4	3.8	50	300	40	-30	54	71	-126	7	B
808	20090817210702	123.6	23.6	3.7	20	276	36	121	60	60	70	5	B
809	20090817212345	123.6	23.6	3.5	20	276	36	301	60	60	250	7	B
810	20090818032154	123.6	23.6	3.8	20	240	30	90	60	60	90	6	B
811	20090818195559	123.4	23.4	3.8	60	300	40	150	54	71	54	7	B
812	20090820153538	123.6	23.6	3.9	20	276	36	121	60	60	70	9	A
813	20090821034912	129.0	28.5	3.4	10	2	80	287	120	20	210	5	B

814	20090907183519	125.8	22.2	4.4	50	20	20	250	221	71	277	3	C
815	20090909092230	131.5	26.5	4	5	166	0	-144	220	90	90	3	C
816	20090915024740	128.0	25.2	3.6	10	212	61	62	80	40	130	3	C
817	20090919032820	125.4	23.8	4.1	20	20	60	70	236	36	121	7	B
818	20090927210759	128.0	25.4	4	10	200	60	230	79	48	318	7	B
819	20090927214431	127.8	25.4	4	30	20	80	10	288	80	170	8	A
820	20091012184143	123.6	23.4	4.2	60	248	80	350	340	80	190	3	C
821	20091017014504	128.0	25.4	3.9	10	215	53	-106	60	40	-70	6	B
822	20091017020416	127.8	25.4	4	20	20	80	30	284	61	168	7	B
823	20091017020741	127.8	25.4	4	50	200	80	-10	292	80	-170	6	B
824	20091017104229	128.0	25.4	3.6	10	259	48	318	20	60	230	4	C
825	20091017104644	128.0	25.4	3.7	10	200	60	50	79	48	138	5	B
826	20091018021525	128.0	25.4	4	10	215	53	74	60	40	110	7	B
827	20091018035032	128.0	25.4	4	10	200	60	50	79	48	138	4	C
828	20091018151816	128.2	25.4	3.9	20	40	40	90	220	50	90	3	C
829	20091018152305	128.2	25.4	4	20	200	60	50	79	48	138	4	C
830	20091018172500	128.2	25.4	3.8	20	259	48	138	20	60	50	5	B
831	20091018183223	128.0	25.6	3.7	20	260	40	130	32	61	62	6	B
832	20091019163027	128.2	25.4	3.8	20	212	61	-118	80	40	-50	4	C
833	20091023173242	129.0	27.0	4	10	20	40	70	225	53	106	3	C
834	20091028135927	130.0	28.0	3.5	20	20	60	130	141	48	42	5	B
835	20091028144234	125.4	23.8	4.2	20	20	60	70	236	36	121	9	A
836	20091028144922	125.4	23.8	4	20	15	53	74	220	40	110	8	A
837	20091028151939	130.0	28.0	3.5	30	34	64	326	140	60	210	5	B
838	20091030184039	130.0	29.0	3.7	5	46	64	34	300	60	150	5	B
839	20091030200050	130.5	29.5	4	20	28	61	298	160	40	230	3	C
840	20091030214140	130.5	29.0	3.7	20	240	80	190	148	80	350	4	C
841	20091031014000	132.5	30.0	3.9	5	260	80	230	158	41	345	4	C
842	20091031084050	130.5	29.5	3.9	30	14	64	146	120	60	30	4	C
843	20091031100925	130.0	29.0	3.9	20	202	84	310	300	40	190	4	C
844	20091031134549	130.0	29.0	3.8	5	48	80	350	140	80	190	5	B
845	20091031234820	130.5	29.0	3.9	10	60	80	-10	152	80	-170	5	B
846	20091102142632	130.4	30.0	3.7	5	185	81	330	280	60	190	3	C
847	20091104103720	130.5	29.0	3.7	10	60	60	190	325	81	330	5	B
848	20091104133334	130.0	29.0	3.8	5	288	61	118	60	40	50	5	B
849	20091104133820	130.0	29.0	4	5	280	40	130	52	61	62	6	B
850	20091104161905	130.5	29.0	3.9	20	60	80	170	152	80	10	5	B
851	20091104163735	130.0	29.0	4.2	5	20	90	90	194	0	84	4	C
852	20091104165920	130.0	29.0	4.1	40	280	20	170	19	67	70	5	B
853	20091104173049	130.0	28.5	3.7	5	260	40	10	162	84	130	5	B
854	20091104180412	129.0	29.5	4.1	40	280	40	90	100	50	90	3	C
855	20091105003549	130.4	30.0	3.7	5	1	87	290	100	20	190	6	B
856	20091105004610	130.4	30.0	3.5	10	360	80	-50	102	41	-165	3	C
857	20091105161642	130.0	29.0	3.9	20	202	84	310	300	40	190	5	B
858	20091105163640	130.5	29.0	3.7	10	68	80	350	160	80	190	4	C
859	20091106053630	130.5	29.0	4.1	10	60	80	10	328	80	170	3	C
860	20091112065230	130.0	29.0	3.9	10	320	20	210	202	80	287	4	C
861	20091112101107	130.5	29.0	3.8	20	240	80	190	148	80	350	4	C
862	20091112103000	130.5	29.0	4	10	60	80	-10	152	80	-170	4	C
863	20091112123900	130.5	29.0	4	10	60	80	170	152	80	10	5	B
864	20091114151029	128.0	25.2	4	10	212	61	62	80	40	130	6	B
865	20091117140730	130.5	29.0	3.7	10	320	40	150	74	71	54	3	C
866	20091118021015	130.0	29.0	4.1	30	202	84	130	300	40	10	4	C
867	20091118125820	130.5	29.0	3.6	10	60	60	10	325	81	150	4	C
868	20091118130030	128.6	27.0	3.6	20	234	64	326	340	60	210	3	C
869	20091118190730	126.4	24.8	3.8	40	60	80	-10	152	80	-170	3	C
870	20091118200506	126.4	24.8	3.5	20	299	48	318	60	60	230	3	C
871	20091118214246	126.4	24.8	4	40	60	80	190	328	50	350	3	C
872	20091121120300	122.8	23.4	3.7	30	60	80	30	324	61	168	3	C
873	20091121123317	123.0	23.8	3.7	10	225	81	150	320	60	10	4	C
874	20091121132948	122.8	23.4	3.8	40	60	80	30	324	61	168	5	B
875	20091122042715	122.8	23.4	3.9	40	60	80	30	324	61	165	7	B
876	20091202032150	128.2	25.2	4	30	12	80	10	280	80	170	5	B
877	20091202183336	128.2	26.0	4	10	40	60	-90	220	30	90	3	C
878	20091205075756	128.2	25.4	4	20	215	53	74	60	40	110	3	C
879	20091205081000	128.2	25.4	3.8	20	240	40	110	35	53	74	3	C
880	20091205092239	128.2	25.4	3.9	20	215	53	74	60	40	110	3	C
881	20091205094200	128.0	25.6	3.7	20	256	36	301	40	60	250	4	C
882	20091205152652	128.2	25.4	4.1	10	215	53	74	60	40	110	5	B
883	20091206034008	128.8	26.0	3.7	10	0	60	50	239	48	138	5	B
884	20091207210723	128.2	25.4	3.6	10	221	48	42	100	60	130	6	B
885	20091207211736	128.0	25.2	3.9	10	240	50	90	60	40	90	6	B
886	20091207212032	128.0	25.4	3.6	10	240	40	110	35	53	74	4	C
887	20091207234918	128.2	25.4	3.6	10	215	53	74	60	40	110	5	B
888	20091208005820	128.2	25.4	3.7	10	212	61	62	80	40	130	5	B
889	20091208015731	128.0	25.4	4.2	20	260	40	130	32	61	62	4	C
890	20091215165756	125.4	23.8	4.1	20	18	75	77	240	20	130	7	B
891	20091215170341	125.4	23.8	4.1	20	18	75	77	240	20	130	8	A
892	20091218021910	129.0	29.0	4.1	40	240	80	70	124	22	153	3	C
893	20091218031644	129.0	29.0	4.1	40	238	84	-130	140	40	-10	4	C
894	20091220073139	123.0	23.8	3.9	50	15	81	30	280	60	170	3	C
895	20091224092730	132.5	26.0	4.1	10	0	0	90	180	90	90	3	C

896	20091224093640	131.0	28.0	4.1	30	240	20	210	122	80	287	3	C
897	20091230142059	128.0	25.5	3.9	10	212	61	-118	80	40	-50	5	B
898	20091230142410	128.0	25.2	3.7	10	220	60	250	76	36	301	5	B
899	20100101074916	127.8	25.4	3.9	40	20	80	10	288	80	170	5	B
900	20100101102429	127.8	25.4	4	30	20	80	10	288	80	170	7	B
901	20100101102653	127.8	25.4	4	30	20	80	10	288	80	170	8	A
902	20100101103550	127.8	25.4	3.7	40	200	80	-10	292	80	-170	7	B
903	20100101152500	128.0	25.4	4	10	200	60	230	79	48	318	3	C
904	20100101183000	127.8	25.2	3.8	20	32	80	10	300	80	170	3	C
905	20100106034206	124.4	23.6	3.5	20	280	40	150	34	71	54	5	B
906	20100108051250	124.4	23.6	3.7	20	256	36	121	40	60	70	7	B
907	20100108071404	124.2	23.8	3.7	20	240	30	90	60	60	90	8	A
908	20100108172022	124.2	23.8	3.6	20	240	30	-90	60	60	-90	8	A
909	20100108172850	124.2	23.8	3.7	20	240	30	-90	60	60	-90	6	B
910	20100108180723	124.2	23.8	3.4	20	260	20	130	38	75	77	6	B
911	20100108181535	124.2	23.8	3.7	20	40	60	90	220	30	90	6	B
912	20100109162121	125.2	23.8	4.1	20	40	60	90	220	30	90	8	A
913	20100111021655	124.2	23.8	3.8	20	240	30	90	60	60	90	8	A
914	20100111022636	124.2	23.8	3.8	20	240	30	-90	60	60	-90	8	A
915	20100111022946	124.4	23.6	3.7	20	40	50	90	220	40	90	6	B
916	20100112210000	123.8	23.4	4	30	35	81	30	300	60	170	4	C
917	20100119211336	131.5	23.0	4	40	180	60	150	266	54	34	3	C
918	20100125010320	132.2	30.4	3.6	10	234	64	164	340	60	30	5	B
919	20100125014912	132.2	30.4	3.7	10	234	64	326	340	60	210	5	B
920	20100125050436	132.2	30.4	3.6	10	324	64	146	340	60	30	5	B
921	20100125075717	132.6	31.2	4.1	10	20	50	-90	200	40	-90	7	B
922	20100125104050	133	31.2	4.1	20	234	64	326	340	60	210	5	B
923	20100125112224	132.6	31.2	4.1	10	40	60	-70	184	36	-121	5	B
924	20100125133530	132.8	31.0	4.1	10	15	53	-106	220	40	-70	8	A
925	20100125153717	128.0	28.5	3.6	5	192	80	-170	100	80	-10	4	C
926	20100126014043	132.4	31.8	3.9	30	28	80	170	120	80	10	7	B
927	20100126030230	132	30.4	3.6	10	234	64	326	340	60	210	5	B
928	20100126054730	132.8	31.0	3.9	10	41	71	97	200	20	70	4	C
929	20100126080217	132.8	31.0	3.8	10	15	53	-106	220	40	-70	7	B
930	20100126090140	134	31.4	4	5	320	50	90	140	40	90	3	C
931	20100126090750	132.8	31.0	3.9	10	40	60	-90	220	30	-90	7	B
932	20100126091720	134	31.4	3.8	5	320	60	90	140	30	90	4	C
933	20100126095000	132.8	31.2	3.9	10	40	50	-90	220	40	-90	8	A
934	20100126123640	132.6	31.0	3.8	10	15	53	-106	220	40	-70	7	B
935	20100126144820	132.2	31.0	3.9	5	345	53	286	140	40	250	4	C
936	20100126154542	132.8	31.0	3.6	10	15	53	74	220	40	110	8	B
937	20100126154820	132.6	31.0	3.8	10	15	53	74	220	40	110	7	B
938	20100126200230	133.8	31.6	4.2	60	62	75	103	200	20	50	4	C
939	20100126201112	131	30.4	4	50	280	40	-70	75	53	-106	3	C
940	20100126205320	133	31.2	3.7	20	40	60	-70	184	36	-121	4	C
941	20100126210550	133.2	31.0	3.9	20	48	61	118	180	40	50	4	C
942	20100127001410	134	31.0	3.9	60	60	60	110	204	36	59	4	C
943	20100127002320	133	31.0	3.7	20	40	60	90	220	30	90	5	B
944	20100127004348	132.8	31.0	4	10	20	60	90	200	30	90	6	B
945	20100127011623	132.6	30.8	3.8	10	40	60	90	220	30	90	6	B
946	20100127061500	133	31.8	3.5	20	220	80	-30	316	61	-168	4	C
947	20100127093640	133	31.8	4.1	20	220	80	150	316	61	12	6	B
948	20100127100550	133	31.2	4	10	48	61	118	180	40	50	4	C
949	20100127122109	132.2	30.2	4.3	10	68	80	350	160	80	190	3	C
950	20100127151640	132.2	32.4	4.1	30	8	80	350	100	80	190	5	B
951	20100127232910	132.2	32.2	4.2	40	12	80	10	280	60	170	5	B
952	20100128023449	132.6	32.2	4.2	20	200	80	150	296	61	12	5	B
953	20100128053714	132.6	32.2	3.9	10	344	36	59	200	50	110	5	B
954	20100128170457	132.2	32.6	4.1	20	360	80	-30	96	61	-168	5	B
955	20100128235418	124.2	23.8	3.6	20	240	30	-90	60	60	-90	7	B
956	20100129000439	124.4	23.6	3.7	20	260	40	130	32	61	62	6	B
957	20100129014717	124.4	23.6	3.9	20	40	50	90	220	40	90	6	B
958	20100129015139	124.4	23.6	3.8	20	240	40	-70	35	53	-106	7	B
959	20100129022155	133.2	31.2	4.2	10	40	50	-90	220	40	-90	5	B
960	20100129033848	124.4	23.6	3.9	20	240	40	110	35	53	74	7	B
961	20100129034115	124.2	23.8	3.7	20	260	20	-50	38	75	-103	5	B
962	20100129034345	124.4	23.6	3.9	20	240	40	-70	35	53	-106	7	B
963	20100129040233	132.6	32.6	3.9	20	320	40	50	188	61	118	4	C
964	20100129125820	132.2	32.8	3.8	20	354	64	326	100	60	210	4	C
965	20100129130550	132.2	32.6	4	40	8	80	350	100	80	190	6	B
966	20100129131657	133	31.2	3.9	10	40	50	-90	220	40	-90	4	C
967	20100129161540	132.6	32.4	4	10	20	50	-90	200	40	-90	4	C
968	20100129172526	132.2	32.6	3.9	20	6	71	306	120	40	210	5	B
969	20100129174730	132.8	32.4	3.9	10	20	50	90	200	40	90	5	B
970	20100130011745	131.6	30.8	3.8	40	340	40	90	160	50	90	4	C
971	20100130130050	132.6	31.2	4	10	0	60	70	216	36	121	5	B
972	20100130164616	132.6	31.2	4.1	10	40	50	-90	220	40	-90	5	B
973	20100131000704	131.8	30.6	3.7	40	300	40	250	145	53	286	5	B
974	20100131034622	132.2	32.6	4.1	20	360	80	150	96	61	12	5	B
975	20100131113820	132.4	32.6	3.8	30	8	80	170	100	80	10	4	C
976	20100131142623	133.2	31.2	4.1	10	240	50	-90	60	40	-90	4	C
977	20100201172801	133.2	31.4	4.6	5	240	40	250	85	53	286	5	B

978	20100201173610	132.8	31.2	4.1	10	15	53	-106	220	40	-70	6	B
979	20100202104140	132.4	32.6	4.4	30	8	80	350	100	80	190	5	B
980	20100202140308	131.8	30.6	3.6	5	215	53	74	60	40	110	6	B
981	20100203045000	132.6	32.8	4.2	20	180	80	150	276	61	12	4	C
982	20100203104440	132.6	32.0	4.1	30	28	80	170	120	80	10	6	B
983	20100203152500	132.6	31.6	3.8	20	220	80	-30	316	61	-168	5	B
984	20100203170639	132.2	32.6	4.2	20	360	80	170	92	80	10	4	C
985	20100203204453	134	31.6	3.8	5	305	53	106	100	40	70	4	C
986	20100203205000	132.8	31.0	4	10	256	36	121	40	60	70	4	C
987	20100204074500	133.2	30.0	3.9	20	68	80	350	168	80	190	4	C
988	20100204162708	132.2	30.0	3.8	5	74	64	326	180	60	210	4	C
989	20100205001434	132.2	30.4	3.8	10	234	64	146	340	60	30	5	B
990	20100205002739	132.4	32.4	4	60	20	80	130	122	41	18	4	C
991	20100206010320	130.4	30.4	3.1	40	239	87	70	140	20	170	3	C
992	20100206120342	132.8	31.0	3.8	10	240	40	-70	35	53	-106	7	B
993	20100206132640	132.8	31.0	3.9	10	15	53	-106	220	40	-70	7	B
994	20100206144617	132.6	31.2	4.1	10	20	50	-90	200	40	-90	9	A
995	20100206172246	132.6	31.4	3.7	10	20	50	-90	200	40	-90	8	A
996	20100207042703	130.8	30.8	4.1	5	15	53	-106	220	40	-70	6	B
997	20100207044734	130.8	30.8	3.6	5	15	53	74	220	40	110	4	C
998	20100207103224	123.8	23.6	3.7	20	276	36	121	60	60	70	5	B
999	20100207115439	125.4	23.8	4	30	12	61	62	240	40	130	9	A
1000	20100208103434	122.8	23.4	3.8	40	60	80	30	324	61	168	6	B
1001	20100208133023	123.6	23.4	3.7	30	279	48	138	40	60	50	7	B
1002	20100208152226	131	30.8	3.8	50	240	60	150	346	64	34	3	C
1003	20100208154910	123.6	23.6	4	20	276	36	121	60	60	70	8	A
1004	20100208162238	123.6	23.6	3.6	20	260	30	60	80	60	90	4	C
1005	20100208170412	123.6	23.6	3.9	20	276	36	121	60	60	70	9	A
1006	20100208171121	123.6	23.6	3.8	20	276	36	121	60	60	70	8	A
1007	20100208183903	130.8	30.8	3.7	5	15	53	-106	220	40	-70	3	C
1008	20100209061550	132.6	32.6	3.9	20	8	61	118	140	40	50	4	C
1009	20100211162016	132.2	30.6	3.9	60	75	81	30	340	60	170	4	C
1010	20100211164015	130.8	30.8	3.8	60	260	40	-10	-368	84	-130	4	C
1011	20100211172110	132.6	32.6	4.2	30	8	80	170	100	80	10	4	C
1012	20100211172614	132.2	32.8	4.2	40	360	80	170	92	80	10	3	C
1013	20100211173240	132.8	32.2	4.2	5	256	36	301	40	60	250	3	C
1014	20100212063542	132.6	31.6	4	20	40	60	-30	136	61	-166	6	B
1015	20100212071119	132.8	31.4	3.9	20	228	80	350	320	80	190	6	B
1016	20100212144730	132.8	32.2	3.9	20	321	48	-138	200	60	-50	7	B
1017	20100212193035	133.2	33.0	3.8	5	200	80	130	302	41	15	4	C
1018	20100212204512	131.8	31.8	3.7	5	58	84	50	320	40	170	3	C
1019	20100214004040	129.0	28.0	3.7	30	360	20	50	222	75	103	5	B
1020	20100215052353	131.8	30.0	3.5	10	39	48	318	160	60	230	4	C
1021	20100215052912	130.2	30.6	3.6	50	188	80	170	280	80	10	4	C
1022	20100217015730	132.8	32.4	3.7	30	28	80	350	120	80	190	4	C
1023	20100217021820	132.6	32.6	3.9	20	8	61	118	140	40	50	4	C
1024	20100219083440	130.2	30.6	4	50	188	80	350	280	80	190	5	B
1025	20100219112518	130	31.0	3.9	60	20	60	-90	200	30	-90	3	C
1026	20100221194959	129.0	27.0	3.6	10	40	50	90	220	40	90	8	A
1027	20100222110640	132.8	32.4	3.9	30	20	80	-10	112	80	-170	5	B
1028	20100223220453	124.4	23.6	3.5	20	260	40	-70	55	53	-106	6	B
1029	20100225105142	132.2	32.6	4.1	30	360	80	-10	92	80	-170	4	C
1030	20100225181140	130.5	29.5	4	40	20	60	-30	126	64	-146	5	B
1031	20100225183535	130.5	29.5	4.1	40	12	80	-170	280	80	-10	6	B
1032	20100225202500	132.0	31.0	4.5	30	42	75	103	180	20	50	3	C
1033	20100228051000	133.2	31.2	3.9	10	40	40	90	220	50	90	4	C
1034	20100228073039	132.6	31.2	3.9	10	40	60	90	220	30	90	5	B
1035	20100228095614	132.8	31.0	4.1	10	40	60	-90	220	30	-90	5	B
1036	20100228163546	132.6	31.0	4	10	15	53	-106	220	40	-70	8	A
1037	20100301172930	133	32.8	4	10	8	80	170	100	80	10	6	B
1038	20100301181910	132.4	32.6	3.8	30	8	80	350	100	80	190	5	B
1039	20100316135820	132.6	32.4	4.2	30	20	80	150	116	61	12	6	B
1040	20100316160033	132.4	32.6	3.9	30	8	80	170	100	80	10	6	B
1041	20100318022522	132.4	32.4	4.1	10	20	60	-90	200	30	-90	5	B
1042	20100318023700	131.4	32.8	4	20	76	61	-168	340	80	-30	4	C
1043	20100318032500	132.4	32.6	4.2	10	20	60	90	200	30	90	3	C
1044	20100318081758	132.2	32.6	4.3	20	360	80	150	96	61	12	6	B
1045	20100318164233	132.4	32.2	4.1	10	20	60	-70	164	36	-121	6	B
1046	20100318164410	132.6	32.2	4.2	20	200	80	150	296	61	12	8	A
1047	20100318201741	132.6	32.0	3.8	20	208	80	350	300	80	190	7	B
1048	20100318203910	132.4	32.0	3.7	10	26	71	126	140	40	30	8	A
1049	20100318210537	132.4	32.4	4	20	320	40	50	188	61	118	5	B
1050	20100319161754	132.4	32.0	4.1	10	28	61	298	160	40	230	5	B
1051	20100319162633	132.6	32.2	4.3	20	200	80	150	296	61	12	7	B
1052	20100319165029	132.4	32.2	4.3	30	20	80	-10	112	80	-170	6	B
1053	20100321043000	132.6	32.0	4.2	30	28	80	350	120	80	190	7	B
1054	20100321183230	133.6	31.0	4.1	5	280	20	-70	79	71	-97	4	C
1055	20100322021033	132.6	32.6	4.1	30	8	80	350	100	80	190	5	B
1056	20100504091050	127.0	24.4	4	5	300	20	30	182	80	107	3	C
1057	20100504092715	127.8	25.4	3.8	10	20	80	50	278	41	165	4	C
1058	20100504095516	127.8	25.4	3.8	20	20	80	10	288	80	170	5	B
1059	20100507221807	126.4	24.8	3.7	30	60	80	10	328	80	170	5	B

1060	20100507223550	127.0	25.8	3.8	5	214	64	146	320	60	30	4	C
1061	20100508215757	129.5	28.0	3.5	5	280	40	250	125	53	286	7	B
1062	20100508221609	130.0	28.0	3.8	30	34	64	326	140	60	210	7	B
1063	20100512172508	128.2	25.4	3.9	40	12	80	-170	280	80	-10	6	B
1064	20100514031526	129.0	28.5	3.8	10	220	60	10	125	81	150	5	B
1065	20100514065226	129.5	28.5	3.8	20	40	20	90	220	70	90	6	B
1066	20100521053230	123.0	23.6	3.7	40	58	84	-130	320	40	-10	7	B
1067	20100521094803	123.0	23.6	3.6	40	60	80	50	318	41	165	8	A
1068	20100521095534	123.0	23.6	3.6	40	60	80	50	318	41	165	8	A
1069	20100521131049	123.0	23.6	3.7	40	58	84	50	320	40	170	8	A
1070	20100521131539	123.0	23.6	3.7	40	58	84	50	320	40	170	9	A
1071	20100521131852	123.0	23.6	3.5	40	225	81	330	320	60	190	7	B
1072	20100523222500	122.6	22.0	4.3	20	320	60	230	199	48	318	3	C
1073	20100607034000	126.8	24.8	3.9	10	245	53	286	40	40	250	3	C
1074	20100607035910	127.0	24.4	4.1	5	16	61	-168	280	80	-30	3	C
1075	20100611040439	122.8	23.8	3.9	5	340	40	210	226	71	306	7	B
1076	20100611041803	122.8	23.4	3.8	40	60	80	30	324	61	168	6	B
1077	20100611043042	122.8	23.4	3.8	40	60	80	30	324	61	168	8	A
1078	20100611044717	122.8	23.4	4	40	60	80	210	324	61	348	9	A
1079	20100611051516	122.8	23.4	3.7	40	60	80	30	324	61	168	9	A
1080	20100618081554	128.0	25.2	4.2	20	200	80	30	104	61	168	8	A
1081	20100618102205	127.2	24.8	4.1	5	300	20	190	201	87	290	3	C
1082	20100618112204	128.0	25.4	4	20	200	80	10	108	80	170	4	C
1083	20100618193500	127.8	25.2	4	40	32	80	10	300	80	170	3	C
1084	20100618194410	127.6	25.8	3.9	5	318	75	77	180	20	130	3	C
1085	20100620115003	127.8	25.4	3.8	40	32	80	10	300	80	170	5	B
1086	20100622075558	123.4	24.6	3.9	20	260	80	230	158	41	345	3	C
1087	20100623023524	128.0	25.8	3.9	10	40	60	90	220	30	90	5	B
1088	20100623111909	125.4	23.8	4.1	30	240	40	110	35	53	74	9	A
1089	20100623235256	128.0	25.8	3.6	20	40	60	-90	220	30	-90	5	B
1090	20100624012152	128.0	25.8	4	10	220	40	250	65	53	286	5	B
1091	20100624020353	128.0	25.4	4.1	40	12	80	10	280	80	170	4	C
1092	20100625043443	130.0	28.0	3.6	30	40	60	150	146	64	34	5	B
1093	20100625043730	129.0	29.5	3.9	20	320	50	90	140	40	90	3	C
1094	20100626133515	130.0	28.0	3.5	20	20	60	130	141	48	42	7	B
1095	20100626135555	130.0	28.0	3.5	20	40	60	-50	161	48	-138	8	A
1096	20100626170520	131.5	28.5	4.1	5	62	80	107	180	20	30	7	B
1097	20100627053504	125.4	23.8	4.2	30	12	61	62	240	40	130	9	A
1098	20100627054035	125.2	23.8	3.9	20	40	60	90	220	30	90	8	A
1099	20100628061914	130.0	28.0	3.8	30	34	64	326	140	60	210	5	B
1100	20100719234843	122.8	22.8	3.9	50	320	80	90	140	10	90	3	C
1101	20100721043032	123.2	23.4	3.9	20	299	48	318	60	60	230	6	B
1102	20100722023044	128.0	25.2	3.9	30	12	80	10	280	80	170	4	C
1103	20100722023549	122.8	23.6	3.7	40	58	84	50	320	40	170	8	A
1104	20100723193517	122.8	23.6	3.9	40	240	80	150	336	61	12	4	C
1105	20100723194140	123.0	23.6	3.6	20	300	40	150	57	71	54	5	B
1106	20100725081000	123.0	22.6	4	40	88	80	170	180	80	10	4	C
1107	20100725082320	123.6	22.2	4	20	280	30	-90	100	60	-90	3	C
1108	20100726231224	123.6	22.4	4.3	20	244	36	59	100	60	110	3	C
1109	20100728182002	125.0	24.0	3.9	10	240	20	110	39	71	83	9	A
1110	20100728191239	125.0	24.0	3.9	10	240	20	110	39	71	83	9	A
1111	20100729062014	125.2	23.8	3.9	20	260	40	150	14	71	54	8	A
1112	20100823045230	123.4	23.8	3.5	20	280	40	50	148	61	118	3	C
1113	20100826141019	130.0	29.0	4.3	20	260	20	-30	18	80	-107	4	C
1114	20100826214921	130.5	29.0	4.1	5	68	80	350	160	80	190	4	C
1115	20100826234918	130.5	29.0	3.9	5	64	61	168	160	80	30	5	B
1116	20100827015134	130.5	29.0	4	10	60	80	170	152	80	10	4	C
1117	20100827053303	130.0	29.0	4.2	5	20	90	90	194	0	84	4	C
1118	20100828030140	130.5	29.0	3.7	5	58	41	345	160	80	230	4	C
1119	20100828151656	129.5	29.5	4.1	10	360	20	-70	159	71	-97	4	C
1120	20100828152603	130.0	29.0	4.1	40	18	75	77	240	20	130	5	B
1121	20100828184820	129.0	29.0	3.7	20	266	71	126	20	40	30	3	C
1122	20100829141136	130.0	29.0	3.9	40	2	84	310	100	40	190	6	B
1123	20100829163530	128.0	25.4	4.1	10	200	60	230	79	48	318	8	A
1124	20100829163901	128.0	25.4	3.8	20	200	60	50	79	48	318	6	B
1125	20100829165820	128.0	25.2	3.6	10	195	81	30	100	60	170	5	B
1126	20100829180335	127.8	25.4	3.9	40	20	80	30	284	61	168	5	B
1127	20100829181850	128.0	25.2	3.9	30	20	80	10	288	80	170	7	B
1128	20100829222219	130.5	29.0	3.9	5	58	41	345	160	80	230	6	B
1129	20100829234932	130.5	29.0	4	5	64	61	168	160	80	30	6	B
1130	20100918042037	125.0	24.0	4	10	18	75	77	240	20	130	7	B
1131	20100919032220	127.8	25.2	4	30	32	80	10	300	80	170	4	C
1132	20100924015851	122.4	24.4	4.1	20	260	60	50	139	48	138	8	A
1133	20100926180755	128.0	25.8	3.9	20	220	40	70	65	53	106	7	B
1134	20100926181110	128.2	25.4	4	30	192	80	10	100	80	170	4	C
1135	20100927064629	128.0	25.6	3.8	20	206	64	34	100	60	150	5	B
1136	20100927075500	127.0	24.4	4	5	260	40	-30	14	71	-126	3	C
1137	20100927111000	131.0	28.0	3.9	5	259	71	-97	100	20	-70	4	C
1138	20100928093316	128.0	25.4	3.8	20	200	60	230	79	48	318	4	C
1139	20100928094305	127.8	25.6	4	20	260	40	-70	55	53	-106	5	B
1140	20101008151315	123.4	23.4	4	60	40	80	230	298	41	345	7	B
1141	20101008163910	123.6	23.6	4.6	40	38	84	50	300	40	170	9	A

1142	20101008170007	123.6	23.4	4	50	40	80	50	298	41	165	7	B
1143	20101008171236	123.4	23.4	4	50	40	80	50	298	41	165	8	A
1144	20101008171836	124.4	24.4	4	20	20	40	160	282	84	310	4	C
1145	20101008175039	123.4	23.4	4	50	40	80	50	298	41	165	8	A
1146	20101008181217	123.4	23.6	3.9	50	40	80	50	298	41	165	7	B
1147	20101008200612	123.4	23.4	4.2	50	40	80	50	298	41	165	9	A
1148	20101008201418	123.6	23.6	3.8	40	284	22	153	40	80	70	9	A
1149	20101009043204	123.6	23.6	3.8	20	276	36	121	60	60	70	7	B
1150	20101009063614	123.6	23.6	3.7	20	276	36	301	60	60	250	4	C
1151	20101009065115	123.6	23.0	4.1	50	220	60	30	114	64	146	4	C
1152	20101031112906	129.0	29.0	4	20	260	60	90	80	30	90	4	C
1153	20101106135307	129.0	27.0	3.5	5	260	80	170	352	80	10	4	C
1154	20101106154758	132.6	31.4	4.3	60	46	81	330	140	60	190	5	B
1155	20101106160140	132.4	30.0	3.6	10	74	64	326	180	60	210	3	C
1156	20101106160956	130.8	30.8	3.6	5	15	53	74	220	40	110	4	C
1157	20101107140412	130.5	27.5	3.5	10	45	53	106	200	40	70	6	B
1158	20101107141314	130.5	27.5	3.5	10	45	53	106	200	40	70	7	B
1159	20101107162044	129.0	27.0	3.8	10	40	50	-90	220	40	-90	5	B
1160	20101110180140	125.5	27.0	3.7	10	200	80	170	292	80	10	3	C
1161	20101110185026	129.0	27.0	3.9	10	40	50	90	220	40	90	5	B
1162	20101110185500	125.5	27.0	3.8	10	20	80	-10	112	80	-170	3	C
1163	20101117154808	127.8	26.4	4.1	40	239	87	70	140	20	170	4	C
1164	20101128062134	130.0	28.0	3.9	40	40	80	170	132	80	10	5	B
1165	20101128062440	130.5	27.5	3.8	10	45	53	286	200	40	250	4	C
1166	20101128063009	130.5	27.5	3.8	10	45	53	286	200	40	250	5	B
1167	20101128064120	130.5	27.5	3.7	10	60	60	110	204	36	59	5	B
1168	20101128110000	127.0	29.5	4.1	40	280	70	90	100	20	90	3	C
1169	20101129043729	129.5	27.5	3.3	20	40	60	90	220	30	90	4	C
1170	20101206051404	128.0	25.4	3.9	10	240	40	110	35	53	74	9	A
1171	20101206061706	128.0	25.2	3.9	20	12	80	-170	280	80	-10	7	B
1172	20101206065128	128.0	25.4	3.9	10	215	53	-106	60	40	-70	6	B
1173	20101206125201	128.2	25.2	3.8	10	212	61	62	80	40	130	5	B
1174	20101206141249	128.0	25.4	3.9	30	12	80	-170	280	80	-10	7	B
1175	20101209175249	128.2	25.4	3.9	20	200	60	230	79	48	318	5	B
1176	20101209180617	128.0	25.6	4	20	240	40	-90	60	50	-90	5	B
1177	20101209183932	128.0	25.6	3.8	10	240	40	90	60	50	90	8	B
1178	20101209223140	128.0	25.6	3.8	30	256	36	121	40	60	70	6	B
1179	20101212053621	125.2	23.8	4	20	260	40	150	14	71	54	6	B
1180	20101213042820	122.8	22.6	3.8	20	215	81	-150	120	60	-10	3	C
1181	20101216225230	125.2	23.8	4	20	260	40	150	14	71	54	6	B
1182	20101217141500	123.0	22.4	4.2	30	2	84	310	100	40	190	3	C
1183	20101219172320	123.0	22.8	3.8	60	192	80	-170	100	80	-10	4	C
1184	20101219173500	123.0	22.8	4	60	192	80	-170	100	80	-10	4	C
1185	20101221073657	124.4	23.6	3.8	20	240	40	-90	60	50	-90	4	C
1186	20101221074320	124.4	23.6	3.7	20	60	40	130	192	61	62	4	C
1187	20101221084948	124.2	23.8	3.7	20	240	30	90	60	60	90	7	B
1188	20101221094816	124.4	23.6	3.6	20	256	36	121	40	60	70	5	B
1189	20101221112320	124.4	23.4	3.9	20	259	48	138	20	60	50	3	C
1190	20101221165632	124.4	23.6	3.7	20	60	40	130	192	61	62	4	C
1191	20101230234443	123.0	23.6	3.8	40	58	84	50	320	40	170	4	C
1192	20110103162547	122.8	23.6	4.0	20	60	80	50	318	41	165	9	A
1193	20110108194735	131.0	29.5	4.0	20	24	61	168	120	80	30	5	B
1194	20110110131346	130.5	29.0	3.9	5	60	60	-30	166	64	-146	6	B
1195	20110110204354	131.0	29.5	3.8	20	40	60	190	305	81	330	4	C
1196	20110116090634	130.0	29.0	4.3	40	48	80	350	140	80	190	6	B
1197	20110116214926	130.0	29.5	4.2	20	296	22	27	180	80	110	7	B
1198	20110117023650	130.5	29.5	4.0	10	40	60	-30	146	64	-146	3	C
1199	20110117125415	130.0	29.0	4.3	40	260	20	150	18	80	73	5	B
1200	20110126131430	132.0	30.0	3.9	30	60	60	10	325	81	150	5	B
1201	20110206052232	125.2	23.8	4.0	30	260	40	150	14	71	54	9	A
1202	20110206053114	125.2	23.8	4.1	20	40	60	90	220	30	90	9	A
1203	20110206053720	125.2	22.6	4.2	5	40	40	190	302	84	310	8	A
1204	20110214013319	125.0	23.8	4.1	20	240	20	90	60	70	90	8	A
1205	20110214112406	128.8	25.2	4.2	10	40	40	90	220	50	90	3	C
1206	20110219010317	128.2	25.4	3.6	10	200	60	30	94	64	146	7	B
1207	20110317015510	131.8	31.0	4.0	5	340	20	90	160	70	90	4	C
1208	20110318094549	131.8	31.6	3.9	60	194	64	326	300	60	210	5	B
1209	20110319011430	133.2	31.0	4.2	20	15	53	-106	220	40	-70	6	B
1210	20110319051028	131.8	30.8	4.0	60	340	40	110	135	53	74	4	C
1211	20110319141559	132.4	32.4	4.0	20	8	80	170	100	80	10	6	B
1212	20110319142934	132.4	32.2	4.0	10	360	60	110	144	36	59	5	B
1213	20110319144925	133.0	32.2	4.1	20	194	64	326	300	60	210	7	B
1214	20110320004439	132.2	30.4	3.8	10	240	60	-30	346	64	-146	5	B
1215	20110320050519	135.2	31.2	4.2	20	1	48	-138	240	60	-50	5	B
1216	20110321005640	131.6	31.0	3.8	10	320	30	90	140	50	90	5	B
1217	20110321064856	131.8	31.0	4.2	50	336	36	121	120	60	70	6	B
1218	20110324131000	122.0	22.4	4.1	40	326	71	126	80	40	30	4	C
1219	20110324133842	122.0	22.4	4.3	40	326	71	126	80	40	30	3	C
1220	20110331052038	124.2	24.6	3.8	10	234	71	54	120	40	150	4	C
1221	20110403020544	124.0	23.8	3.9	60	62	75	103	200	20	50	3	C
1222	20110409165941	132.5	29.5	4.0	10	280	40	-70	75	53	-106	5	B
1223	20110409171708	132.5	29.5	3.9	10	280	40	110	75	53	74	7	B

1224	20110409182000	132.5	29.5	3.8	10	285	53	106	80	40	70	5	B
1225	20110409182906	132.2	30.6	3.8	10	341	48	-138	220	60	-50	6	B
1226	20110409223904	132.2	30.4	3.7	10	234	64	326	340	60	210	6	B
1227	20110410030404	132.4	30.0	3.8	10	68	61	118	200	40	50	4	C
1228	20110410031109	132.2	30.2	3.6	10	68	80	350	160	80	190	4	C
1229	20110410043848	132.0	30.5	4.0	10	234	64	326	340	60	210	7	B
1230	20110501033309	126.2	24.4	4.3	40	60	80	10	328	80	170	4	C
1231	20110507042710	124.8	24.8	4.0	30	240	80	50	138	41	165	3	C
1232	20110512101206	124.4	23.4	3.9	40	75	81	-150	340	60	-10	3	C
1233	20110512105855	124.4	23.8	3.8	10	260	20	90	80	70	90	3	C
1234	20110514042128	125.2	23.2	4.0	20	240	30	90	60	60	90	5	B
1235	20110516045816	124.4	23.4	4.0	40	80	80	230	338	41	345	3	C
1236	20110608115235	123.0	23.6	4.1	20	300	40	-30	54	71	-126	7	B
1237	20110609065940	122.8	23.4	4.0	50	60	80	30	324	61	168	5	B
1238	20110620042715	123.6	23.6	4.2	10	312	61	-118	180	40	-50	4	C
1239	20110620072050	123.6	23.6	4.3	10	194	64	326	300	60	210	6	B
1240	20110620163109	123.8	23.8	3.8	20	220	20	30	102	80	107	3	C
1241	20110629021737	128.0	25.4	3.9	10	200	60	230	79	48	318	5	B
1242	20110629022651	127.8	25.4	4.0	30	20	80	10	288	80	170	7	B
1243	20110629024754	128.0	25.4	4.2	10	200	60	50	79	48	138	8	A
1244	20110629035119	128.0	25.4	3.9	10	200	60	50	79	48	138	7	B
1245	20110629124944	128.0	25.4	4.1	20	200	60	50	79	48	138	7	B
1246	20110629130020	128.0	25.4	3.9	10	200	60	50	79	48	138	7	B
1247	20110629133009	128.2	25.4	4.0	10	200	60	230	79	48	318	8	A
1248	20110629142835	127.4	24.6	4.0	5	300	20	30	182	80	107	5	B
1249	20110630032909	128.0	25.2	4.0	20	200	80	30	104	61	168	5	B
1250	20110630184044	128.0	25.6	3.9	20	220	40	250	65	53	286	6	B
1251	20110630185810	128.0	25.4	3.5	10	200	60	50	79	48	138	8	A
1252	20110702051358	128.0	25.4	3.8	10	200	60	50	79	48	138	6	B
1253	20110702051801	128.0	25.4	3.7	10	200	60	50	79	48	138	6	B
1254	20110704154007	128.0	25.8	4.1	10	60	60	110	204	36	59	5	B
1255	20110707083852	128.2	25.2	4.1	20	212	80	-170	120	80	-10	3	C
1256	20110714021009	125.0	24.0	4.6	10	280	20	-50	58	75	-103	3	C
1257	20110714021729	124.4	25.0	4.2	10	0	20	190	261	87	290	3	C
1258	20110715041110	124.4	23.8	3.9	10	280	20	110	79	71	83	3	C
1259	20110715041930	124.4	24.0	3.9	10	260	30	90	80	60	90	3	C
1260	20110715132531	124.2	24.6	3.8	40	260	80	90	80	10	90	3	C
1261	20110727072707	124.2	24.6	3.9	10	234	71	54	120	40	150	3	C
1262	20110731041241	128.0	25.4	3.9	10	200	60	50	79	48	138	8	A
1263	20110825051208	125.0	24.0	4.3	10	260	20	-70	59	71	-97	3	C
1264	20110825052208	125.2	23.4	4.2	20	240	30	90	60	60	90	3	C
1265	20110829125421	130.5	27.5	4.0	10	25	53	286	180	40	250	6	B
1266	20110928034834	128.0	25.4	3.9	10	259	48	318	20	60	230	8	A
1267	20110928043558	128.2	25.4	4.0	10	240	50	90	60	40	90	7	B
1268	20110928044159	128.0	25.4	4.1	20	195	81	30	100	60	170	7	B
1269	20110928064745	128.0	25.2	4.0	50	20	80	190	288	80	350	7	B
1270	20110928071820	127.8	25.4	4.1	30	20	80	190	288	80	350	5	B
1271	20111012160357	125.0	23.8	4.0	20	220	20	70	61	71	97	8	A
1272	20111012161431	125.0	24.0	4.1	10	62	75	103	200	20	50	8	A
1273	20111012161940	125.0	23.8	3.9	10	240	20	90	60	70	90	8	A
1274	20111016215237	123.6	23.4	4.3	40	20	80	210	284	61	348	9	A
1275	20111016220754	123.4	23.4	3.9	40	40	80	50	298	41	165	9	A
1276	20111016224651	123.4	23.4	3.9	50	40	80	30	304	61	168	8	A
1277	20111016232933	123.4	23.6	4.0	40	40	80	230	298	41	345	9	A
1278	20111016233838	123.4	23.6	3.9	40	38	84	50	300	40	170	9	A
1279	20111016235038	123.4	23.4	4.4	50	35	81	30	300	60	170	7	B
1280	20111017000328	123.4	23.6	4.1	50	40	80	50	298	41	165	9	A
1281	20111017001511	123.4	23.4	4.0	60	40	80	50	298	41	165	9	A
1282	20111017002314	123.4	23.4	4.1	60	40	80	50	298	41	165	9	A
1283	20111017003352	123.4	23.4	4.0	50	40	80	50	298	41	165	9	A
1284	20111017015722	123.4	23.6	4.0	40	38	84	50	300	40	170	9	A
1285	20111017020656	123.4	23.4	3.9	50	40	80	230	298	41	345	7	B
1286	20111017130414	123.4	23.6	3.9	60	300	20	-10	39	87	-110	9	A
1287	20111019181343	125.0	23.8	4.0	10	240	20	90	60	70	90	9	A
1288	20111021065410	123.0	23.6	3.8	50	58	84	50	320	40	170	9	A
1289	20111021115146	123.0	23.6	3.8	30	55	81	-150	320	60	-10	9	A
1290	20111021122425	123.0	23.6	4.0	40	58	84	-130	320	40	-10	9	A
1291	20111021123050	123.0	23.6	3.8	40	58	84	50	320	40	170	9	A
1292	20111021124212	123.0	23.6	3.9	40	58	84	-130	320	40	-10	9	A
1293	20111022121355	123.2	23.4	3.9	20	255	53	74	100	40	110	4	C
1294	20111023075348	123.8	23.6	3.5	20	280	40	150	34	74	54	5	B
1295	20111027153646	127.6	25.2	3.9	50	32	80	-170	300	80	-10	6	B
1296	20111027161000	129.8	24.0	4.4	5	256	0	86	80	90	90	3	C
1297	20111031030204	126.6	24.8	4.0	50	52	80	10	320	60	170	5	B
1298	20111109165918	128.2	25.4	4.1	30	12	80	10	280	80	170	5	B
1299	20111110044533	129.0	27.0	3.9	20	40	60	-90	220	30	-90	5	B
1300	20111110052109	129.0	27.0	3.9	10	24	36	-121	240	60	-70	7	B
1301	20111111143330	129.0	27.0	3.9	10	40	50	90	220	40	90	5	B
1302	20111113035203	124.4	26.0	4.1	40	340	40	70	185	53	106	3	C
1303	20111113164729	129.0	27.0	3.7	10	40	50	90	220	40	90	5	B
1304	20111117212514	128.0	25.8	3.7	10	40	60	-90	220	30	-90	3	C
1305	20111117212919	128.0	25.8	3.7	20	256	36	121	40	50	70	4	C

1306	20111118203130	127.8	25.4	4.1	30	40	80	190	308	80	350	6	B
1307	20111118234539	128.0	25.8	3.7	20	256	36	301	40	60	250	4	C
1308	20111122164616	131.5	27.5	3.9	30	80	80	170	172	80	10	3	C
1309	20111123110308	130.0	27.0	3.9	10	68	61	118	200	40	50	3	C
1310	20111126174756	131.5	28.5	3.9	5	62	80	107	180	20	30	5	B
1311	20111204204812	128.8	25.8	3.6	10	201	48	42	80	60	130	5	B
1312	20111215164640	127.2	24.2	4.3	10	260	40	-30	14	71	-126	4	C
1313	20111215212621	127.8	25.6	3.9	20	280	40	130	52	61	61	3	C
1314	20111220101959	125.0	23.8	4.0	20	240	20	90	60	70	90	9	A
1315	20111227212610	127.8	25.4	4.0	20	26	64	34	280	60	150	3	C
1316	20111228051412	127.8	25.4	3.8	30	20	80	10	288	80	170	6	B
1317	20111228171925	128.0	25.4	3.7	10	200	60	50	79	48	138	6	B
1318	20120114135304	130.5	28.5	3.6	5	75	81	-150	340	60	-10	4	C
1319	20120115075637	129.0	29.0	3.9	40	238	75	-103	100	20	-50	5	B
1320	20120121141256	129.0	28.0	3.7	30	360	20	50	222	75	103	4	C
1321	20120204024251	130.0	28.0	3.7	30	48	80	170	140	60	10	6	B
1322	20120204130259	127.8	25.2	4	30	20	80	190	288	80	350	5	B
1323	20120209065803	130.0	28.0	3.6	30	40	80	150	136	61	12	5	B
1324	20120209084416	130.0	28.0	3.8	30	48	80	350	140	80	190	6	B
1325	20120215202330	130.0	29.5	3.9	20	320	20	50	182	75	103	3	C
1326	20120218120331	130.5	29.5	4.1	5	230	87	70	140	20	170	3	C
1327	20120219022226	130.0	29.5	4.1	20	296	22	-153	180	80	-70	5	B
1328	20120219123308	130.5	29.0	4.1	5	64	61	346	160	80	210	6	B
1329	20120219202724	130.5	29.0	3.7	5	72	80	10	340	80	170	5	B
1330	20120219221531	130.5	29.0	4	5	239	87	70	140	20	170	6	B
1331	20120223210224	130.0	28.0	3.7	30	48	80	170	140	80	10	5	B
1332	20120225042050	123.8	23.6	3.8	20	280	40	130	52	61	62	5	B
1333	20120227020229	123.4	23.4	4.2	50	35	81	30	300	60	170	9	A
1334	20120227025208	123.4	23.4	3.9	60	40	80	50	298	41	165	9	A
1335	20120227054059	123.6	23.6	4.4	40	38	84	50	300	40	170	9	A
1336	20120227073121	123.4	23.4	4.3	50	35	81	-150	300	60	-10	9	A
1337	20120227073450	123.4	23.4	4.2	60	40	80	230	298	41	345	8	A
1338	20120227073840	123.4	23.4	4	50	40	80	50	298	41	165	9	A
1339	20120227074440	123.4	23.4	3.9	40	40	80	50	298	41	165	9	A
1340	20120227110111	123.4	23.4	3.8	60	40	80	50	298	41	165	9	A
1341	20120227221042	123.4	23.4	4	50	40	80	230	298	41	345	6	B
1342	20120227235459	123.4	23.4	4.3	60	40	80	50	298	41	165	9	A
1343	20120228074229	123.4	23.4	4.1	50	40	80	50	298	41	165	9	A
1344	20120228090524	123.4	23.4	4	60	40	80	50	298	41	165	8	A
1345	20120228090755	123.4	23.4	4	60	40	80	50	298	41	165	9	A
1346	20120228102251	123.4	23.6	4.2	50	40	80	230	298	41	345	9	A
1347	20120228204939	123.2	23.4	4.1	20	280	50	90	100	40	90	6	B
1348	20120228231914	123.2	23.6	4	20	280	40	-70	75	53	-106	6	B
1349	20120229234546	123.2	23.6	3.9	60	58	84	-130	320	40	-10	8	A
1350	20120229235155	123.2	23.6	3.8	60	222	84	310	320	40	190	8	A
1351	20120301031914	123.2	23.6	3.8	60	222	84	310	320	40	190	9	A
1352	20120301032246	123.2	23.6	3.9	60	22	84	310	320	40	190	8	A
1353	20120301032746	123.2	23.6	3.6	30	300	40	150	54	71	54	7	B
1354	20120301061346	123.2	23.4	3.7	30	200	80	-10	292	80	-170	8	A
1355	20120301110507	123.0	23.4	4.1	30	212	80	10	120	80	170	9	A
1356	20120301122031	123.0	23.4	4	30	212	80	10	120	80	170	8	A
1357	20120301132214	123.8	23.6	3.9	20	280	40	-50	52	61	-118	6	B
1358	20120301144937	123.8	23.6	4.2	20	280	40	-50	52	61	-118	7	B
1359	20120301145554	123.8	23.8	3.9	10	280	20	130	58	75	77	7	B
1360	20120301151112	123.8	23.6	3.6	20	276	36	121	60	60	70	6	B
1361	20120301151515	123.8	23.6	3.7	20	280	40	130	52	61	62	7	B
1362	20120301185101	123.0	23.8	3.8	10	222	84	130	320	40	10	7	B
1363	20120301185730	123.0	23.6	3.8	40	58	84	50	320	40	170	9	A
1364	20120301190834	123.0	23.8	3.8	20	225	81	150	320	60	10	8	A
1365	20120301202109	123.0	23.6	3.8	40	58	84	50	320	40	170	9	A
1366	20120302030226	122.8	23.6	4.1	30	225	81	330	320	60	190	9	A
1367	20120302061445	125.4	24.0	4	30	252	80	-170	160	80	-10	9	A
1368	20120302094817	126.0	25.4	4	5	18	75	-103	240	20	-50	4	C
1369	20120303213730	125.4	22.6	3.9	5	320	40	-70	115	53	-106	6	B
1370	20120303221408	124.2	23.8	3.9	20	240	30	-90	60	60	-90	7	B
1371	20120304124439	127.8	25.4	4.1	20	20	80	190	288	80	350	8	A
1372	20120304144903	128.0	25.4	3.9	10	200	60	50	79	48	138	8	A
1373	20120307165630	128.0	25.4	4.1	30	12	80	10	280	80	170	5	B
1374	20120307172055	128.2	25.2	4.1	50	12	80	10	280	80	170	6	B
1375	20120307180355	128.2	25.4	3.8	30	20	60	210	274	64	326	5	B
1376	20120308034516	124.4	23.6	3.8	20	60	40	-50	192	61	-118	7	B
1377	20120310030140	122.8	23.4	3.9	30	55	81	30	320	60	170	7	B
1378	20120310074549	122.8	23.4	3.9	40	60	80	30	324	61	168	9	A
1379	20120310075033	122.8	23.4	3.9	40	60	80	30	324	61	165	9	A
1380	20120311062606	123.0	23.4	4.2	60	55	81	-150	320	60	-10	9	A
1381	20120313020426	122.8	23.4	3.9	40	60	80	30	324	61	165	8	A
1382	20120313021552	122.8	23.4	3.9	40	60	80	30	324	61	168	8	A
1383	20120314164142	122.6	23.4	4	30	68	80	170	160	80	10	6	B
1384	20120404151919	128.0	25.6	3.7	10	84	61	168	180	80	30	5	B
1385	20120405002805	128.0	25.6	3.8	5	268	80	350	0	80	190	6	B
1386	20120405003815	128.0	25.6	3.8	10	88	80	170	180	80	10	5	B
1387	20120405020124	128.0	25.6	3.9	5	360	80	170	92	80	10	5	B

1388	20120405035500	127.4	24.4	3.8	10	26	64	34	280	60	160	3	C
1389	20120405112317	128.0	25.6	4.1	10	40	50	90	220	40	90	5	B
1390	20120406031656	128.2	26.2	3.9	5	180	60	-10	275	81	-150	4	C
1391	20120408160054	122.0	22.0	3.9	60	268	61	298	40	40	230	4	C
1392	20120421141000	131.5	29.5	3.8	5	66	71	126	180	40	30	5	B
1393	20120428003000	129.0	27.0	4	10	240	40	-70	35	53	-106	5	B
1394	20120428003006	129.4	26.8	4	10	40	50	-90	220	40	-90	5	B
1395	20120511065146	125.2	24.0	4.2	30	252	80	10	160	80	170	7	B
1396	20120511065819	125.0	24.0	4	10	62	75	103	200	20	50	8	A
1397	20120511083028	125.2	24.0	4.1	30	252	80	-170	160	80	-10	8	A
1398	20120518235434	122.6	22.2	3.8	50	24	36	59	240	60	110	3	C
1399	20120522212808	125.2	23.5	4.1	30	260	40	-30	14	71	-126	8	A
1400	20120524044453	123.8	23.2	4	60	0	50	90	180	40	90	4	C
1401	20120526134841	129.4	26.4	3.8	30	281	71	97	80	20	70	4	C
1402	20120621081052	125.0	24.0	4	10	18	75	-103	240	20	-50	8	A
1403	20120622175155	124.2	24.8	3.6	10	240	60	30	134	64	146	3	C
1404	20120630105808	122.4	24.4	4	50	258	75	77	120	20	130	4	C
1405	20120701040934	124.2	23.6	3.8	20	260	40	110	55	53	74	5	B
1406	20120703094140	131.5	29.0	3.8	40	300	40	70	145	53	106	4	C
1407	20120716035934	128.0	25.6	3.7	5	180	80	-10	272	80	-170	5	B
1408	20120716130211	127.6	26.4	3.9	20	60	80	50	318	41	165	5	B
1409	20120716130729	127.6	26.4	4	20	55	81	30	320	60	170	5	B
1410	20120716131049	127.6	26.4	4	30	55	81	30	320	60	170	4	C
1411	20120727204606	125.0	23.6	4.1	20	240	30	90	60	60	90	8	A
1412	20120727205448	125.0	23.6	4	20	240	30	90	60	60	90	8	A
1413	20120727211149	125.0	23.6	3.9	20	240	30	90	60	60	90	8	A
1414	20120727225204	125.0	23.4	4	50	280	40	130	52	61	62	9	A
1415	20120806215359	123.6	23.4	4.3	50	200	80	150	296	61	12	6	B
1416	20120821002035	128.0	25.6	3.8	5	360	80	-10	92	80	-170	5	B
1417	20120821002945	128.2	25.4	3.8	10	40	50	90	220	40	90	6	B
1418	20120821011311	128.0	25.6	3.6	5	360	80	170	92	80	10	4	C
1419	20120821154341	127.8	25.0	4.1	50	28	80	170	120	80	10	5	B
1420	20120821160005	127.8	25.2	4.1	50	32	80	10	300	80	170	4	C
1421	20120821194252	127.8	25.4	3.9	20	20	80	30	284	61	168	6	B
1422	20120822205301	128.0	25.4	4.1	40	20	80	10	288	80	170	5	B
1423	20120822210858	128.0	25.8	3.8	20	256	36	121	40	60	70	5	B
1424	20120822220059	128.0	25.6	3.8	20	260	40	130	32	61	62	5	B
1425	20120822224044	127.6	24.4	4.2	5	280	20	190	181	87	290	5	B
1426	20120823035820	127.6	24.6	4.1	5	300	20	30	182	80	107	4	C
1427	20120824005348	127.8	25.8	3.9	5	180	60	130	282	41	15	3	C
1428	20120914030906	130.0	28.0	3.8	30	48	80	350	140	80	190	5	B
1429	20120914115308	130.0	28.0	3.7	30	34	64	146	140	60	30	7	B
1430	20120917170929	129.0	27.5	3.7	5	198	41	345	300	80	230	5	B
1431	20120922200440	130.0	28.0	3.4	5	34	64	326	140	60	210	5	B
1432	20120922200710	130.0	28.0	3.4	20	40	60	150	146	64	34	4	C
1433	20120924015736	122.0	24.4	3.6	30	280	60	-70	64	36	-121	3	C
1434	20121001145410	128.5	25.0	3.7	10	260	60	150	6	64	34	5	B
1435	20121001160410	129.0	25.5	3.6	20	199	87	-110	100	20	-10	5	B
1436	20121003195907	129.5	27.5	3.7	20	260	20	110	59	71	83	5	B
1437	20121003203630	129.0	28.5	3.4	10	88	80	350	180	80	190	5	B
1438	20121004034636	129.5	27.5	3.7	20	260	20	-50	38	75	-103	5	B
1439	20121006173901	129.0	29.0	3.9	20	260	60	-90	80	30	-90	3	C
1440	20121006175245	129.0	29.0	3.7	20	261	71	97	60	20	70	5	B
1441	20121017100124	133.0	31.2	4.2	40	260	80	90	80	10	90	5	B
1442	20121017112416	132.2	30.4	4.1	10	234	64	326	340	60	210	6	B
1443	20121017124710	130.2	30.6	4	50	188	80	170	280	80	10	6	B
1444	20121017125419	132.2	30.4	3.8	10	234	64	146	340	60	30	5	B
1445	20121017144906	132.2	30.4	3.8	10	234	64	326	340	60	210	5	B
1446	20121017155640	132.2	30.4	3.9	10	234	64	326	340	60	210	4	C
1447	20121018150600	130.2	30.6	4.1	50	188	80	170	280	80	10	5	B
1448	20121019052322	130.2	30.6	3.8	50	188	80	350	280	80	190	5	B
1449	20121019145803	132.6	31.4	4	60	45	81	330	140	60	190	6	B
1450	20121019163855	132.4	30.6	4	10	341	48	42	220	60	130	5	B
1451	20121019184140	133.6	31.0	3.9	5	280	20	-70	79	71	-97	3	C
1452	20121020004445	123.0	23.6	3.8	40	60	80	50	318	41	165	9	A
1453	20121020143009	128.2	26.0	4.1	50	52	80	-170	320	80	-10	4	C
1454	20121022221741	127.6	26.4	4.1	50	236	84	-130	140	40	-10	7	B
1455	20121025131000	123.4	23.4	4.1	60	205	81	150	300	60	10	8	A
1456	20121025131256	123.4	23.4	4	50	35	81	30	300	60	170	9	A
1457	20121025134800	123.4	23.2	4	50	35	81	30	300	60	170	9	A
1458	20121025144432	123.4	23.2	4	60	40	80	30	304	61	168	9	A
1459	20121025152406	122.8	22.2	4.1	5	320	20	210	302	80	287	4	C
1460	20121025154728	123.6	23.4	3.9	40	280	40	150	34	71	54	9	A
1461	20121025155429	123.0	22.8	3.8	5	316	22	-153	200	80	-70	6	B
1462	20121025162724	123.4	23.2	4.1	60	35	81	30	300	60	170	7	B
1463	20121025164033	123.0	22.8	3.9	5	200	80	-50	302	41	-165	5	B
1464	20121025171230	122.6	22.2	3.9	5	38	84	50	300	40	170	6	B
1465	20121025183926	123.4	23.4	4.1	60	38	84	50	300	40	170	9	A
1466	20121025185123	123.6	23.6	3.8	20	276	36	121	60	60	70	7	B
1467	20121025200932	123.6	23.6	3.7	20	276	36	121	60	60	70	8	A
1468	20121025202824	123.6	23.6	3.8	20	276	36	301	60	60	250	8	A
1469	20121026112943	123.6	23.6	3.7	20	284	22	153	40	80	70	7	B

1470	20121027010733	124.0	26.0	3.9	30	240	80	-10	332	80	-170	3	C
1471	20121027030825	123.8	23.6	3.5	20	276	36	121	60	60	70	5	B
1472	20121027182150	123.4	23.4	4.1	60	40	80	50	298	41	165	7	B
1473	20121029004939	123.0	23.6	3.9	40	60	80	50	318	41	165	9	A
1474	20121029015613	123.0	23.6	4	40	225	81	330	320	60	190	9	A
1475	20121029022308	123.0	23.6	4.2	40	58	84	-130	320	40	-10	8	A
1476	20121029051746	123.0	23.8	4	20	225	81	150	320	60	10	3	C
1477	20121029053343	123.2	23.8	3.9	20	280	20	-50	58	75	-103	3	C
1478	20121029062116	123.0	23.6	4	40	58	84	50	320	40	170	4	C
1479	20121030083853	122.8	23.4	4	40	60	80	30	324	61	168	8	A
1480	20121030084651	122.8	23.4	3.9	40	60	80	30	324	61	168	9	A
1481	20121030085348	122.8	23.4	3.7	30	60	80	30	324	61	168	9	A
1482	20121101184319	127.8	26.0	4.4	40	60	80	-10	152	80	-170	5	B
1483	20121101201049	123.2	23.2	4	20	234	71	-126	120	40	-30	4	C
1484	20121103031000	122.8	23.6	3.8	40	240	80	-10	332	80	-170	7	B
1485	20121103035640	122.8	23.4	3.8	30	60	80	30	324	61	168	8	A
1486	20121103042708	122.8	23.4	3.8	40	60	80	30	324	61	168	8	A
1487	20121105205632	129.0	26.5	4.1	5	15	53	-106	220	40	-70	6	B
1488	20121113165846	124.2	24.6	3.5	10	240	60	-10	335	81	-150	3	C
1489	20121113170213	124.2	23.8	3.6	20	240	30	90	60	60	90	8	A
1490	20121113171448	124.4	23.6	4	20	260	40	130	32	61	62	9	A
1491	20121113193529	124.2	23.6	3.9	20	220	40	70	65	53	106	8	A
1492	20121113200742	124.2	23.8	3.8	20	240	30	-90	60	60	-90	7	B
1493	20121114032259	125.4	22.6	4.1	5	320	40	110	115	53	74	3	C
1494	20121130054920	129.0	26.5	4	10	40	40	90	220	50	90	5	B
1495	20121130060500	128.5	26.5	4.1	10	220	80	250	104	22	333	4	C
1496	20121204200628	128.5	27.0	3.8	20	66	64	34	320	60	150	7	B
1497	20121212123150	129.0	26.5	4	5	15	53	74	220	40	110	3	C
1498	20121212132706	128.5	27.0	3.9	20	299	48	138	60	60	50	7	B
1499	20121212133646	128.5	27.0	3.7	30	300	40	-30	54	71	-126	5	B
1500	20121212135640	128.5	27.0	3.8	30	300	40	-30	54	71	-126	5	B
1501	20121212160320	129.0	25.5	3.8	10	248	80	350	340	80	190	4	C
1502	20121213004820	128.5	25.5	3.9	10	260	60	190	165	81	330	4	C
1503	20121213132550	129.0	27.0	3.8	5	80	80	-10	172	80	-170	4	C
1504	20121230182044	128.2	26.0	4	5	80	80	-10	172	80	-170	4	C

Supplementary 1-F1

24-hour seismograms showing VLFE activation caused by the Mw 8.3 Kuril earthquake

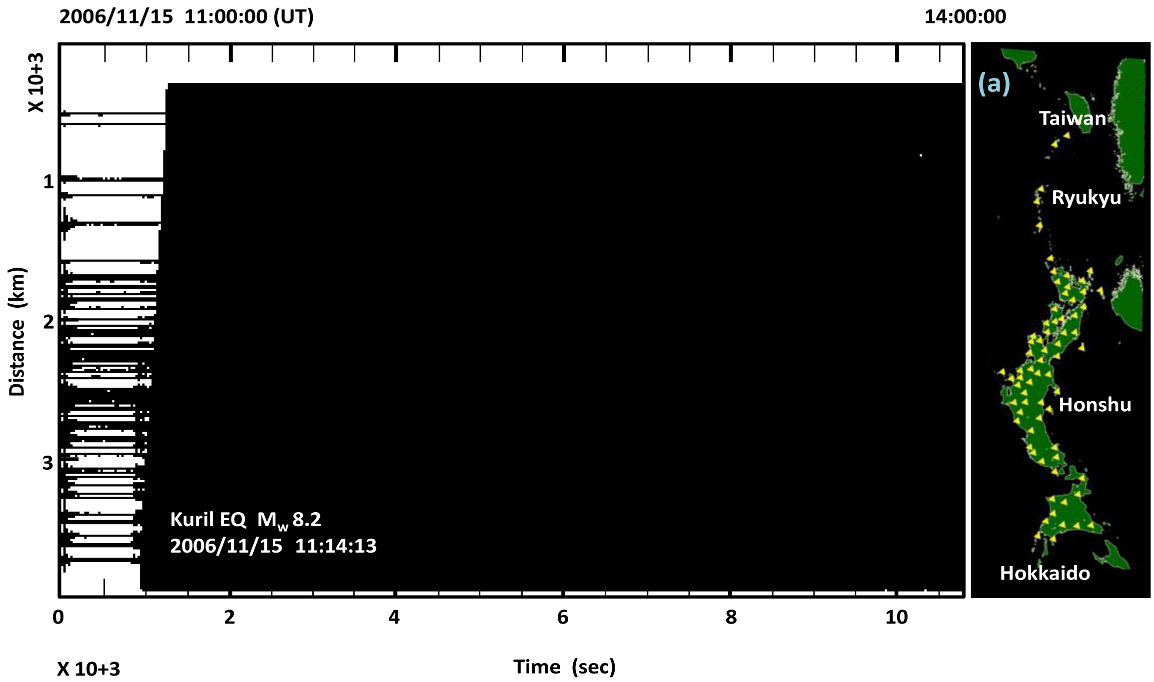
2006/11/15 11:00:00 (UT)
14:00:00
X 10+3
Distance (km)
Time (sec)
X 10+3
Kuril EQ M_w 8.2
2006/11/15 11:14:13
(a)
Taiwan
Ryukyu
Honshu
Hokkaido

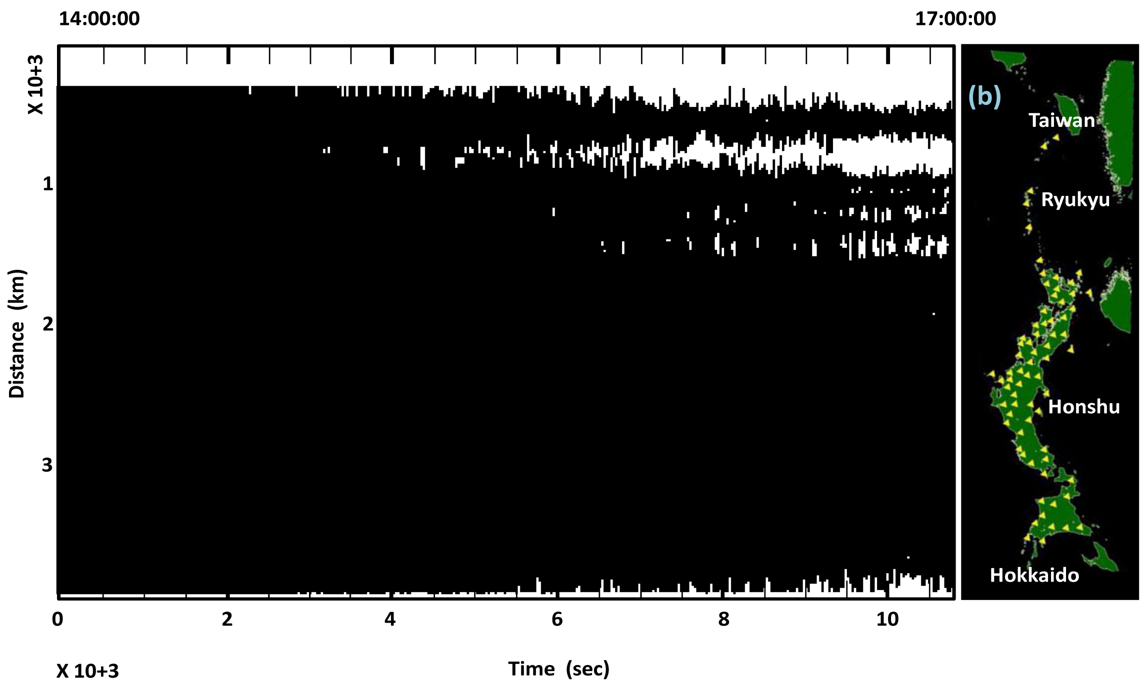
14:00:00
17:00:00
X 10+3
Distance (km)
Time (sec)
X 10+3
(b)
Taiwan
Ryukyu
Honshu
Hokkaido

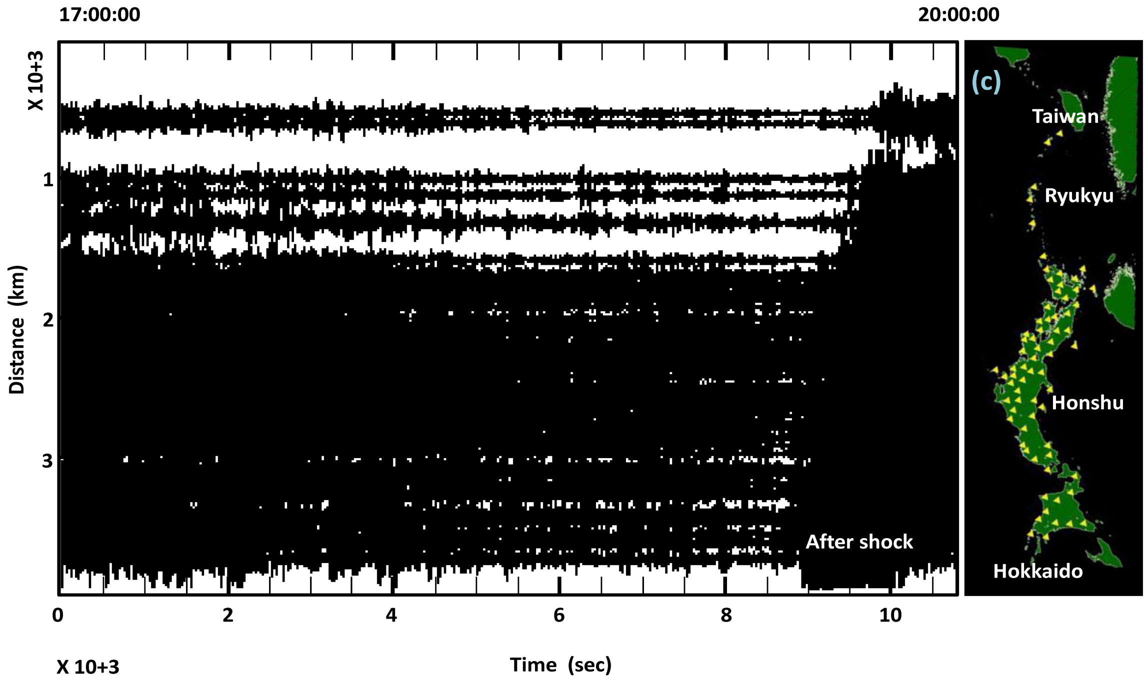
17:00:00
20:00:00
X 10+3
Distance (km)
1
2
3
After shock
0
2
4
6
8
10
X 10+3
Time (sec)
(c)
Taiwan
Ryukyu
Honshu
Hokkaido

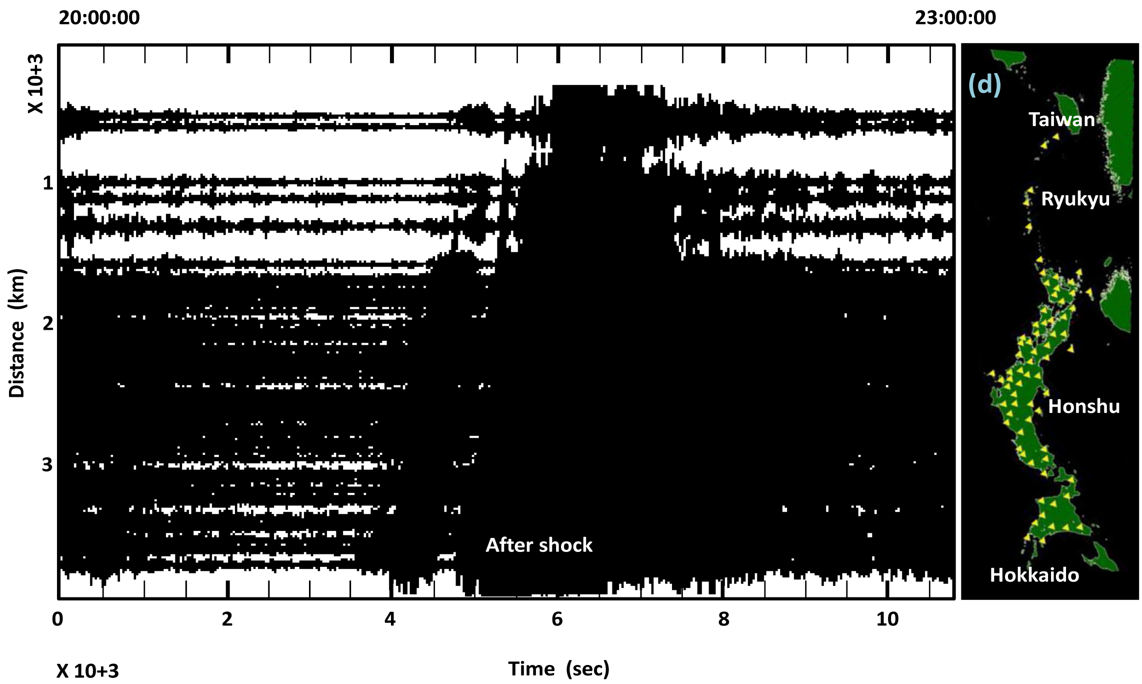
20:00:00
23:00:00
X 10+3
Distance (km)
1
2
3
After shock
0
2
4
6
8
10
X 10+3
Time (sec)
(d)
Taiwan
Ryukyu
Honshu
Hokkaido

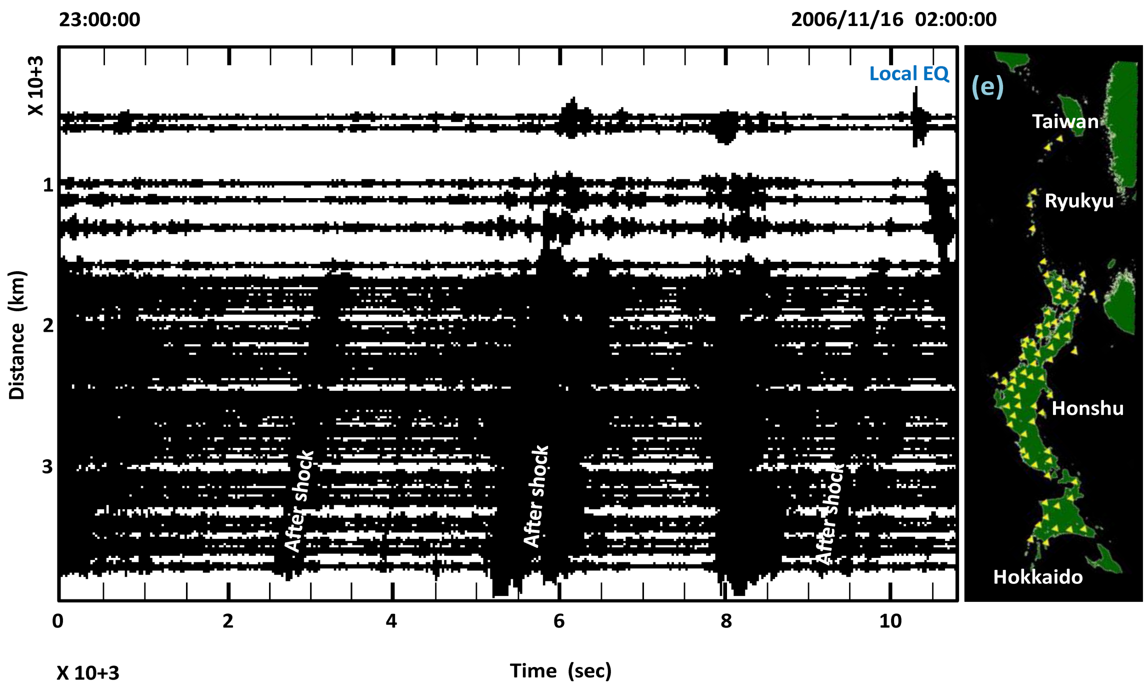
23:00:00
2006/11/16 02:00:00
Local EQ
(e)
Taiwan
Ryukyu
Honshu
Hokkaido
After shock
After shock
After shock
X 10+3
Distance (km)
1
2
3
0
2
4
6
8
10
X 10+3
Time (sec)

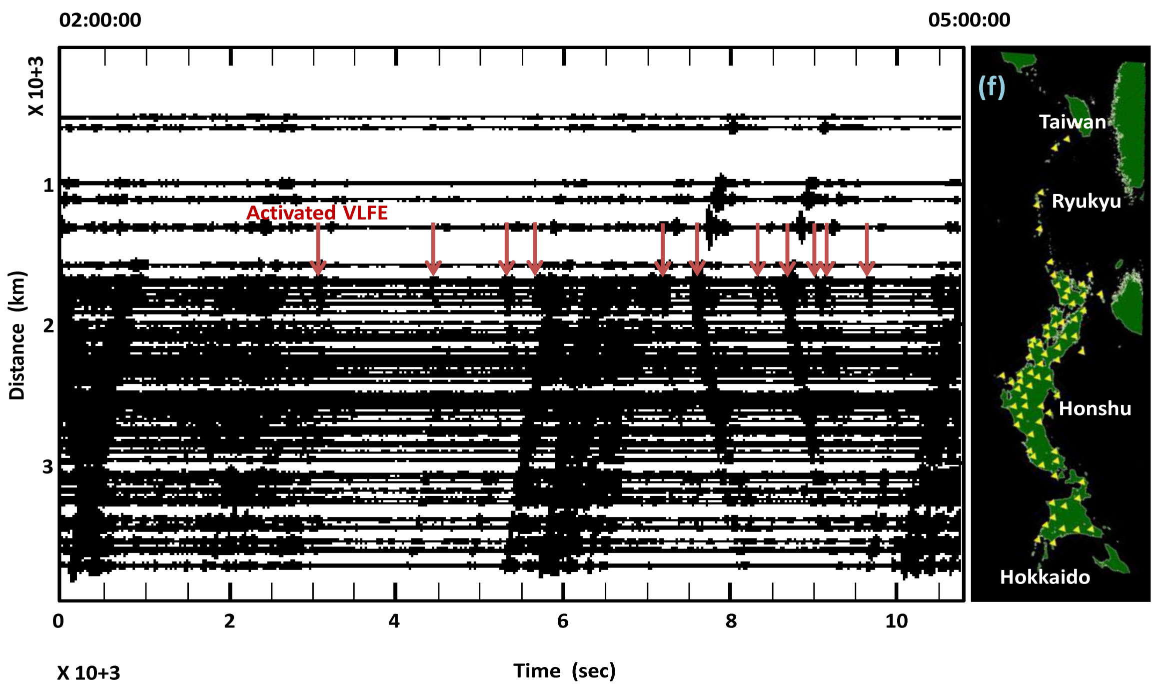
02:00:00
05:00:00
Activated VLFE
(f)
Taiwan
Ryukyu
Honshu
Hokkaido
X 10+3
Distance (km)
1
2
3
0
2
4
6
8
10
X 10+3
Time (sec)

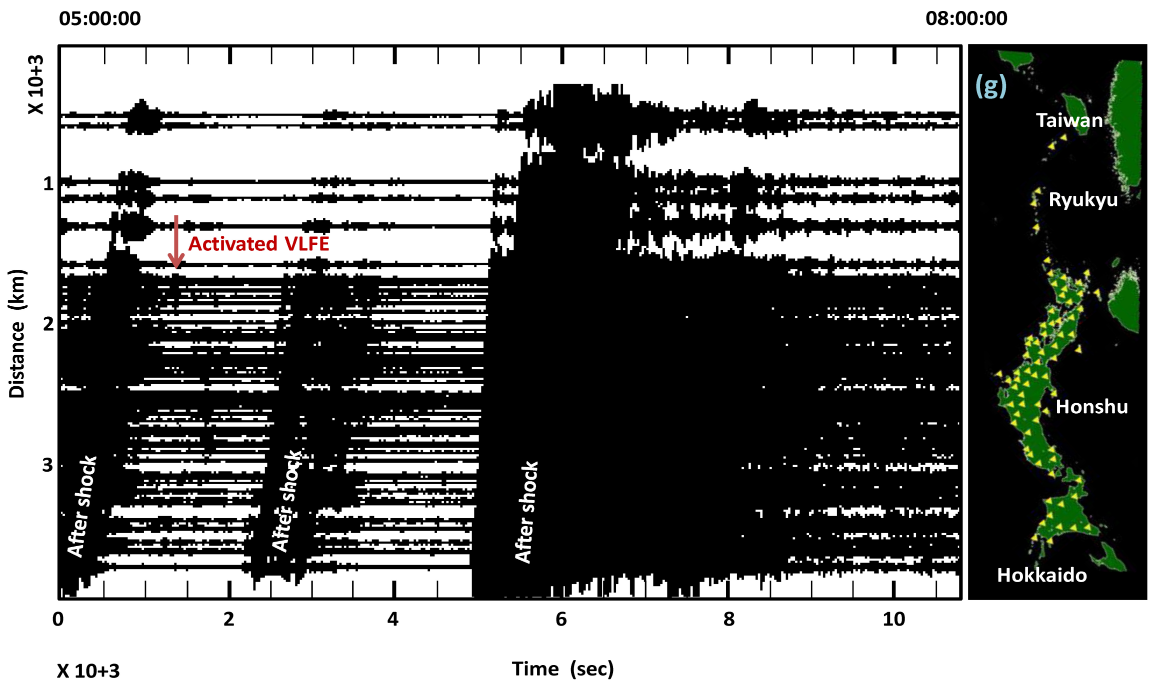

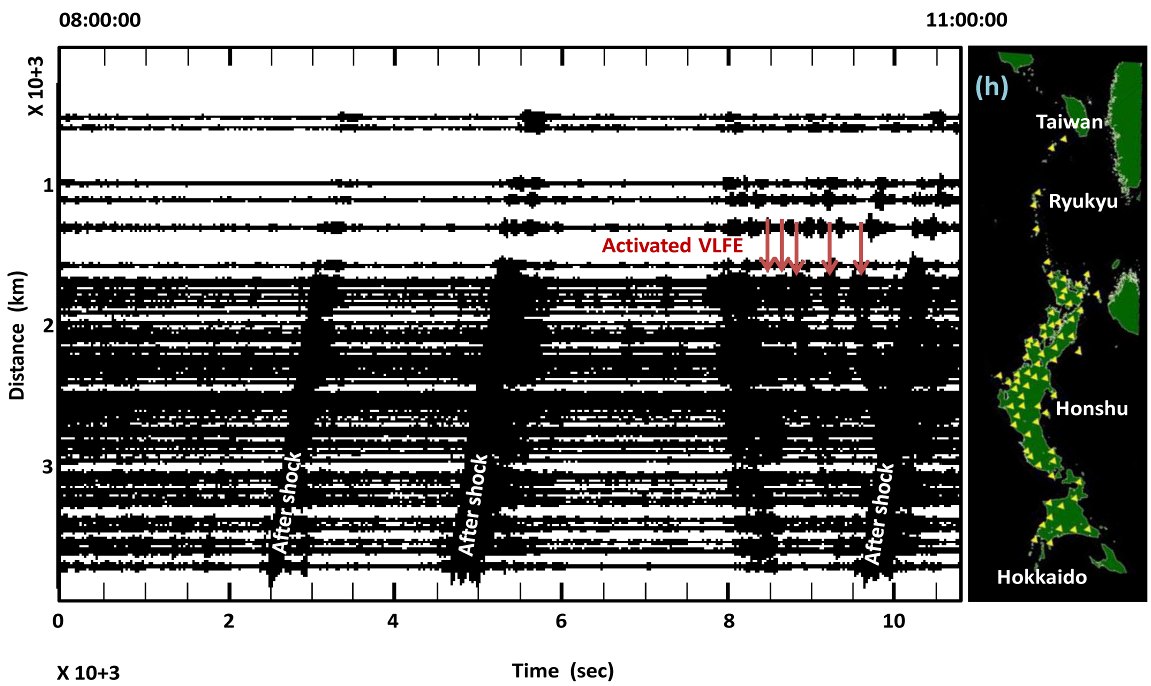

Supplement 1-F1. Twenty-four-hour vertical component seismograms after the M_w 8.3 Kuril earthquake occurrence obtained from the broadband seismic stations of F-net (triangles in the right diagram). The seismogram filtered at 0.02-0.06 Hz is arranged from top to bottom based on increasing distance northward from 120°E, 20°N. The time zero in (a) is comparable to (UT) 11:00:00, on Nov. 15, 2006. The time spacing in each diagram (a-h) is three hours.

Supplementary 2

The catalog of RVLFEs in 2005-2012

Table S1. Occurrence times, locations, magnitudes and source parameters of the 97 RVLFEs south of Miyako Island.

No.	Time	Log (°E)	Lat (°N)	M_w	Depth (km)	Strike 1	Dip 1	Rake 1	Strike 2	Dip 2	Rake 2	Quality value	Quality rank	CCC (γ)	Sequence	M_0 (e+15Nm)
1	20050306123904	125.2	23.9	4.1	20	0	80	50	258	41	165	9	A	0.99	1-1	1.70
2	20050306124629	125.4	23.8	4.0	30	12	61	62	240	40	130	6	B	1.00	1-2	1.42
3	20050306125726	125.3	23.9	4.0	20	20	60	70	236	36	121	8	A	1.00	1-3	1.06
4	20050306133847	125.3	23.9	3.9	20	20	60	70	236	36	121	8	A	0.99	1-4	1.02
5	20050420034835	125.3	23.9	4.0	20	240	40	150	354	71	54	4	C	0.94	2-1	1.32
6	20050420040629	125.3	23.9	4.1	20	20	60	70	238	36	121	8	A	0.99	2-2	1.53
7	20050427174543	125.2	23.9	4.0	20	0	80	50	258	41	165	8	A	0.93	2-3	1.36
8	20050621104939	125.1	23.9	4.0	20	14	71	64	260	40	150	4	C	0.89	3-1	1.26
9	20050621110723	125.2	23.8	4.0	20	40	60	90	220	30	90	5	B	0.99	3-2	1.44
10	20050807180602	125.3	23.9	4.0	20	20	60	70	236	38	121	5	B	0.98	4-1	1.49
11	20050807181218	125.2	23.9	4.0	20	20	60	70	236	36	122	5	B	0.99	4-2	1.10
12	20051109233209	125.2	23.9	3.9	20	14	71	64	260	40	150	8	A	0.98	5-1	0.93
13	20051109233836	125.2	23.9	4.0	20	20	60	70	236	36	121	8	A	1.00	5-2	1.19
14	20060108075950	125.3	23.9	3.9	20	20	60	70	236	36	121	5	B	0.99	6-1	0.96
15	20060108080649	125.3	23.9	4.0	20	20	60	70	236	36	121	6	B	1.00	6-2	1.07
16	20060211094253	125.3	23.9	4.0	20	20	60	70	236	36	121	7	B	1.00	7-1	1.11
17	20060212131130	125.1	23.9	4.0	20	14	71	54	260	40	150	7	B	0.97	7-2	1.14
18	20060603055500	125.3	23.9	3.8	20	12	61	62	240	40	130	5	B	0.87	8-1	0.67
19	20060603061338	125.3	23.9	4.0	20	20	60	70	236	36	121	8	A	1.00	8-2	1.10
20	20060603074433	125.2	23.9	4.0	20	40	60	90	220	30	90	7	B	1.00	8-3	1.48
21	20060609033819	125.2	23.8	4.0	20	14	71	54	260	40	150	7	B	0.91	8-4	1.44
22	20060715204947	125.2	23.9	4.0	20	40	70	90	220	20	90	5	B	0.96	9-1	1.42
23	20061111114018	125.2	23.9	4.1	20	0	80	50	258	41	165	5	B	0.98	10-1	1.59
24	20061111114500	125.4	23.8	4.1	30	12	61	62	240	40	130	3	C	1.00	10-2	2.08
25	20070112055346	125.2	23.8	3.9	20	14	71	54	260	40	150	9	A	0.97	11-1	1.05
26	20070112060022	125.2	23.9	4.0	20	0	80	50	258	41	165	8	A	1.00	11-2	1.11

27	20070323140753	125.3	23.9	3.9	20	12	61	62	240	40	130	6	B	0.91	12-1	0.91
28	20070503013304	125.2	23.8	4.0	20	14	71	54	260	40	150	6	B	0.75	13-1	1.44
29	20070503014109	125.4	23.8	4.0	30	12	61	62	240	40	130	6	B	1.00	13-2	1.33
30	20070611114039	125.2	23.9	4.1	20	0	80	50	258	41	165	7	B	0.98	14-1	2.03
31	20070611114602	125.3	23.9	3.9	20	20	60	70	236	36	121	6	B	1.00	14-2	0.84
32	20070611120305	125.3	23.9	3.9	20	20	60	70	236	36	121	5	B	1.00	14-3	0.99
33	20070731065125	125.4	23.8	4.2	30	12	61	62	240	40	130	8	A	0.99	15-1	2.22
34	20070731065637	125.4	23.8	4.0	30	12	61	62	240	40	130	7	B	1.00	15-2	1.49
35	20070731070758	125.3	23.9	3.9	20	20	60	70	236	36	121	8	A	1.00	15-3	0.92
36	20071222002451	125.4	23.8	4.2	30	12	61	62	240	40	130	8	A	0.99	16-1	2.46
37	20071222002826	125.3	23.9	3.9	20	20	60	70	236	36	121	8	A	1.00	16-2	0.95
38	20080211033516	125.2	23.9	4.1	20	0	80	50	258	41	165	8	A	0.98	17-1	1.68
39	20080211034133	125.4	23.8	4.0	30	12	61	62	240	40	130	7	B	1.00	17-2	1.37
40	20080211035341	125.2	23.8	3.9	20	40	60	90	220	30	90	7	B	0.99	17-3	0.86
41	20080215103433	125.2	23.9	3.9	20	20	60	70	236	36	121	5	B	0.92	17-4	0.94
42	20080507055343	125.2	23.9	4.0	20	14	71	54	260	40	150	3	A	0.93	18-1	1.45
43	20080507055953	125.3	23.9	4.0	20	20	60	70	236	36	121	7	B	1.00	18-2	1.44
44	20080607271119	125.2	23.8	4.0	20	40	60	90	220	30	90	5	B	0.91	19-1	1.47
45	20080627073009	125.3	23.9	4.0	20	20	60	70	236	36	121	6	B	1.00	19-2	1.14
46	20080701010642	125.1	23.9	3.9	20	14	71	54	260	40	150	6	B	0.93	20-1	0.82
47	20080901171245	125.2	23.9	4.1	20	0	80	50	258	41	165	8	A	0.96	21-1	1.96
48	20080901192605	125.3	23.9	4.0	20	20	60	70	236	36	121	9	A	1.00	21-2	1.40
49	20080910061242	125.1	23.9	3.9	20	0	80	50	258	41	165	4	C	0.85	21-3	0.94
50	20081020164605	125.2	23.9	4.0	20	260	40	170	358	84	50	7	B	0.91	22-1	1.80
51	20081209131102	125.2	23.8	4.1	20	40	60	90	220	30	90	7	B	0.98	23-1	1.57
52	20081209131835	125.3	23.8	4.0	20	20	60	70	236	36	121	4	C	0.99	23-2	1.16
53	20081209134602	125.3	23.9	4.0	20	20	60	70	236	36	121	5	B	0.99	23-3	1.31
54	20090126155349	125.1	23.9	4.0	20	14	17	54	260	40	150	7	B	0.83	24-1	1.32
55	20090126160209	125.3	23.9	4.1	20	20	60	70	236	36	121	7	B	1.00	24-2	1.64
56	20090331090046	125.2	23.9	4.1	20	20	60	70	236	36	121	6	B	0.95	25-1	1.71
57	20090331090639	125.2	23.9	4.0	20	0	80	50	258	41	165	6	B	0.99	25-2	1.07
58	20090331092232	125.4	23.8	3.9	30	12	61	62	240	40	130	4	C	1.00	25-3	0.77
59	20090711050347	125.3	23.9	4.0	20	20	60	70	236	36	121	5	B	0.99	26-1	1.12
60	20090711051544	125.3	23.9	3.9	20	20	60	70	236	36	121	5	B	0.99	26-2	0.99

61	20090716144520	125.2	23.9	4.1	20	20	60	70	236	36	121	6	B	0.99	26-3	1.86
62	20090813042022	125.2	23.9	4.0	20	0	80	50	258	41	165	6	B	0.99	27-1	1.22
63	20090919032831	125.3	23.9	4.0	20	20	60	70	236	36	121	7	B	0.99	28-1	1.34
64	20091028144249	125.2	23.9	4.1	20	20	60	70	236	36	121	8	A	0.95	29-1	2.06
65	20091028144929	125.2	23.9	4.0	20	20	60	70	236	36	121	7	B	0.98	29-2	1.06
66	20091215165807	125.2	23.9	4.1	20	0	80	50	258	41	165	7	B	0.97	30-1	1.57
67	20091215170305	125.2	23.9	3.9	20	0	80	50	258	41	165	7	B	1.00	30-2	1.02
68	20100109162125	125.0	23.9	4.1	10	62	75	103	200	20	50	7	B	0.97	31-1	1.78
69	20100207115443	125.1	23.9	3.9	20	14	71	54	260	40	150	7	B	0.98	32-1	0.82
70	20100623111918	125.2	23.9	3.9	20	40	60	90	220	30	90	7	B	0.98	33-1	0.95
71	20100627053506	125.3	23.9	4.1	20	20	60	70	236	36	121	8	A	0.99	33-2	1.89
72	20100627054038	125.2	23.9	3.9	20	20	60	70	236	36	121	6	B	1.00	33-3	0.81
73	20100728182002	125.2	23.9	4.0	20	0	80	50	258	41	165	5	B	0.99	34-1	1.12
74	20100728191232	125.2	23.9	3.9	20	0	80	50	258	41	165	8	A	0.99	34-2	0.90
75	20100729062012	125.1	23.9	3.9	20	14	71	54	260	40	150	7	B	0.78	34-3	0.80
76	20100918042155	125.3	24.0	4.1	20	240	40	150	354	71	54	4	C	0.99	35-1	2.05
77	20101212053619	125.2	23.8	4.0	20	14	71	54	260	40	150	4	C	0.95	36-1	1.12
78	20101216225239	125.2	23.9	4.0	20	0	80	50	258	41	165	6	B	0.99	36-2	1.36
79	20110206052236	125.1	23.8	4.0	20	14	71	54	260	40	150	8	A	0.56	37-1	1.37
80	20110206053115	125.3	23.9	4.0	20	20	60	70	236	36	121	8	A	0.99	37-2	1.44
81	20110214013319	125.2	23.9	4.1	20	0	80	50	258	41	165	4	C	0.98	37-3	1.79
82	20110825051208	125.0	23.9	4.1	10	58	75	77	280	20	130	3	C	0.90	38-1	2.04
83	20111012160404	125.1	23.9	4.0	20	0	80	50	258	41	165	9	A	0.97	39-1	1.33
84	20111012161427	125.3	23.9	4.0	20	20	60	70	236	36	121	8	A	****	39-2	1.32
85	20111012161910	125.2	23.9	3.8	20	20	60	70	238	36	121	8	A	0.99	39-3	0.69
86	20111019181343	125.1	23.9	4.1	20	14	71	54	260	40	150	9	A	0.91	39-4	1.55
87	20111220102024	125.0	23.9	4.0	10	62	75	103	200	20	50	7	B	0.99	40-1	1.23
88	20120302061428	125.2	23.9	4.0	20	14	71	54	260	40	150	6	B	0.95	41-1	1.26
89	20120511065139	125.0	23.9	4.0	10	62	75	103	200	20	50	4	C	0.92	42-1	1.25
90	20120511065807	125.3	23.9	3.9	20	20	60	70	238	36	121	8	A	1.00	43-1	0.97
91	20120511083028	125.3	23.9	4.0	20	20	60	70	236	36	121	9	A	1.00	43-2	1.35
92	20120522212813	125.1	23.9	3.9	20	14	71	-126	260	40	-30	7	B	0.91	43-3	0.86
93	20120621081035	125.0	23.9	4.0	20	18	80	73	260	20	150	5	B	0.99	44-1	1.43
94	20120727204612	125.0	23.6	4.1	20	60	60	90	240	30	90	4	C	0.92	45-1	2.09

95	20120727205444	125.0	23.6	4.0	20	60	60	90	240	30	90	4	C	1.00	45-2	1.23
96	20120727211153	125.0	23.6	4.0	20	60	60	90	240	30	90	4	C	1.00	45-3	1.16
97	20120727225209	125.0	23.7	3.9	20	60	60	90	240	30	90	4	C	0.96	45-4	0.94

*** The master event for the calculation of cross-correlation coefficients (γ)